May 31, 2017

DOE Award Number: DE-EE0005124

System Reliability Model for Solid-State Lighting (SSL) Luminaires

Recipient: RTI International
PO Box 12194
Research Triangle Park, NC 27709-2194

Sub-Recipient: Auburn University

Other Teaming Members: Cree Inc., SAS Institute, PPG Industries, State of North Carolina, LED Systems Reliability Consortium

Principal Investigator: Dr. J. Lynn Davis

RTI Project Number 02013159

RTI INTERNATIONAL

RTI Project Number
0213159

System Reliability Model for Solid-State Lighting (SSL) Luminaires

May 31, 2017

Prepared for U.S. Department of Energy

Prepared by RTI International

RTI International
3040 E. Cornwallis Road
Research Triangle Park, NC 27709

CONTENTS

Section **Page**

List of Acronyms **xv**

1. Acknowledgements **1-1**

2. Executive Summary **2-1**

3. Comparison of Actual Accomplishments with the Goals and Objectives **3-1**

4. Summary of Activities for Entire Funding Period **4-1**

4.A Models Overview 4-1
4.A.1 Background 4-1
4.A.2 Empirical Models of Lumen Maintenance Behavior of LEDs 4-2
4.A.3 Kaplan-Meier Models of Lumen Maintenance Failures 4-12
4.A.4 Physics of Failure Models of Chemical Degradation of SSL Devices 4-18
4.A.5 Projection of Chromaticity Shift 4-35
4.A.6 Virtual Models of the Impact of Lumen Degradation 4-37
4.A.7 Weibull Models of SSL Device Failure 4-41

4.B Individual LED Behavior 4-44
4.B.1 Industry Data on Lumen Maintenance of Individual LEDs 4-44
4.B.2 Industry Data on Chromaticity Stability of LEDs 4-50
4.B.3 Accelerated Testing of Luminous Flux and Chromaticity Maintenance 4-53

4.C LED Lamp Behavior 4-93
4.C.1 Elevated Ambient Testing of PAR38 Lamps 4-94
4.C.2 Elevated Ambient Testing of A19 Lamps 4-99
4.C.3 Accelerated Stress Testing of A19 Lamps 4-100

4.D LED Luminaire Behavior 4-113
4.D.1 Luminaire Operation at Room Temperature 4-113
4.D.2 Guidance Document for SSL Luminaire and Lamp Use 4-134
4.D.3 Accelerated Stress Testing 4-135
4.D.4 Hammer Test Results 4-137
4.D.5 Remote Phosphor Disk Studies 4-144
4.D.6 Luminaire Operation in Accelerated Stress Tests 4-145
4.D.7 Organic Light Emitting Diodes (OLEDs) 4-168
4.D.8 Luminaire Driver Behavior 4-175

4.D.9 AST Results of SSL Drivers and Luminaires..... 4-198

References **R-1**

Appendix

A: Devices Under Test (including Auburn work) **A-1**

B: Products—Experimental Methods **B-1**

C: Products—List of Papers and Presentations **C-1**

D: Products—Networks and Collaborations Fostered **D-1**

E: Products—Inventions/Patent Applications **E-1**

FIGURES

Number **Page**

2-1. Product Hazard Function as Represented by the Bathtub Curve 2-1
2-2. Three-Pronged Approach to Building a Knowledge Base of SSL Device Failure 2-2
2-3. Luminous Flux Decay Rate Constants (α) for LEDs by Package Type 2-5
2-4. CSMs of PAR38 Lamps Classified by LED Package Type 2-6
2-5. Example of Chromaticity Shift Modeling for SSL Devices 2-7
2-6. Weibull Probability Plot for 6" Downlights in WHTOL 2-9

4A-1. Three-Pronged Approach to Building a Knowledge Base of SSL Device Failure 4-1
4A-2. Breakout of the LM-80-08 Reports by Package Type, Collected from Major Manufacturers 4-3
4A-3. Residual Distributions for the Fitted Linear Models 4-6
4A-4. Decay-Rate Constant Values of Representative Test Populations of One HP-LED Product Tested at One of Three Different Temperatures 4-8
4A-5. Illustration of the Components of Double Model for Luminous Flux Maintenance 4-11
4A-6. L70 Survivorship Curves and 95% Confidence Interval (CI) Levels for a Randomly Selected Population of Generic HP-LEDs Operated and 1,000 mA and 100°C 4-15
4A-7. L90 Survivorship Curves and 95% CI Levels for a Randomly Selected Population of Generic HP-LEDs Operated at 1,000 mA and 100°C 4-15
4A-8. L70 (Left) and L90 (Right) Survivorship Curves and 95% CI Levels for a Randomly Selected Population of Generic HP-LEDs 4-16
4A-9. Kaplan-Meier L70 Survivorship Curves for a Random Sample of MP-LEDs Assuming the Generic Model in Table 4A-2 4-17
4A-10. Comparison of the L70 Survivorship with Different Assumptions of the Level of Conservatism Incorporated Into the α Value 4-17
4A-11. (Left) L70 Kaplan-Meier Survivorship Curve for a Random Population of Industry Average COB-LEDs. (Right) Comparison of the L70 Survivorship Curves for Random Populations of Industry Average, Conservatively Derated, and Very Conservatively Derated COB-LEDs 4-18
4A-12. Examples of Equation (4A.14) Solved for $k_2 = 100k_1$ (i.e., $k_2 >> k_1$) and $k_1 = 5k_2$ (i.e., $k_1 > k_2$) 4-21
4A-13. Derivatives of the Functions Shown in 4A-12 4-21
4A-14. Time Dependent Change in the Transmittance Spectra of Polycarbonate Observed During 7575 4-24
4A-15. Time Dependence of the Change in Lens Transmittance at Wavelengths of 450 nm and 750 nm for a Polycarbonate Lens Material for 7575 Exposure 4-26

4A-16. Graph of the Slopes ($d\%T_\lambda/dt$) for Select Wavelengths in 7575 4-26
4A-17. Fitting Coefficients for Polycarbonate Lenses as a Function of Wavelength for Exposure to 7575 4-27
4A-18. Representative Example of the Change in $\Delta u'v'$ of an LED Showing the Three Major Stages of Chromaticity Shift During LED Lifetime 4-31
4A-19. Data and Chromaticity Model Fits for a MP-LED Product Under Low Stress Condition (Left) and High Stress Condition (Right). 4-33
4A-20. Projected Time to 3-Step (Orange Diamonds) and 7-Step (Blue Circles) Chromaticity Shifts for HP-LEDs 4-36
4A-21. Projected Time for 7-Step Chromaticity Shift for MP-LEDs 4-37
4A-22. Weibull Probability Plot for the Luminaires Subjected to the Hammer Test [37] 4-43
4B-1. Breakout by LED Package Type of the LM-80 Reports That Have Been Collected From Major Manufacturers 4-46
4B-2. Graph of the Decay Rate Constants (α) Calculated Using TM-21-11 for the 250+ Datasets Collected by RTI 4-47
4B-3. Decay Rate Constant, α, Scatter Plot as a Function of Junction Temperature and Forward Current for the LEDs Examined in this Study 4-48
4B-4. Graph of the Decay Rate Constants (α) Calculated Using TM-21-11 on Manufacturers' LM-80 Data for the MP-LEDs, Broken out by Housing Material ... 4-50
4B-5. CSM Distribution of the Available LM-80 Data Sorted by LED Package Type 4-51
4B-6. Models of the Chromaticity Changes of a Typical MP-LED Under Lower-Stress (Top Graph) and Higher-Stress (Bottom Graph) Conditions 4-52
4B-7. Image of the Mounting Configuration Used for Testing Individual LEDs 4-55
4B-8. Schematic Cross-Section of the Package Design for the XR-C HP-LED Along with Potential Sites Where Failure Can Occur 4-56
4B-9. SPDs of Warm White XR-C Samples Subjected to Test Condition 1 for Varying Times 4-58
4B-10. SPD of Warm White XR-C Samples Subjected to Test Condition 2 for Varying Times 4-58
4B-11. I-V Curve of Warm White XR-C Samples Taken at Different Times During Exposure to Test Condition 1 4-59
4B-12. I-V Curve of a Warm White XR-C Sample Taken at Different Times During Exposure to Test Condition 2 4-60
4B-13. Absolute Radiant Flux Measurements of Product XR-C at Different Times in 8585 Testing 4-61
4B-14. Change in Average Chromaticity Coordinates ($\Delta u'$ and $\Delta v'$) for the Population of five XR-C HP-LEDs Operated at 350 mA in 8585 4-61
4B-15. SEM Images of a Pristine Sample of the XR-C HP-LED and an Analogous XR-C Sample After 5,708 Hours of Exposure to 8585 4-62
4B-16. Total Chromaticity Shift Data ($\Delta u'v'$) for XR-C HP-LED Exposed to 8585 for 5,708 Hours (Blue Squares) and Future Chromaticity Projection Using a Bound Exponential Model 4-63
4B-17. I-V Curve at Different Exposure Times for a XR-C Sample Subject to 8585 Conditions 4-64

4B-18. Schematic Cross-Section of the Package Design for the Product G HP-LED 4-65
4B-19. Picture of the Phosphor-Silicone Layer from Product G After 8,000 Hours of Testing at 125°C and 1,000 mA. 4-66
4B-20. Average Luminous Flux Maintenance for the Test Samples of Product G LEDs in WHTOL Tests 4-67
4B-21. SPD Measurements for the Warm White Version of Product G in 7575 (Top) and 8585 (Bottom) as a Function of Exposure to the WHTOL Environment 4-69
4B-22. SPD Measurements for the Cool White Version of Product G in 7575 (Top) and 8585 (Bottom) as a Function of Exposure to the WHTOL Environment 4-70
4B-23. Chromaticity Shift for Warm White (Top) and Cool White (Bottom) Versions of Product G HP-LEDs 4-72
4B-24. Charges in CCT Values for XP-G Product During WHTOL Testing 4-73
4B-25. Cross-Section SEM Image of the Interface Between the Die and the Silicone-Phosphor Layer for a Control Sample of Product G (Left) and a Sample Subjected to 5,352 Hours of 8585 (Right) 4-74
4B-26. Schematic Cutaway of the General Package Structure of HP-LED Devices, Such as Product LR, That Use the Phosphor Plate Structure 4-75
4B-27. Average Luminous Flux Maintenance for the Test Samples of Product LR Devices 4-76
4B-28. SPD Measurements for Warm White Version of Product LR in 7575 (Top) and 8585 (Bottom) as a Function of Exposure to the WHTOL Environment 4-78
4B-29. SPD Measurements for Cool White LEDs in the Product LR Package Exposed to 7575 (Top) and 8585 (Bottom) as a Function of Exposure to the WHTOL Environment 4-79
4B-30. Pictures of Three-Dimensional, Shaped LED Chips Used for Lighting 4-80
4B-31. Picture of the High-Voltage Version of Product T, Which Contained Multiple Small LEDs in the Same Footprint 4-81
4B-32. Picture of the Luminaire Used to Test the High Voltage, Multichip Version of Product T 4-81
4B-33. Chromaticity Shift, as Measured by $\Delta u'v'$, for the High-Voltage Version of LED Product T 4-82
4B-34. Picture of the LED Modules Tested as Part of DOE Project DE-EE0007081 and Included Here for Completeness 4-83
4B-35. Reflectance Spectra of the Solder Mask from an Unexposed Board and Boards Following 8,000 Hours of Exposure of Separate Populations to 75°C and 95°C Elevated Ambient Environments 4-85
4B-36. Chromaticity Shifts Measured for Cool White LEDs from the Tested MP-LED Modules 4-86
4B-37. Chromaticity Shifts Measured for Warm White LEDs from the Tested MP-LED Modules 4-87
4B-38. Chromaticity Shift Models for the Cool White Assemblies in the MP-LED Modules 4-90
4B-39. Chromaticity Shift Models for the Warm White Assemblies in the MP-LED Modules 4-91
4C-1. Plots of Chromaticity Changes, as Measured by $\Delta v'$ Versus $\Delta u'$ for Five PAR38 LED Lamp Products, with Five Samples for Each Product [27] 4-96

4C-2. CSMs Observed in PAR38 Lamps Categorized by the LED Package Types Used in the Lamps [27] 4-97
4C-3. Model of the Chromaticity Shift for Sample 12-97 [27] 4-98
4C-4. CSMs Observed in A19 60-watt Equivalent Lamps Sorted According to LED Package Types (Data from [63]). 4-100
4C-5. Models of Time Dependence of Changes in $\Delta u'$ and $\Delta v'$ for PNNL Sample 13RT-08 4-100
4C-6. Photo of the A19 Lamps Examined in This Study and the Configuration of These Lamps for the Room Temperature Operational Life Test (protocol SSL3) 4-102
4C-7. Comparison of the Luminous Flux Maintenance of A19 Lamps under AST Conditions G1, G2, and G3 4-103
4C-8. Photo of the Configuration of A19 Lamps during the SSL1 and SSL2 Testing Protocols 4-104
4C-9. Luminous Flux Maintenance of A19 Lamp Samples Examined by Auburn University in the Room Temperature Operational Life Test (Protocol SSL3) 4-105
4C-10. Model of the Chromaticity Shift for A19 Lamp Sample ChWW in the Room Temperature Operational Lamp Study Performed by Auburn University, in Which the Lamp Was Operated for 10,000 Hours in Protocol SSL3 Testing 4-106
4C-11. Luminous Flux Maintenance Profiles for the 10 CWW Samples Exposed to SSL1 Testing Protocol 4-108
4C-12. Luminous Flux Maintenance Profiles for the 10 ChWW Samples Exposed to SSL1 Testing Protocol 4-108
4C-13 Luminous Flux Maintenance Profiles for the 10 PWW Samples Exposed to SSL1 Testing Protocol 4-109
4C-14. Luminous Flux Maintenance Profiles for the 10 CCW Samples Exposed to SSL2 Testing Protocol 4-109
4C-15. Luminous Flux Maintenance Profiles for the 10 PCW Samples Exposed to SSL2 Testing Protocol 4-110
4C-16. Luminous Flux Maintenance Profiles for the 10 PSL Samples Exposed to SSL2 Testing Protocol 4-110
4C-17. Weibull Chart Showing the Failure Time of A19 Lamps Subjected to the SSL1 Test Protocol (8585) 4-111
4C-18. Electrical Driver Used in ChWW with Key Components Identified 4-112
4D-1. Picture of the Downlights Used in the RTOL Test After Installation in a Ceiling in a Common Area in RTI Offices 4-114
4D-2. Average Luminous Flux Maintenance for Each Luminaire Product in This Normal Operational Life Test 4-116
4D-3. Luminous Flux Maintenance for Each of the 12 Samples in the Normal Operational Life Test 4-117
4D-4. Picture of the LED Board Used with the Philips Lightolier Calculite Downlight Examined in This Study 4-118
4D-5. Cutaway View Showing the Components of the Philips Lightolier Calculite Luminaire 4-119
4D-6. Luminous Flux of Philips Lightolier Calculite Luminaires 4-120

4D-7. Picture of the Reflector From a Philips Lightolier Calculite 6” Downlight Sample That Exhibited Excessive Lumen Maintenance Loss 4-121
4D-8. Values Over Time for u' and v' of the Three Philips Lightolier Calculite Luminaries in Normal Operational Life Tests 4-122
4D-9. SPD of Lightolier DUT-030 During RTOL Test 4-122
4D-10. The SPDs Over Time Shown in 4D-9 for Calculite Sample #30 Normalized to the Maximum of the Blue Emission Peak at ~450 nm for Each Measurement .. 4-123
4D-11. Picture of the Housing and Driver of the Cree LR6 (left) and the Hybrid Light Engine (right) 4-124
4D-12. SPDs for Cree CR6 Luminaires in the RTOL Tests 4-124
4D-13. Luminous Flux of Cree LR6 Luminaires in Real-Time Life Tests 4-125
4D-14. Values for u' and v' of Cree LR6 Luminaires in RTOL Tests Show Complex Changes Over Time 4-125
4D-15. Flicker Waveform of Cree LR6 DUT-006 4-126
4D-16. Pictures of the LSG Glimpse Luminaire Showing the Back of the Housing and the Potted Driver (left) and the Light Engine (right) 4-127
4D-17. Luminous Flux Over Time of the LSG Glimpse Luminaires in Real-Time Life Tests 4-127
4D-18. Change Over Time for u' and v' for the Two LSG Glimpse Luminaires in Normal Operational Life Tests 4-128
4D-19. Picture of the Sylvania RT-6 Downlight Examined in RTOL Tests, Along With the Driver and LED Boards 4-129
4D-20. Luminous Flux Over Time of the Sylvania RT6 Luminaires in RTOL Tests 4-130
4D-21. Changes With Time for u' and v' for the Two Sylvania RT6 Luminaires in Normal Operational Life Tests 4-130
4D-22. The Spectral Radiant Flux of the Sylvania RT6 luminaire. 4-131
4D-23. Picture of the Cree CR6 Downlight and Driver (left) and Hybrid LED Light Engine (right) 4-132
4D-24. Luminous Flux Over Time of Cree CR6 Luminaires in RTOL testing. 4-133
4D-25. Values for u' and v' Over Time of Three Cree CR6 Luminaires in RTOL Tests Show a Dominance by v' and a Yellow Shift Over Time, Which Can Be Categorized as CSM-3 4-134
4D-26. Temperature, Relative Humidity, and Electrical Bias Profile of Each Loop of the Hammer Test 4-139
4D-27. Failure Times of the Luminaires in the Hammer Test 4-141
4D-28. Weibull Probability Plot for the Luminaires Subjected to the Hammer Test 4-142
4D-29. Distribution of Failure Modes for Luminaires Examined During the Hammer Test 4-143
4D-30. Temperature Change of LED Drivers in Environmental Chamber With the Chamber Controls Turned Off 4-148
4D-31. Example of the DUT Temperature Change During 7575 WHTOL Experiments With the Chamber Controls Fully Engaged 4-149
4D-32. Example of Device Failure During 7575 Experiments 4-150
4D-33. Pictures of Lithonia Security Lamp 4-151

4D-34. $\Delta u'$ and $\Delta v'$ Data and Chromaticity Shift Models for Lithonia Security Lamp in 8585 4-152
4D-35. $\Delta u'$ and $\Delta v'$ Data and Chromaticity Shift Models for Lithonia Security Lamp in 7575 4-153
4D-36. Picture of Cree Essentia Luminaire Subjected to 8585 Testing by RTI 4-154
4D-37. Models of the Shift in $\Delta u'$ and $\Delta u\ v'$ for the Cree Essentia Downlight in 8585 . 4-155
4D-38. Radiant Flux Spectra Measured for the Same Cree Essentia Luminaires in 8585 Testing at Different Exposure Times 4-156
4D-39. Pictures of the Light Engines Used in the OptiLED 6" Downlight—Neutral White (Left) and Warm White (Right) 4-157
4D-40. Chromaticity Shift Data and Associated Models for Total Chromaticity Shifts for Warm White OptiLED Round150 Luminaire (left) and Neutral White Luminaire (right) 4-158
4D-41. Chromaticity Shift Data ($\Delta u'$ and $\Delta v'$) and Associated Models for the Warm White Version of the OptiLED Round150 Product 4-159
4D-42. Chromaticity Shift Data ($\Delta u'$ and $\Delta v'$) and Associated Models for the Neutral White Version of the OptiLED Round150 Product 4-159
4D-43. Total Chromaticity Shift Data and Associated Models for Chromaticity Shifts for Warm White OptiLED Round150 Luminaire (left) and Neutral White Luminaire (right) 4-160
4D-44. Picture of the LSG Glimpse Indirect Luminaire (left) and Its LED Board (right) 4-161
4D-45. Average Chromaticity Shift ($\Delta u'v'$) of the LSG Glimpse Indirect Lamps During 7575 4-162
4D-46. Average Change in $\Delta u'$ and $\Delta v'$ for the LSG Glimpse Indirect Luminaire During 7575 4-163
4D-47. SPD of DUT-B Equipped With Warm White MP-LEDs as Initially Recorded and After 4,000 and 7,000 Hours of Exposure to 7575 4-164
4D-48. SPD Normalized to the Phosphor Emission Maximum for Both the Initial Measurement of DUT-B and After 4,000 and 7,000 Hours of Exposure to 7575 4-164
4D-49. Picture of the Commercial Electric T-65 6" Luminaire With the Front Lens Removed 4-165
4D-50. Comparison of the Chromaticity Change, as Measured by $\Delta u'v'$, for the Commercial Electric T-65 Luminaire in Various WHTOL Tests 4-166
4D-51. Data and Associated Models for $\Delta u'$ and $\Delta v'$ of a Population of Commercial Electric T-65 6" Downlights Exposed to the 7575 Environment 4-167
4D-52. Data and Associated Models for $\Delta u'$ and $\Delta v'$ of a Population of Commercial Electric T-65 6" Downlights Exposed to the 6590 Environment 4-168
4D-53. Picture of the Acuity Chalina OLED Luminaire (left) and an Individual OLED Panel With Light Diffuser Film Applied to the Top Surface (right) 4-169
4D-54. Picture of Two Acuity Chalina OLED Luminaires in Elevated Ambient Temperature Bake Test of 45°C 4-170
4D-55. Power Consumption of the Control Luminaire and Four DUTs (#224, #225, #226, and #227) Subjected to Elevated Ambient Conditions of 45°C for Extended Periods of Time 4-171

4D-56. Luminous Flux Maintenance of Commercial OLED Products in an Elevated Ambient Environment of 45°C 4-173
4D-57. Graph of $\Delta u'v'$ vs. $\Delta u'$ for OLED Luminaires Subjected to Elevated Ambient Conditions of 45°C 4-174
4D-58. SPD Measurements for DUT 226 at Different Stages of Elevated Ambient Exposure at 45°C 4-174
4D-59. Locations of Catastrophic Failure in SSL Luminaires 4-176
4D-60. Generalized Schematic of the Electrical Circuits Commonly Used in SMPS Drivers for SSL Devices 4-178
4D-61. Simple Drivers Used in SSL Lamps 4-180
4D-62. Drivers Used in More Complex SSL Devices, Such as Downlights 4-181
4D-63. Multi-stage and Multi-channel Drivers Used with TWL Luminaires 4-181
4D-64. Comparison of the Characteristic I-V Curves from Two MOSFETs from Equivalent Downlights 4-183
4D-65. Failed MOSFET from a 6" Downlight 4-184
4D-66. SAM Images of MOSFETs from Equivalent Luminaires Subjected to 7575 4-184
4D-67. One-side of a Driver Board for a 6" LED Downlight with the Parts Labeled 4-185
4D-68. Typical Structure of an Electrolytic Capacitor after Disassembly 4-186
4D-69. Driver for 6” Downlight that Exhibited Multi-component Failure 4-187
4D-70. Side View of a Failed Film Capacitor from LED Drivers 4-188
4D-71. Top View of a Failed Film Capacitor Showing the Schoop Metallization and the Winding 4-188
4D-72. Failed Resistors from WHTOL Testing on 6" Downlights 4-189
4D-73. The Most Common Single-stage Driver Topologies Found in SMPS Devices Used in LED Drivers 4-191
4D-74. Driver Structure for Multi-channel Drivers Such as Those Used in TWL Luminaires 4-193
4D-75. Two-stage Driver with a Flyback Typology in Stage 1 and a Buck Typology in Stage 2. 4-193
4D-76. PCB of the LED Driver Product Used in this Study and the Associated Electrolytic Capacitors and their Location on the PCB 4-199
4D-77. Test Setup Used in this Study 4-200
4D-78. Comparison of the Temperature Profile of Three Drivers during 7575 4-204
4D-79. Interior of Environmental Chamber Used to Simultaneously Expose both LEDs and Drivers in a Luminaire to AST Environments 4-206
4D-80. Process Flow for Determining Failure Mechanisms of Luminaires Examined in this Study 4-207
4D-81. Component Failure Distribution for 6" Downlights in 7575 Testing 4-208
4D-82. Weibull Probability Plot Based on Temperature and Humidity Parameterization for 6" Downlights in WHTOL 4-210
4D-83. Weibull Probability Plot for 6" Downlights Using Temperature as the only Parameter 4-211
4D-84. Average Power Consumption of Select Luminaires as a Function of Time in 7575 4-212

4D-85. Comparison of Data for Average Power Consumption and Appropriate Model for Two Luminaires Tested in this Study 4-213
4D-86. MOSFET Switching Waveform for Lithonia Security Lamp Samples Unexposed (left) and after 6,000 Hours of 7575 Exposure (right) 4-215
4D-87. Picture of the Top of the CR6 Driver PCB with Key Component Labeled..... 4-216
4D-88. Block Circuit Diagram of a Buck Driver Used in a 6" Downlight 4-217
4D-89. MOSFET Switching Waveforms for CR6 Luminaires..... 4-218
4D-90. Top View of the Driver PCB for the Commercial Electric T-65 Downlight..... 4-220
4D-91. Comparison of the MOSFET Switching Waveforms for the Commercial Electric T-65 Downlight 4-220

TABLES

Number		Page
3-1.	Project Milestones	3-3
4A-1.	Types of Reliability and Degradation Models Developed in This Work	4-2
4A-2.	Parameter Estimates for the Four Main LED Package Architectures Examined in This Study	4-5
4A-3.	Typical Models Used to Describe the Kinetics Occurring in Materials Used in LED Lighting Devices	4-23
4A-4.	Common Materials Found in SSL Luminaires, Lamps, and LED Modules	4-27
4A-5.	Chemical Reactions Responsible for Chromaticity Shifts in LEDS	4-29
4A-6.	Chemical Reactions Responsible for Chromaticity Shifts in LEDs	4-30
4A-7.	Models and Fitting Parameters Used in Least Squares Optimization of the Data Shown in Figure 4A-19	4-34
4A-8.	*k* Values for the HP-LED Shown in Figure 4A-12 for All Measured Values of Temperature and Current	4-35
4A-9.	Optical Ray Tracing Simulation Inputs, Outputs, and Comparison to a Model for a Virtual 2 × 4 Troffer With a 3-Inch Deep Optical Mixing Cavity	4-39
4A-10.	Values of the Exponents *l* and *r* for Different Luminaire Designs	4-40
4B-1.	Time to Reach Certain Levels of Lumen Maintenance for Assumed α Values	4-49
4B-2.	Logistic Fit Parameters for Chromaticity Shift Models of a MP-LED Product Using Available LM-80-08 Data	4-53
4B-3.	Individual HP-LEDs Subjected to Accelerated Stress Testing During This Project	4-54
4B-4.	Experimental Protocols Used During WHTOL Testing	4-55
4B-5.	Rates of Exponential Decay for WHTOL Test of XP-G LEDs Compared with Temperature Alone	4-68
4B-6.	Logistic Fit Parameters for CCT Values of LEDs in WHTOL Testing	4-74
4B-7.	Rates of Exponential Decay for WHTOL Test of Product LR LEDs Compared with Temperature Alone	4-77
4B-8.	α Values Calculated with the Energy Star® TM-21-11 Calculator for the MP-LED Modules Under Different Ambient Temperatures and Forward Currents	4-84
4C-1.	Breakout of the LED Package Types Found in the 32 Different LED PAR38 Lamps Examined in CALiPER 20.5 [27]	4-95
4C-2.	Primary CSMs Observed in PAR38 Samples [27; 66]	4-95
4C-3.	Physical, Electrical, and Photometric Characteristics of the A19 60-watt Equivalent Lamps Studied by Auburn University during This Work	4-101
4C-4.	AST Protocols Used by Auburn University for Initial Testing of A19 Lamps	4-103
4C-5.	AST Protocols Used by Auburn University for Extended Testing of A19 Lamps	4-104

4C-6. Chromaticity Properties of Individual A19 Lamps in the Room Temperature Operational Life Test[a] 4-105
4C-7. Decay Rate Constant of A19 Lamps in Room Temperature Operational Life Test (Protocol SSL3) 4-107
4D-1. Specifications for the 6” Downlight Luminaire Models Used in RTI’s RTOL Test 4-115
4D-2. Summary of the Standards for Thermal and Biased Humidity Test Procedures Used in This Work 4-137
4D-3. Remaining Luminaires Examined in the Hammer Test [37] 4-138
4D-4. Photometric, Electrical, and Physical Properties of Luminaires Examined in this Study 4-147
4D-5. Parameters for the Chromaticity Shift Models of Lithonia Security Lamp in 8585 and 7575 4-153
4D-6. Coefficients for the Generalized Logistic Models of the Chromaticity Coordinates of the LSG Glimpse Indirect Luminaire 4-162
4D-7. Least-Squares Fit Coefficients of Bounded Exponential Models From the Chromaticity Shift of the Commercial Electric T-65 Population 4-168
4D-8. Average Impedance of Individual OLED Panels From the Control Luminaires, Fully Operational Panels from 45°C Tests, and Failed Panels from 45°C Tests. 4-172
4D-9. Common Topologies Found in LED Drivers 4-190
4D-10. Summary of Common AST Methods Used 4-196
4D-11. Change in Capacitor Properties during 2,280 Hours of 135°C HTSL Testing 4-201
4D-12. Change in Capacitor Properties during 5,352 Hours of 8585 WHTSL Testing ... 4-202
4D-13. Properties of the Multi-stage Drivers Examined by RTI in a WHTOL Environment of 757 4-202
4D-14. Change in Electrical and Photometric Properties for Two-stage, One-channel Drivers 4-203
4D-15. Change in Electrical and Photometric Properties for Multi-stage, Four-channel Drivers 4-203
4D-16. Electrical Properties of LED Drivers and Controls after Operational Testing in 7575 4-213
4D-17. Comparison of the Properties of Key Components in the CR6 Luminaire 4-219

List of Acronyms

AC	Alternating current
ALT	Accelerated life test
AST	Accelerated stress test
CCT	Correlated color temperature
CI	Confidence interval
COB-LED	Chip-on-board LED
CSP	Chip-scale package
DC	Direct current
DLM	Downlight module
DMM	Digital multimeter
DOE	U.S. Department of Energy
DUT	Device under test
EMC	Epoxy molding compound
EMI	Electromagnetic interference
EPRI	Electric Power Research Institute
ESR	Equivalent series resistance
FIT	Failure in time
HAST	Highly accelerated stress test
HP-LED	High-power LED
HTOL	High-temperature operational life
HTSL	High-temperature storage life
IC	Integrated circuit
IES	Illuminating Engineering Society of North America
I_D	Current at the MOSFET drain
I_f	Forward current
I-V	Current - Voltage
LED	Lighting emitting diode
LSG	Lighting Science Group
LSRC	LED Systems Reliability Consortium
LM-DST	Lumen maintenance decision support tool
MOSFET	Metal-oxide-semiconductor field-effect transistor
MP-LED	Mid-power LED
NEMA	National Electrical Manufacturers Association
NIST	National Institute of Standards and Technology
NGLIA	Next-Generation Lighting Industry Alliance
PC	Polycarbonate
pcLED	Phosphor-converted LED
PCT	Polycyclohexylenedimethylene
PDF	Probability density function
PFC	Power factor correction
PLCC	Plastic leaded chip carrer
PMMA	Polymethyl methacrylate
PPA	Polyphthalamide
RH	Relative humidity
RTI	Trade name of the Research Triangle Institute
RTOL	Room temperature operational life
RUL	Remaining useful life
SAM	Scanning acoustical microscopy
SEM	Scanning electron microscope
SMC	Silicone molding compound

SMPS	Switched-mode power supply
SMT	Surface-mount technology
SPD	Spectral power distribution
SSE	Sum of the squared errors
SSL	Solid-state lighting
SSL1	8585 test protocol for lamps
SSL2	5565 test protocol for lamps
SSL3	RTOL test protocol
SSR	Sum of the squared residuals
SSTHS	Steady-state temperature and humidity soak
THD	Total harmonic distortion
TiO_2	Titanium dioxide
T_j	Junction temperature
TWL	Tunable white light
V_{DD}	Voltage at the MOSFET drain
V_{GS}	Voltage between the MOSFET gate and source
WHTOL	Wet high-temperature operational life
WHTSL	Wet high-temperature storage life

1. ACKNOWLEDGEMENTS

Many RTI team members contributed to this work and made the project so successful.

- J. Lynn Davis, PhD
- Karmann Mills
- Cortina Johnson
- Robert Yaga
- Georgiy Bobashev, PhD
- Nick Baldasaro
- Michelle Conner
- Sarah Shepherd
- Mike Lamvik, PhD
- Eric Solano
- Curtis Perkins
- Mike Levine
- James Bittle
- Kimberly Guzan
- Karen Hall
- Cathy Sabodish
- Joe Young (intern)
- William Pridgen (intern)
- Curtis Perkins (intern)

RTI would like to also gratefully acknowledge the partners and external contributors for this project. More details on their specific contributions are listed in Appendix D.

- **Auburn University**, Auburn, Alabama. Especially Dr. Pradeep Lall, Dr. Peter Sakaluakus, and Dr. Hao Zhang.
- **Cree**, Sturtevant, Wisconsin and Research Triangle Park, North Carolina, especially Ralph Tuttle and Eric Haugaard.
- Agencies within the **state government of North Carolina** including the State Construction Office, Department of Environmental Quality, Department of Public Instruction, Department of Public Safety, North Carolina State University, and University of North Carolina at Chapel Hill.
- **SAS Institute**, Cary, North Carolina

Other Significant Collaborators:

- LED Systems Reliability Consortium, led by Morgan Pattison and Fred Welsh
- Dr. Willem van Driel, Philips Inc.—participated in discussions on analyzing the ALT data.
- Dr. Monica Hansen—consultation on LED performance, leading efforts to acquire LM-80 data from manufacturers, and industry practices
- Dr. Troy Trottier—consultation on LED phosphors, encapsulants, and projection of chromaticity shifts
- Praneet Athalye, Ph.D., LC, of Buck Boost LLC—consultation on LED drivers and electrical failure analysis
- Marc Chason of Marc Chason and Associates, Inc.—advisory board member
- Jennifer Einberg of Iota Ink, LLC—contributions to DST programming
- LTIOptics—performing Photopia simulations on virtual luminaires
- C&C Technologies—use of environmental test chambers

2. EXECUTIVE SUMMARY

Solid-state lighting (SSL) technologies have made significant market gains over the past decade, but still account for less than 10% of the total sockets in the United States. SSL technologies continue to deliver higher levels of performance and to provide new capabilities to meet the rising market demand; however, the one universal axiom that has been present from the outset is that SSL products must meet or exceed customer expectations, including reliability. Bob Talley, of the State Construction Office of North Carolina, eloquently made this point at the Department of Energy (DOE) SSL Research and Development Workshop in 2016 when he told of his less than satisfying experiences with SSL technologies, including excessive color shifts, high driver failure rates, and control system compatibility. Although SSL technologies have made significant gains in the market, reliability clearly remains a potential impediment to future growth and has been identified by DOE as one of the primary barriers to the adoption of SSL technologies.

All products will fail over time, but some number of a population of products will fail quickly while others will take longer to fail. The failure rate of a population of a product can be described with a hazard function, such as the Bathtub Curve shown in **Figure 2-1**. In this approach to product reliability, some of the population contain latent defects and will fail quickly during the short burn-in stage when a device is first turned on. Fortunately, these early failures are sorted out quickly and the remaining population enters a region of normal operation that is typically characterized by a long time with a constant failure rate. As the usage time for the population grows, parts begin to wear-out and the failure rate increases. SSL devices can fail in three main ways: loss of luminous flux with time, excessive chromaticity shift with time, and abrupt or catastrophic failure. Understanding the influence of each lighting system component on these failure pathways is critical to maintaining the growth rate enjoyed by SSL technology.

Figure 2-1. Product Hazard Function as Represented by the Bathtub Curve

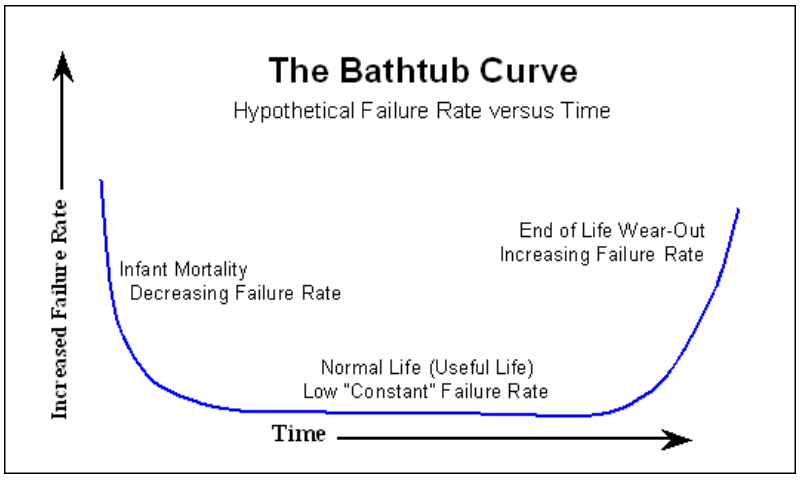

Building models of the reliability of SSL lamps, luminaires, and devices is a complex endeavor requiring a multi-physics approach. A lighting system consists of many components including light-emitting diodes (LEDs), lenses, reflectors, printed circuit boards (PCBs), driver electronics, and heat sinks, and many of these system components are comprised of sub-assemblies. During operation, parts of an SSL lighting system must endure extreme stress such as high temperatures (perhaps greater than 150°C), low temperatures (perhaps below -20°C), high levels of actinic radiation, electric transients and surges, and environmental stresses such as moisture and chemicals. SSL devices are expected to withstand this gauntlet of environmental stress and operate reliably from 10,000 hours (for disposable lamps) to more than 50,000 hours (for infrastructure lighting in schools). Achieving this level of performance requires a knowledge of the primary failure mechanisms in SSL devices and models to help predict their remaining useful life.

A three-pronged approach was used in this project to gather data on SSL device failures, build models based on that data, and validate the models in the real world. As shown in **Figure 2-2**, multiple sources were used to acquire information about SSL device failures (i.e., loss of luminous flux, excessive chromaticity shift, and abrupt or catastrophic "lights out" failures). These data sources included the scientific and technical literature, publicly available data sets [from sources such as Pacific Northwest National Laboratory (PNNL)], and data acquired through accelerated stress testing (AST) in the laboratories of RTI International and our partner Auburn University.

Figure 2-2. Three-Pronged Approach to Building a Knowledge Base of SSL Device Failure

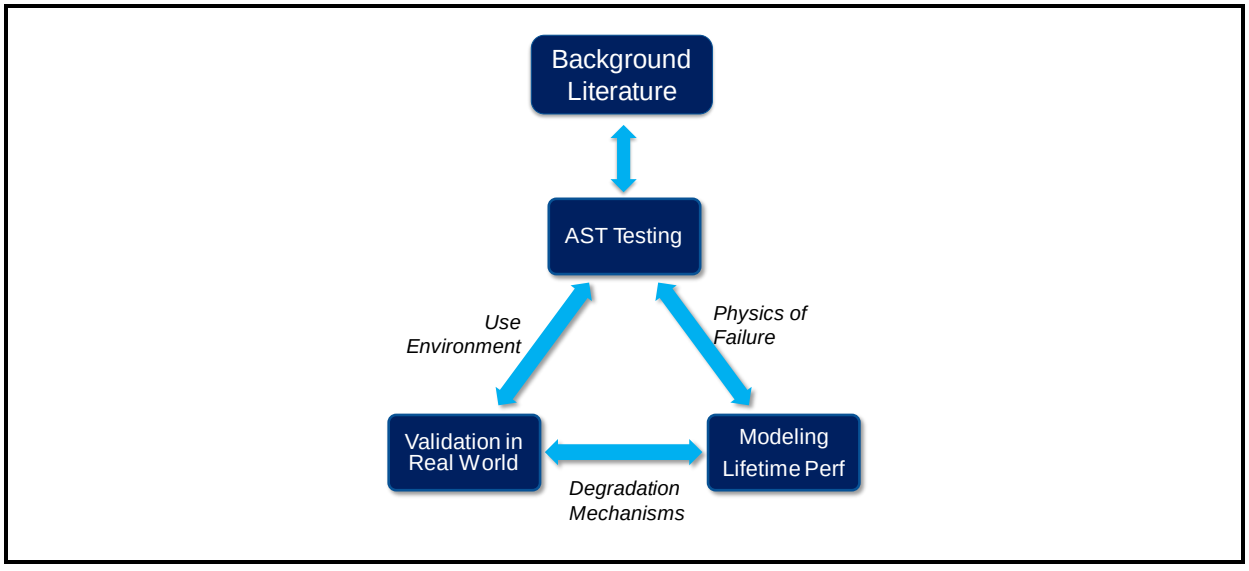

From the beginning, this project was designed around the concept that models for the reliability of SSL luminaires can be built from data on accelerated aging studies on 6"

downlights and key system components, such as LEDs and lenses. By analogy to the field of genetics, where fruit flies are widely used in studies because they share 75% of the genes that cause human diseases, 6" downlights are the "fruit flies" of the lighting industry because

- LED downlights are widely used in most lighting markets around the world and accounted for more revenue in 2014 than any one single luminaire type;
- downlights incorporate a wide range of LED technologies including high-powered LEDs (HP-LEDs), mid-power LEDs (MP-LEDs), chip-on-board LEDs (COB-LEDs), remote phosphor devices, and hybrid LEDs;
- a wide variety of design features are available with downlights, including various sizes of optical mixing cavities and indirect lighting;
- materials used in downlights are similar to those used in other luminaire designs;
- downlights can use either integrated or stand-alone drivers;
- downlight products are regularly refreshed by lighting manufacturers and product developments closely track those occurring in LEDs; and
- downlights are small, inexpensive and in most instances can be purchased for under $30 per sample;

Consequently, the bulk of this project was spent studying the behavior of 6" downlights under accelerating stress conditions, and this report summarizes the major findings from this work. The findings for downlights are believed to be applicable for nearly every luminaire design, if proper consideration is given to the impact of device design on luminous flux and chromaticity maintenance.

The initial foray for this project into gathering data to understand the reliability of SSL devices was a highly accelerated stress test (HAST), also called a Hammer Test, that was applied to 6" downlights. RTI developed the Hammer Test in cooperation with the LED Systems Reliability Consortium, and this testing protocol used aggressive stress tests such as elevated temperature, biased humidity, and temperature shocks to push the downlights to the maximum. Several major insights resulted from this study, including that SSL technologies are incredibly robust and can withstand extreme environmental stresses and continue to operate properly. A second finding was that the LEDs themselves were incredibly robust and only 2 LED failures were observed in more than one million operational hours. This work was summarized in a report on the DOE website that has been downloaded more than 700 times, demonstrating the significant value that this work is providing to the industry.

In addition to experimental findings, RTI's status as a not-for-profit research institute allowed us to forge agreements with leading LED manufacturers and gain access to their LM-80-08 data of LED performance. We were able to collect more than 250 different data sets from leading manufacturers, covering all LED package types. This information was

combined with experimental data on lenses and reflectors to create RTI's lumen maintenance decision support tool (LM-DST). The goal of this tool is to allow manufacturers and lighting professionals to look at different luminaire designs and model the expected change in lumen maintenance of the design with aging, given the initial decisions that were made as part of the luminaire design stage. Incorporated into the LM-DST, is the relative impact of lens and reflector aging on total luminaire efficiency. These aging models were created through an innovative and cost-effective approach in which experimental data on luminaire materials was combined with commercial ray-tracing software to create virtual luminaires. The properties of the luminaire materials were then systematically degraded, based on experimental findings, and the impact of these changes were modeled with the ray-tracing software. Through this approach, RTI developed accurate models of the impact of the degradation of luminaire materials (e.g., LEDs, lenses, reflectors) on luminaire efficiency for multiple luminaire designs. This approach greatly improved the accuracy and breadth of the models in the LM-DST, all with minimal costs.

Failure of a conventional light source is typically easy to define. When the device stops producing light, a catastrophic or "lights-out" failure has occurred. This process typically takes 5,000 to 10,000 hours to occur. One year of operation for 12 hours per day equates to nearly 4,400 hours of operation per year. In most cases, the lighting device can be made operational in a short period by replacing a ballast or lamp; consequently, other failure modes, such as excessive chromaticity shift or loss of luminous flux are often ignored, even though they are occurring, because the lamp will be replaced soon.

However, for SSL devices failure is often not as well defined. First, SSL luminaires and lighting installations are often expected to operate for much longer than conventional lighting technologies, which places greater emphasis on parametric properties, such as luminous flux and chromaticity maintenance. Since LEDs lose luminous flux and typically change colors slowly over long periods of time, it may not be obvious to the observer when a parametric failure has occurred. In addition, over such extended time periods, luminaire components, such as lenses, housings, and reflectors may be more responsible for parametric shifts than the LEDs themselves. A second factor is that the expected long lifetime of SSL devices places increased reliability demands on LED drivers and control electronics used in this lighting system. These electronics are expected to perform flawlessly for time periods longer than traditional ballast and to maintain adequate lighting levels without introducing flicker, affecting other electronics through electromagnetic interference (EMI) emissions, or introducing harmonic distortions onto the branch circuit.

In this project, the RTI team systematically investigated each potential failure pathway. Leveraging our relationships with the leading LED manufacturers, we demonstrated a relationship between LED package types and luminous flux maintenance across a broad slice of the industry, as shown in **Figure 2-3**. This data allowed us to create general models of LED behavior covering average performance for a given package type. This work also allows

an investigation of the phenomena that the efficiency of some LED products initially improves and then begins to decrease in an exponential decay fashion. The models that we built for the efficiency improvement are based on bounded exponential functions and represent the first attempts in the industry to capture this behavior.

Figure 2-3. Luminous Flux Decay Rate Constants (α) for LEDs by Package Type

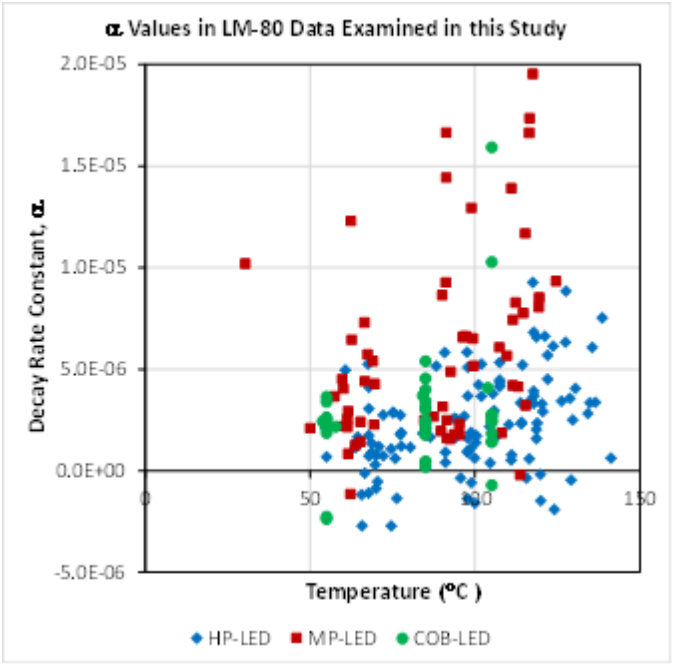

At the beginning of this project, chromaticity shift in LED devices was thought to be too random and too unpredictable to be included into a reliability assessment. However, RTI took on this task and demonstrated that chromaticity shift proceeds in an orderly and predictable fashion. To achieve this level of understanding, one of the industry's first detailed studies into the nature of chromaticity shift in LEDs was performed by combining the luminous flux information from LM-80-08 reports, experimental data from our accelerated testing, and data from sources such as PNNL. The outcome was conclusive proof that chromaticity shift proceeds according to one of five chromaticity shift modes (CSMs) which align with color directions on the 1976 universal color space. In addition, different LED packages were found to favor certain CSMs over others, as shown in **Figure 2-4** for PAR38 lamps.

Figure 2-4. CSMs of PAR38 Lamps Classified by LED Package Type.

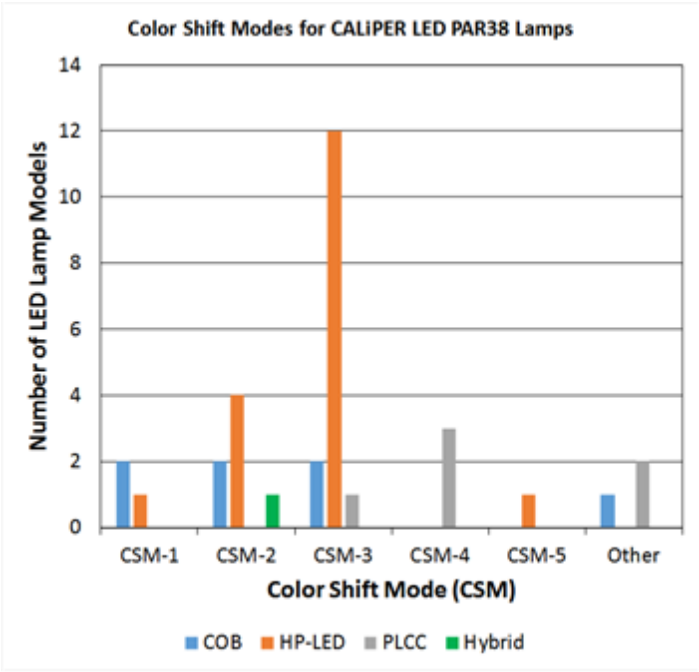

In the next step of this project we assembled the information on chromaticity shift and luminous flux maintenance to create a process for modeling chromaticity shift. While projecting chromaticity shifts is significantly more difficult than projecting luminous flux, the material degradations that occur during SSL device aging produce chemical changes in materials, and these processes can be followed spectroscopically using the light emitted from the luminaire. Through analyzing numerous samples, we determined that the processes responsible for chromaticity shifts in SSL devices can be divided into two broad categories—a fast process that typically occurs only in the first 1,000 to 2,000 hours of operation and a slow process that may take several thousand hours to emerge from the background. These processes can be modeled using a bounded exponential function for the fast process and a generalized logistic function for the slow process. The coefficients of the models can be correlated with environmental conditions and time, which enables not only a projection of chromaticity at a future time but also an estimation of the behavior for conditions that have not been measured yet. An example of these types of models is shown in **Figure 2-5**, where a bounded exponential function is used for the initial chromaticity shift and two sequential logistic functions are used for the subsequent chromaticity shifts.

Figure 2-5. Example of Chromaticity Shift Modeling for SSL Devices

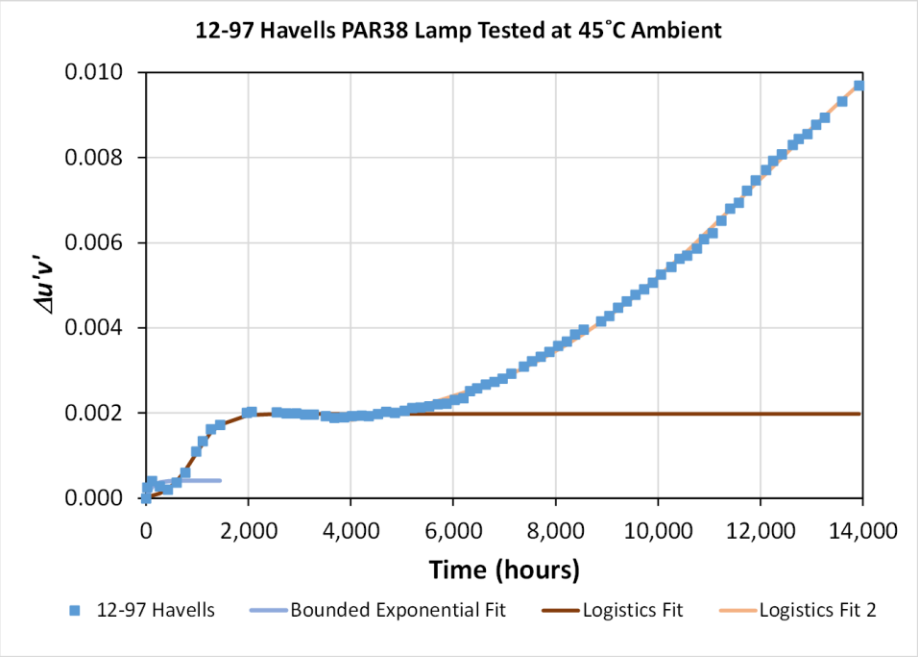

In building these models, the RTI team demonstrated several significant characteristics of chromaticity shifts in SSL devices. These are:

- Chromaticity shifts are predictable and can be modeled with bounded exponential and generalized logistic functions
- Chromaticity shifts have an upper limit and do not proceed indefinitely
- Within common operating conditions, chromaticity shifts follow similar trends although the timing and magnitude of the shifts will differ depending on conditions.

Concurrent with this effect, extensive accelerated stress tests (AST) were conducted on LED driver electronics. Various AST protocols were used in this work including wet high-temperature operating life (WHTOL) tests, high-temperature operating life (HTOL) tests, and high-temperature storage life (HTSL) tests. Early work at Auburn University conclusively demonstrated that the capacitance and equivalent series resistance of electrochemical capacitors can change significantly during use; however, the performance of properly-designed LED drivers using these components remains steady. Other parts of the SSL driver were found to be more susceptible to aging with the switched-mode control and the power factor correction (PFC) circuits being the most sensitive.

The switched-mode control circuit serves as the voltage regulator for the SSL driver and delivers a constant current to the LEDs. At the heart of this circuit is a metal-oxide-semiconductor field-effect transistor (MOSFET) that is controlled by an integrated circuit.

The on/off switching time of the MOSFET determines the current supplied to the LEDs which in turn determines their light output. The MOSFET has been shown to be susceptible to thermal stress that causes failure in the component through electrical shorting. In many of the samples that we tested, this failure mode produced a cascade of failures in other components, including electrochemical capacitors, leaving little external trace of the failure in the MOSFET itself.

The PFC circuit in an SSL driver minimizes the non-linear load characteristics of switched mode power supplies (SMPS) and makes the load appear to be more linear. High power factors (> 0.80) are desirable in SSL devices to minimize the amount of unused power that is reflected back to the grid. The PFC circuit also feeds the switched-mode controller and our experiments demonstrated that degradation of the capacitors in the PFC stage can have a significant effect on the operation of SSL drivers and ultimately the failure of key components.

The findings from AST studies were used to build Weibull models of the reliability of 6" downlights in three different WHTOL environments, 85°C and 85% relative humidity (8585), 75°C and 75% relative humidity (7575), and 65°C and 90% relative humidity (6590). These models are shown in **Figure 2-6** as a Weibull probability plot. These models demonstrate that the WHTOL test is an excellent screening tool for rapid assessment of product reliability in less than 2,000 hours of testing. Higher humidity environments (e.g., 8585 and 6590) produced higher initial failure rates in the first 1,000 hours of testing, which can be attributed to poor designs and latent defects. The long-term trends followed the Weibull models for these test conditions. For 7575 testing, Weibull models were followed closely throughout.

Figure 2-6. Weibull Probability Plot for 6" Downlights in WHTOL

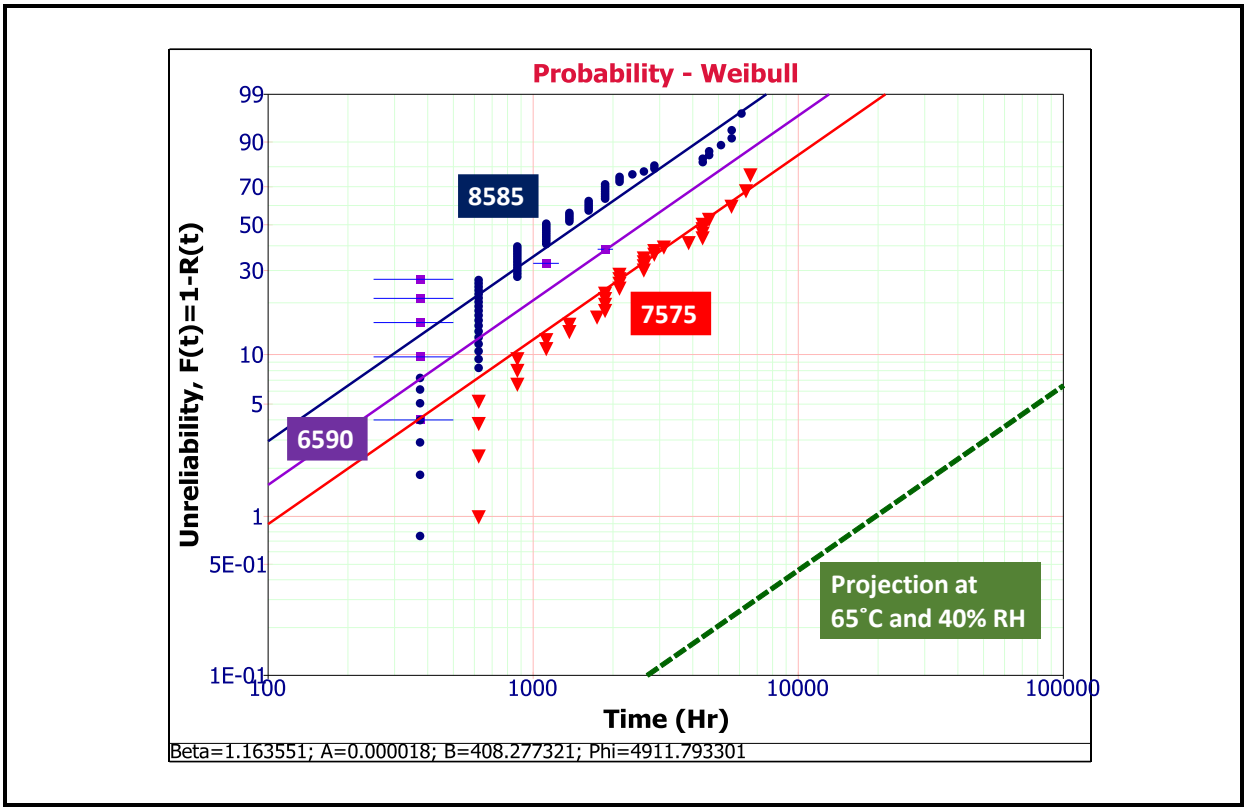

This project also achieved several major milestones which are listed below:

- Combined, the LEDs examined in the study have been tested for more than **25,000,000** hours of exposure, and LED failures have been exceeding rare.
- A decision support tool (DST) was developed to estimate the luminous flux maintenance of SSL luminaires during aging depending upon the choice of LED package, luminaire device, and optical materials used in the design.
- Failure analysis has been performed on more than 400 different SSL devices and the locations of device failure have been pinpointed. This has led to a shift from thinking that electrolytic capacitors are the primary source of failure to looking at other components such as MOSFETs and film capacitors in the PFC circuit as likely sources of failure.
- This project has successfully demonstrated that WHTOL methods can be applied to SSL devices including luminaires and we have demonstrated that poorly designed devices will fail in less than 1,500 hours of WHTOL. Well-designed devices will fail in a random manner during WHTOL testing and this behavior can be modeled with Weibull statistics.
- In collaboration with Pacific Northwest National Laboratory (PNNL), RTI conducted some of the first publicly available accelerated testing of organic light-emitting diodes (OLEDs), an emerging lighting technology. The results identified potential

areas of research to increase the reliability of OLED technologies to be more competitive with inorganic LED light sources.

- A significant part of this project has been the sharing of our results with the domestic lighting industry. To date, we have authored or contributed to 5 major reports that are available on the DOE website. These reports have been downloaded more than 2,300 times from the DOE website. In addition to these reports, we have published a total of 27 papers to date in the technical literature and two PhD dissertations. When added together, this project is producing more than one public outreach event (i.e., presentations or publications) per month.

This summary report on DOE Award Number DE-EE0005124 is divided into sections to cover the major efforts of the endeavor. Section 3 provides a comparison of the actual accomplishments with the original goals and objectives of this project. Section 4 provides a summary of activities for the entire funding period (September 15, 2015 – February 28, 2017). It is divided into four main sections followed by appendices of support information:

- Section 4A provides an overview of the modeling techniques that were developed during this study. These models, which did not exist before this work, cover most aspects of SSL technologies including the failure probability of populations of LEDs, chromaticity shift, luminaire design-dependent factors and their impact on lumen maintenance and chromaticity shift, and Weibull models for electrical driver reliability.

- Section 4B concentrates on the findings for LEDs produced by this work including our analysis of industry data (i.e., LM-80-08 reports), public data from PNNL, and our accelerated testing findings. The results of this section form the basis for chromaticity shift analyses of luminaires discussed later in the report.

- Section 4C provides a summary of AST performed at Auburn University on LED lamps and discusses the findings that were derived from a deeper analysis of lamp data taken under the CALiPER program, in partnership with PNNL.

- Section 4D describes the behavior of SSL luminaires from the perspective of the three principal failure outcomes: luminous flux loss, chromaticity shift, and catastrophic failure. Information covered in this section ranges from room temperature performance of 6” downlights to findings from HAST and AST testing and cover lighting system components from LEDs to drivers.

- Appendix A provides a list of the devices tested in this study, and the tests that were performed on each product.

- Appendix B provides a synopsis of innovative experimental and modeling approaches that were developed during this work. Full details of these methods are provided in the body of the report.

- Appendix C provides a listing of the 30 technical publications produced by this project.

- Appendix D provides a synopsis of some of the collaborations formed during this work.

In summary, understanding the reliability of SSL technologies is critical to the continued market growth of this energy savings technology. Without consumer confidence in the reliability of the technology, market adoption will slow, potential energy savings will be lost, and lighting costs (both from an energy consumption and maintenance perspective) will rise. The importance of SSL technology reliability will become even more significant as SSL technologies transition to additional capabilities such as human-centric white tunable lighting (WTL), light-based communications such as LiFi, horticultural lighting, and other uses of the SSL lighting platform that have not yet been envisioned. This project laid the foundation for the continued growth of a domestic lighting industry by providing models and a greater understanding of the issues affecting the reliability of SSL devices. While this project is ending, the goal of providing highly reliable SSL technologies is just getting started and additional research and analysis will be required as SSL technologies mature and transition into these new growth areas.

3. COMPARISON OF ACTUAL ACCOMPLISHMENTS WITH THE GOALS AND OBJECTIVES

Solid-state lighting (SSL) is an emerging illumination technology that offers the promise of greater energy efficiency and longer product lifetimes. Studies by the U.S. Department of Energy (DOE) have concluded that 18% of all total site electricity consumption in the United States goes to provide general illumination. Further, according to a second DOE report, SSL technologies have the potential to save 261 terawatt-hours (TWh), or about one-third of lighting site electricity consumption, by 2030. That savings in site electricity consumption corresponds to about 4.5 quadrillion British thermal units (quads) of primary energy, which is approximately equal to the forecasted 2030 energy production from "other" renewable sources such as wind and solar. Consequently, SSL technologies have the potential to be a significant contributor to energy supply issues by reducing the demand on energy resources.

Initial SSL products, including lamps and luminaires, are readily available on the market today, but the total market penetration of this emerging technology is still less than 20% in most applications. SSL products with claimed lifetimes of 50,000 hours are becoming readily available. However, this projected lifetime is based solely on lumen maintenance estimations for the LEDs and does not account for the performance of other system components that may not be able to operate that length of time. Methods to provide more realistic estimates of luminaire system lifetimes are need by the lighting industry and key stakeholders such as electric utility companies and taxpayers to increase confidence in the lifetime of SSL products.

To realize the benefits of lower energy consumption and reduced CO_2 emissions, SSL technologies must be rapidly accepted by the marketplace and displace less-efficient light sources such as incandescent lamps. However, based on lessons learned from the initial introduction of the compact fluorescent lamp, purchasers are skeptical of claims made by new lighting technologies. Therefore, rapid and sustainable market penetration of SSL technologies requires that manufacturers deliver products that provide excellent appearance (i.e., pleasing correlated color temperatures [CCT]) and high color-rendering indices (CRI) and deliver on promised energy efficiency and long lifetimes. Failure to achieve these goals could delay the market acceptance of SSL products, rendering the expected benefits of reduced energy consumption and lower CO_2 emissions unrealized.

This creates two conundrums for the lighting manufacturers and key stakeholders: (1) How to ensure the promised product reliability of 15 years for a rapidly changing technology platform, and (2) What will the usage and maintenance profiles be for a product that lasts for 15 years? Both DOE and the lighting industry are attempting to answer these questions in a timely manner. In the 2016 DOE SSL Multi-Year Program Plan (MYPP), both lifetime and testing were identified as significant barriers to successful acceptance of SSL technologies by end users. Regarding the barrier of lifetime, the MYPP states, “These (i.e., SSL) are new

technologies with extreme lifetimes and new failure mechanisms, so the reliability of these products is not well understood." The MYPP also states that "A better understanding of the luminaire system lifetime and reliability is necessary to provide confidence that SSL products will meet stated lifetime claims and achieve a reduced cost of lighting."

Creating an accurate reliability model requires a team that is capable of designing an appropriate experimental matrix for accelerated life test (ALT) studies, analyzing the complex data from manufacturers' data and ALT trials, conducting detailed failure analysis work to ensure that acceleration methodologies are reproducing field mortality results, and building an accurate, predictive model of future reliability from convoluted data sets. Strong expertise in statistical methods and proficiency in common statistical software are mandatory for creating this model in a format that can be widely shared with the SSL industry. **RTI International** (**RTI**) and its associates SAS Institute, Cree, PPG Industries, and Auburn University's–National Science Foundation's Center for Advanced Vehicle and Extreme Environment Electronics (henceforth referred to as the RTI Team), received an award (Award DE-EE0005124) from DOE to build such reliability methods in response to Area of Interest 4: System Reliability Methods of FOA DE-FOA-0000329.

The planned milestone achievements of this project are listed in the table below. The primary objectives of the work proposed by the RTI team were to develop and validate a reliability models and accelerated stress testing (AST) methodologies, which would be targeted to predict the lifetime of integrated SSL luminaires using less than 3000 hours of testing. RTI has accomplished this objective by evaluating luminaire and component performance using standard SSL test methods, including those from the Illumination Engineering Society (IES) and other standards organizations, new methods developed during the project (Appendix B), and data from outside sources, such as LED manufacturers and PNNL. The initial build of the reliability model was based on assumed Arrhenius behavior and was constructed during Phase I of the project. During Phase II, a more accurate multivariable reliability model was developed. This second-generation model was based on measured statistical distributions of experimental and literature values, such as LM-80 data from LED manufacturers. Degradation factors were determined from a statistical analysis of the experimental data, considering the accelerating effects of environmental stressors and their impacts on system reliability. This effort culminated in the development of a Decision Support Tool (DST) which contained models for LEDs (high-power, mid-power, and chip-on-board), lenses (polymethyl methacrylate and polycarbonate), and reflectors (Toray, Furukawa, WhiteOptics, coil coatings, and high reflectance white paint). In addition, the DST includes models for different luminaire geometries to capture the relative contributions of degradation in optical and reflector materials on changes in luminaire efficiency.

In the continuation years of this project (BP4 and 5), the focal points of RTI's research were chromaticity shift and modeling the electrical behavior over time in SSL luminaires. Before

this project began, chromaticity shift was thought to be too complicated for simple modeling. RTI was able to prove otherwise. RTI has provided models and an experimental foundation for thinking about chromaticity shift at both the LED and luminaire levels. These results were presented at several conferences, DOE meetings, and will be published in a book chapter in 2017. The model for electrical parameter changes of SSL luminaires was achieved by identifying the critical driver components influencing lifetime. The myriad of architectures used in LED drivers greatly complicates the effort to build a unified model. RTI was able to use a system health standpoint to identify key components and understand driver reliability

Table 3-1. Project Milestones

	Milestone	Anticipated Completion Date	Actual Completion Date	Status at End of Project
M1	Complete the formulation of the advisory board and hold the first board meeting via teleconference	Dec-11	Dec-11	An advisory board (AB) was selected and utilized in the decision-making process of this project. Regular AB meetings occurred through 2015 and were supplemented with inputs from the LSRC throughout.
M2	Complete the initial accumulation of publicly available data from manufacturers and literature sources	Mar-12	Mar-12	A large body of data was collected from manufacturers, including LM-80 reports, and used in model creation. A database of relevant literature has also been compiled and will be made available upon request.
M3	Complete gap analysis and develop an experimental matrix for ALT studies of SSL luminaire components	Jun-12	Jun-12	Tests created to fill known gaps included the Hammer Test, 8585, and 7575.
STAGE GATE 1	Complete initial Arrenhius-based model of integrated SSL luminaire reliability	Sep-12	Sep-12	These models were completed and built in the LM-DST for SSL luminaire components.
M4	Complete at least two rounds of accelerated life tests	Mar-13	Mar-13	The first tests were completed using RTI's Hammer Test procedure and follow-up tests initially used 8585.

(continued)

Table 3-1. Project Milestones (continued)

	Milestone	Anticipated Completion Date	Actual Completion Date	Status at End of Project
M5	Create an initial iteration of a probabilistic reliability model	Sep-13	Sep-13	The probabilistic reliability model for LEDs was developed using the Kaplan-Meier approach and was built into RTI's Decision Support Tool.
M6	Develop an accelerated test method for measuring lumen depreciation arising from dirt accumulation	Sep-13	Sep-14	The results of this work were presented at the DOE site visit to RTI in August 2014 and a manuscript is being finalized and will be submitted for peer review in 2017.
M7	Complete at least two rounds of ALTs based on an experimental matrix derived from initial model	Jun-13	Jun-13	Over 400 samples of 6" downlights, lamps, LEDs, and troffers have been tested over the course of this project.
STAGE GATE 2	Create a refined probabilistic reliability model	Sep-13	Sep-13	This model was incorporated into the Decision Support Tool and was been updated and refined.
M9	Use the refined probabilistic reliability model to develop a test method for lumen depreciation	Mar-14	Mar-14	Methods developed during this project for lumen depreciation study included 8585, 7575, and 6590.
M10	Analysis of color shift in LM-80 data	Jun-14	Jan-15	This analysis was used to create estimated Color Shift Models are described in CALiPER 20.5.
M11	Remote phosphor color shift factors determined	Sep-14	Sep-14	This analysis was used to developed a manuscript that was published in the 2017 book on SSL device reliability by van Driel, Fan, and Zhang.
M12	ALT studies and failure mode determination completed on at least 150 SSL devices	Dec-15	Dec-15	Over 400 samples of 6" downlights, lamps, LEDs, LED modules, and troffers have been tested over the course of this project.
M13	Paper on common failure modes for SSL luminaires submitted	Mar-16	Mar-16	These results were submitted for publication as a book chapter in March 2016 and final publication should occur in June 2017.

(continued)

Table 3-1. Project Milestones (continued)

	Milestone	Anticipated Completion Date	Actual Completion Date	Status at End of Project
M14	Factors impacting color shift at the LED level determined for major LED types	Mar-16	Mar-16	The initial results of this work were presented at several events in 2015, including LED ART Symposium, and Strategies in Light, in February 2016.
M15	Luminaire level determination of factors impacting color shift	Jun-16	Jun-16	The initial results of this work were presented at several events in 2015, including LED ART Symposium, and Strategies in Light, in February 2016.
M16	Paper on changes in luminous flux and color point for remote phosphor configurations submitted for publication	Jun-16	Mar-16	These results were submitted for publication as a book chapter in March 2016 and final publication should occur in June 2017.
M17	Complete ALT studies and failure mode determination for 250 SSL devices	Sep-16	Sep-16	Over 400 samples of 6" downlights, lamps, LEDs, LED modules, and troffers have been tested over the course of this project.
M18	High-level model providing general trends for luminaire color shift developed	Sep-16	Sep-16	These results were presented at Strategies in Light in 2016 and have been shared with the IES color shift project sub-committee (TM-31) during the spring and summer of 2016.
M19	Paper on electrical parameter changes for integrated SSL luminaires submitted for publication	Dec-16	Oct-16	These results were submitted for publication as a book chapter in March 2016 and final publication should occur in June 2017.
M20	Model for electrical parameter changes of SSL luminaires developed	Feb-17	Feb-17	Weibull models were developed to characterized the behavior of SSL drivers. Models were also developed for power consumption changes and tied to driver morphology.
M21	Present the test methods and reliability model to at least one national standards organization	Sep-16	Sep-16	RTI has worked closely with the IES since 2015 on methods to project chromaticity shifts (TM-31). Several presentations on our findings have been given to this sub-committee including one in Aug. 2016.

(continued)

Table 3-1. Project Milestones (continued)

	Milestone	Anticipated Completion Date	Actual Completion Date	Status at End of Project
M22	Probabilistic reliability model that provides accurate prediction of SSL lifetime based on test times of 3,000 hours	Feb-17	Feb-17	We have demonstrated that WHTOL methods can be used as a screening tool for SSL device reliability with as little as 1,500 hours. These methods have been shown to have predictable failure rates that follow a Weibull model.

4. SUMMARY OF ACTIVITIES FOR ENTIRE FUNDING PERIOD

4.A Models Overview

4.A.1 Background

This project focused on understanding the lifetime and reliability of solid-state lighting (SSL) products, and building this knowledge base required a three-pronged approach consisting of obtaining data on SSL device failures, building models based on that data, and validating the data in the real world. As shown in ***Figure 4A-1***, multiple sources were used to acquire information about SSL device failures, including the scientific and technical literature, publicly available data from sources such as Pacific Northwest National Laboratory (PNNL), and data acquired through accelerated stress testing (AST) in the laboratories of RTI International and our partner Auburn University. Data was acquired on most system components, including the light-emitting diodes (LEDs), lenses, reflectors, drivers, electrical components, that comprise SSL systems. In some instances, we found the available data were out of date and not representative of the typical use conditions of SSL devices. For example, handbook methods for calculating failure rates often rely on failure-in-time (FIT) data from the 1990s, which does not reflect modern advances in electronics reliability.

Figure 4A-1. Three-Pronged Approach to Building a Knowledge Base of SSL Device Failure

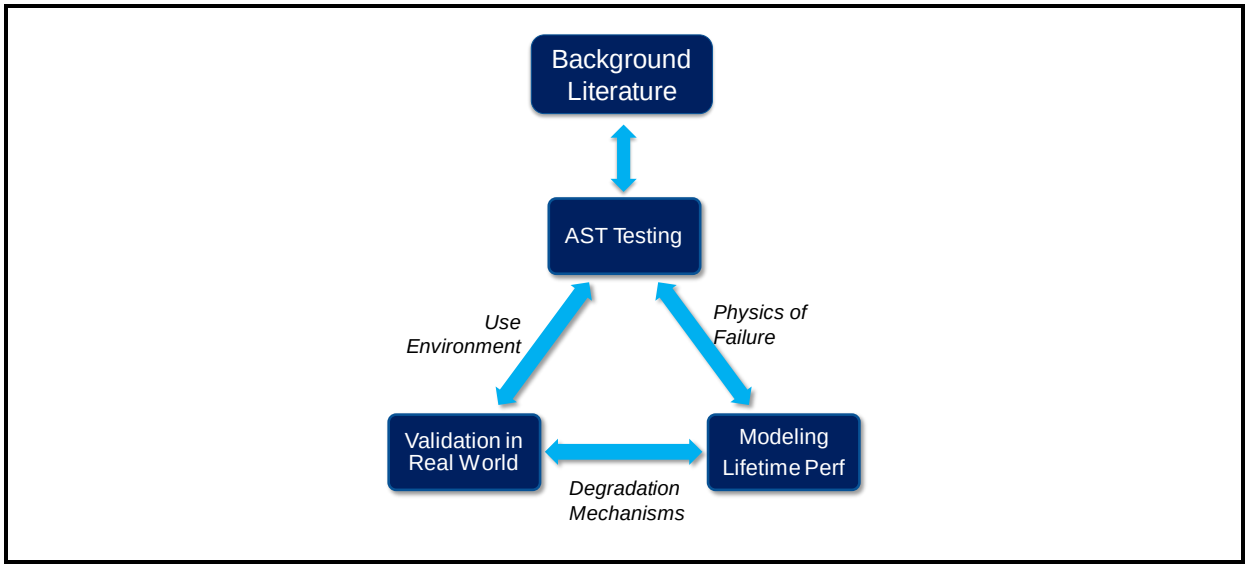

Models of a given phenomenon can be constructed by leveraging available data from industrial sources and laboratory experiments. In some instances, the industry already has developed standard methods, such as TM-21-11 [1], for projecting long-term performance

based on data collected using standard procedures, such as LM-80-08 [2], and we adhered to those methods as much as possible. However, in most of the project, there were no acceptable models or methods to create models, so they were developed as part of this project. In general, several different approaches outlined in ***Table 4A-1*** were used to create models described in this report, depending on the type of data. This section provides an overview of the methods used to create the models. Examples of actual implementation of the models are given in subsequent sections.

Table 4A-1. Types of Reliability and Degradation Models Developed in This Work

Basis for Model	Description	Examples
Empirical	Models built directly from data typically using optimization approaches, such as least squares, to find acceptable model coefficients. These models often do not have a theoretical basis but provide adequate representations of actual performance.	General models of LED lumen maintenance behavior for different packages
Kaplan-Meier Models	Models developed from the distribution about the mean for various types of data (e.g., lumen data) that provide the probability of failure at a given time.	Probability of lumen maintenance failure for a given distribution of α values
Weibull Models	Parametric models of failure probabilities in time using the two-parameter form of the Weibull equation. This approach allows the calculation of FIT rate, and the probability distribution.	Electronic device failure probability
Physics of Failure	Models developed by leveraging knowledge of the underlying mechanisms responsible for failure. There is a direct cause and effect of physical degradation of key components and failure.	Degradation of lens and reflectors Chromaticity shift
Simulation Models	Models developed using commercial ray-tracing software but leveraging new methods developed in this study to initially degrade materials in the simulation to study the effect on luminous flux maintenance.	Degradation models for luminaires
Principal Components Analysis	Models built from a statistical procedure that converts a set of observations of possibly correlated variables into an orthogonal array of linearly uncorrelated variables of fewer number.	Models of lamp lifetime, from its design & physical characteristics
Kalman Filtering Models	A technique for predicting the future behavior of a device, including residual useful life, based on previous behavior over an extended period.	LED lumen maintenance and CCT changes

Note: CCT = correlated color temperature.

4.A.2 Empirical Models of Lumen Maintenance Behavior of LEDs

During this work, general models of the performance of LEDs by package type were created based on decay rate constants (α) calculated directly from LM-80-08 data using the TM-21-11 projection method. The data that were used in building these models were obtained from

six of the top seven LED manufacturers and represented a broad slice of the LED market. LM-80-08 reports from a total of more than 250 different LED test populations were analyzed. This sample set consisted of 135 high-power LEDs (HP-LEDs), 95 mid-power LEDs (MP-LEDs), 43 chip-on-board LEDs (COB-LEDs), and 9 chip-scale package (CSP) datasets. The test reports analyzed in this study were published by the manufacturers between 2011 and 2015, with most of the collected test reports published in 2012 to 2014. A break-out of the LM-80-08 reports, by publication year, is shown in ***Figure 4A-2***. Only the most recent LM-80-08 reports for each product were included in this analysis.

The ubiquity of HP-LED products is indicated by the large number of LM-80-08 reports that were collected for this package, whereas the growth in COB-LED LM-80-08 reports reflects the recent introduction of this package style into the market. While MP-LEDs have been widely used, additional packaging materials began in 2013 to be incorporated into these products. Commodity MP-LEDs tend to use packages with lead frames overmolded with polyphthalamide (PPA) or polycyclohexylenedimethylene terephthalate (PCT), whereas premium MP-LED packages tend to contain higher performing materials, such as epoxy molding compound (EMC), silicones, and ceramics. Consequently, the number of updated LM-80-08 reports for MP-LED products continues to increase.

Figure 4A-2. Breakout of the LM-80-08 Reports by Package Type, Collected from Major Manufacturers

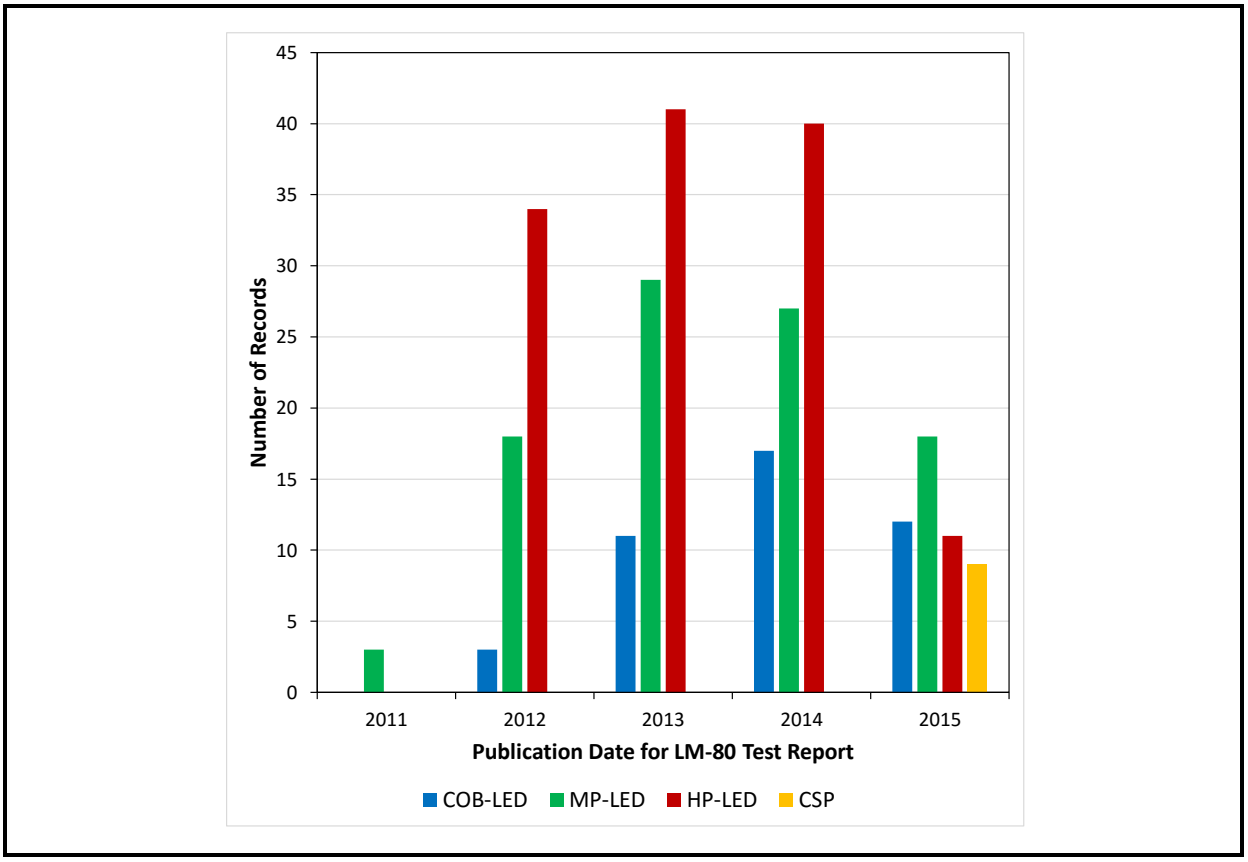

Each LM-80-08 test report contains not only summary information of the test population, such as an average value for α, but also test results (e.g., lumen maintenance and total chromaticity shifts) for each LED in the test population. This allowed α values and TM-21-11 projections to be calculated for the entire population, which is widely done. In addition, TM-21-11 projections can also be made for each LED in the test population along with a decay rate constant, α. An analysis of the data from these LM-80-08 reports is given in Section 4.B.1, while this section will concentrate on the methods used to develop the models. One of the primary motivations for creating general models of lumen maintenance by LED package was to provide an indication of how a general LED package of a particular design (e.g., HP-LED, MP-LED, COB-LED) would perform in an application. In addition, LM-80-08 data are often considered proprietary by manufacturers and not widely shared, making it difficult to get actual data. Development of such general models for common LED packages may provide a means to evaluate the different LED options in an application; however, when a final decision is made, the actual LM-80 data from the manufacturer are recommended to be used.

In developing the general models of lumen maintenance behavior according to LED package type, the LM-80-08 datasets were found to include the potential predictor variables current, ambient temperature, voltage, junction temperature, and the response variable decay rate constant (α) for each sample. Exploratory data analyses were conducted on the datasets to detect correlations between the predictors and the dependent variable. This analysis determined that current and junction temperature had the highest statistical correlation with the response variable.

Multiple linear regression was used to describe the decay rate α for each package type as a function of the predictor variables. **Equation (4A.1)** shows the general form followed by these regression models, where α is the decay rate, T is temperature—junction temperature (T_j) is used in the models, except for the COB models where substrate temperature is used—I_f is the forward current (current per die is used in the COBs), and ε is the residual error which is the difference between the data and the model. Low residual error values indicate that the models account for most of the behavior in the data.

$$\alpha = \beta_0 + \beta_1 * T_j + \beta_2 * I_f + \varepsilon \quad (4A.1)$$

where:

α = decay rate

T_j = junction temperature (substrate temperature for COB-LEDs)

I_f = forward current

β_0, β_1, β_2 = regression parameters

ε = residual error

Substrate temperature, which is approximately equal to ambient temperature in LM-80-08 tests, is used for COBs, because the junction temperature of the LEDs in the array may vary. Likewise, the current per die is used for arrays to allow scaling of the models. It is possible that there exist an interaction between I_f and T_j; however, the data did not support a complete factorial design structure and the estimate of the interaction was confounded.

The open-source statistical software package R was used to fit the regression models (estimation of parameters β_0, β_1, and β_2) and to compute regression statistics (R package "lm") [3]. For each regression model, the overall p-value and the p-value for each predictor variable were obtained. P-value is a measure of the statistical significance of the data and of each coefficient for the model. Standard regression statistics were obtained, including the adjusted coefficient of determination (R^2) and the residual standard error (RSE). For the selected models, the relative importance of the predictor variables was calculated using R package "relaimpo" by computing several estimators, including the R^2 contribution averaged over orderings among predictors. Cross validation was performed on each model using the R package "DAAG" by calculating the mean squared error (MSE) that results from a 10-fold cross-validation.

The multiple parameter linear regression model depicted in Equation (4A.1) was used to describe the relationship between average decay rate α for each package type as a function of I_f and T_j. ***Table 4A-2*** shows the results of the multiple linear regression model, and the values of the outcome, α, were first calculated for each individual LED using the standard TM-21-11 algorithm.

Table 4A-2. Parameter Estimates for the Four Main LED Package Architectures Examined in This Study

	HP-LED	MP-LED Gen 1	MP-LED Gen 2	COB-LED
β_0	$-6.72*10^{-6}$	$-1.31*10^{-5}$	$-3.25*10^{-6}$	$-4.58*10^{-6}$
β_1	$7.57*10^{-8}$	$3.13*10^{-7}$	$7.55*10^{-8}$	$1.07*10^{-9}$
β_2	$3.11*10^{-9}$	$9.00*10^{-9}$	$9.07*10^{-9}$	$4.41*10^{-9}$
RSE	$2.50*10^{-6}$	$9.09*10^{-6}$	$2.15*10^{-6}$	$1.50*10^{-6}$
Adjusted R^2	0.68	0.69	0.84	0.75
N	1,242	347	402	319
*All calculated parameters were found to be statistically significant.				
Equation	$\alpha = -6.72*10^{-6} + 7.57*10^{-8}*T_j + 3.11*10^{-9}*I_f$	$\alpha = -1.31*10^{-5} + 3.13*10^{-7}*T_j + 9.0*10^{-9}*I_f$	$\alpha = -3.25*10^{-6} + 7.55*10^{-8}*T_j + 9.07*10^{-9}*I_f$	$\alpha = -4.58*10^{-6} + 1.07*10^{-8}*T_j + 4.41*10^{-9}*I_r$

Figure 4A-3 shows plots of the residuals versus the fitted values for each one of the models. The randomness of the model residuals supports the appropriateness of the model. A more in-depth discussion of the models for each package type is given Section 4.B.1.

Figure 4A-3. Residual Distributions for the Fitted Linear Models

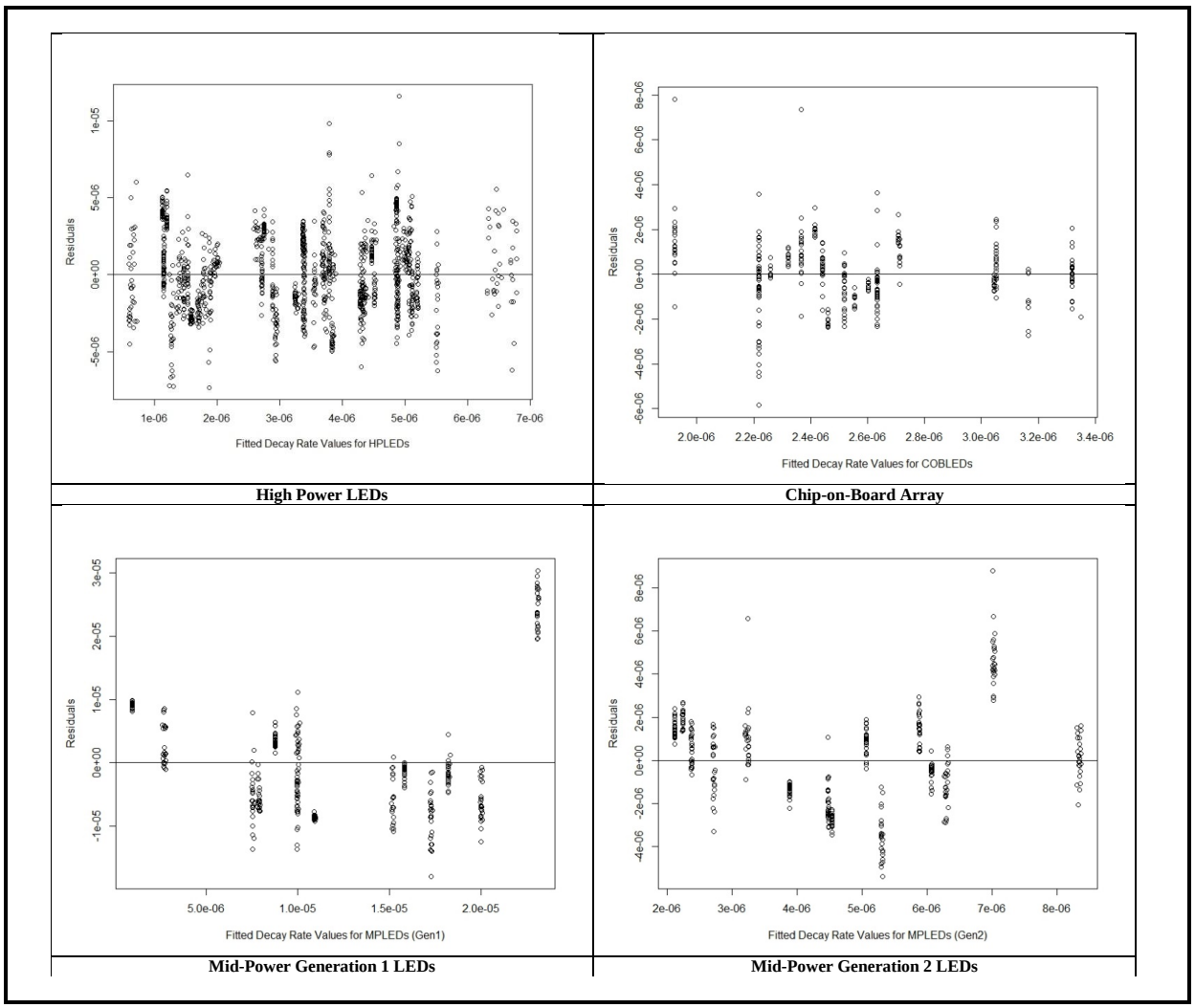

The LM-80-08 method provides a standard test procedure for measuring lumen maintenance changes of LEDs. The method was recently updated to reduce testing burden on the manufacturers; the revised standard is LM-80-15 [4]. Due to the lag time between approval of the revised standard test method and the completion of product tests, no data in our analysis were acquired under the LM-80-15 protocol.

Because all LED manufacturers perform this testing, LM-80 reports are available on many LED products. Consequently, this vast data resource is available and provides a good foundation to build general models for LED performance. However, the LM-80 method has

several significant limitations, including (1) the calculated α value will depend on the length of testing [5-7]; (2) some experimental parameters, especially low currents and temperatures, produce minimal changes in the LEDs and can result in negative α values [8]; and (3) other helpful properties such as chromaticity coordinates and forward voltage are not usually included in the LM-80 report.

Although the LM-80 method specifies a minimum test time of 6,000 hours, the manufacturer can choose to run the test for longer periods of time. However, to get information into the marketplace as quickly as possible, results are often published once the minimum of 6,000 hours of testing has been reached, then updated as necessary when additional data become available. The calculated α values have been shown to depend on test length [5-7], so α values recorded with shorter test durations may vary from those from longer tests. Moreover, if additional failure modes arise outside the test period, this behavior may not be accurately reflected in the calculated α values, introducing additional errors in the reported α values. Thus, although the manufacturers reported α values contain several potentially significant sources of errors, these data are the most complete dataset that is currently available. The models developed in this study may suffer from these same limitations, but a methodology is provided to overcome these limitations to some degree by derating the α values to build in conservatism in any luminaire and lamp lifetime models.

While the models described in this report consider a population of a given LED package type and are generally conservative, additional margin can be added by increasing the mean or average α values (represented by μ) by the standard deviation (σ) of the entire population. This approach is useful when considering the average performance of a particular LED package type. As shown in ***Figure 4A-4****,* there is a spread in α values within a given LED population. In Figure 4A-4, the average value for test population is shown as the black circle, while the results from each LED in the test population are shown as a blue diamond (55°C), red square (85°C), or green triangle (105°C). Because the methods described herein calculate α for each LED, the distribution of α values can be accounted for by calculating σ for each product. Thus, a moderately conservative estimate of α can be obtained by calculating $\mu+\sigma$ using the methods described here, including the population distribution of the data evaluated in this report.

An even more conservative estimate can be computed as $\mu+2\sigma$. According to standard statistical theory, for a normally distributed population, 84% of the values will be less than the mean plus one standard deviation (assuming a one-sided distribution) and 97.5% of the values will be less than the mean plus two standard deviations. Thus, the added conservatism included in the reported method provides a mechanism to derate the generalized LED α values to increase the probability that the true α value of the chosen population is equal to or better than the calculated μ value.

This approach provides additional margin for designers of SSL lamps and luminaires to accommodate unforeseen circumstances in field operation. In addition, σ provides a measure of the population distribution and random sampling from the population can be used to emulate the variability of α values for multi-LED devices. In this way, synthetic LED populations can be created using this approach by selecting random values about the mean, weighted by a normal distribution with standard deviation σ.

Figure 4A-4. Decay-Rate Constant Values of Representative Test Populations of One HP-LED Product Tested at One of Three Different Temperatures

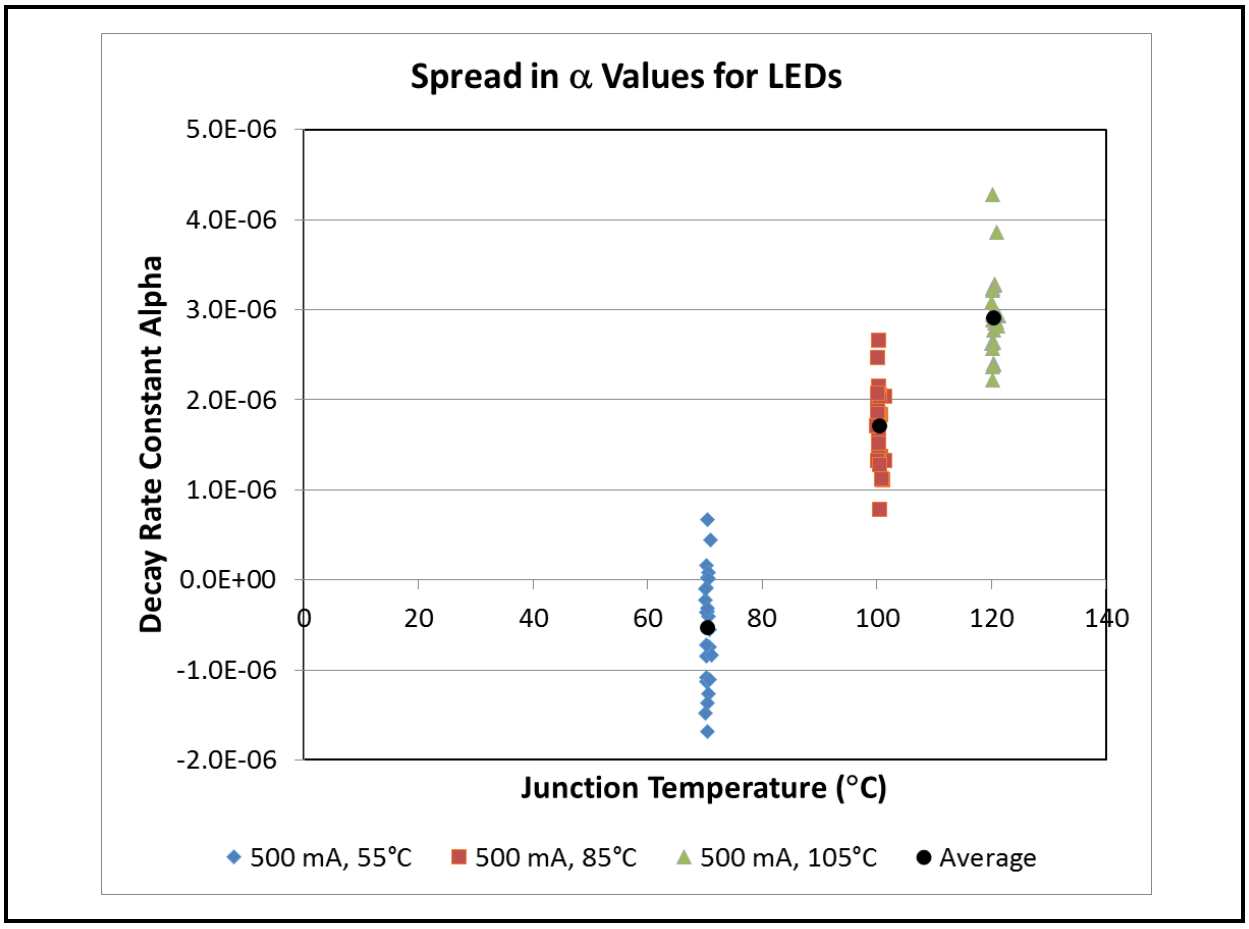

As noted earlier, LED lumen maintenance data sometimes can show a temporary increase in luminous flux over time. This increase can be the result of several effects, including annealing of defects in the LED epitaxial layer, annealing of defects in the phosphor layer, reduction in contact resistances, and changes in the refractive index of materials in the light path (e.g., silicone binder in LED phosphors). TM-21-11 does not fit this increase, which is one of the reasons the TM-21-11 protocol dictates that the first 1,000 hours of data be discarded. Such an increase in luminous flux can occur during early operation time (i.e.,

first 1,000 hours) or under low stress conditions (e.g., low operational currents combined with low ambient temperatures). In such instances, luminous flux often increases slightly to a normalized value greater than 1.0 (usually before the first 1,000 hours) and then slowly decays. Because the single exponential model used in TM-21-11 does not describe the increase in efficiency and the extended decay over time, an empirical rule in TM-21-11 is to drop observations obtained during the first 1,000 hours and calculate the exponent based on the remaining data. Such an approach is undesirable because of the loss of potentially important data and because 1,000 hours is an arbitrary period, which may vary from LED to LED.

Even with the removal of the first 1,000 hours, there are some LEDs that show an increase in luminous flux with time during LM-80-08 testing. This increase, although often followed by an eventual decrease, biases the value of the decay rate constant toward more optimistic, lower values. In fact, when the decay is slower, the decay constant is smaller, and the time to reach L70 is longer. In extreme cases, the luminous flux does not decrease over the observed period, leading to unrealistic, negative decay rate constants and infinite lifetime forecast.

Temporary increases in a measurable property followed by a decrease are often generically described by a Weibull function commonly used in reliability. The challenge, however, is to find a more interpretable "mechanistic" approach to the description of this phenomenon. Several unelucidated mechanisms may be responsible for a temporary increase in luminous flux, and a model for this phenomenon was developed under this work and published in the literature [8].

Although there is not great certainty in the literature regarding the physical origin (or origins) of these short-term improvements in luminous flux, different functional forms can be proposed and tested if certain mechanistic assumptions are made. Thus, estimating the temporal form of the burn-in period from among a limited number of temporal forms, associated with common physical processes like diffusion or chemical reactions, might be possible. For example, a kinetic process could arise when a catalyst continues the curing of the silicone encapsulant to produce an end form with a different index of refraction or when defects in the epitaxial or interconnect layers are annealed during LED operation, increasing device efficiency. Zero-, first-, and second-order kinetic processes such as these would proceed at different rates with known (or easily parameterized) forms as a function of time [9-11]. For simplicity, a physical process that involves a first-order rate of change was assumed in this analysis. Such processes lead to a model with a single dominant exponent with two easily interpreted empirical parameters.

For the maximum observed luminous flux improvement, the assumption of first-order behavior yields a time-dependent lumen improvement that could be represented by a bounded exponential function as given in **Equation (4A.2)**:

$$\lambda(1 - e^{-\beta t}) \tag{4A.2}$$

where λ corresponds to the maximum asymptotic increase in efficiency as $t \to \infty$, and β is a special decay coefficient, such that 1/ β corresponds to the time when the efficiency increases by about 0.63 of the maximum value. As discussed later, the same functional form was found to model the rapid change in chromaticity during the burn-in stage.

If all data acquired using the LM-80-08 method were to be considered, a functional form would need to be developed that accounts for the potential increase in luminous flux under certain conditions in addition to the exponential loss that follows. We propose a model that explicitly fits both the exponential decay and the increase in efficiency. The total model in **Equation (4A.3)** would fundamentally be:

$$\Phi_{total} = M1*M2 \tag{4A.3}$$

where M1 is a model for luminous flux increase, and M2 is the model for luminous flux decrease given by TM-21-11. Specifically, M2 is an exponential decay model, $e^{-\alpha t}$, as shown in **Figure 4A-5**, and M1 is a 2-parameter bounded exponential model, as shown in **Equation (4A.4)**:

$$M1 = B + \lambda(1 - e^{-\beta t}) \tag{4A.4}$$

where B corresponds to projected initial normalized luminous flux value, λ corresponds to the maximum asymptotic increase in efficiency as $t \to \infty$, and 1/β corresponds to the time when the efficiency increases by about 0.63 of the maximum value. If there is no increase in efficiency (λ = 0), the model becomes equivalent to a simple exponential model because M1 will be equal to B. The combined model is given in **Equation (4A.5)** and depicted graphically in Figure 4A-5:

$$\Phi_{total} = e^{-\alpha t}(B + \lambda(1 - e^{-\beta t})) \tag{4A.5}$$

Figure 4A-5. Illustration of the Components of Double Model for Luminous Flux Maintenance

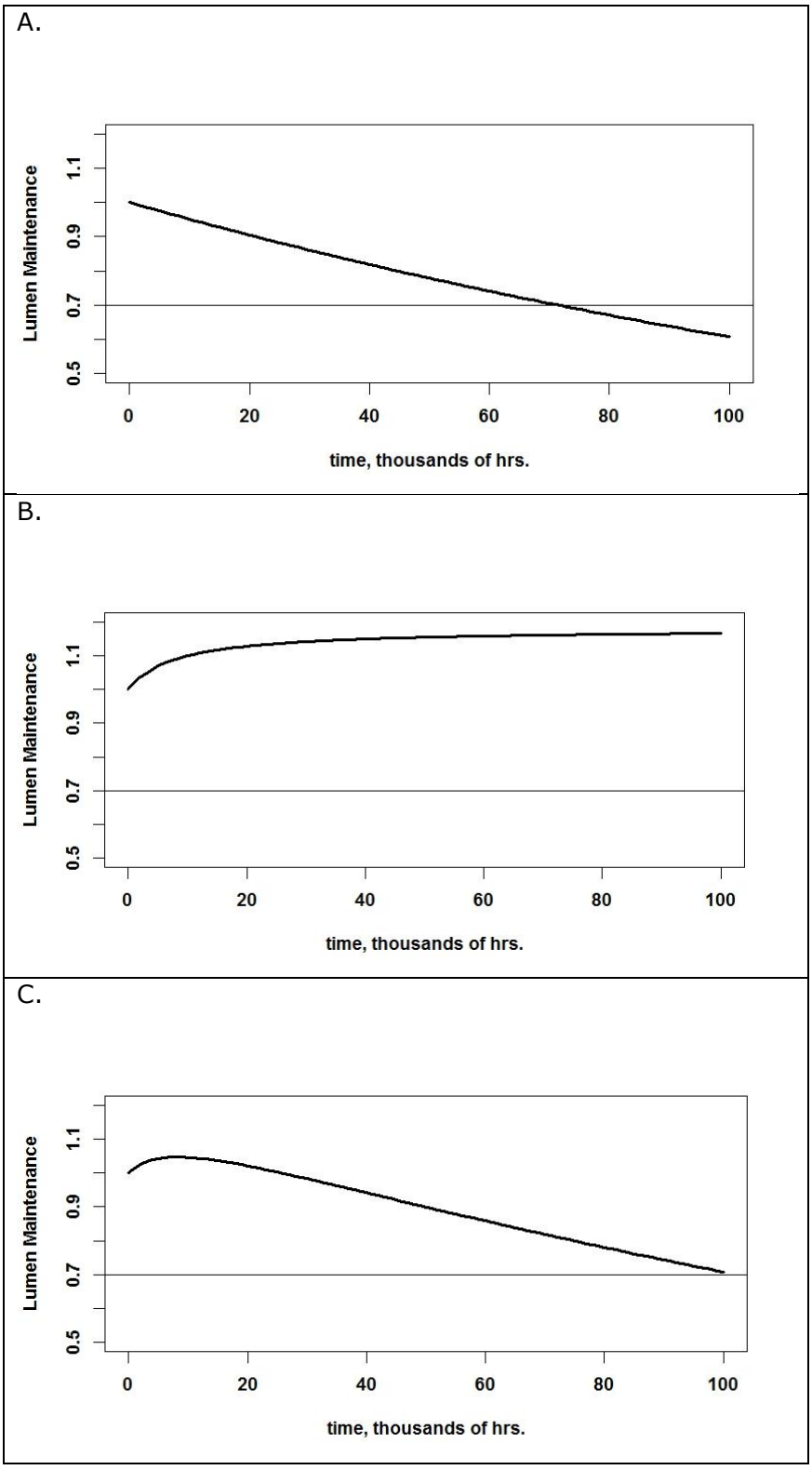

In Figure 4A-5, panel A represents lumen maintenance corresponding to an exponential decay model (i.e., TM-21-11); Panel B corresponds to the bounded exponential model; and Panel C illustrates the shape of the full model.

Automatic algorithms that find the best model fit using the observed data generally are sensitive to the initial conditions and require setting up boundaries for plausible parameter values. We used a hybrid approach, in which a grid search was used to identify plausible initial conditions, then the solution was refined by using restricted nonlinear, least square models with an automated "port" algorithm. In selecting a model with the best fit, an MSE criterion was used, rather than an R^2 criterion. R^2 values can be misleading when the fit is close to a horizontal line, because R^2 is close to zero even if the model shows a good fit. Such situations are not uncommon in lumen maintenance data, when the level of noise is high and α is small.

A nonlinear grid search starts in a space of four parameters and about 10 values for each of the parameters. After obtaining the approximate values of the best parameter combination, these values were used as an initial approximation in an automated search in the same range of the parameter values. We considered several automatic fitting algorithms (Gauss-Newton, Golub-Pereyra, and Port), but preferred the "port" algorithm, which allows for the physical restriction of parameter values. The fitting algorithm usually converged very close within the size of the grid cell. As expected, the double model of luminous flux maintenance produced a better fit (measured in terms of MSE) compared to an exponential model using all the available data. TM-21-11 models that consider estimation starting at 5,000 hours often produced a similar fit to the double model, but when the model was extended to the entire range of observational times, the double model produced better fits. In presenting the results, we follow convention and use R^2 to illustrate goodness of fit.

4.A.3 Kaplan-Meier Models of Lumen Maintenance Failures

Using estimates of decay rates, α, the TM-21-11 method can be used to project lumen maintenance (*L(t)*), for any length of time as $L(t) = e^{-\alpha t}$. This project might be misleading if the actual decay rate follows a different distribution and the exponential model used in TM-21-11 is not a valid simplification across all times. The time-based luminous flux behavior of this population can be calculated using a non-parametric method such as a Kaplan-Meier survivorship analysis.

As suggested by the data collected in this study and additional LM-80-08 data analyzed from manufacturers, LEDs typically have a long lifetime, and abrupt failures are extremely rare. Because LEDs do not often fail in an abrupt fashion, parametric failure is often defined as the reduction of the luminous flux below a predetermined level. In this study, time to failure will be defined as the time in hours when the LED lumen depreciation reaches a threshold of the initial lumen output. For example, failure may be defined as the time when the L70 condition is reached, which corresponds to a reduction in luminous flux to 70% of

the initial value. Other definitions of failure, such as L50 or L90, also can be used, but L70 and L90 are used in this work to be representative. However, with the variation in α values that naturally occurs in a population of LEDs, the time required to reach L70 may vary for each LED. In creating these survivorship models, the data from each LED population undergoing test is used to represent the variation in the overall sample population; this variation also is reflected in the population drawn for the Kaplan-Meier survivorship analysis.

The survivorship probability for new LED units is the probability that the LED is functional at time *t* (i.e., is surviving at time *t*) and is estimated by randomly sampling new units from the population. The decay rate values are predicted using the prediction intervals and variances calculated previously for each package type, for example using LM-80-08 data. This approach allows the estimation of the α values for a random sample of the LEDs of mean μ and standard deviation σ, and the survivorship probability can be calculated using the Kaplan-Meier method.

The Kapan-Meier estimator of survivorship is of the form

$$\widehat{S(t)} = \prod_{t_i<t} \frac{n_i - d_i}{n_i}$$

where:

$\widehat{S(t)}$ = estimator of survival at time *t*

t_i = time required for luminous flux to drop below the threshold value for specimen *i*

d_i = number of LEDs at time t_i with luminous flux below threshold

n_i = number of surviving LEDs at time t_i with luminous flux above threshold

The 95% confidence interval for the Kaplan-Meier estimator of the survival time depends on its variance. The estimator of the variance can be calculated using the method proposed by Greenwood [12]:

$$\widehat{Var(S(t))} = \widehat{S(t)}^2 * \sum_{t_i \le t} \frac{d_i}{n_i(n_i - d_i)}$$

Kaplan-Meier calculations were performed on the data in this study using the following assumptions:

- All units in the randomly selected sample population are of same LED package type.
- All units are tested at the same current and generated the same T_j.
- Decay rate values are predicted using the prediction intervals and variances described earlier.

Kaplan-Meier survivorship curves can be calculated for specific LEDs as well as any generic LEDs represented by the models given in Table 4A-2. In building these models, including the

data for individual LEDs and the variance is essential. For example, the L70 survivorship curve for a randomly selected population of generic HP-LEDs operated at I_f = 1,000 mA and T_j = 100 C is shown in ***Figure 4A-6***, and the corresponding L90 survivorship curve for a different randomly selected population in given in ***Figure 4A-7***.

If L70 is the parametric failure criterion and the luminous flux of each individual LED is greater than 70% of the initial value, then each LED is deemed to have survived to at least the next period. As shown in Figure 4A-6, roughly 50% of the HP-LED population survive (i.e., exhibits luminous flux greater than L70) for almost 85,000 hours under these operational conditions. This is the median failure time of the population, which is also called the B50 number. Likewise, other B-values can be determined with this procedure. Two key findings can be made by examining Figure 4A-6 and Figure 4A-7. First, as might be expected, the time to reach B50 and L90 is much shorter than time necessary to reach B50 and L70. Perhaps more unexpectedly, the survivorship of a random LED population does not decrease in a continuous fashion, but instead has regions where many units fall below the parametric threshold (i.e., do not survive and can be considered parametric failures), followed by a prolonged period where fewer failures are observed. This trends is most easily observed in Figure 4A-7 and is an outcome of the property of the randomly selected LED population.

Using the models discussed herein, representative curves can be generated by randomly drawn samples of the industry average LED at any current and temperature level covered by the models in Table 4A-2. Successive calculations of the Kaplan-Meier estimator may give slightly different results, because the estimator draws a different random sample each time it is calculated. In addition, more conservative models can be created by increasing the mean (μ) decay rate constant by one standard deviations (i.e., $\mu + \sigma$) and very conservative models can be created by increasing the mean decay rate constant by two standard deviations (i.e., $\mu + 2\sigma$). This approach allows for compensation of population variation and uncertainty in the true α value. For each randomly selected sample, we calculated both the overall value of α for the sample and the Kaplan-Meier estimate. The L70 and L90 survivorship curves of a typical sampling are shown in ***Figure 4A-8***.

Figure 4A-6. L70 Survivorship Curves and 95% Confidence Interval (CI) Levels for a Randomly Selected Population of Generic HP-LEDs Operated and 1,000 mA and 100°C

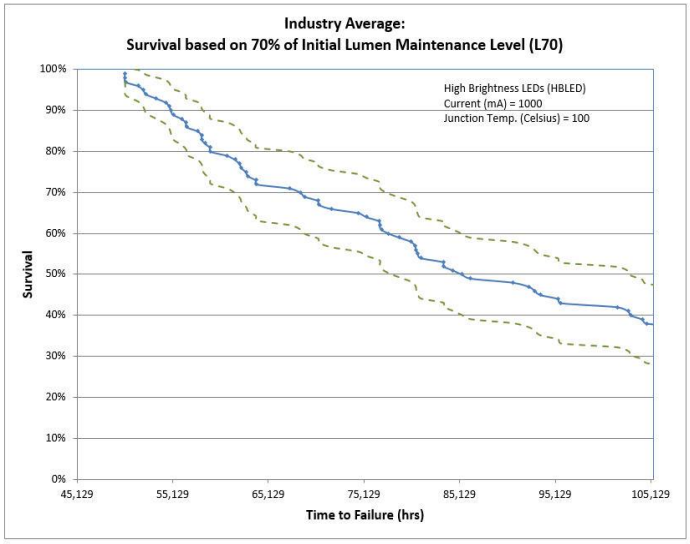

Figure 4A-7. L90 Survivorship Curves and 95% CI Levels for a Randomly Selected Population of Generic HP-LEDs Operated at 1,000 mA and 100°C

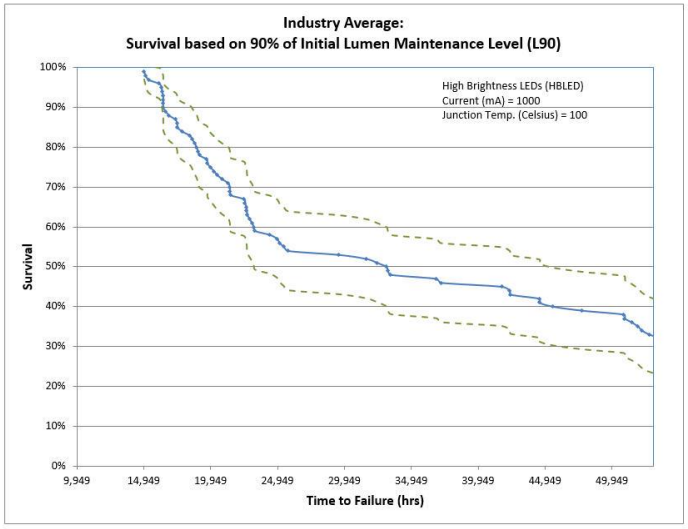

Figure 4A-8. L70 (Left) and L90 (Right) Survivorship Curves and 95% CI Levels for a Randomly Selected Population of Generic HP-LEDs

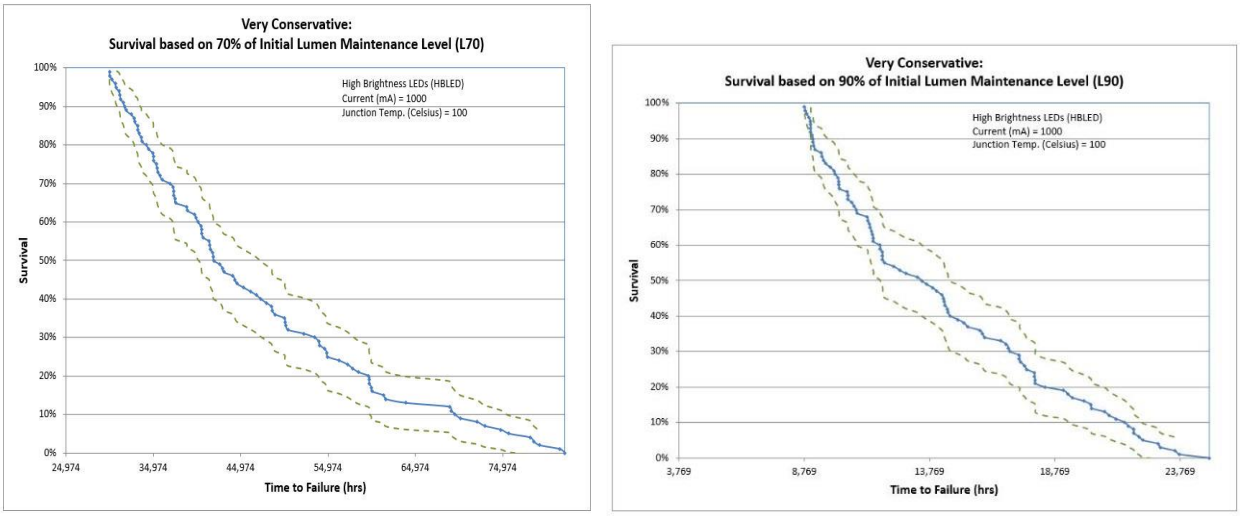

NOTE: The LEDs are assumed to be operated at 1,000 mA and 100°C and with an assumed very conservative (i.e., $\mu + 2\sigma$) Decay Rate Constant

Figure 4A-9 shows the reliability curves for a MP-LED population model calculated with the generic model given in Table 4A-2 and operated at I_f = 200 mA and T_j = 60°C. The curves were generated for populations created from random samples of the generic MP-LED model, assuming the industry average decay rate and very conservative values for the decay rate. Clearly, the two populations exhibited slightly different behaviors due to the differences in assumed α values that were randomly drawn for the samples. ***Figure 4A-10*** shows additional samples for MP-LEDs, and the behaviors are different from those given in Figure 4A-9 simply due to the random way in which α values were selected.

Figure 4A-9. Kaplan-Meier L70 Survivorship Curves for a Random Sample of MP-LEDs Assuming the Generic Model in Table 4A-2

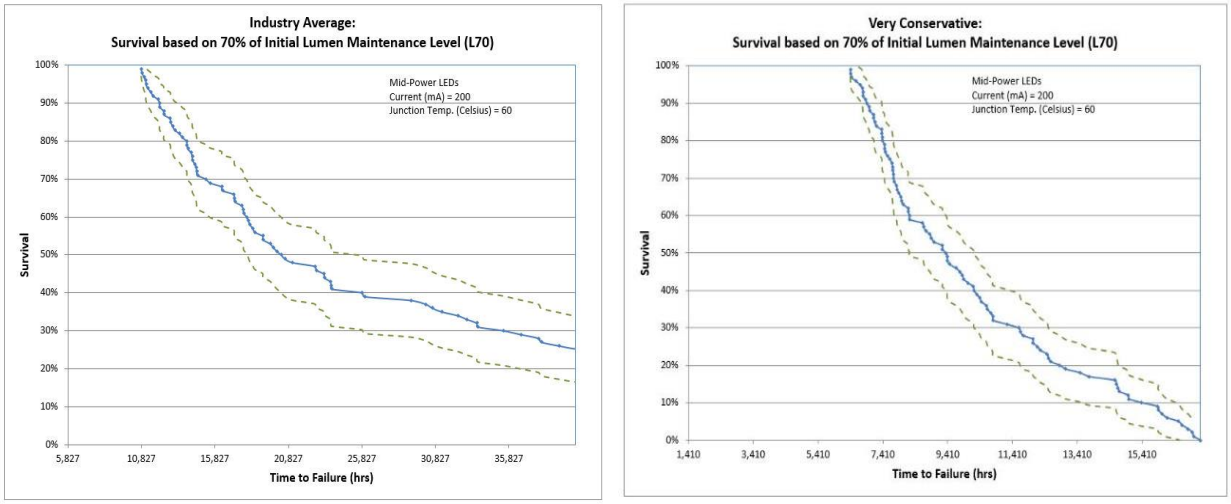

Figure 4A-10. Comparison of the L70 Survivorship with Different Assumptions of the Level of Conservatism Incorporated Into the α Value

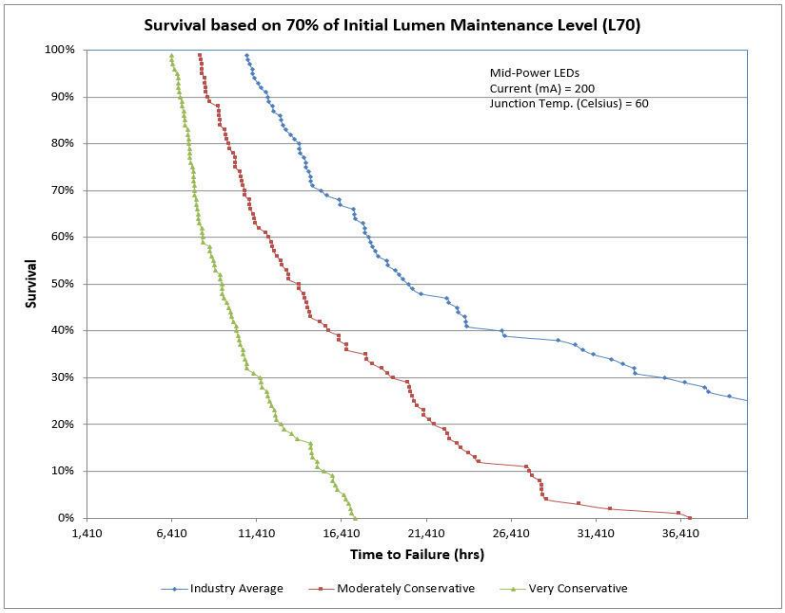

For completeness, the L70 Kaplan-Meier survivorship curve for a population of COB-LEDs is given in ***Figure 4A-11*** for a randomly selected, generic COB-LED population tested with at a current of 100 mA and a junction temperature of 100°C. The curves were generated for the industry average decay rate and for very conservative values of the decay rate.

Figure 4A-11. (Left) L70 Kaplan-Meier Survivorship Curve for a Random Population of Industry Average COB-LEDs. (Right) Comparison of the L70 Survivorship Curves for Random Populations of Industry Average, Conservatively Derated, and Very Conservatively Derated COB-LEDs

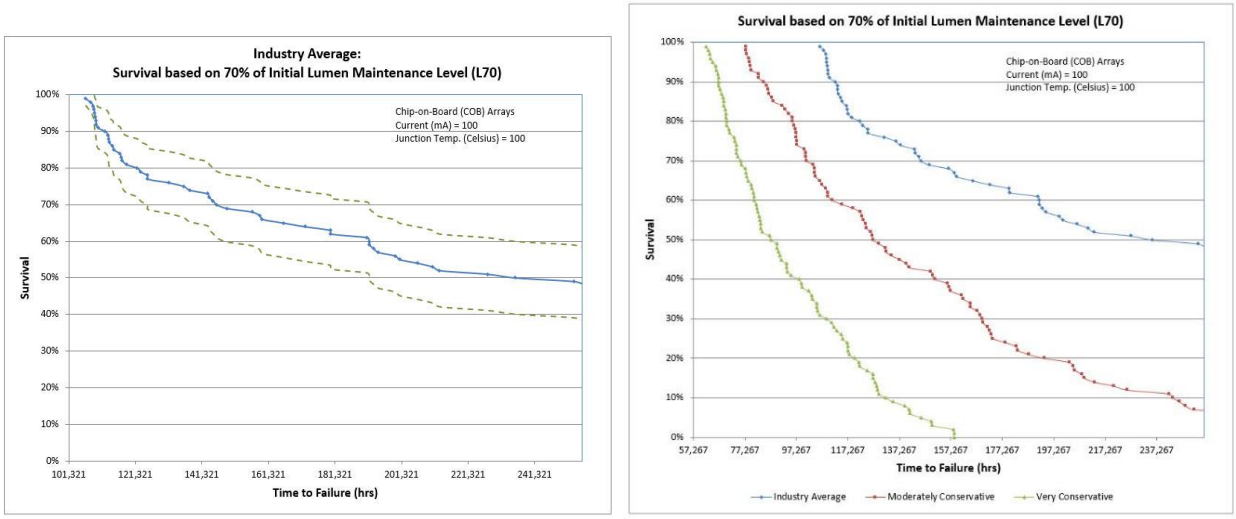

4.A.4 Physics of Failure Models of Chemical Degradation of SSL Devices

A variety of chemical processes occur in SSL devices that can produce either parametric or abrupt failure of the device. Such chemical processes include corrosion of wirebond pads and weakening of solder joints, which can cause abrupt failure in LED devices [13; 14]. Chemical processes are also responsible for many parametric failures of SSL devices, such as excessive loss of luminous flux or excessive chromaticity shifts. These kinetic processes can impact the LEDs [15], encapsulants [16-18], lenses [19; 20], reflectors [20; 21], and other materials used in LED devices. Understanding the kinetic process responsible for a given failure mode provides an understanding of a particular failure mechanism, and this level of detail allows models to be built for time to failure and remaining useful life (RUL).

Perhaps one of the best examples of the application of chemical kinetics in lighting is the TM-21-11 procedure for projecting luminous flux maintenance for LEDs. Although no specific chemical process is assumed in TM-21-11, the materials degradation processes responsible for the decline of luminous flux can be expressed using chemical kinetic theory, as shown here. The application of assumed chemical kinetics in TM-21-11 results in the expression of luminous flux decay as an exponential degradation process shown in **Equation (4A.6)**:

$$\Phi(t) = \Phi_0 e^{-\alpha t} \tag{4A.6}$$

where:

$\Phi(t)$ = luminous flux at time t

Φ_0 = initial luminous flux

α = decay rate constant

For temperatures between two measurement values (T_1 and T_2), the activation energy (E_a) responsible for the luminous flux decay can be calculated using the Arrhenius equation; this form of this equation is given in **Equation (4A.7)**. The linkage of lumen maintenance to the Arrhenius equation demonstrates the chemical kinetic nature of lumen maintenance processes.

$$\frac{E_a}{k_B} = \frac{(ln\alpha_1) - (ln\alpha_2)}{\left(\frac{1}{T_2} - \frac{1}{T_1}\right)} \tag{4A.7}$$

where:

E_a = activation energy (expressed in electron volts [eV])

k_b = Boltzmann's constant (8.617 x 10^{-5} eV/Kelvin)

T = temperature

As discussed earlier, a generic chemical process, assumed in these models where A is converted to C, can this reaction can be expressed as **Equation (4A.8)**:

$$A \rightarrow C \tag{4A.8}$$

This formalism clarifies the relationship between lumen maintenance, chromaticity shift, and chemical kinetics. This type of reaction, including more complicated versions, occurs in a variety of processes responsible for parametric failures of SSL devices; specific examples will be discussed later. For the generic chemical reaction in Equation (8), the reaction rate, $k(T)$, changes with temperature according to the Arrhenius equation, as given in **Equation (4A.9)**:

$$k(T) = A\exp(-E_a/k_b T) \tag{4A.9}$$

where A is a pre-exponential factor.

Knowledge of the rate of the chemical reactions involved in the degradation of LED devices is important, because these reactions determine the time necessary for the device properties to change to such an extent that the LED device crosses the predetermined parametric failure threshold (e.g., L70 or $\Delta u'v' > 0.007$).

Many of the processes involved in lumen light loss and chromaticity shift often involve the transformation of a material from one state to another. In many instances, this transformation proceeds through an intermediate state. If the influence of outside reactants is ignored for now, the sample reaction given earlier can be expanded into a more

complicated sequential reaction, in which A is first converted to an intermediate state B and then into the final state C, as shown in **Equation (4A.10)**:

$$A \rightarrow B \rightarrow C \tag{4A.10}$$

The concentration of A decreases by the same amount that the concentration of B increases, which can be expressed by **Equation (4A.11)**:

$$\frac{dA}{dt} = -k_1[A] = k_1[B] \tag{4A.11}$$

where:

$[A]$ = concentration of A

$[B]$ = concentration of B

k_1 = reaction rate constant for transformation of A into B, governed by Equation (4A.9)

The conversion of B into C can be written in a similar manner, as given by Equation (4A.12):

$$\frac{dc}{dt} = -k_2[B] = k_2[C] \tag{4A.12}$$

where:

$[C]$ = concentration of C, the end product

k_2 = reaction rate for the transformation of B in C

By solving these differential equations, expressions for the starting material concentration as a function of time (i.e., $[A]$ versus time) and the end product (i.e., $[C]$ versus time) can be developed as shown in **Equation (4A.13)** and **Equation (4A.14)**:

$$[A] = A_0 e^{-k_1 t} \tag{4A.13}$$

$$[C] = A_0 \left(1 - \left(\frac{1}{k_2 - k_1}\right)\left(k_2 e^{-k_1 t} - k_1 e^{-k_2 t}\right)\right) \tag{4A.14}$$

where A_0 is the initial concentration of A.

For lumen maintenance and chromaticity shift, the parameter [C] is needed, because it is directly linked to the observed lighting change.

Several different situations may arise for this sequential reaction, including the situations where the conversion of B to C is fast (i.e., $k_2 >> k_1$) and where the conversion of A to B is faster than the conversion of B to C (i.e., $k_1 > k_2$). Both situations are shown in in ***Figure 4A-12***. Examples of Equation (4A.14) solved for *k2* = 100k1 (i.e., *k2* >> *k1*) and *k1* = 5k2

(i.e., *k1* > *k2*) is shown in Figure 4A-12 and the derivatives of these solutions are shown in ***Figure 4A-13***.

Figure 4A-12. Examples of Equation (4A.14) Solved for $k_2 = 100k_1$ (i.e., $k_2 >> k_1$) and $k_1 = 5k_2$ (i.e., $k_1 > k_2$)

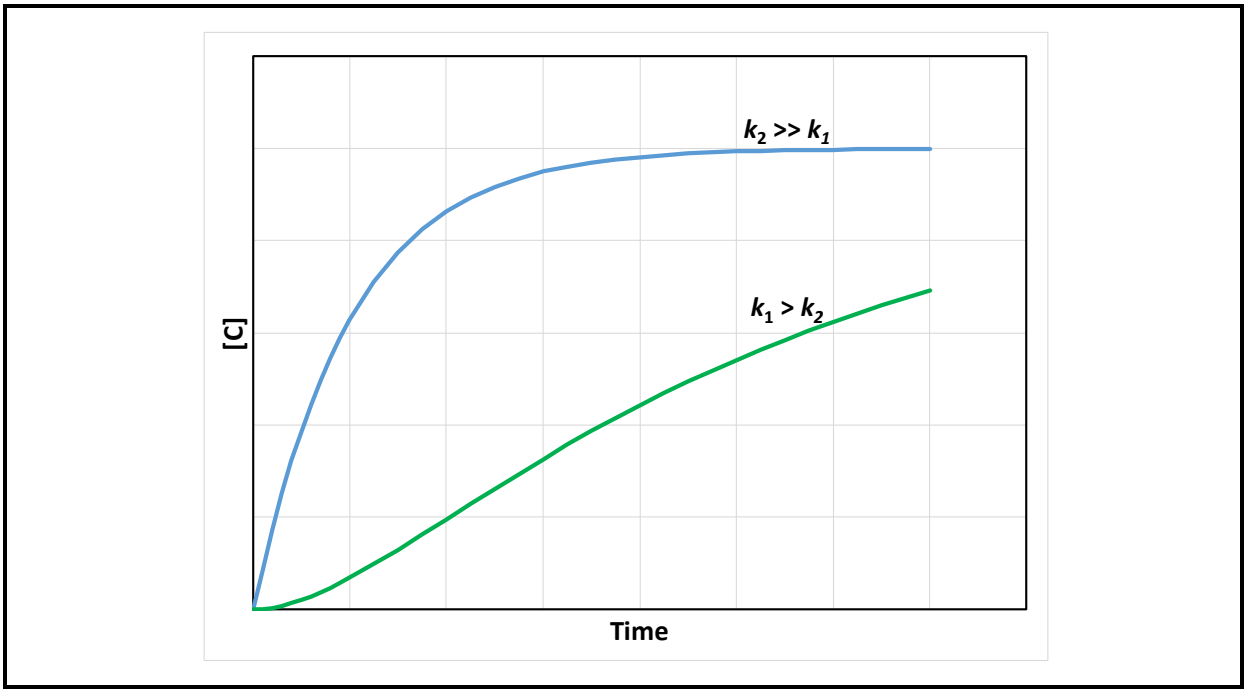

Figure 4A-13. Derivatives of the Functions Shown in Figure 4A-12

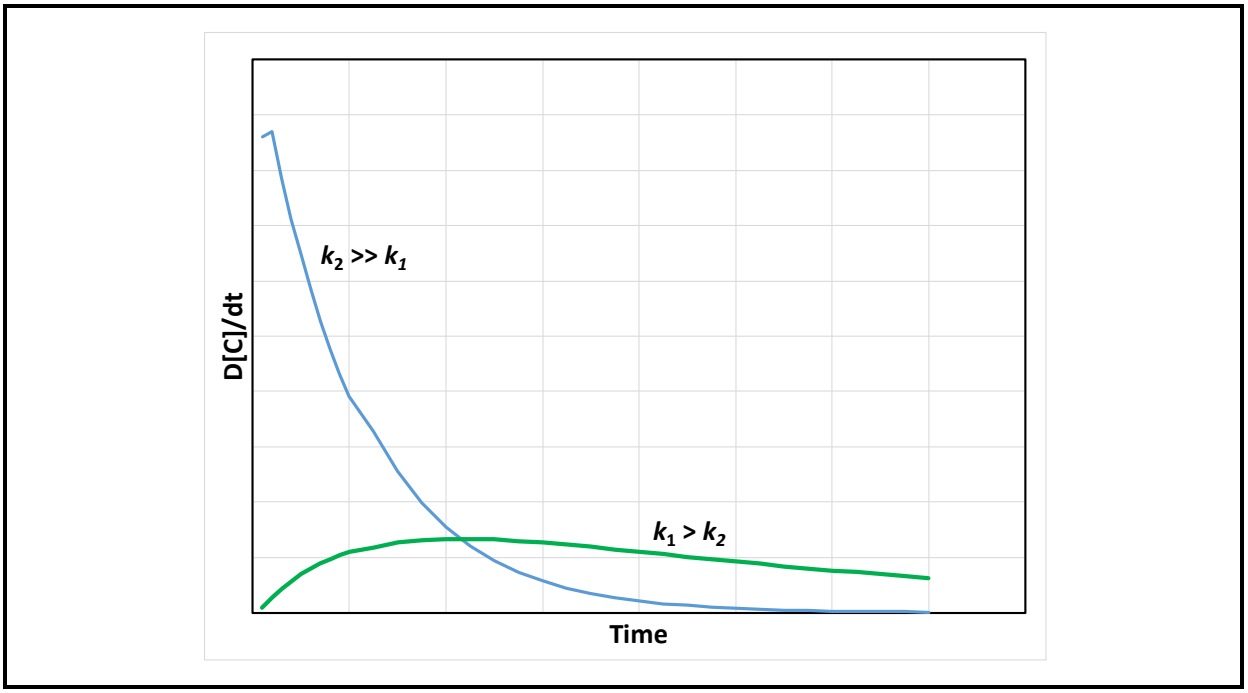

By comparing Figure 4A-12 and Figure 4A-13, the example where $k_2 >> k_1$ can be seen to be another manifestation of the bounded exponential function that we have already demonstrated is applicable to modeling LED lifetimes [8]. Indeed, a closer examination of Equation (4A.14) reveals that it reduces to Equation (4A.4) (i.e., the bounded exponential equation) if $k_2 >> k_1$. An examination of the derivative of this function given in Figure 4A-13 shows that growth rate in this instance is highest in the beginning and then rapidly decreases to an asymptotic value.

In contrast, the situation where $k1$ is just slightly larger than $k2$ results in a significantly different profile. Initially, the change in $[C]$ is miniscule and not easily detected in Figure 4A-12 although the growth rate can be seen to be increasing gradually by examining the derivative in Figure 4A-13. Essentially, an incubation process is occurring during this stage. Eventually, the reaction proceeds to a sufficient extent to be detected, and there is an emergent stage in Figure 4A-12 where $[C]$ grows quickly. As this emergent stage continues, the rate remains essentially constant (i.e., $d[C]/dt$ given in Figure 4A-13 is essentially flat indicating a linear rate of change). After an inflection point, the rate slows down (i.e., $d[C]/dt$ is negative in Figure 4A-13) and the value of $[C]$ approaches a limiting asymptote. When k_1 and k_2 have similar values, Equation (4A.14) can be shown in reduce to the logistic equation given in **Equation (4A.15)**

$$\frac{A}{1+Ce^{-kt}} \tag{4A.15}$$

where:

A = maximum or asymptotic value

C = a fitting parameter

K = rate of change in the curve

In examining large amounts of data from manufacturers, public sources, and our experimental findings, we have concluded that many phenomena associated with lumen maintenance and chromaticity shifts in SSL devices can be modeled using either the exponential decay, bounded exponential, or generalized logistic functions. In addition, as shown in Figure 4A-13, the logistic function and the bounded exponential function can be reduced to a linear form over a limited time frame. Examples of the use of these models to characterize the decay of materials commonly used in SSL devices is given in **Table 4A-3.** The bounded behavior of the generalized logistic and bounded exponential functions arises from limitations on the concentration of at least one of the reactants, possibly by other physical processes (e.g., available concentration for reaction, changes in light flux levels, preceding reactions, surface absorption, mass transport). At this point, the rate of reaction slows down (see Figure 4A-12) and approaches an asymptote.

Although they both approach asymptotic values, a significant difference between bounded exponential and logistic behavior is that the bounded exponential reaction initially proceeds very fast while the logistic model undergoes an incubation period, perhaps prolonged, where minimal reactions occur. Consequently, many processes occurring during the LED burn-in stage can be modeled with a bounded exponential function, and many slower acting processes can be modeled with a generalized logistic function.

Table 4A-3. Typical Models Used to Describe the Kinetics Occurring in Materials Used in LED Lighting Devices

Model	Equation	Parameters	Example in LED Devices
Exponential Decay	$Be^{-\alpha t}$	B = initial value α = decay rate constant t = time	Lumen Maintenance—TM-21-11
Exponential Growth	$A(1 + k)^t$	A = initial value k = growth rate constant t = time	Theoretical possible but not observed in LED devices. May describe some capacitor properties
Bounded Exponential	$C + A[1 - \exp(-kt)]$	A = Maximum value C = Initial value often 0 k = rate constant t = time	Lumen maintenance growth Initial chromaticity shifts Moisture ingress
Logistic Function	$A/[1 + C\exp(-kt)]$	A = maximum value C = fitting parameter k = rate constant t = time	Yellowing of lenses Chromaticity shift
Linear	$kt + b$	k = slope, rate constant b = intercept, initial value t = time	Can be used to locally approximate the exponential functions listed above under certain conditions.

Degradation of Common Luminaire and Lamp Components

One element of the change in luminaire efficiency during aging is the degradation of optical components such as lenses. To accurately model lens aging, the change in the transmittance spectrum of the lens needs to be determined over a timescale that simulates the natural aging process. Because SSL luminaires can be operated for 50,000 hours or more, such data cannot be acquired in the laboratory unless the aging process is accelerated.

RTI has performed accelerated stress testing (AST) studies on the degradation of common materials used in LED luminaires, and these models have been collected in RTI's Lumen Maintenance Decision Support Tool (LM-DST). In building the models contained in the LM-

DST, individual models have been developed for common lens materials, such as polymethyl methacrylate (PMMA), polycarbonate (PC), and silicone. These models were generated using data acquired during AST of the materials used in SSL luminaires. This discussion will concentrate on the techniques used to build the models for lenses and reflectors in the LM-DST, while details of the AST experiments for these materials are described elsewhere [20].

The models for lens transmittance changes during normal use were built from measurements of the change in the transmittance spectra of the material at different times. An example of such data for PC lenses housed in 6-inch downlights in an accelerating environment of 75°C and 75% relative humidity (7575) is shown in ***Figure 4A-14***. The 7575 environment is intended to achieve the natural aging of the lens that would occur during normal operation and uses higher temperatures and humidity levels than the lens would normally experience, to accomplish more than 50,000 hours of aging in less than 4,000 hours of experimental testing.

Figure 4A-14. Time Dependent Change in the Transmittance Spectra of Polycarbonate Observed During 7575

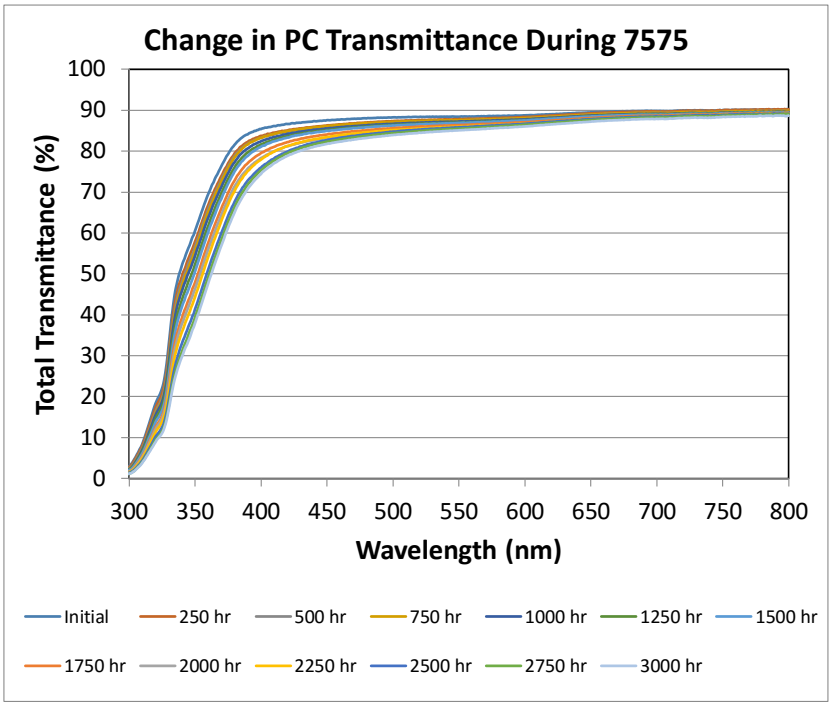

As shown in Figure 4A-14, the transmittance of the polycarbonate lens degrades at each wavelength as the time in 7575 increases. Chemical degradation in the polymer have been shown to be responsible for this process and several mechanisms have been proposed [22-26]. An important finding from previous studies is that photo-oxidation of polycarbonate

does not occur immediately, but instead, there is an incubation period lasting approximately 1,000 hours [22-25], suggesting that a logistic function may be used to model this process.

The extent of the transmittance changes in polymer also shows a wavelength dependence, with the transmission at low wavelengths decreasing faster than at longer wavelengths. For example, the transmittance at 450 nm decreased by 9.5% during 4,000 hours of 7575 while the transmittance at 750 nm decreased by only 2.72%. Consequently, the wavelength dependent change in transmittance (i.e., $d\%T_\lambda/dt$) needs to be considered in building these models. The differential change in transmittance also has a potential impact on the performance of SSL devices, because lumen maintenance and chromaticity stability will be affected.

By studying the aging of optical components under AST conditions, the values for $d\%T_\lambda/dt$ can be determined from Figure 4A-14 for PC and similar measurements for other materials. Graphs of the time-dependent changes in transmittance measured at wavelengths of 450 nm and 750 nm are given in ***Figure 4A-15***. The calculated slope of each graph corresponds to the first derivative of transmittance (i.e., $d\%T_\lambda/dt$) for that wavelength. To understand the impacts across the visible spectrum, such graphs must be created at each wavelength of interest, and ***Figure 4A-16*** shows a plot of the $d\%T_\lambda/dt$ values at select wavelengths between 400 nm and 750 nm. A least squares fit to the data is shown as a dotted line in Figure 4A-16 using the bounded exponential model. The least square fit was determined by minimizing the sum of the squared residuals (SSR), which is also termed sum of the squared errors of prediction (SSE). The resulting coefficient of determination (R^2) was computed to be 0.993. To further validate this model, we also calculated the Durbin-Watson statistic, which measures the degree of autocorrelation among the residuals. Ideally, the residuals should occur randomly around the fit line (as shown in Figure 4A-3). If the residuals have a high degree of autocorrelation and occur predominantly on one side of the fit line or another for four or more consecutive data points, the least squares fit may not be appropriate, even if R^2 is high. For the fit shown in Figure 4A-16, the Durbin-Watson (DW) statistic was calculated to be 2.34, which provides strong evidence that the residuals are not autocorrelated. Consequently, the least squares fit can be judged to be excellent.

The plot shown in Figure 4A-16 can be linearized by plotting the reciprocal of $d\%T_\lambda/dt$ versus wavelength as shown in ***Figure 4A-17***. By determining the $d\%T/dt$ values at different wavelengths, the change in optical properties of the polycarbonate lens used in SSL device can be calculated at any time during the AST measurements and can be correlated to the expected luminaire performance in the use environment, if the acceleration factors have been determined. The same procedure can be repeated for any material used in an SSL device to obtain the coefficients to model the degradation of the material during normal use. Common materials often found in SSL devices are listed in ***Table 4A-4.***

Figure 4A-15. Time Dependence of the Change in Lens Transmittance at Wavelengths of 450 nm and 750 nm for a Polycarbonate Lens Material for 7575 Exposure

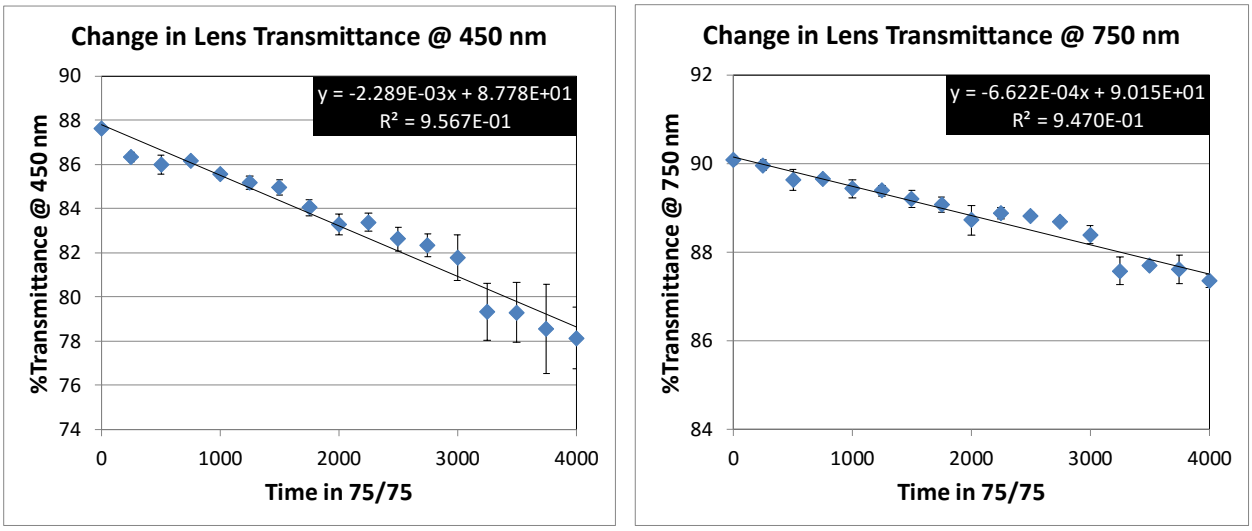

Note that the y-axis scales of the two graphs are different.

Figure 4A-16. Graph of the Slopes ($d\%T_\lambda/dt$) for Select Wavelengths in 7575

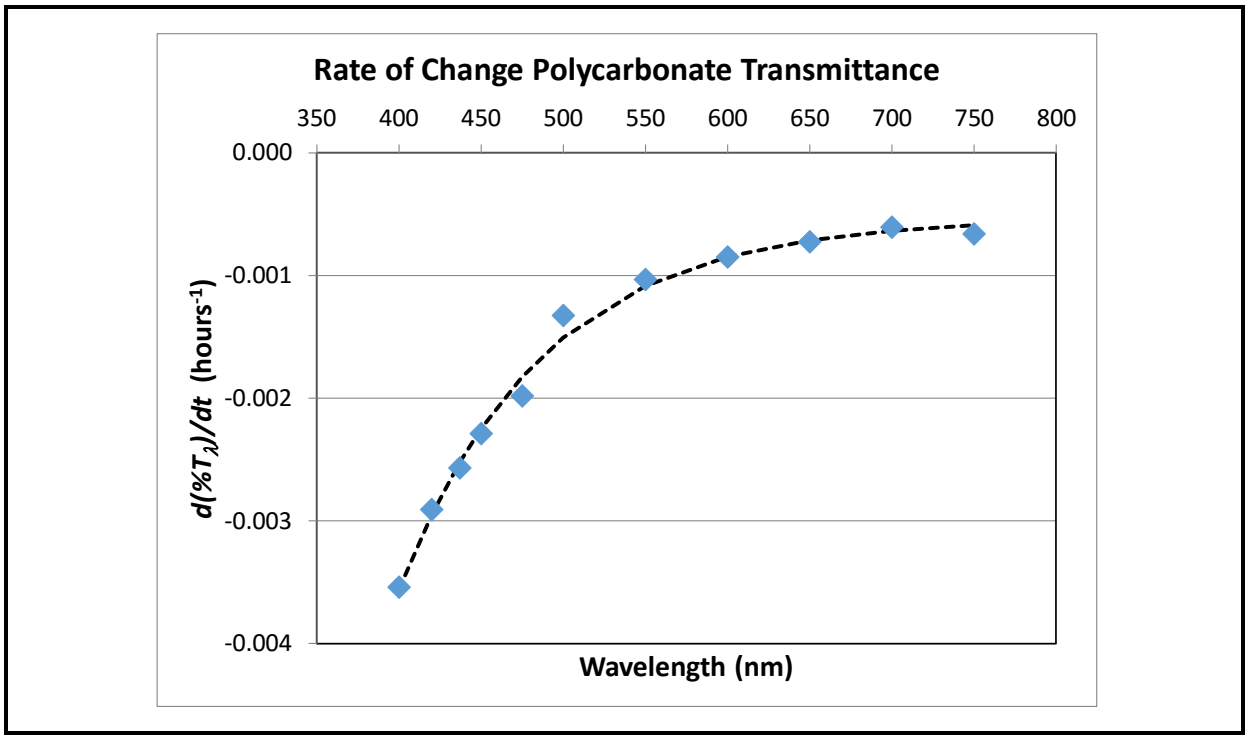

Note: The dotted line indicates the least squares fit using a bounded exponential model, $d\%T_\lambda/dt = 3.56*10^{-3} + 7.79*10^{-7}*(1 - e^{-(1.14*10-2)t})$. The least squares fit was judged to be excellent, because the R^2 value was 0.993, and the DW statistic was calculated to be 2.34.

Figure 4A-17. Fitting Coefficients for Polycarbonate Lenses as a Function of Wavelength for Exposure to 7575

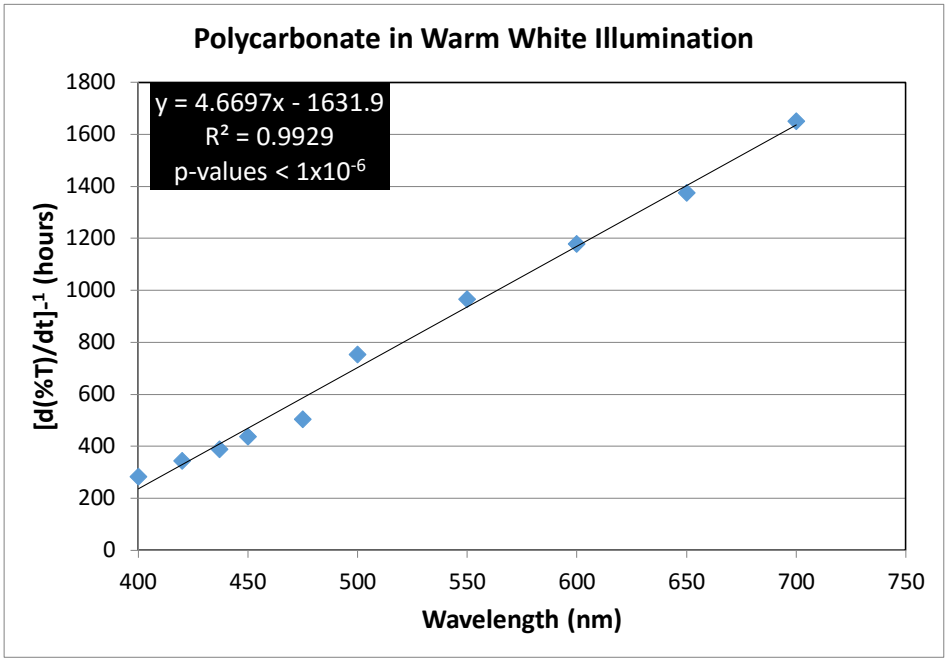

Table 4A-4. Common Materials Found in SSL Luminaires, Lamps, and LED Modules

SSL Device Element	Common Materials
Secondary Lenses	Polycarbonate (PC) Polymethyl methacrylate (PMMA) Silicones Glass
Secondary Reflectors	Polyethylene terephthalate (PET) films Microcellular foams of PET Silicone filled with rule-phase TiO_2 Polyolefin films surface coated with TiO_2 Paints usually filled with TiO_2 Polished aluminum Silver-coated aluminum
Solder masks	Photoimageable epoxies filled with additives
Encapsulants	Silicones Epoxies

Note: TiO_2 = titanium dioxide

In accelerated testing, the lens transmittance at each wavelength ($\%T_\lambda$) is degraded during use as shown in Figure 4A-14**.** This allows the transmittance at any given time to be calculated using **Equation (4A.16)**:

$$\%T_\lambda(t) = \%T_\lambda(0) + \frac{d(\%T_\lambda)}{dt} * t \qquad (4A.16)$$

where:

t = time

$\%T_\lambda(0)$ = initial lens transmittance (i.e., $t = 0$) for wavelength λ

$\%T_\lambda(t)$ = lens transmittance at time t for wavelength λ

$d(\%T_\lambda)/dt$ = change in lens transmittance with time (experimentally derived from 7575 data)

The values of $d(\%T_\lambda)/dt$ can be determined from either Figure 4A-16 or the linearized form in Figure 4A-17. These models have been built into the LM-DST for many of the secondary lens and reflector materials listed in Table 4A-4.

Chromaticity Shifts in LEDs

Kinetic models also can be constructed for the processes responsible for chromaticity shift in LEDs. The major white LED structure (i.e., phosphor-converted LED [pcLED]) uses emission from a blue LED and a broadband phosphor to produce white light. Therefore, kinetic processes affecting either the blue LED or the phosphor may be responsible for chromaticity shifts. In addition, some packages, such as mid-power LEDs (MP-LEDs), can have contributions to lumen maintenance loss and chromaticity shifts from the molding resin used in the LED [27-29]. Because the average emission wavelength of the phosphor is typically in the yellow to orange spectral regions, a change in the relative emissions from the phosphor or the blue LED causes a chromaticity shift along the blue-yellow line. In contrast, changing the emission properties of the phosphor can produce a chromaticity shift in the green or red directions. Because the processes involved in shifting chromaticity in the blue-yellow directions are fundamentally different from those in the green-red directions, the spectral behavior for these shifts, not surprisingly, is also different.

Fortunately, the chromaticity shifts that occur in LEDs provide spectroscopic markers of the transformation and degradation of materials involved in the optical path. At a high level, the chemical reactions that result in the spectroscopic changes that produce chromaticity shifts are either simple first-order conversion reactions—see (Equation (4A.8)—or the sequential first-order reaction process shown in (Equation (4A.10). The reactants A and B can be a variety of materials in the LED package, and the chromaticity shift process can involve a variety of chemical reactions, as outlined in ***Table 4A-5***.

In addition, A and/or B also can represent external chemical species such as water, oxygen, and volatile organic carbons that react with components inside the LED package to produce a chromaticity shift. Examples of this type of behavior include the intrusion of atmospheric oxygen to cause either oxidation of nitride [30-33].

Table 4A-5. Chemical Reactions Responsible for Chromaticity Shifts in LEDS

Chromaticity Shift Mode	Direction of Shift	Responsible Chemical Processes
1	Blue	▪ Annealing processes in epi layers ▪ Additional curing of silicones ▪ External cracks in the binder layer ▪ Expansion of the phosphor binder layer ▪ Moisture-induced expansion of the phosphor-binder layer
2	Green	▪ Oxidation of nitride phosphors
3	Yellow	▪ Delamination of phosphor-binder layer ▪ Internal cracks in the binder layer ▪ Yellowing of encapsulants
4	Yellow then Blue	▪ Photo-oxidation of molding resin
5	Red	▪ Partial quenching of green-emitting phosphor likely caused by oxygen

The reactions responsible for chromaticity shift in LEDs can be followed spectroscopically, because the properties of light emission from the LED change during the chromaticity shift, due to the kinetic processes associated with materials degradation. For example, a change in the relative populations of oxidized and unoxidized phosphor will change the emission profile of the LED and will alter its spectral power distribution (SPD) [30; 33]. Because chromaticity properties—such as u', v', $\Delta u'$, $\Delta v'$, $\Delta u'v'$, and CCT—are calculated from the SPD, any changes in the spectral emissions of the phosphor will also be reflected in these parameters.

RTI has developed a multiparameter procedure for modeling the chromaticity shift in LEDs, and this approach also can be used to project the chromaticity shift at future times. This procedure allows determination of the time required for parametric failure, due to excessive chromaticity shift, to be estimated. The chromaticity modeling procedure developed by RTI as part of this work was built from an examination of hundreds of datasets on chromaticity shift taken on LEDs, lamps, and luminaires. A key element of our procedure is a determination that chromaticity shifts can be modeled using the functions given in Table 4A-3. ***Table 4A-6*** summarizes the models that we have found often provide the best fit to

the different chromaticity shift modes (CSMs) [27]. In many cases, the models can be approximated by a straight line over the limited chromaticity shift range of interest in SSL applications (i.e., $\Delta u'v'$), because the bounded exponential and logistic functions approximate linear behavior (see Figure 4A-13) for a finite range of values.

Table 4A-6. Chemical Reactions Responsible for Chromaticity Shifts in LEDs

Chromaticity Shift Mode	Direction of Shift	Likely Model
1	Blue	Bounded Exponential
2	Green	Bounded Exponential and Logistic
3	Yellow	Logistic
4	Yellow then Blue	Logistic
5	Red	Logistic

In determining the nature of chromaticity shift in LEDs, dividing the shift process into three stages is beneficial, as shown in ***Figure 4A-18***. For simplicity, these stages are shown using a $\Delta u'v'$ plot, although the changes could as be shown using time-based plots of u', v', $\Delta u'$, or $\Delta v'$, as will be shown throughout the remainder of this report.

There are two processes responsible for the chromaticity shift in Figure 4A-18**,** one that is dominant from the time the LED is turned on until around 2,000 hours, when the second process becomes dominant. We term the first process the burn-in stage of chromaticity shift, and this process in analogous to the initial luminous flux increase discussed earlier. The second stage is the emergent stage, which becomes dominant after an incubation period of roughly 2,000 hours in this instance. For the results shown in Figure 4A-18, The emergent stage continues until the terminal chromaticity shift (i.e., $\Delta u'v' > 0.007$) is reached, and the device becomes a parametric failure for excessive chromaticity shift.

Figure 4A-18. Representative Example of the Change in $\Delta u'v'$ of an LED Showing the Three Major Stages of Chromaticity Shift During LED Lifetime

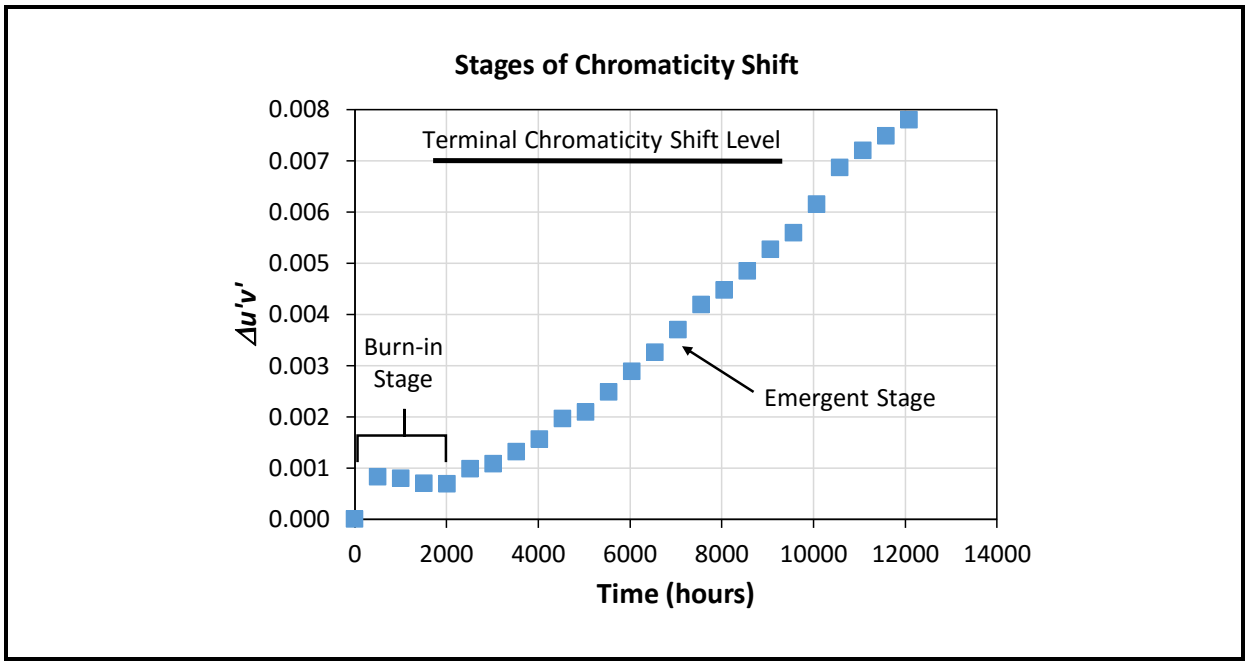

This burn-in stage is characterized by a rapid change in chromaticity, often in the blue or green directions, when the device is first turned on, followed by a period of essentially little change in chromaticity. This chromaticity behavior is found in most LED devices including luminaires [33] and LED lamps [27]. An analogous effect is often found for luminous flux maintenance during the early stage of LED operation [8]. The rapid rise to an asymptote observed during this stage is suggestive of bounded exponential behavior.

In contrast, the emergent stage, which is characterized by a period of monotonic change in chromaticity, occurs after the burn-in stage and becomes observable after a prolonged period of device operation. The rise of the emergent stage is easiest to detect in the time-dependent profiles of the u' and v' chromaticity coordinates, because one of these coordinates usually changes before the other [27]. In some cases, the emergent stage continues until the terminal chromaticity shift is reach (e.g., $\Delta u'v' > 0.007$) and the device becomes a parametric failure. As will be shown later in this report, more than one emergent stage is possible, each with separate incubation periods, if multiple processes are necessary to reach the terminal shift point. In that instance, the first emergent stage will typically reach an asymptotic value short of the parametric failure threshold, and a second process, usually occurring at a different rate, eventually emerges and may produce parametric failure. Emergent stage chromaticity shifts are often best modeled with a generalized logistic model, and the monotonic increase can be approximated by a linear function for a limited time.

The procedure that RTI uses to model chromaticity shifts consists of the following steps:

Step 1. **Build a model for the lowest stress condition**. Often this model will be a bounded exponential value and provides an indication of the maximum value of the initial chromaticity shift during the burn-in stage. This model can be used as a starting point for coefficient estimates in models for higher stress conditions.

Step 2. **Build a model for highest stress conditions, using combinations of the bounded exponential and generalized logistic functions shown in Table 4A-6.** The highest stress condition occurs at the highest temperature and current setting and usually results in the largest chromaticity shift in the test data. A key point to note when examining this data is the appearance of asymptotic values (i.e., *A* for logistic and bounded exponential models). The onset of an asymptote in the experimental data sometimes can be detected early by looking for deviations from linearity in the emergent stage. The determination of asymptotic values is important, because this number can be used in building models under lower stress conditions.

Step 3. **The models for the highest stress and lowest stress conditions help to set the appropriate parameters for deconvoluting the chromaticity behavior at in-between values.** For example, with the logistic model, determining the coefficients is often easier under high stress conditions, and these values can be used as starting points for lower stress conditions.

Step 4. **Build generalized logistic and bounded exponential models for lower stress conditions, as appropriate**. Deconvolute the chromaticity behavior using the models and model parameters from the lowest stress (for bounded exponential models during the burn-in stage) and highest stress (for generalized logistic models during the emergent stage) conditions as starting points. The rate constant (*k*) should change between experimental conditions, but other parameters will stay relatively steady.

Step 5. **Perform a linear regression fit on the values of the rate constant *k*,** once the parameters for the model fit have been determined for the different conditions, to determine values at stress conditions that were not tested.

An example of the use of this procedure is given in ***Figure 4A-19*** for a MP-LED product. For simplicity, the chromaticity shift procedure is only demonstrated for $\Delta u'v'$, although the same procedure can be used on u' and v' individually.

Figure 4A-19. Data and Chromaticity Model Fits for a MP-LED Product Under Low Stress Condition (Left) and High Stress Condition (Right).

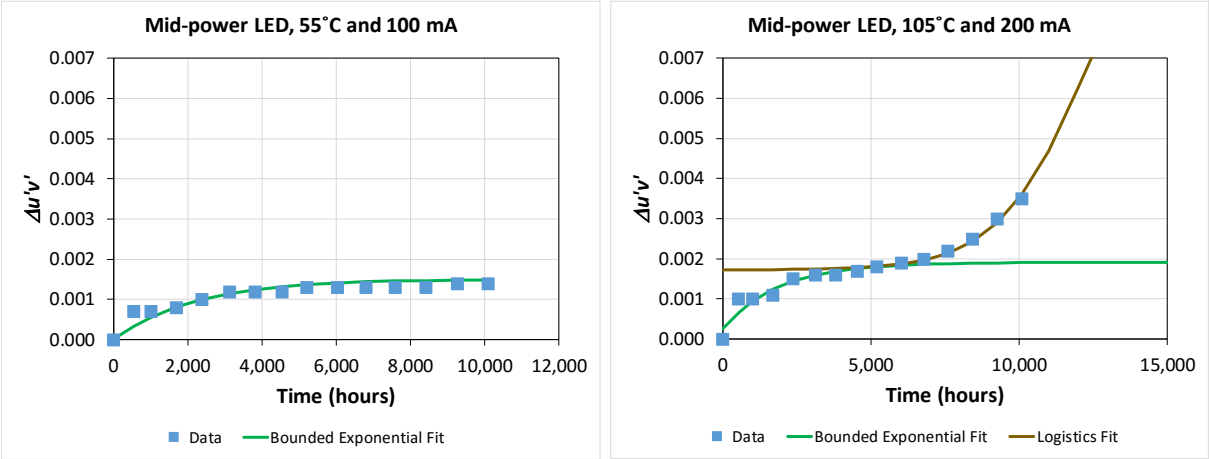

In this example, the lowest stress condition (i.e., 55˚C and 100 mA) and the highest stress conditions (i.e., 105˚C and 200 mA), given in the LM-80-08 report for this product, is modeled in Figure 4A-19. In addition, other information reveals that the initial chromaticity of this product is in the green direction, followed by a shift in the blue direction. By examining all the data, we determined that this product exhibits CSM-1 behavior with the terminal chromaticity shift being in the blue direction. The terminal chromaticity shift is the process that causes the chromaticity to exceed a predetermined limit, which we assume to be a total chromaticity shift ($\Delta u'v'$) greater than 0.007 in accordance with EnergyStar® requirements [34]. We attribute the initial green shift to oxidation of the Eu-doped nitride phosphors in the warm white product [30-33], while the blue shift is attributed to photo-oxidation of the molding resin used in the MP-LED package [27; 28].

The initial chromaticity shift, which is in the green direction, can be modeled with a bounded exponential; however, the terminal blue shift that is characteristic of CSM-4 behavior is best modeled with a logistic function. The parameters produced by a least squares fit of a bounded exponential model to the data acquired under low stress conditions are given in ***Table 4A-7***. For the high stress condition shown in Figure 4A-19, a bounded exponential model provided a good explanation of the initial green shift behavior of the LED, and the parameters of this model closely align with those of the low stress condition, as shown in Table 4A-7. The *k*-value (i.e., reaction rate) is higher at 105˚C and 200 mA, as might be expected. However, around 6,000 hours, a new chromaticity shift mechanism becomes dominant. Accordingly, a logistic model was used for this behavior and the equation of the least squares optimized least squares fit is given in Table 4A-7. Because the output from the logistic model is offset by the initial chromaticity condition (i.e., Model 1) for the high stress condition, the logistic model is shifted accordingly by the parameters C_1 and C_2 in Table 4A-7. Only the generalized logistic model can be used to project the time for parametric

failure due to chromaticity shift, because the initial green shift does not cause more than a 0.002 change in $\Delta u'v'$. Based on this analysis, the time required for $\Delta u'v'$ to exceed 0.007 is projected to be 12,450 hours at 105°C and 200 mA.

Table 4A-7. Models and Fitting Parameters Used in Least Squares Optimization of the Data Shown in Figure 4A-19

	Low Stress Condition	High Stress Condition
Model 1	Bounded Exponential	Bounded Exponential
Applicable Time	0 – 10,000 hours	0 – 6,000 hours
Model 1 Equation	$\Delta u'v' = (1.50 \times 10^{-3})*\{1 - \exp[(-4.58 \times 10^{-4})*t]\}$	$\Delta u'v' = (2.44 \times 10^{-4}) + (1.66 \times 10^{-3}) * (1 - \exp[(-5.35 \times 10^{-4})*t]$
Model 1 SSE[a]	2.75×10^{-7}	2.12×10^{-7}
R^2	0.913	0.956
Model 2		Generalized Logistic
Applicable Time		> 6,000 hours
Model 2 Equation		$\Delta u'v' = C_1 + (1.00 \times 10^{-2})/\{1 + 114.9*\exp[(6.71 \times 10^{-4})*(t - C_2)]\}$[b]
Model 2 SSE[a]		3.39×10^{-8}
R^2		0.994

[a] SSE is the sum of the squared errors and is used in optimizing the least squares fit.

[b] C_1 and C_2 are x-axis and y-axis adjustment parameters that are used to shift the logistic function, because its impact occurs after the green shift represented by Model 1.

By performing this analysis at all measured values in the LM-80-08 dataset, a correlation was found with LED T_j and I_f as the predictor variables and the reaction rate constant (k) as the dependent variable. In performing this analysis at different settings, the parameters for the high stress condition are used as guides for the initial estimate of parameters such as A (i.e., the maximum shift) for both the bounded exponential and generalized logistic functions. The least squares optimization process adjusts the remaining parameters in the model until the optimal least squares fit is obtained, given this starting point and parameter constraints. The parameters for this MP-LED product at different values of the predictor variables is given in ***Table 4A-8*** along with the model for total chromaticity shift ($\Delta u'v'$) at 10,000 hours based on T_j and I_f values.

Table 4A-8. *k* Values for the HP-LED Shown in Figure 4A-12 for All Measured Values of Temperature and Current

Predictor Variables		Logistic Model Parameters				
Temperature (˚C)	**Current (mA)**	**C**	***k* value**	**A**	**X-Axis Offset (C_1)**	**Y-Axis Offset (C_2)**
105	100	120.00	3.342E-04	1.200E-02	6000.0	0.00155
55	150	131.00	3.342E-04	1.100E-02	8000.0	0.00145
85	150	131.14	3.366E-04	1.084E-02	5000.0	0.0016
105	150	121.44	4.992E-04	1.121E-02	5123.3	0.0018
55	200	115.00	4.042E-04	1.200E-02	7000.0	0.00158
85	200	116.34	6.581E-04	1.267E-02	5500.0	0.0017
105	200	114.95	6.708E-04	1.000E-02	5210.0	0.00172
$\Delta u'v'$(10,000 hours) = $(4.41 \times 10^{-6}) * T_j + (3.54 \times 10^{-7}) * I_f - 4.94 \times 10^{-4}$						
$R^2 = 0.88$ Sum of Squares of Errors (SSE) = 1.64×10^{-8}						

Note: °C = degrees Centigrade; mA = milliampere.

4.A.5 Projection of Chromaticity Shift

Projecting chromaticity shift over time is more difficult than projecting luminous flux maintenance, and to date there is no chromaticity shift analog for TM-21-11. This is because the direction of chromaticity shift can change in time, which not only creates uncertainty in the shift direction but in the magnitude. While luminous flux maintenance generally decreases after the burn-in stage, the magnitude of chromaticity shift can decrease after the burn-in period during the early parts of the emergent stage and then increase for an indeterminate period.

The Illuminating Engineering Society (IES) has formed a subcommittee to work on developing a method for projecting chromaticity shift, which will be called TM-31. The goal of the TM-31 subcommittee is to develop a single, parameterized equation for projecting chromaticity in the future. This subcommittee is looking at a quadratic fit calculated on either the derivative of the individual chromaticity changes with time (i.e., differential chromaticity analysis) [35] or an analytical equation of the form $at^2 + bt + c$, where t is time and a, b, and c are fitting coefficients. However, the approach currently under consideration by the TM-31 subcommittee always will produce a conservative estimate, and the estimated chromaticity maintenance always will be lower than the actual value. This fact is a consequence of the use of a quadratic model, because the impact of time on the calculated chromaticity maintenance increases as t^2. In addition, the approach being considered by the TM-31 subcommittee does not have the necessary upper and lower bounds on the chromaticity shift as discussed in this report. Although the TM-31 subcommittee approach has several limitations, it does produce a number for chromaticity maintenance that can be used to compare products.

One approach to increasing the accuracy of chromaticity shift projections is to wait for the emergent stage to appear and project chromaticity from that time. As discussed earlier, the terminal chromaticity shift of a pcLED can be accurately modeled with a generalized logistic function, and a generalized logistic function can be modeled by a line over much of the function, except for the beginning and end. By fitting only the chromaticity shift of u', v', or $\Delta u'v'$ during the emergent stage, reasonable estimates can be obtained of the time necessary for a given level of chromaticity shift (e.g., 7-step or 3-step) to occur. Examples of such projections for HP-LEDs and MP-LEDs are shown in ***Figure 4A-20*** and ***Figure 4A-21***, respectively. A close examination of both figures illustrates that an informed selection of LED products and operating conditions allows a consistent chromaticity point to be maintained for an extended period. Conversely, the selection of a poorly performing product and operating conditions will result in low chromaticity maintenance. The data points shown in red in Figure 4A-21 are for the same LED product operated under conditions between 55°C and 65 mA and 105°C and 100 mA. Clearly, this product will perform poorly under all operating conditions, but there are other MP-LED products that will maintain a stable chromaticity point (within a 7-step MacAdam ellipse) for 100,000 hours or longer.

Figure 4A-20. Projected Time to 3-Step (Orange Diamonds) and 7-Step (Blue Circles) Chromaticity Shifts for HP-LEDs

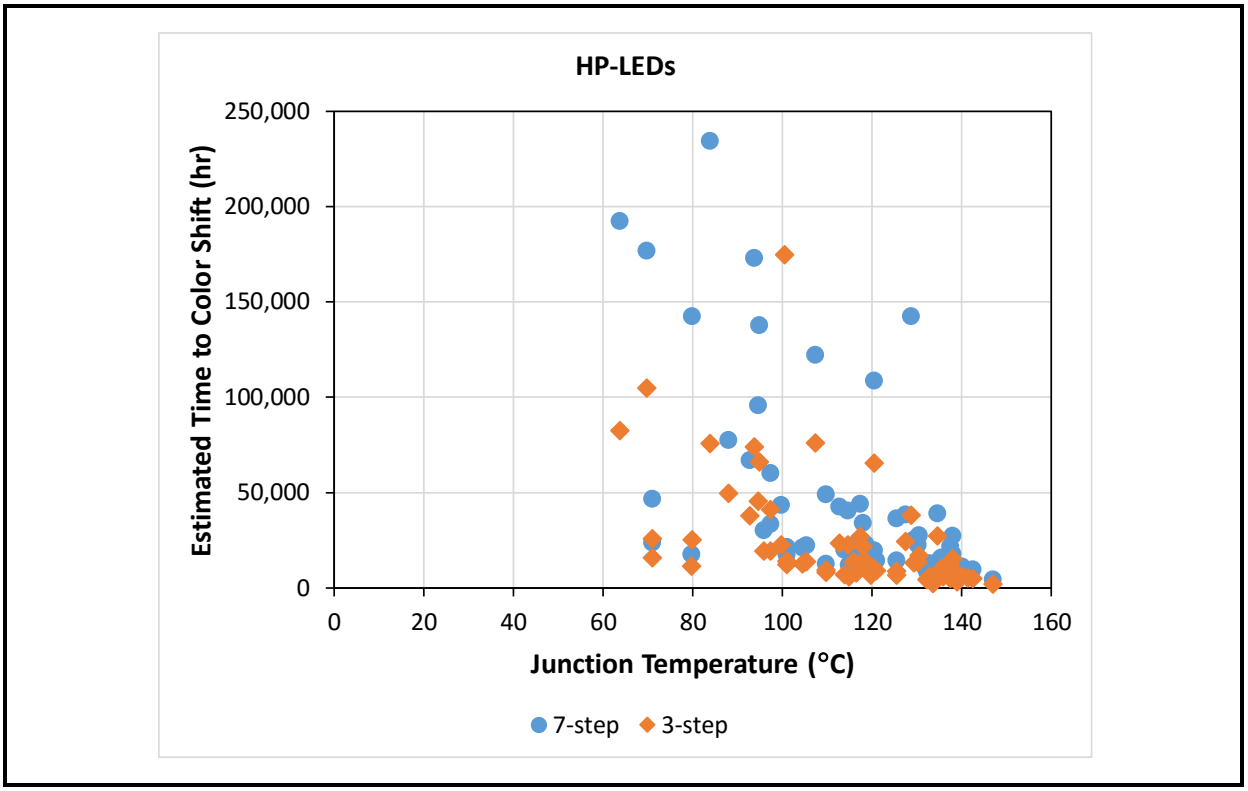

Figure 4A-21. Projected Time for 7-Step Chromaticity Shift for MP-LEDs

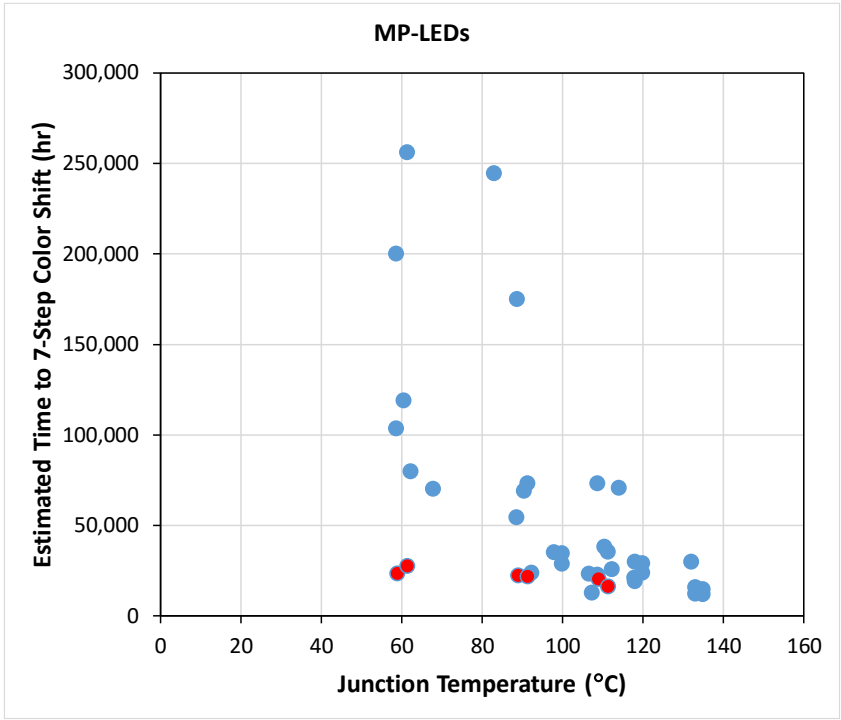

4.A.6 Virtual Models of the Impact of Lumen Degradation

When a luminaire is new, its luminaire efficiency, which is defined as the ratio of luminous flux (lumens) emitted by a luminaire to that emitted by the light source (e.g., LEDs or lamps used therein) is at its maximum value. As the optical components of the luminaire age, the luminaire efficiency will degrade in a systematic manner which can change the chromaticity point. Thus, when considering the chromaticity maintenance of LED-based lighting source, changes in the LEDs and the optical components (i.e., lenses and reflectors) of the luminaire, such as those described in Equation (4A.16), need to be considered. In addition, the relative impacts of lens and reflector degradation will depend on the design of the luminaire. For example, a design without an optical mixing cavity will not be affected greatly by reflector degradation but will be impacted by lens degradation, because all photons go through the lens. This phenomenon can be studied for nearly any luminaire design by using optical simulation tools. This simulated or "virtual" luminaire approach, which is illustrated here, involves designing a luminaire in an optical ray-tracing simulation tool, such as Photopia, that includes the selection of the initial optical properties of the lenses and reflectors. Then, the properties of these materials can be degraded in a systematic manner, and the impacts on luminaire performance can be determined.

For this analysis, any luminaire design can be modeled for any expected physical parameters, including size and optical cavity depth. As a first step, the reflectance and transmittance of optical components in the luminaire are normalized to their initial values. Aging of materials used in luminaires could be accommodated easily in the simulation by attenuating the optical properties of the materials. For example, the impact of a 10% drop in lens transmittance can be simulated by reducing normalized lens transmittance by 10% to a normalized value of 90%. Transmittance is normalized by the initial transmittance of the pristine material. By systematically changing the design parameters and simulating aging of the optical surfaces by introducing new values for normalized transmittance and reflectance, a model can be created to determine the change in luminous flux produced by the luminaire during aging of its optical components. A simple power-law model of the form shown in **Equation (4A.17)** captures the impact of optical materials degradation on lumen maintenance for the LED device:

$$\Phi_{tot}(t) = \Phi_{init} F_{LEDs} [L(t)]^m [R(t)]^n \quad (4A.17)$$

where:

Φ_{tot} = total luminous flux from the luminaire at time t

Φ_{init} = initial luminous flux from the luminaire at time zero. This value is also the product of the luminous flux from the light engine and the luminaire efficiency when both are new.

F_{LEDs} = lumen maintenance factor of the LED at time t

$L(t)$ = change in the normalized lens transmittance *[%T(t)/%T(t = 0)]* at time t

M = design-dependent factor for the lens as determined from a least squares fit on the simulation results

$R(t)$ = change in the normalized reflector reflectance *[%R(t)/%R(t = 0)]* at time t

N = design-dependent factor for the reflector as determined from a least square fit on the simulation result

An example of the output from a typical simulation for a 2-foot × 4 foot troffer (hereafter termed 2x4) with a 3-inch optical mixing cavity is shown in ***Table 4A-9***. Inputs to the optical simulation tool are provided in the yellow boxes in Table 4A-9, outputs from the simulation are given in the green boxes, and the model prediction using Equation (4A.17) with m = 2.04 and n = 0.52 are given in the blue boxes.

In this simulation, the light engine for the luminaire consisted of 121 MP-LEDs, the luminaire lens was a common PMMA lens material, and the reflector was a high-performance PET reflector. As shown in Table 4A-9, various "virtual luminaires" were

created by attenuating the lens transmittance and reflector reflectance in 5% increments from their normalized initial values. The impact of these materials changes luminaire efficiency and will likely change the chromaticity of any light produced by the luminaire as well. Ignoring the effects of LED lumen depreciation, Equation (4A.17) can be recast into a model for luminaire optical efficiency degradation as shown in **Equation (4A.18)**.

$$LE(t) = LE(t=0)[L(t)]^{l}[R(t)]^{r} \quad (4A.18)$$

where:

LE(t) = luminaire efficiency at time *t*

LE(t = 0) = initial luminaire efficiency

L(t) = change in the normalized lens transmittance *[%T(t)/%T(t=0)]* at time *t*

l = design-dependent factor for the lens as determined from a least squares fit of the simulation results.

R(t) = change in the normalized reflector reflectance *[%R(t)/%R(t=0)]* at time *t*

r = design-dependent factor for the reflector as determined from a least squares fit of the simulation results.

Table 4A-9. Optical Ray Tracing Simulation Inputs, Outputs, and Comparison to a Model for a Virtual 2 × 4 Troffer With a 3-Inch Deep Optical Mixing Cavity

Inputs to Photopia	Test 1	Test 2	Test 3	Test 4	Test 5	Test 6	Test 7	Test 8	Test 9
Reflector % (of orginal reflectance)	100%	100%	100%	95%	95%	95%	90%	90%	90%
Lens % (of orginal trasmittance)	100%	95%	90%	100%	95%	90%	100%	95%	90%
Cavity Height	3"	3"	3"	3"	3"	3"	3"	3"	3"
Photopia Calculated Values									
Luminaire Efficiency	94.7%	85.2%	76.3%	92.5%	83.4%	74.7%	90.6%	81.6%	73.2%
Output Lumens	4582	4125	3694	4479	4034	3614	4385	3952	3541
Intensity at Nadir (cd)	1637.4	1474.7	1324.7	1608.8	1450.9	1298.9	1572.2	1429.9	1272.6
Full Beam Angle (90-270° plane)	108.6	108.4	108.3	108.2	107.8	108.0	107.8	107.4	107.7
Spacing Criterion (90-270° plane)	1.27	1.27	1.27	1.27	1.27	1.27	1.27	1.26	1.27
RTI Model Prediction	94.7%	85.3%	76.5%	92.6%	83.4%	74.8%	90.4%	81.5%	73.0%
Difference Between RTI and Photopia	0.0%	0.1%	0.2%	0.1%	0.0%	0.1%	-0.2%	-0.1%	-0.2%
Percent of Luminaire Efficiency	0.0%	0.2%	0.2%	0.1%	0.0%	0.1%	-0.2%	-0.1%	-0.3%
Absolute Value of Percent Efficiency	0.0%	0.2%	0.2%	0.1%	0.0%	0.1%	0.2%	0.1%	0.3%

The parameters *l* and *r* take into account the impact of the luminaire design on the relative contributions of lens and reflector aging upon the degradation in luminaire efficiency. For example, in the 2 × 4 troffer design shown in Table 4A-9, *l* is approximately 2 and *r* is approximately 0.44, indicating that the degradation of the lens has a much greater impact

on changes in luminaire efficiency, and by extension chromaticity stability, than the degradation of the reflectors. However, for luminaires with smaller apertures and proportionally deeper optical mixing cavities, the value of *r* can equal or surpass the value of *l*, indicating that reflector degradation has a significant impact on overall luminaire efficiency changes in some designs [20].

This finding is illustrated in ***Table 4A-10***, which provides the values of *l* and *r* for different luminaire designs. These values were calculated for different luminaire designs using the procedure described above. An examination of the values of *l* or *r* provides insights into the impact of lens and reflector degradation on the luminous efficacy maintenance of luminaires. In virtually every design, the impact of the lens is the dominant factor, especially in designs with a small optical mixing cavity. However, as the optical mixing cavity becomes deeper, degradation of the reflector has an increased impact.

There are two designs that deserve special attention. For the 6-inch circular downlight, the walls of the mixing cavity tapered from 3 inches at the base of the optical cavity to 5 inches at the light exit. In this case, degradation of the reflector covering the walls has a much greater impact than if the walls were vertical. In fact, for the 3-inch deep tapered optical cavity, the impact of the reflector is greater than that of the lens. A second special luminaire design that merits discussion is a parking garage lamp in which a secondary lens is placed directly over the LED, and there is no separate mixing cavity. In this design, the reflector has no impact (i.e., $r = 0$) and the degradation of the lens impacts luminous flux maintenance by a power of 0.45, which is roughly a square root dependence.

Table 4A-10. Values of the Exponents *l* and *r* for Different Luminaire Designs

Luminaire Type	LED Type	Value of *l*	Value of *r*
2' x 4' Troffer, 3” deep optical cavity	MP-LED	2.03	0.44
2' x 2' Troffer, 3” deep optical cavity	MP-LED	2.04	0.52
6” x 24” linear, 3” deep optical cavity	MP-LED	2.10	1.33
6” x 24” linear, 2” deep optical cavity	MP-LED	2.11	0.91
6” x 24” linear, 1” deep optical cavity	MP-LED	2.09	0.48
6” x 12” linear, 3” deep optical cavity	MP-LED	2.12	1.49
6” x 12” linear, 2” deep optical cavity	MP-LED	2.11	1.02
6” x 12” linear, 1” deep optical cavity	MP-LED	2.08	0.50
6” x 6” square downlight, 3” deep optical cavity	MP-LED	2.10	1.92
6” x 6” square downlight, 2” deep optical cavity	MP-LED	2.12	1.25
6” x 6” square downlight, 1” deep optical cavity	MP-LED	2.10	0.57
6” circular downlight with straight walls, 3” deep optical cavity	MP-LED	2.07	1.13

(continued)

Table 4A-10. Values of the Exponents *l* and *r* for Different Luminaire Designs (continued)

Luminaire Type	LED Type	Value of *l*	Value of *r*
6" circular downlight with straight walls, 2" deep optical cavity	MP-LED	2.05	0.73
6" circular downlight with straight walls, 1" deep optical cavity	MP-LED	2.03	0.30
6" circular downlight with tapered walls, 3" deep optical cavity	HP-LED	1.00	1.35
6" circular downlight with tapered walls, 2" deep optical cavity	HP-LED	1.03	0.95
6" circular downlight with tapered walls, 1" deep optical cavity	HP-LED	1.05	0.55
Park garage lamp with secondary lens directly over LED	HP-LED	0.45	0

Conceptually, the value of *r* can be thought of as being proportional to the likelihood that light emitted by an LED at the base of an optical cavity will strike the reflector in that optical cavity and be impacted by reflector degradation. For example, with for a 6-inch downlight with a 3-inch optical mixing cavity with tapered walls (i.e., the aperture is 6 inches, and the optical mixing cavity depth is 3 inches, for a 6:3 ratio), there is an increased likelihood that aging of the reflector will impact luminaire efficiency and chromaticity stability, so the value of *r* is high. In contrast, for a 6-inch downlight with a 1-inch optical mixing cavity (i.e., the aperture is 6 inches, and the optical mixing cavity depth is 1 inch, for a 6:1 ratio), the impact of reflector aging on luminaire efficiency is reduced, so *r* is less. In either case, the light must pass through the lens so the impact of its degradation on luminaire efficiency and chromaticity stability changes little. Consequently, the impact of reflector degradation on lumen maintenance and chromaticity stability can be reduced by shrinking the optical mixing cavity, but this also may change the distribution and homogeneity of the light emitted by the luminaire. In addition, the impact of lens degradation varies widely with luminaire design, and the value of the exponent *l* ranges from 0.45 for the parking garage luminaire to ~2 for luminaires with vertical walls on the optical cavity.

4.A.7 Weibull Models of SSL Device Failure

The two-parameter Weibull distribution is widely used in reliability statistics to model failure rates as a function of time. The exponential form of the Weibull equation is given in **Equation (4A.19)** and the linear form of the equation is given in **Equation (4A.20)**.

$$F(t) = 1 - \exp(-t/\eta)^{\beta} \tag{4A.19}$$

$$\ln(-\ln(1-F(t)) = \beta\ln(t) + \beta\ln(\eta) \quad (4A.20)$$

where:

$F(t)$ = population fraction failing at time t

β = Weibull shape parameter. $\beta = 1$ is for constant failure rate, and $\beta > 1$ is for wearout phenomena

t = time

η = Weibull scale parameter (characteristic life).

There are multiple sources of additional information about using the Weibull equation in accelerated life testing (ALT) and in assessing product reliability. The textbook by Nelson is a good reference [36].

The Weibull distribution is a common tool that is used in the evaluation of product life, and it can model decreasing (e.g., $\eta < 1$ due to the burn-in stage), stable (e.g., $\eta = 1$), and increasing (i.e., $\eta > 1$ in wear-out stage) failure rates. The linearize form of the Weibull equation given in **Equation (4A.20)** facilitates the creation of Weibull plots that facilitate an analysis of data. In a typical Weibull analysis, the fraction of the population that has failed—F(t)—is plotted against time in a log-log graph, and the slope of the plot gives the value of β. β values of 1 indicate that the failure rate is constant in time, while β values greater than 1 indicate a rate of failure that increases with time. The intercept of the linearized Weibull equation is the characteristic life (η), which is equal to the time when 63.2% of the population has failed. In some uses, β is termed the shape parameter, because changing β affects the shape of the distribution, and η is termed the scale parameter, because changing η affects the scale of the failure time.

An example of the use of the Weibull parameter is given in the Hammer test report and reproduced in ***Figure 4A-22*** [37]. A two-parameter Weibull model was used to fit the data, and maximum likelihood estimator (MLE) methods were used to account for censored data. Censored data are data where the experiment has stopped or been suspended, whereas MLE methods provide an estimate of the failure time of samples where failure occurred in the interval between measurements (i.e., interval censored) and testing has been suspended (i.e., censored data). Because the performance of the luminaires was tested before each loop of the Hammer test, and their continued performance (or lack thereof) is verified after each loop (i.e., after 42 hours of testing), the exact failure time is unknown. This prompted the data to be treated as interval censored data for all failures in the Weibull analysis. In other words, the sample failed during this 42-hour span; although the exact failure time is not known, it can be approximated with MLE methods. Devices that were still operational at the end of the Hammer test were treated as right censored data, meaning

that they will likely fail in the future. Median rank methods were applied to the censored data. This treatment of the data resulted in the following parameters for the Weibull model:

- Shape parameter (β) = 1.935
- Characteristic lifetime or scale parameter (η) = 995.9

Because the β value was greater than 1, wear out phenomena are responsible for the failure of the luminaires. This observed value of β demonstrates that the Hammer Test is an acceleration test.

Figure 4A-22. Weibull Probability Plot for the Luminaires Subjected to the Hammer Test [37]

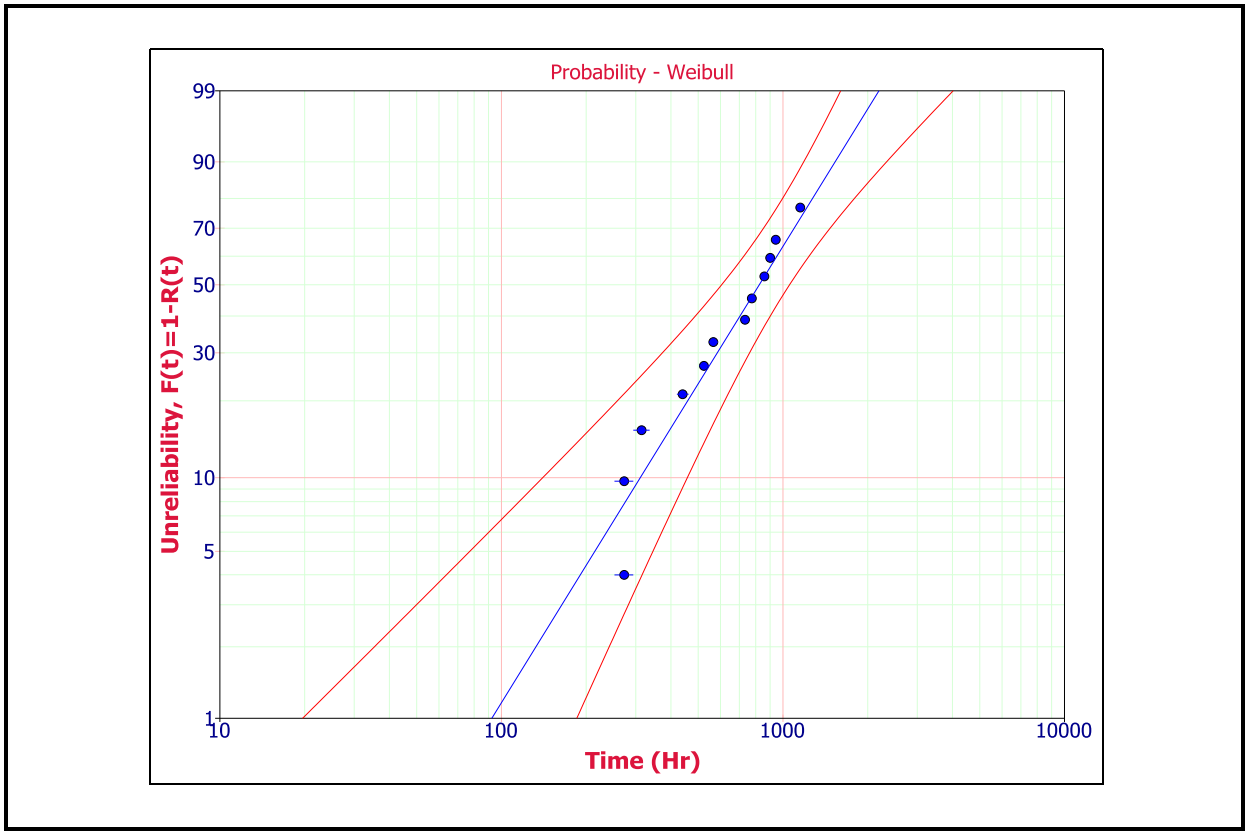

An advantage of the Weibull approach to building reliability models is that the basic Weibull equation can be used to calculate a variety of statistical parameters that describe the reliability of a sample population, including product reliability, failure rate in time (FIT), probability density function (known as pdf), and cumulative failure probabilities [36]. Multiple examples of the use of Weibull function are given in this report, especially during the discussion of luminaire failure rates.

4.B Individual LED Behavior

4.B.1 Industry Data on Lumen Maintenance of Individual LEDs

A LED manufacturer typically provides lamp and luminaire manufacturers with data on the long-term luminous flux and chromaticity maintenance of the LEDs it sells. The Illuminating Engineering Society of North America (IES) has established a standard test method (LM-80-08) that has been adopted by the lighting industry to ensure uniformity in reporting this information [2]. The LM-80-08 method consists of regular measurements of luminous flux after exposure of a population (typically 25 samples or more) of LED packages, arrays, or modules to elevated temperatures. LM-80-08 specifies that at least three test temperatures must be used in testing: 55°C, 85°C, and a third temperature of the manufacturer's choosing. Separate populations of LEDs are used for each test temperature. LM-80-08 also requires that the total chromaticity shift be reported as $\Delta u'v'$, but makes no requirements that the individual chromaticity coordinates also be given. Although $\Delta u'v'$ is a scalar property that provides information on the magnitude of the total chromaticity shift of the LED, it does not provide any information on the direction of the shift. Recently, the IES LM-80-08 standard was updated with an eye toward reducing testing burden. The LED manufacturers must now provide reports on data at two temperatures, one of which must be either 55°C or 85°C, and a second of the manufacturer's choosing [4]. In addition, LM-80-15 reports must now include the individual chromaticity coordinates, u' and v', which provides additional insights into the chromaticity behavior of the LEDs.

The data produced by the LM-80-08 and LM-80-15 testing protocols can then be used to project the long-term lumen maintenance of LED light sources at each test temperature using methods described in IES TM-21-11 [1]. The projection protocol assumes an exponential decay in LED lumen maintenance after the first 1,000 hours. The form of the luminous flux maintenance decay can be expressed by Equation (4B.1):

$$\Phi(t) = Be^{-\alpha t} \tag{4B.1}$$

where $\Phi(t)$ is the normalized luminous flux output at time t, B is a projected initial constant of normalized luminous flux, and α is the decay rate constant. In addition to an exponential fit, a series of empirical rules are applied in the TM-21-11 fitting protocol, including (1) requiring a minimum of 6,000 hours of test data at each test temperature; (2) using only the last half of the data set for tests lasting 10,000 hours or longer; and (3) discarding the first 1,000 hours of test data in the exponential fit. The parameter, α, provides an inverse measure of the lumen maintenance of the light source. Larger α values indicate lower luminaire maintenance levels (i.e., higher lumen depreciation). LED junction temperature has been shown to have a significant influence on α values. LED junction temperature in turn is a function of the current flowing through the junction, ambient temperature, and the specifics of the LED package structure as designed by the manufacturer.

Building models of lumen maintenance for SSL luminaires requires knowledge of the luminous flux maintenance of the LEDs used in the luminaire, as the LED is a principal contributor to luminaire-level performance. However, many LED products are on the market, and their performance specifications are constantly improving. Furthermore, LM-80 data and TM-21-11 projections are often viewed as confidential information by LED manufacturers and are not readily available to the general lighting public. Therefore, it is difficult and costly to build and maintain an up-to-date library of the large amount of TM-21-11 data being generated. Koh et al. showed that it is possible to use LEDs with α values below a threshold value and still meet certain product requirements, such as EnergyStar, depending on the design goals for the luminaire [34]. Therefore, instead of building models for every LED product, RTI decided to construct general models for each major package architecture. These models are based on linear regression models of a sampling of TM-21-11 projections from available LM-80 data. This information can help facilitate luminaire-level models by providing consistent information about average LED performance, by package type, across a range of operational conditions. After consultation with DOE, this approach was pursued in the research reported here. Additional information on the models developed using this method is provided in Section 4.A. This section will concentrate on the application of these models to SSL devices and the resulting findings.

As part of our efforts to collect data from the industry, beginning in 2011, we contacted major LED manufacturers about supplying data for the project team to evaluate. Dr. Monica Hansen of LED Lighting Advisors was enlisted in 2013 to help lead the effort, and we continued to push major LED manufacturers to provide updated LM-80 reports and, when possible, additional information, such as chromaticity coordinates. During this project, we collected more than 250 LM-80 reports, covering most major package types, as shown in **Figure 4B-1**. All of the data collected were LM-80-08 data, as there has not been sufficient time for tests to be completed under the LM-80-15 standard. In addition to data on the three major package types, we collected limited data on emerging CSP LEDs at the end of this project. Unfortunately, not many test reports were available on this package type because of its relatively recent market introduction.

Figure 4B-1. Breakout by LED Package Type of the LM-80 Reports That Have Been Collected From Major Manufacturers

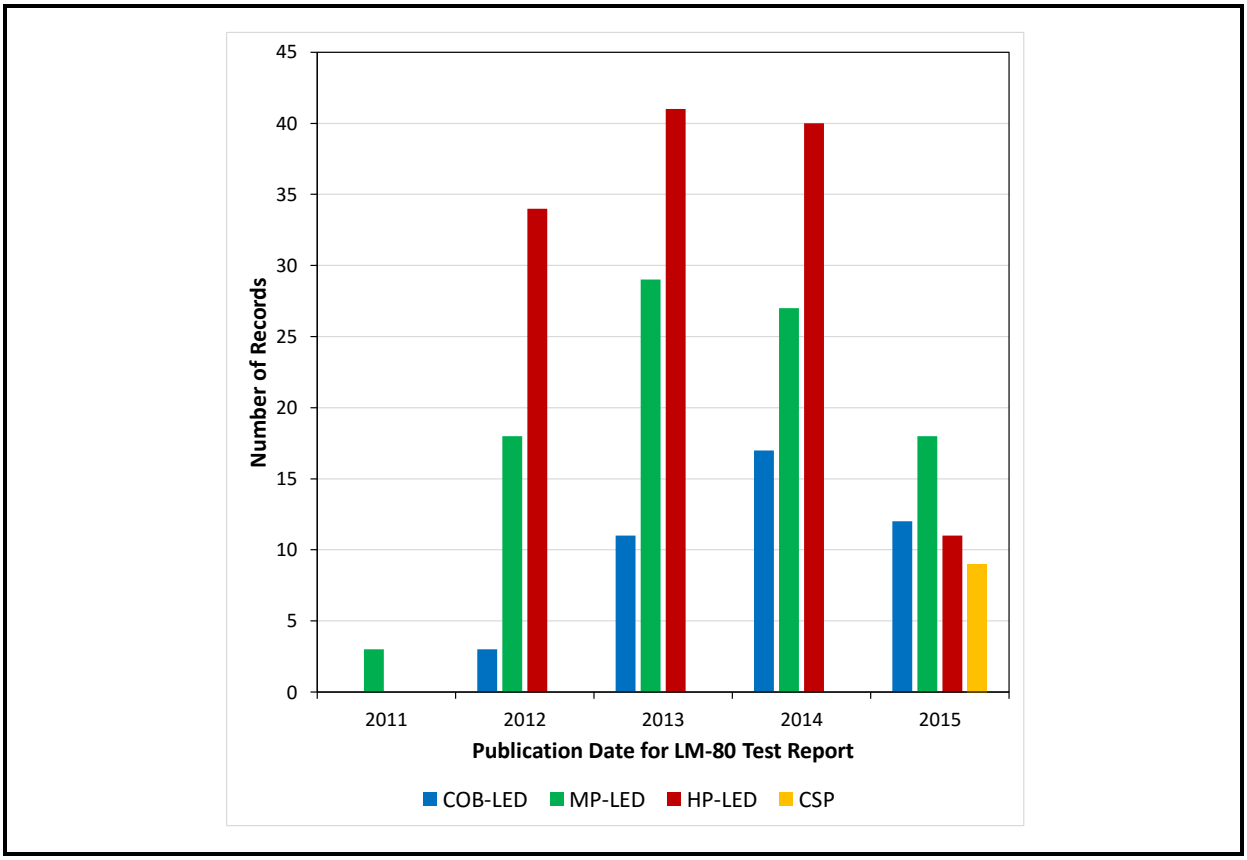

A first-level analysis can be conducted on the TM-21-11 results obtained from LED manufacturers by examining the average α values of each LED population as a function of T_j at the various currents measured. This analysis is shown in **Figure 4B-2,** and several trends are immediately clear. First, α values tend to increase with temperature. As a result, a model of LED α values would likely need to include T_j as a parameter. Second, α values for MP-LEDs are generally greater than the values for HP-LEDs, which are in turn generally greater than the values for COB arrays. There also appears to be a bifurcation of the mid-power data, with the older first generation (Gen1) product based on PPA and PCT technology having higher α values than newer (Gen2) products incorporating different packaging materials (e.g., epoxy molding compounds [EMC], silicone molding compounds [SMC], and ceramics). This finding suggests that models should be created for each LED package type, with separate models for Gen1 and Gen2 MP-LED technologies. Finally, some data sets produce a negative α value, which is equivalent to the unrealistic condition of a perpetual increase in lumen maintenance. LEDs that demonstrate this behavior were typically HP-LEDs and COB-LEDs operated at low I_f and T_j values. This situation requires

further data analysis beyond that typically performed with TM-21-11 and is addressed in detail in Section 4.A and elsewhere [8].

Figure 4B-2. Graph of the Decay Rate Constants (α) Calculated Using TM-21-11 for the 250+ Datasets Collected by RTI

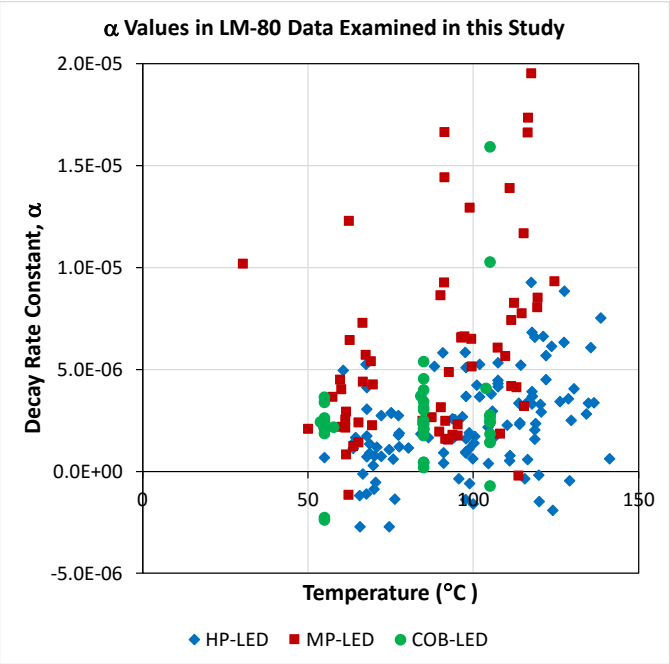

Note: The data are separated by LED package type and show examples of HP-LEDs (blue diamonds), MP-LEDs (red squares), and COB-LEDs (green triangles).

RTI found that the α values of LEDs are dependent on multiple variables, including the following:

- Junction temperature
- Forward Current
- LED package type (i.e., HP-LED, MP-LED, COB-LED)
- Manufacturer (not used in these models)

RTI analyzed industry data from a cross-section of the leading LED manufacturers. The distribution of LED α values can be visualized using a three-dimensional scatter chart with the α values depending on I_f and T_j **(Figure 4B-3**). The distribution about the mean for most manufacturers has a similar shape, although averages may vary, and this distribution can be assumed to be Gaussian. This finding allows an estimate of the distribution about the mean value for LED models of each package type constructed from composites of α values from different manufacturers.

Figure 4B-3. Decay Rate Constant, α, Scatter Plot as a Function of Junction Temperature and Forward Current for the LEDs Examined in this Study

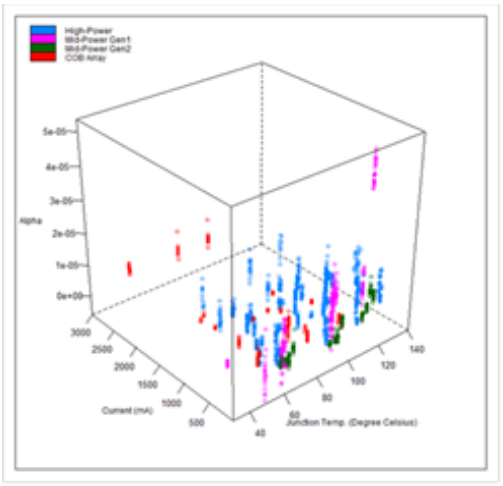

The LM-80-08 data collected in this work from LED manufacturers were analyzed for major trends in α values as a function of T_j. TM-21-11 assumes that the luminous flux maintenance follows the exponential behavior given in Equation (4B.1); consequently, the smaller the value of α, the better the luminous flux maintenance. Examples of the time to reach certain levels of luminous flux maintenance, assuming a given α value, are shown in **Table 4B-1**. The time required to reach a certain level of luminous flux maintenance is denoted by Lx, where x is the remaining percentage of luminous flux, relative to the starting point. For example, a luminous flux maintenance level of 90% of the initial value is denoted by L90, and a luminous flux maintenance level of 70% of the initial value is denoted by L70. In projecting the time to reach a certain Lx level for a given α, TM-21-11 limits the projection time to no more than six times that of the data collection interval, as noted in Table 4B-1 [1]. Although the data that we have accumulated from LED manufacturers suggest that the lumen maintenance of many LED products is very good under the conditions used in an LM-80 test, the unrealistic decay rate constants (i.e., negative α values) demonstrate a limitation in the TM-21-11 method. We have developed a procedure to overcome this limitation, termed the "Double Models" approach, which is described further in Section 4.A and in the peer-reviewed literature [8].

Table 4B-1. Time to Reach Certain Levels of Lumen Maintenance for Assumed α Values

Assumed α Value	L90 (hours)[a]	L80 (hours)[a]	L70 (hours)[a]
5×10^{-7}	210,720[b]	446,287[b]	713,350[b]
1×10^{-6}	105,361[b]	223,144[b]	356,675[b]
5×10^{-6}	21,072	44,629	71,355[b]
1×10^{-5}	10,536	22,314	35,667

[a] L90 denotes a luminous flux level of 90% of the initial value, L80 denotes a luminous flux level of 80% of the initial value, and L70 denotes a luminous flux level of 70% of the initial value.

[b] TM-21-11 limits the maximum time that can be reported for the luminous flux to decay to a certain level: no more than 6 times the LM-80 experiment length. Consequently, the reported times for these values would be "> 60,000 hours" if the LM-80 experiment was conducted for 10,000 hours.

A deeper inspection of Figure 4B-2 leads to the conclusion that α values are strongly dependent on the LED package types. In particular, the α values for HP-LEDs and COB-LEDs were generally lower than that of MP-LEDs, implying that HP-LEDs and COB-LEDs have better luminous flux maintenance. Both HP-LED and COB-LED packages use thermally stable substrate materials (e.g., ceramics or metal-core materials) that can withstand the effects of high heat. In contrast, MP-LEDs use a housing formed from plastic resins that can undergo a photo-oxidation reaction under certain conditions [28; 29; 39]. The molding resin most frequently used in MP-LEDs is PPA, a low-cost, nylon-type material that provides some heat resistance but will undergo photo-oxidation under some conditions. To overcome this limitation, the LED manufacturers developed more-stable molding compounds for use in MP-LEDs, including EMC and SMC. In addition, the PPA materials have improved through the addition of new antioxidant formulations to the molding resin. Consequently, the performance of the current generation of MP-LEDs is much better than initial products, and this generation of MP-LEDs is becoming commercially available (see **Figure 4B-4**). MP-LEDs also continue to benefit from the general trends in improved LED efficiency, which will lower internal temperatures. Modern MP-LEDs containing PPA resins can achieve a lumen maintenance of > 50,000 hours, provided the operational conditions are chosen judiciously [40]. The choice between Gen 1 and Gen 2 MP-LED package types often comes down to a choice of operating the Gen 1 package at lower currents and temperature, requiring more chips to achieve a certain luminous flux level, whereas the Gen 2 package can be driven harder and fewer chips are needed. Gen 2 packages also generally have higher costs, which must be considered when designing SSL devices.

Figure 4B-4. Graph of the Decay Rate Constants (α) Calculated Using TM-21-11 on Manufacturers' LM-80 Data for the MP-LEDs, Broken out by Housing Material

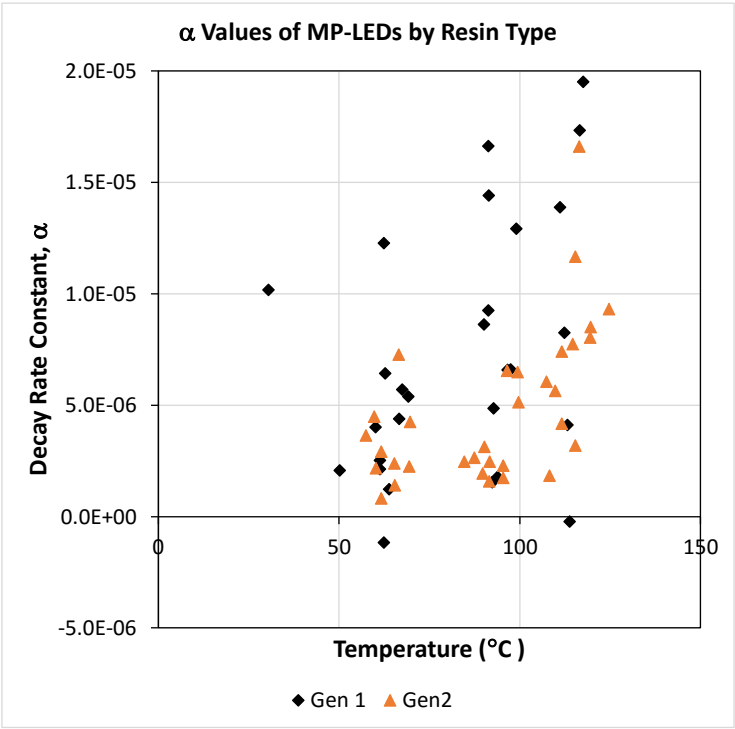

Note: The MP-Gen 1 devices use low-cost resins, such as PPA, whereas the MP-LED Gen 2 devices use higher-performing resins, such as EMC and SMC. Manufacturers' LM-80 Data for the MP-LEDs is also shown in Figure 4B-2.

On the basis of this data collection, RTI was able to build general models for LEDs by package types. These models are given in Table 4A.2. A key utility of these models is their incorporation into RTI's Lumen Maintenance-Decision Support Tool (LM-DST).

4.B.2 Industry Data on Chromaticity Stability of LEDs

LED manufacturers typically report total chromaticity shifts in LM-80-08 data sets as $\Delta u'v'$ values, which denotes the magnitude of the chromaticity shift, but not the direction. In general, we found it difficult to obtain actual chromaticity coordinate values for samples tested under the LM-80-08 protocol. The only LM-80-08 dataset that was readily available and contained full chromaticity coordinates (i.e., u' and v' values) was that of the Lumileds Luxeon Rebel HP-LED product. RTI's status as a not-for-profit research institute eventually allowed us to gain access to some of the protected data from LED manufacturers but with tightly controlled data rights. The efforts of our consultant, Dr. Monica Hansen of the LED Lighting Advisors, were especially critical in obtaining this information. We anticipate that the data will be more readily available when manufacturers begin releasing data acquired

under the LM-80-15 protocols, which mandates the reporting of chromaticity coordinates. However, LM-80-15 data will likely be acquired only on new products, and the currently installed base of SSL products was tested under the more-limited requirements of LM-80-08.

The RTI team reached agreements with some LED manufacturers to acquire chromaticity coordinates for 81 LM-80 datasets, which represents less than one-third of our total database of LM-80 reports. As part of our analysis, the available data were classified into appropriate chromaticity shift modes (CSMs), and the results, broken out by LED package type, are shown in **Figure 4B-5**. A large percentage of the available data was from HP-LED products, and most of the HP-LEDs shifted in a CSM-3 fashion (i.e., terminal/emergent shift in the yellow direction). The COB-LED products that were tested shifted mainly in a CSM-2 fashion (i.e., in the green direction), although some products exhibited either CSM-1 (i.e., blue shift) or CSM-3 shifts. A limited amount of the MP-LED data that we acquired also included chromaticity coordinates. According to the limited data that we have, the MP-LEDs tended to exhibit either CSM-1 or CSM-2 shifts. Interestingly, none of the available data showed a CSM-4 shift for MP-LEDs. A CSM-4 shift would involve a short initial blue shift, followed by a yellow shift, and ending with a second blue shift. This CSM has previously been shown to occur almost exclusively in plastic-leaded packages such as MP-LEDs [27], and the absence of this type of chromaticity shifts may arise from either (1) insufficient test times and conditions or (2) package improvements. This finding demonstrates that the CSM procedure that we developed for classifying LED chromaticity shifts can be extended beyond PAR38 and A19 lamps and is broadly applicable at the LED level.

Figure 4B-5. CSM Distribution of the Available LM-80 Data Sorted by LED Package Type

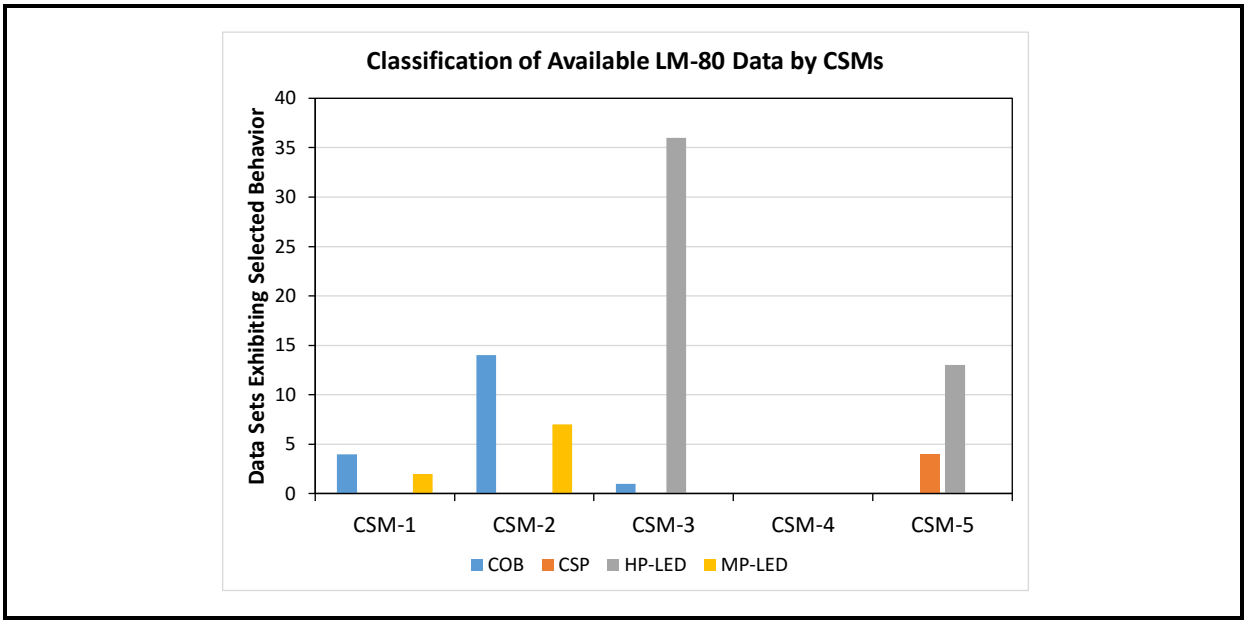

As a second step in our review, we modeled the chromaticity shift of selected LED products using the methods described in **Section 4.A**. One example of this analysis is shown in **Figure 4B-6** for a common MP-LED product in a lower-stress test condition (55˚C and 100 mA) and a higher-stress test condition (105˚C and 200 mA). The only chromaticity shift of this product during 10,000 hours of testing at 55˚C and 100 mA was a shift in the green direction. However, at higher temperatures and higher currents, a new chromaticity shift process arises that is in the blue direction. As shown in Figure 4B-6, the initial green shift can be modeled by a bounded exponential function since it changes quickly when the device turns on and then reaches a limiting value. In contrast, the changes in the LED package responsible for the blue shift take time to have an impact (i.e., the incubation period) and are projected to ultimately lead to an increase in $\Delta u'v'$ greater than 0.007.

Figure 4B-6. Models of the Chromaticity Changes of a Typical MP-LED Under Lower-Stress (Top Graph) and Higher-Stress (Bottom Graph) Conditions

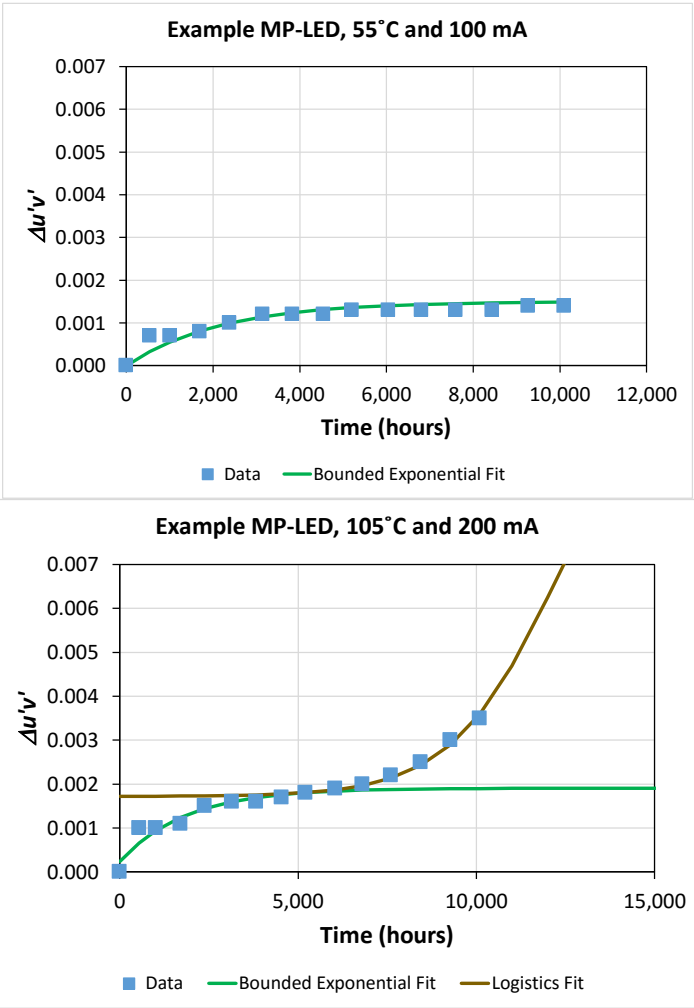

Using these models, logistics functions can be fit to much of the data in the data set for this LED, and the results are shown in **Table 4B-2**. In addition, there is a correlation between the *k* value of the logistic function for each data set and the temperature and current used during the test, and this correlation can be captured with a multivariate linear regression model. The *k* value gives the rise of the logistic function and corresponds to the rate at which the chromaticity shift is occurring if the other fitting coefficients are similar. Although the test data given in Figure 4B-6 did not show the emergence of the second shift process (i.e., blue shift) at mild conditions such as 55°C and 100 mA, we can obtain projected results under these test conditions by extrapolating using the multivariate linear regressions models given in Table 4B-2. Using this approach, the *k* value for 55°C and 100 mA is estimated to be 1.027×10^{-4}, which indicates that it will take more than 55,000 hours for this product to shift by $\Delta u'v' = 0.007$ under these test conditions.

Table 4B-2. Logistic Fit Parameters for Chromaticity Shift Models of a MP-LED Product Using Available LM-80-08 Data

Predictor Variables		Logistic Model Parameters					
Temperature (°C)	Current (mA)	A	*k* value	C	X-Axis Offset	Y-Axis Offset	SSE
55	100						
85	100						
105	100	120.00	3.342E-04	1.200E-02	6000.0	0.00155	1.23E-08
55	150	131.00	3.342E-04	1.100E-02	8000.0	0.00145	5.14E-08
85	150	131.14	3.366E-04	1.084E-02	5000.0	0.0016	3.38E-08
105	150	121.44	4.992E-04	1.121E-02	5123.3	0.0018	5.02E-08
55	200	115.00	4.042E-04	1.200E-02	7000.0	0.00158	2.06E-08
85	200	116.34	6.581E-04	1.267E-02	5500.0	0.0017	4.89E-08
105	200	114.95	6.708E-04	1.000E-02	5210.0	0.00172	3.39E-08

Notes: Multivariate linear regression model: $k = (4.41 \times 10^{-6})T_j + (3.54 \times 10^{-6})I_f - 4.94 \times 10^{-4}$.
All coefficients were found to be statistically significant with p values ≤ 0.05 and R2 = 0.88.

4.B.3 Accelerated Testing of Luminous Flux and Chromaticity Maintenance

Accelerated testing was conducted on individual HP-LEDs by both RTI and Auburn University as part of this project to examine the failure modes of individual LEDs. A variety of HP-LED products were examined in these studies, as shown in **Table 4B-3**, and several different experimental conditions were employed, including wet high-temperature operational lifetime testing (WHTOL) and high-temperature operation lifetime (HTOL) tests using elevated ambient bakes. In performing these tests, individual LEDs pre-mounted on metal-core printed circuit boards were purchased from distributors. The use of distributors to purchase

these products limited the selection of available manufacturers to Cree and Philips. However, these products are believed to be representative of the state of the industry at the time of purchase, which was from 2012–2014.

The small metal-core boards containing the HP-LED packages were attached to heat sinks via either pre-cut thermal adhesives or thermal grease and secured to the heat sinks with screws, as shown in **Figure 4B-7**. The study of lumen maintenance of individual LEDs included blue, warm white, and cool white LEDs to investigate the behavior of different phosphor formulations. In all instances, the white LEDs (both cool white and warm white) were fabricated in the pcLED configuration with the phosphor residing on top of the die.

Table 4B-3. Individual HP-LEDs Subjected to Accelerated Stress Testing During This Project

Sample ID	Emitter Type	Conversion Layer	CCTs Tested	Comment
XR-C	Surface	Phosphor-silicone	2750	Example of early pcLED product with silicon-phosphor conversion layer
LR	Surface	Phosphor-ceramic	3100 and 5500	Example of early product with phosphor-plate conversion layer
E	Surface	Phosphor-silicone	Blue only	Larger die size than earlier products
G	Surface	Phosphor-silicone	3000 and 5300	Competitive product to LR but in phosphor-silicone format
T	Bulk	Phosphor-silicone	3000 and 6500	Single die with truncated pyramid structure (i.e., shaped chip) in same package size as products E and G
T-HV	Bulk	Phosphor-silicone	2700	16 die connected in series in package with same footprint as E, G, and T

The tested products included both surface-emitting LEDs and the newer bulk-emitting LED structures. The surface-emitting LED devices produce photons from a planar epitaxial layer, and the photons are directed through a phosphor layer, composed of phosphor and a binder, that is present on one side of the device. For surface emitters, the phosphor conversion layer can be applied as a film on one side of the LED die because emission only occurs on one side. In forming this structure, a binder is added to the phosphor to achieve the desired mechanical performance and environmental stability. Typically, LED manufacturers will either use a silicone binder to hold the phosphor (phosphor-silicone) or combine a glass/ceramic binder with the phosphor (phosphor-ceramic). A bulk emitter consists of a three-dimensional emission structure formed by etching and faceting the epitaxial layer. Because of its nonplanar geometry, the phosphor-conversion layer must be

applied around a complex structure. To date, only phosphors mixed with silicone binders have been used in this type of structure. Similarly, other non-planar structures such as MP-LEDs typically use a variation of the phosphor-silicone conversion material to achieve white light. Therefore, examining both the phosphor-silicone and phosphor-ceramic structures for the conversion layer will provide some insights into the performance of the materials used to make white light in multiple LED packages.

Figure 4B-7. Image of the Mounting Configuration Used for Testing Individual LEDs

WHTOL tests were used to accelerate aging of the LEDs, and three different WHTOL environments were used in testing, as shown in **Table 4B-4**. For example, WHTOL tests performed at 85˚C and 85% RH (hereafter termed 8585) followed procedures outlined in JESD22-A101B, which call for a continuous soak at 8585 with electrical power to the luminaires cycled on and off at 1-hour intervals [41]. The power cycling promotes moisture ingress when the unit is powered off followed by a higher operating temperature when the unit is powered on, which tends to drive the moisture off.

Table 4B-4. Experimental Protocols Used During WHTOL Testing

Protocol Name	Temperature (˚C)	Relative Humidity (%)	Electrical Cycling
8585	85	85	1 hour on, 1 hour off
7575	75	75	1 hour on, 1 hour off
6590	65	90	1 hour on, 1 hour off

The LEDs were mounted on a common heat sink and were connected in series with five LEDs The heat sink containing the LED assembly was placed in the environmental chamber under the designated conditions, and the LEDs were powered by a constant-current driver that was kept outside of the environmental chamber. The test population of LEDs typically consisted of 10 blue LEDs, 10 cool white LEDs, and 10 warm white LEDs. The LEDs were operated at current levels to match the conditions in the LM-80-08 report. For the Product G LEDs, this was 500 mA, and for the Product LR LEDs, this was 700 mA. After each round of WHTOL exposure, the individual LEDs were measured at RTI in a 10" integrating sphere using a 2π configuration with the LEDs and the heat sink mounted outside of the integrating sphere. At Auburn University, the LEDs were placed in the center of a 1-meter integrating sphere and measured in a 4π configuration. Both approaches allowed each LED to be measured separately. During the measurements, corrections were made for zero level and self-absorbance as outlined in LM-79. Calibrations were performed using a NIST-traceable standard, including radiometric standards at Auburn University and forward flux standards (Labsphere Model Number FFS-100-400) at RTI.

Behavior of XR-C HP-LED in Accelerating Testing

Introduced in 2006, the XR-C was one of the first white HP-LEDs available on the market and was used in many early-generation SSL devices, including LED lamps and luminaires. The general structure of the LED package is shown in **Figure 4B-8**. The XR-C package design was unique in that a small glass lens sat on top of a low-durometer (i.e., soft) silicone encapsulant with only the tack of the silicone holding the lens in place. Because the silicone is permeable to water and most volatile organic carbons, there is a direct path for these chemicals to access the LED and phosphor.

Figure 4B-8. Schematic Cross-Section of the Package Design for the XR-C HP-LED Along with Potential Sites Where Failure Can Occur

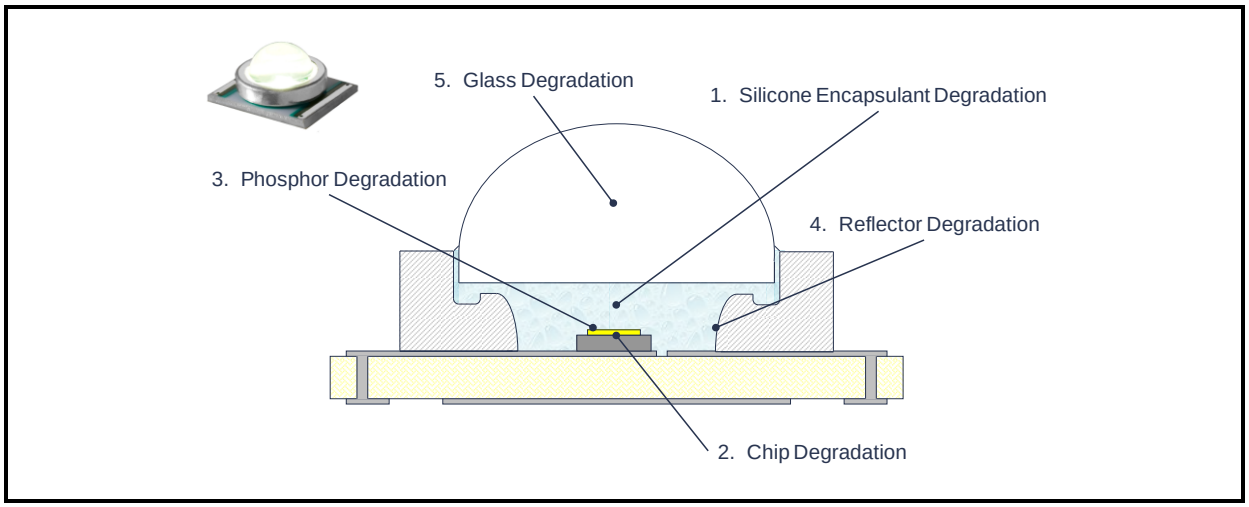

Graphic is courtesy of Cree Inc.

Initial experiments performed by Auburn University during this project examined the influence of temperature alone on the performance of the XR-C package. Two different test conditions were used in this experiment. Test Condition 1 consisted of a 105°C elevated ambient environment and a forward current of 350 mA. Test Condition 2 consisted of a 175°C elevated ambient environment and a forward current of 500 mA. Although Test Condition 2 was outside the specified operational range of the device, such a test can provide insights into the ultimate failure mode of LED devices. All tests were operational tests in which the LED was cycled between the on state and the off state once per hour (i.e., 1 hour on followed by 1 hour off).

The photometric properties of the XR-C samples were measured in a calibrated integrating sphere every 2 weeks (i.e., 336 hours). In addition, the characteristic Current-Voltage (I-V) curve of the LED was measured with a Keithley 2401 power source. In performing this measurement, the sweep current was changed from 0 mA to 500 mA, and the forward voltage was measured. The I-V curve of the LED was recorded to monitor the electrical properties of the die and to detect any degradation in the electrical performance of the LED itself. After completion of photometric and electrical measurements, all samples were returned to the environmental chamber for further exposure to the accelerating stress test (AST) conditions.

The spectral power distributions (SPDs) obtained from warm white Cree XR-C samples are shown in **Figure 4B-9** and **Figure 4B-10** as a function of time. Although the luminous flux of the device dropped by roughly 15%, the drop in emission intensity was relatively uniform, and virtually no change in the spectrum profile was found after more than 5,000 hours of exposure to Test Condition 1. Further, no LED failures were observed during the tests conducted under Test Condition 1. Under Test Condition 2, there was a slight change in the spectral profile, resulting in a decrease in the CCT value, and the loss of luminous flux was higher. In addition, three of the five LEDs undergoing tests failed during the 1,392 hours of Test Condition 2. The key findings from this tests are that elevated temperatures within the specified operational range require a long time to produce detectable levels of degradation in HP-LEDs and that different test strategies are needed to reduce test times to less than 3,000 hours.

Figure 4B-9. SPDs of Warm White XR-C Samples Subjected to Test Condition 1 for Varying Times

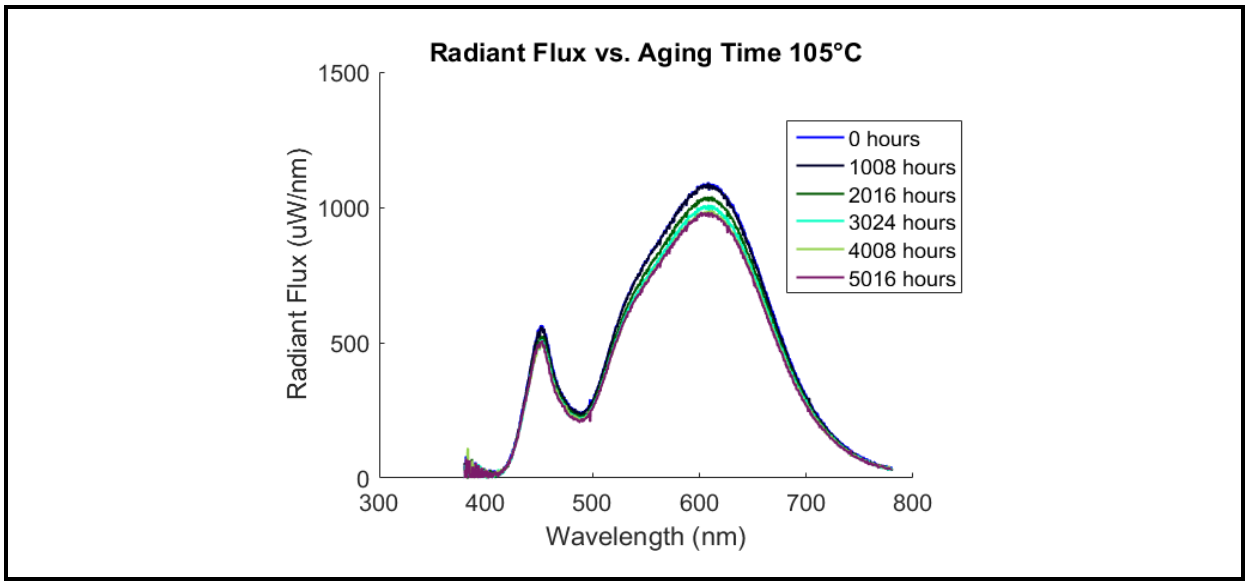

Figure 4B-10. SPD of Warm White XR-C Samples Subjected to Test Condition 2 for Varying Times

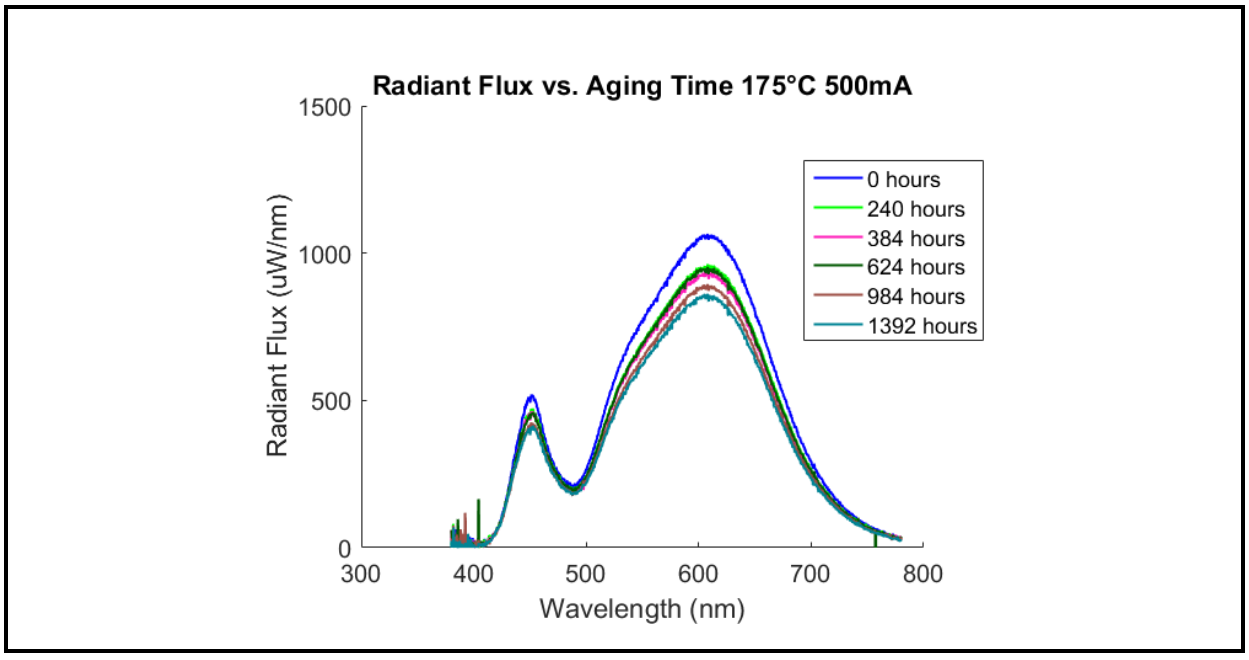

LEDs are semiconductor devices that will pass current when forward biased above a threshold voltage. Measuring the I-V curve of the LED samples provides a means to monitor the p-n junction inside the package and to provide insights into material degradation or

other changes that affect the electrical performance of the device. The I-V curve of the XR-C package under Test Condition 1 is shown in **Figure 4B-11,** and the corresponding I-V curve under Test Condition 2 is shown in **Figure 4B-12**. Figure 4B-11 indicates that increasingly higher voltages are required to achieve a given forward current after prolonged exposure to Test Condition 1, which means that more power is required to achieve the same drive current. This finding indicates that the device has become less efficient, likely because of degradation within the package (e.g., epitaxial layer, contacts, etc.). As a result, the efficiency of the device decreases, which may explain at least part of the emission decrease in the SPD shown in Figure 4B-9. Under the more strenuous Test Condition 2, the level of degradation was higher, as shown in Figure 4B-12, indicating that device efficiency is further compromised. This finding helps to partially explain the drop in the SPD shown in Figure 4B-10.

Figure 4B-11. I-V Curve of Warm White XR-C Samples Taken at Different Times During Exposure to Test Condition 1

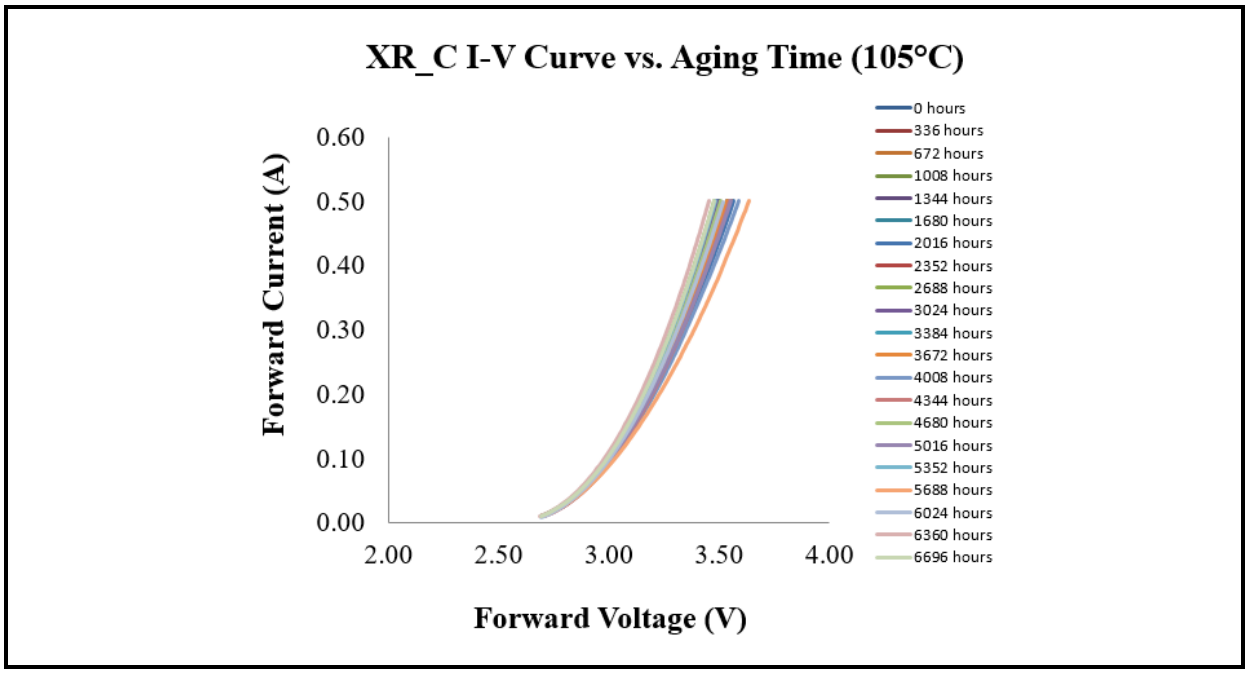

Note: Test times are given in hours on the right-hand side.

Figure 4B-12. I-V Curve of a Warm White XR-C Sample Taken at Different Times During Exposure to Test Condition 2

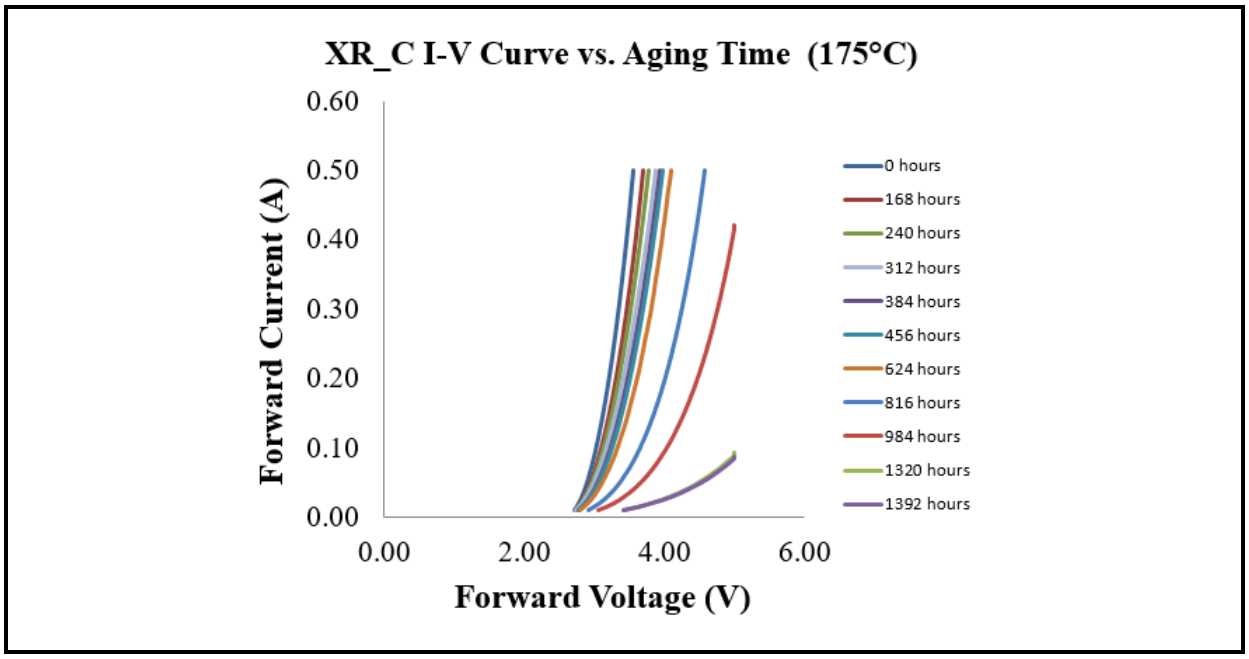

Note: Test times are given in hours on the right-hand side.

Following the high-temperature experiments, five warm white XR-C LEDs were tested at Auburn University in a WHTOL environment of 8585 for 5,708 hours. The devices were operated at 350 mA during this test, and power was supplied to the devices on a 1-hour duty cycle. The time-dependent radiant flux spectrum obtained from one of the samples is shown in **Figure 4B-13**, and two major trends are immediately obvious. First, the phosphor emission peak is shifting to lower wavelength values (i.e., a shift toward the green), and the rate of this shift appears to be higher initially and then slows down. This finding is confirmed in the time-dependent plot of the change in chromaticity coordinates (i.e., $\Delta u'$ and $\Delta v'$) given in **Figure 4B-14**. Second, the intensity of blue emissions is actually *increasing* with time, and the radiant flux at nominal blue wavelengths (~ 450 nm) is higher, by roughly a factor of 2, after 5,708 hours of exposure than the initial value. These findings contrast sharply with those of high-temperature exposure alone (see Figure 4B-9 and Figure 4B-10) and provide a clear indication that WHTOL testing is a more-aggressive accelerated test for LEDs and produces greater degradation than heat alone. In addition, previous studies have shown that moisture ingress into LED packages reduces the package extraction efficiency and accelerates luminous flux decay at a faster level than temperature alone [29; 42-45]. Therefore, WHTOL testing was used in this study as a major acceleration test for LED devices.

Figure 4B-13. Absolute Radiant Flux Measurements of Product XR-C at Different Times in 8585 Testing

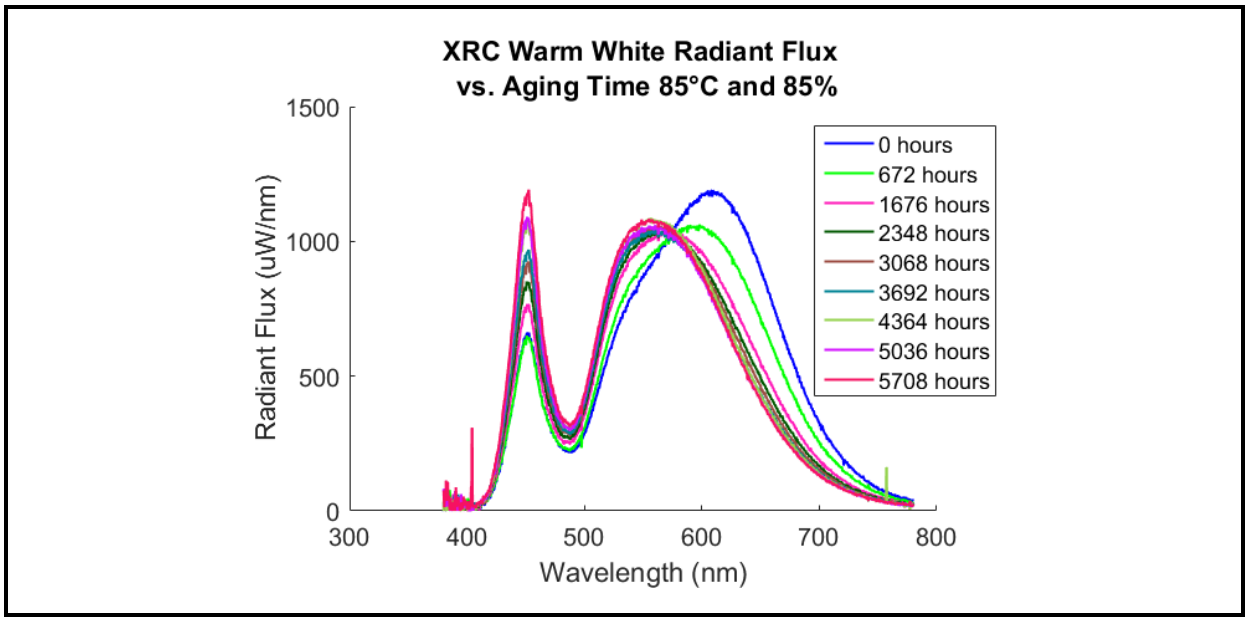

Note: Test times are given in hours on the right-hand side.

Figure 4B-14. Change in Average Chromaticity Coordinates ($\Delta u'$ and $\Delta v'$) for the Population of five XR-C HP-LEDs Operated at 350 mA in 8585

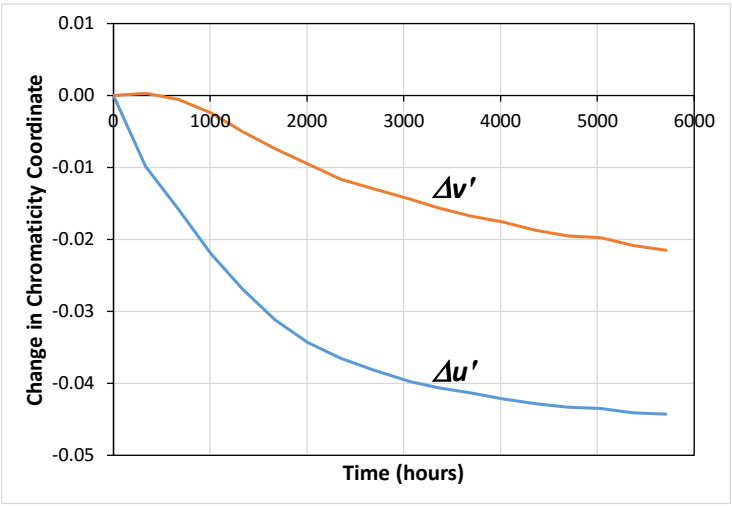

The timing of the chromaticity coordinate changes (see Figure 4B-14) for the XR-C provides significant insight into the degradation of the device in 8585. Initially, the chromaticity shifts in the green direction, as evidenced by the negative change in $\Delta u'$ and the approximately 0 slope of $\Delta v'$. However, after 500 hours of exposure, $\Delta u'$ continues to shift in a negative

direction and $\Delta v'$ begins to shift in a negative direction, which indicates a period of shifting in a more cyan-like direction. Thus, there appears to be an incubation period before a change in v' occurs, whereas the change in u' occurs nearly instantaneously with WHTOL exposure. As the $\Delta u'$ shift slows, the change in v' rises in relative importance, and the shift is toward blue, as we have reported previously [46]. The processes responsible for the green chromaticity shift can be assigned to oxidation of the phosphor and will be discussed in more detail later.

Additional investigation was required to determine the cause of the blue chromaticity shift, especially because this shift is delayed and exhibits the unusual property of a significant increase in blue radiant flux. As part of this investigation, a detailed analysis of the phosphor-binder layer of the XR-C package was performed using a scanning electron microscope (SEM). **Figure 4B-15** shows the SEM images of the XR-C LED package binder layer at a magnification of 2,580X for both a pristine sample and a sample after exposure to 5,708 hours of 8585.

The thickness of the phosphor layer, indicated by the white line in Figure 15, differs between the pristine and exposed samples. For the pristine sample, the phosphor particles are evenly distributed in the binder layer in a dense fashion on the top of the LED die, and the thickness of the phosphor-binder layer in the pristine sample is approximately 25.87 µm. For the sample exposed to 8585, the phosphor-binder layer was thicker, suggesting that this layer swelled some during WHTOL. SEM measurements determined that the phosphor-binder layer was 45.56 µm thick after 5,708 hours of 8585, roughly 75% thicker than the initial thickness. The finding of swelling of the phosphor-silicone layer in pcLEDs was recently confirmed by Khalilullah et al. [16].

Figure 4B-15. SEM Images of a Pristine Sample of the XR-C HP-LED and an Analogous XR-C Sample After 5,708 Hours of Exposure to 8585

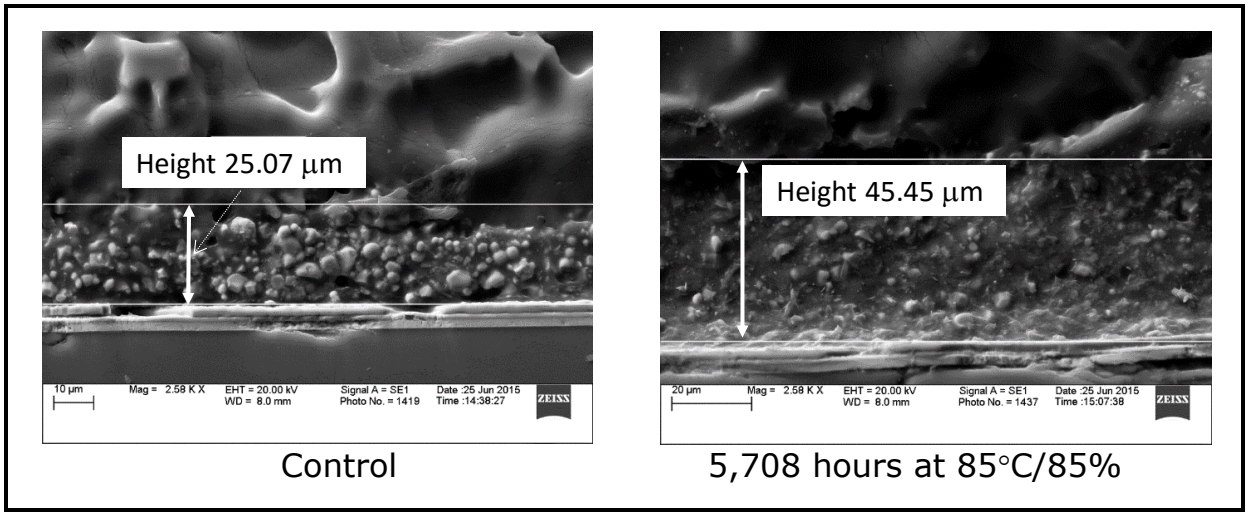

Note: The white horizontal line indicates the approximate thickness of the phosphor-binder layer in each sample. The images were taken at a magnification of 2,500X and a working distance of 8.0 mm.

The extent of the reaction responsible for the swelling of the phosphor-binder layer also can be followed through the change in the chromaticity point (i.e., $\Delta u'v'$). As shown in **Figure 4B-16**, the total chromaticity (i.e., $\Delta u'v'$) data follows a bounded exponential form, which is consistent with moisture ingress into the package because the amount of swelling that can occur in the phosphor-binder layer is finite. This model also predicts that the chromaticity shift will stabilize after a shift of 0.050 (i.e., 50-step MacAdam ellipse), which is well beyond the chromaticity limits of EnergyStar. As will be discussed later, we have not seen this failure mode in other products. Because the XR-C was one of the first HP-LED products on the market, it is not surprising that later products exhibit better performance in this type of test.

Figure 4B-16. Total Chromaticity Shift Data ($\Delta u'v'$) for XR-C HP-LED Exposed to 8585 for 5,708 Hours (Blue Squares) and Future Chromaticity Projection Using a Bound Exponential Model

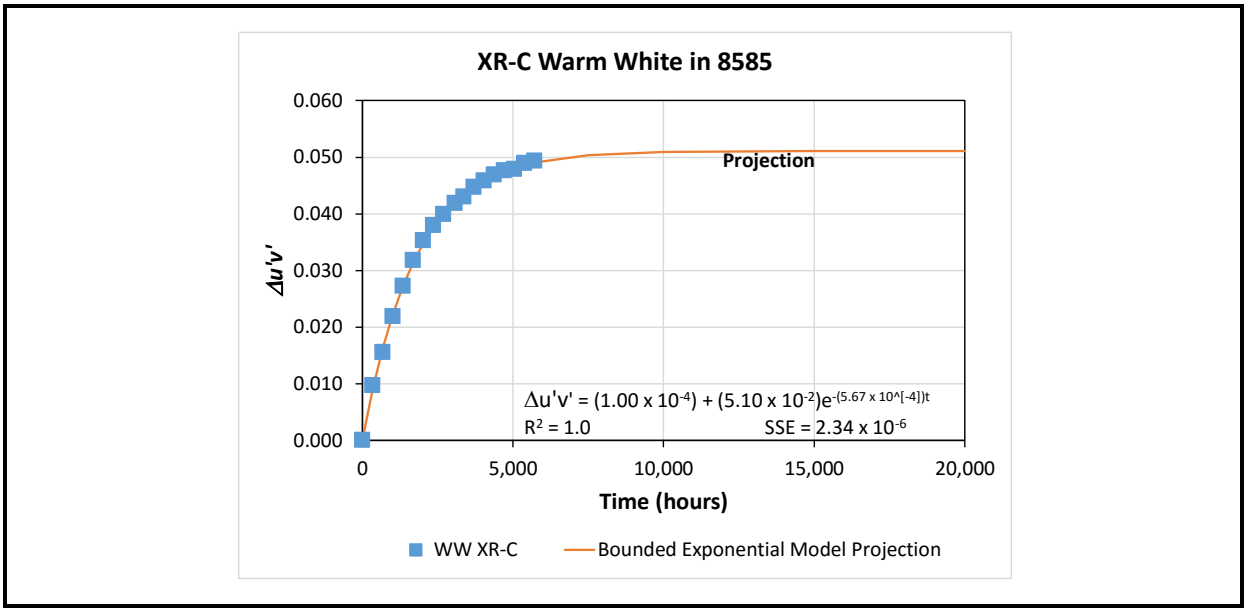

The I-V curve of the LEDs in 8585 tests were measured, and a typical example is shown in **Figure 4B-17.** Compared with Figure 4B-11, the LED was less degraded at the end of the test. The extent of degradation was lower because a smaller increase in voltage was required to maintain a given forward current. Thus, even though the 8585 environment produces significant changes in the LED SPD profile, the impact on the blue LED itself was lower than the impact of elevated ambient environments. Therefore, we conclude that

WHTOL testing more elements of the LED package, and at a higher rate, than temperature alone.

Figure 4B-17. I-V Curve at Different Exposure Times for a XR-C Sample Subject to 8585 Conditions

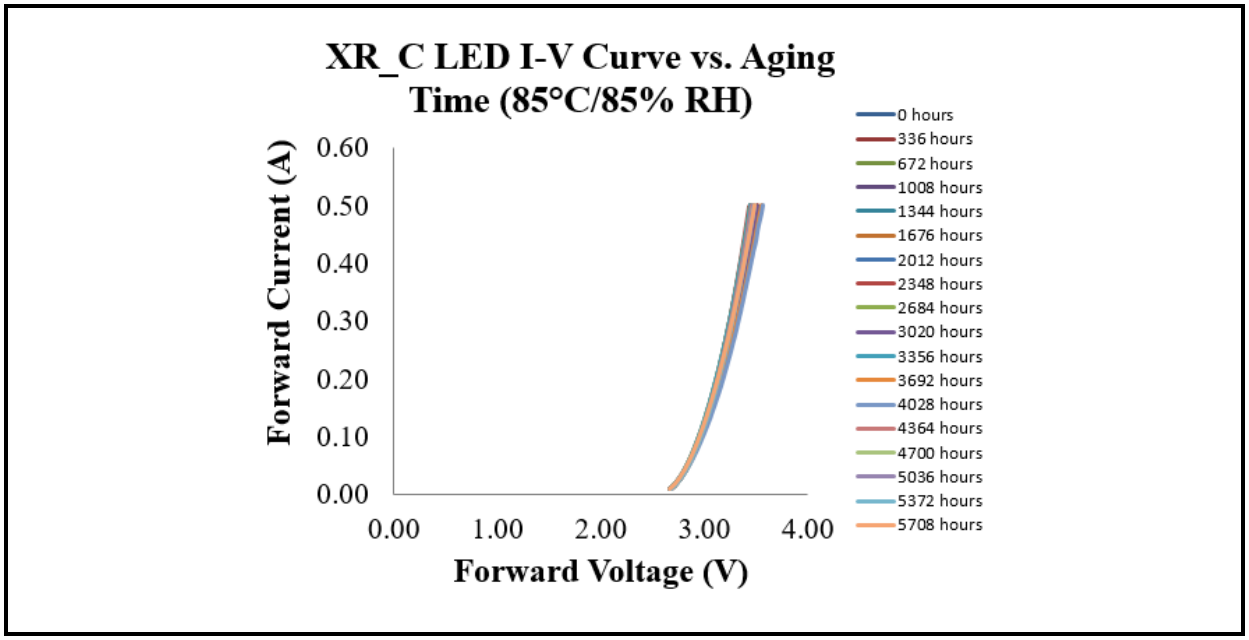

Note: Test times are given in hours on the right-hand side.

Surface-Emitting HP-LEDs with Silicon-Phosphor Conversion Layers in WHTOL Testing

Product G was introduced to the market as a second-generation HP-LED product in 2010 and was quickly adopted by many SSL lamp and luminaire manufacturers. An earlier version of this product, referred to as Product E here, was introduced first. It is similar to Product G in most respects but has a smaller die area. Product G has a significantly different package structure from that of the XR-C; a schematic of this LED package is shown in **Figure 4B-18**. The Product G design uses a larger die area to provide a higher luminous flux than earlier products. This design also uses a molded silicone lens on top of the LED and its encapsulant. Although the durometer of the silicone was increased, the package is still susceptible to moisture and chemical ingress under certain conditions [47]. The performances of Product G and its competitive analog, Product LR, were closely examined in this study because the basic LED package architecture has many similarities to current LED products on the market.

Figure 4B-18. Schematic Cross-Section of the Package Design for the Product G HP-LED

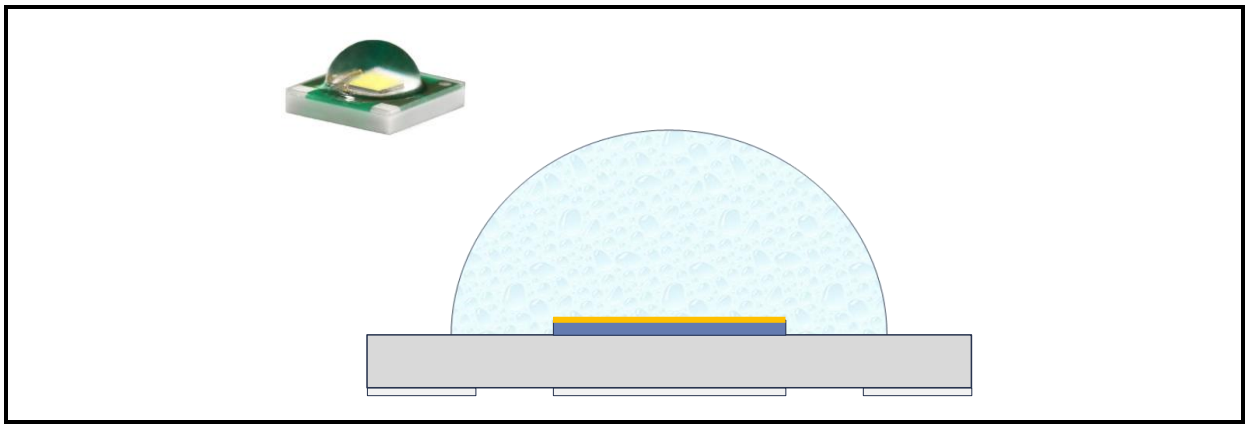

Source: Graphic is courtesy of Cree Inc.

Product G testing was conducted at both RTI and Auburn University. Both cool white and warm white products were examined during this study, and a variety of testing conditions (e.g., 8585, 7575, and 6590) were used at the two test sites. The devices were typically operated at 500 mA, and power was supplied to the devices on a 1-hour duty cycle.

Auburn University used HTOL testing to examine the change in the phosphor binder layer with thermal aging. As shown in **Figure 4B-19**, hairline cracks of roughly 1 μm in width became visible in the top of the phosphor-silicone layer with aging, and these cracks will likely affect the LED's light emission. In particular, the appearance of cracks in the phosphor-silicone layer can change the path of unconverted blue photons (favoring increased secondary conversion) or can provide a path for direct emission of photons to the outside and completely bypass the phosphor layer [27].

Figure 4B-19. Picture of the Phosphor-Silicone Layer from Product G After 8,000 Hours of Testing at 125°C and 1,000 mA.

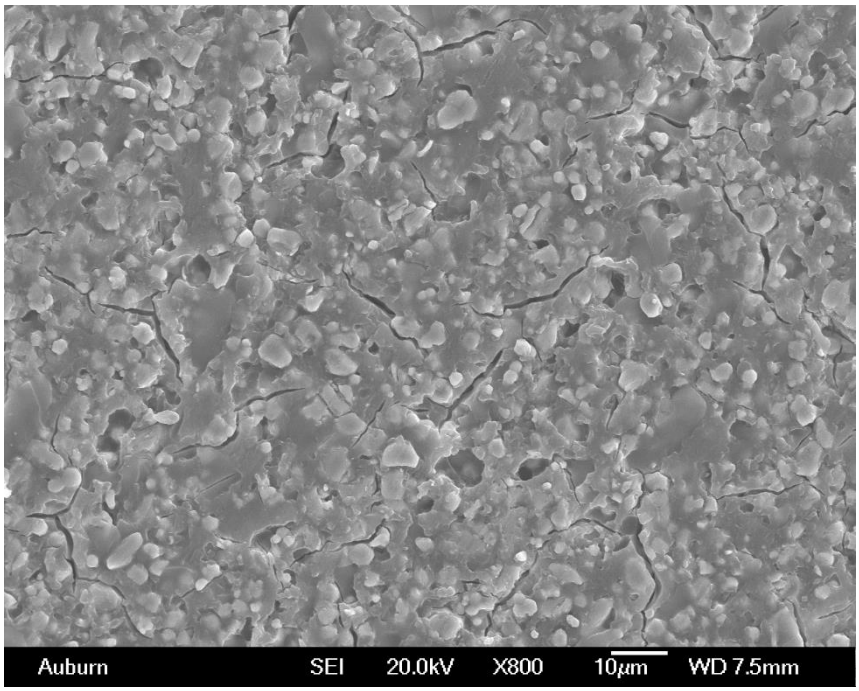

The luminous flux maintenance behavior of Product G LEDs is given in **Figure 4B-20**, and the value of this parameter depended upon the WHTOL test that was used and the CCT value of the LED. For the warm white LEDs, the luminous flux rose as high as 11.3% above the starting point in 8585, and a more modest 2.3% increase above the starting value was found in 7575. In both cases, we attribute the initial increase in luminous flux to oxidation of the warm white nitride phosphor, which produces a green shift of the primary phosphor emission peak and a net increase in luminous flux. As shown below, the extent of this nitride phosphor oxidation was higher in 8585 than in 7575 and, as a result, the maximum luminous flux was highest in the 8585 test. For the cool white LEDs, there was a modest initial increase in luminous flux of 4.3% above the initial value in 8785 and 1.9% above the initial value in 7575.

Figure 4B-20. Average Luminous Flux Maintenance for the Test Samples of Product G LEDs in WHTOL Tests

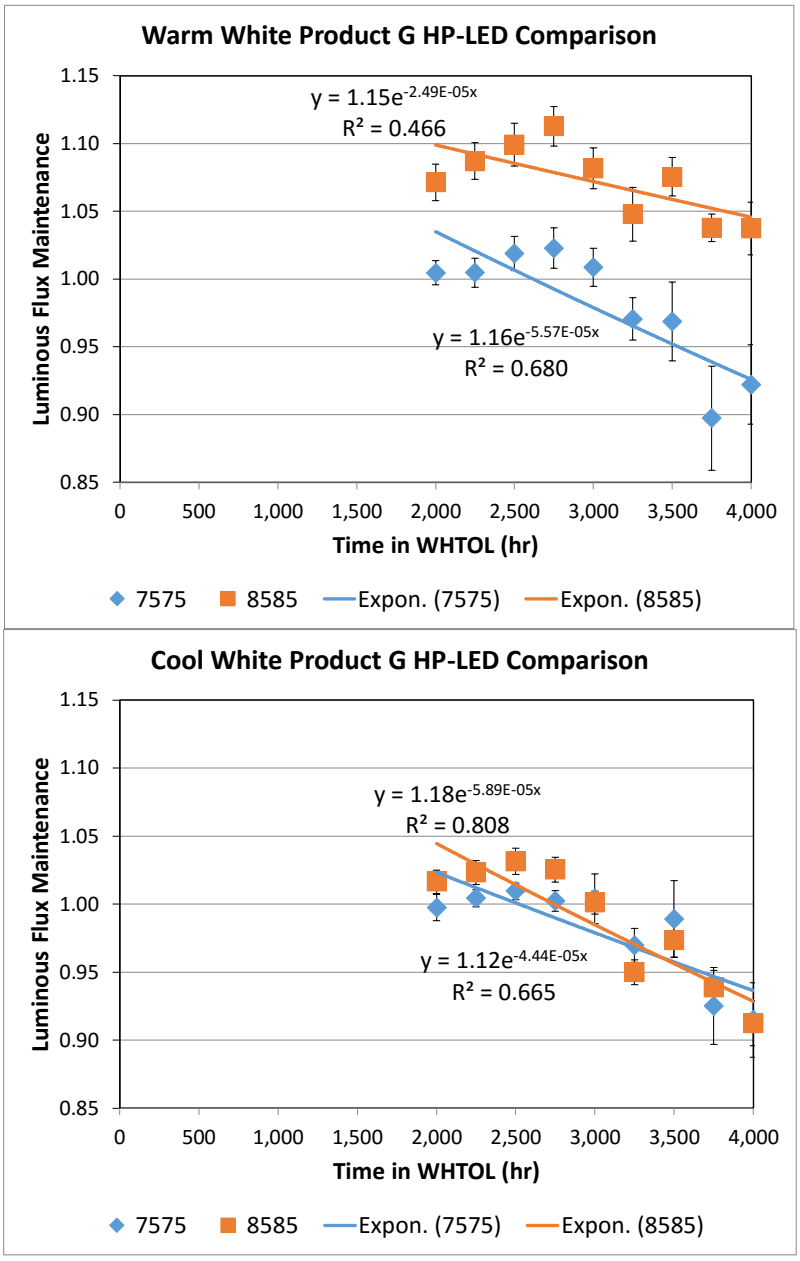

Note: The results for warm white LEDs are shown on the top, and the results for cool white LEDs are shown on the bottom. The error bars represent one standard deviation about the average.

It is not possible to use the TM-21-11 projection method to analyze the data obtained in our WHTOL studies because (1) our data acquisition is more highly accelerated than that anticipated in TM-21-11 and (2) our tests stopped at 4,000 hours and did not reach the 6,000-hour minimum specified in TM-21-11. Nonetheless, we can use a method like TM-21-11 to analyze the data. Because our WHTOL data is highly accelerated, we decided to calculate lumen maintenance using only the last half of the data set. As a result, only data

between 2,000 and 4,000 hours were used in calculating the rate of exponential decay, and no data before 2,000 hours were used in the calculations. The resulting fits, which assume an exponential decay model, are also given in Figure 4B-20, and the results are summarized in **Table 4B-5**. According to this analysis, the exponential decay rate of the luminous flux value for the warm white phosphors is higher than that of the cool white phosphors. In addition, the TM-21-11 decay rate constant (α values) reported by the manufacturer for Product G operated at 85°C and 500 mA indicate that there is a net 1% increase in luminous flux maintenance at the end of the 10,000-hour test period. Therefore, α has a negative value in the manufacturer's data, which suggests that luminous flux is always increasing, which has no real physical meaning [8]. Therefore, it can only be stated that the WHTOL environments used in these tests are highly accelerating compared with environments with high temperature alone, but an acceleration factor cannot be calculated in this case.

Table 4B-5. Rates of Exponential Decay for WHTOL Test of XP-G LEDs Compared with Temperature Alone

LED Color	WHTOL Test	Exponential Decay Rate
Warm white	7575—WHTOL	5.57×10^{-5}
Warm white	8585—WHTOL	2.49×10^{-5}
Cool white	7575—WHTOL	4.44×10^{-5}
Cool white	8585—WHTOL	5.89×10^{-5}
Warm white	85°C and 500 mA	-1.06×10^{-6}

To provide an additional layer of detail, the time-dependent SPD measurements obtained from the warm white version of Product G in 8585 and 7575 are shown in **Figure 4B-21**, and the corresponding SPD measurements for the cool white version of Product G are shown in **Figure 4B-22**. When examining the spectra in Figure 4B-21, a significant shift to lower wavelengths can be seen for the phosphor emissions occurring between 480 nm and 800 nm. The impact of this oxidation reaction is very obvious in the 8585 environment but is more subtle in 7575 testing, in line with the lumen maintenance data summarized in Table 4B-5. The doped-nitride phosphors are likely a component of the phosphor mix for this LED, and the marked shift in the wavelength has been attributed to the impact of lattice oxidation and, to a lesser extent, oxidation of the Rare-Earth dopant [30; 33]. It is also noteworthy that a slight increase in the blue emission peak occurred in 8585 testing, whereas a slight decrease in this peak occurred in 7575. This effect may be due to moisture-induced swelling of the phosphor-binder layer in 8585, as discussed above for Product XR-C. However, this effect appears to be much smaller than the effect observed for the XR-C.

Figure 4B-21. SPD Measurements for the Warm White Version of Product G in 7575 (Top) and 8585 (Bottom) as a Function of Exposure to the WHTOL Environment

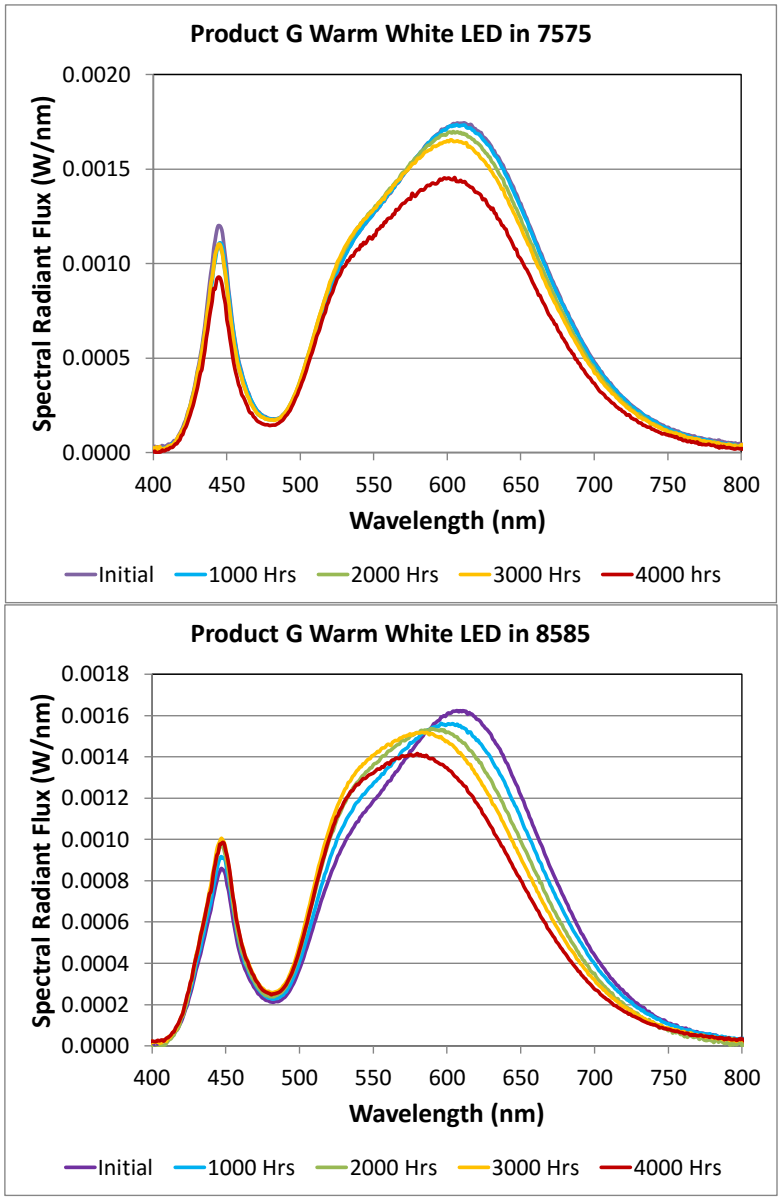

Figure 4B-22. SPD Measurements for the Cool White Version of Product G in 7575 (Top) and 8585 (Bottom) as a Function of Exposure to the WHTOL Environment

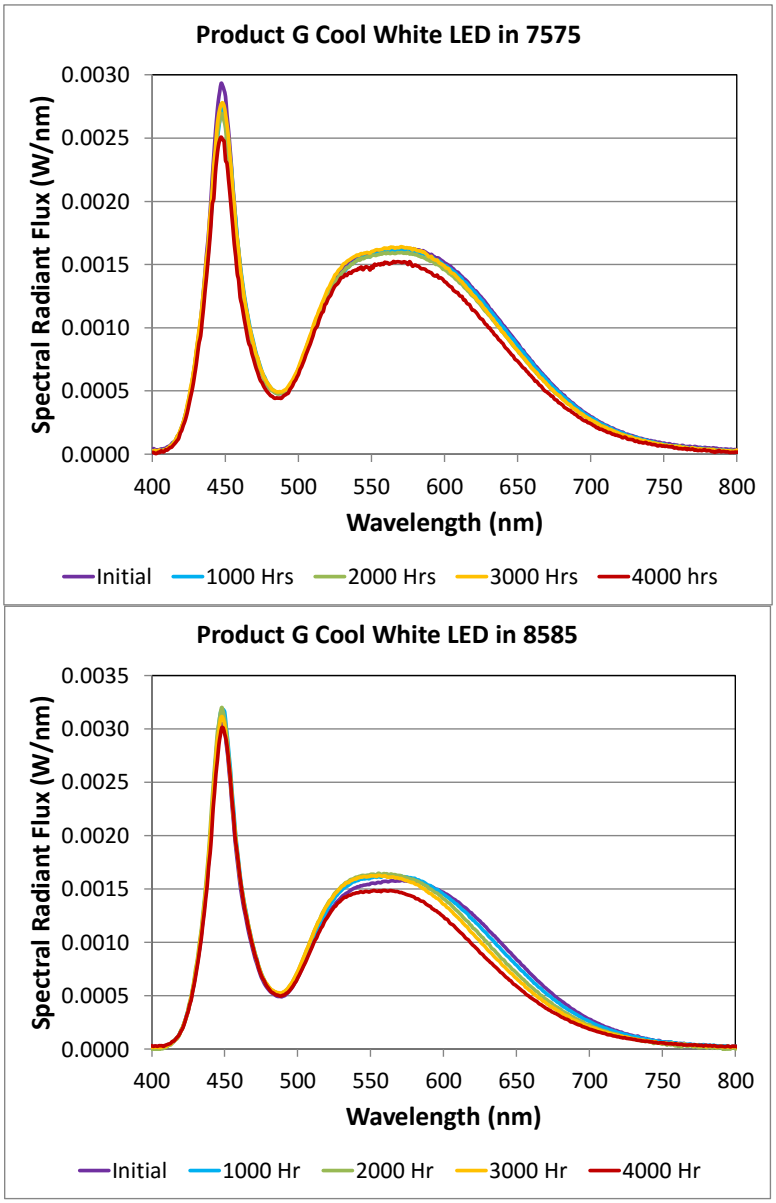

Although the SPD profile of the cool white LED product did not show the major changes that were observed for the warm white version of Product G, there was nonetheless a small loss in emission intensity at longer wavelengths (i.e., greater than ~600 nm). This change may be due to a shift in emission wavelengths of one component phosphor in the phosphor mix, as discussed above, so that it is not distinguishable from the main phosphor peak. Alternatively, this reduction in long wavelength emissions could be due to quenching of that component of the phosphor mix.

Because the chromaticity coordinates are calculated from the SPD, an examination of the chromaticity shifts with WHTOL exposure times provides additional information on changes of the materials used in Product G and, by extension, similar products throughout the industry. The average chromaticity coordinates for 10 samples of warm white and cool white versions of Product G are given in **Figure 4B-23**. Several major trends are evident from examining the chromaticity coordinates. First, although the shifts were generally in the same direction for a given color of LED, the amount of chromaticity shift was greater in 8585 (dotted line) than in 7575 (solid line). This finding agrees with the lumen maintenance and SPD data at the higher stress levels (and more-accelerating environment) of 8585 compared with 7575. Second, although both warm white and cool white LEDs shifted in the same direction, the magnitudes of the shifts were larger with the warm white samples than with the cool white ones. Figure 4B-21 and Figure 4B-22 demonstrate that the chromaticity shift in the warm white LEDs occurs mainly because of oxidation of the warm white phosphor, resulting in a shift of the emission peak to lower wavelengths. As we have discussed elsewhere, this behavior is indicative of both surface and bulk oxidation of the nitride phosphors in warm white LEDs [20; 30; 33]. It is reasonable to assume that the larger chromaticity shifts observed for the warm white LEDs in WHTOL are due to a higher content of the red (i.e., doped-nitride) phosphor. For the cool white LEDs, no new emission feature appeared in the range 480 nm to 550 nm. Instead, there was a general loss of emission intensity above 570 nm, and this loss of orange and red emissions is believed to be the cause of the chromaticity shift. It is likely that the small amount of red phosphor added to the phosphor mix in the cool white LEDs that were tested (i.e., initial CCT ~ 5,300 K) is shifting as well, which leads to the loss of emission intensity above 575 nm. Consequently, the larger chromaticity shift found for the warm white product is thought to be due to the higher concentration of red-emitting doped-nitride phosphors.

Figure 4B-23. Chromaticity Shift for Warm White (Top) and Cool White (Bottom) Versions of Product G HP-LEDs

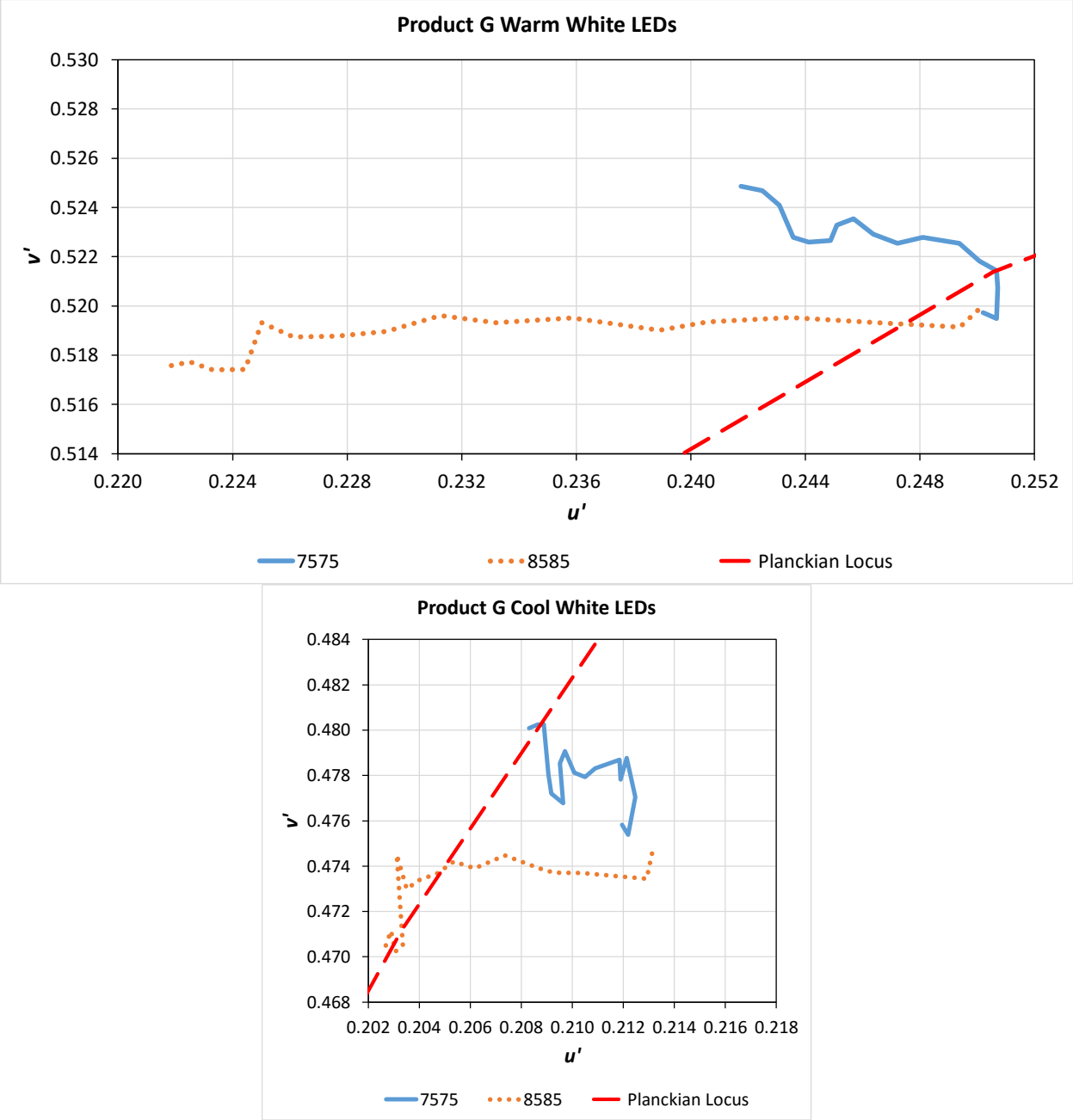

The CCT values of the Product G LEDs in 7575 and 8585 were also analyzed, and the results are shown in **Figure 4B-24**. For both warm white and cool white versions, the CCT value increased with longer exposure times in WHTOL. For the 8585 samples, the magnitude of the CCT change is larger than found for the 7575 tests. In all cases, these data can be modeled with logistic curves; however, the maximum shift appears to be higher in 8585

than in 7575. This finding suggests that either additional processes are involved in the chromaticity shift in 8585 compared with 7575 or the difference in moisture concentration produces a higher rate in 8585. The parameters for these models are shown in **Table 4B-6**. In general, the fit to a logistic function was better in the samples exposed to 8585, which is not surprising, as the magnitude of the effect is greater under these conditions. Most of the range of this data can also be fit with a line; however, the rate of change in CCT values slows for both warm white and cool white LEDs in 8585, which will not be adequately modeled using a linear fit. The observed increase in CCT values is consistent with a green chromaticity shift, as the shift would be paralleling the Blackbody Locus for part of the time. It is speculated that the lower asymptotic shift occurring in 7575 arises from the oxidation of only surface sites, whereas bulk sites may be oxidized in 8585, producing a large chromaticity shift and a bigger change in CCT.

Figure 4B-24. Charges in CCT Values for XP-G Product During WHTOL Testing

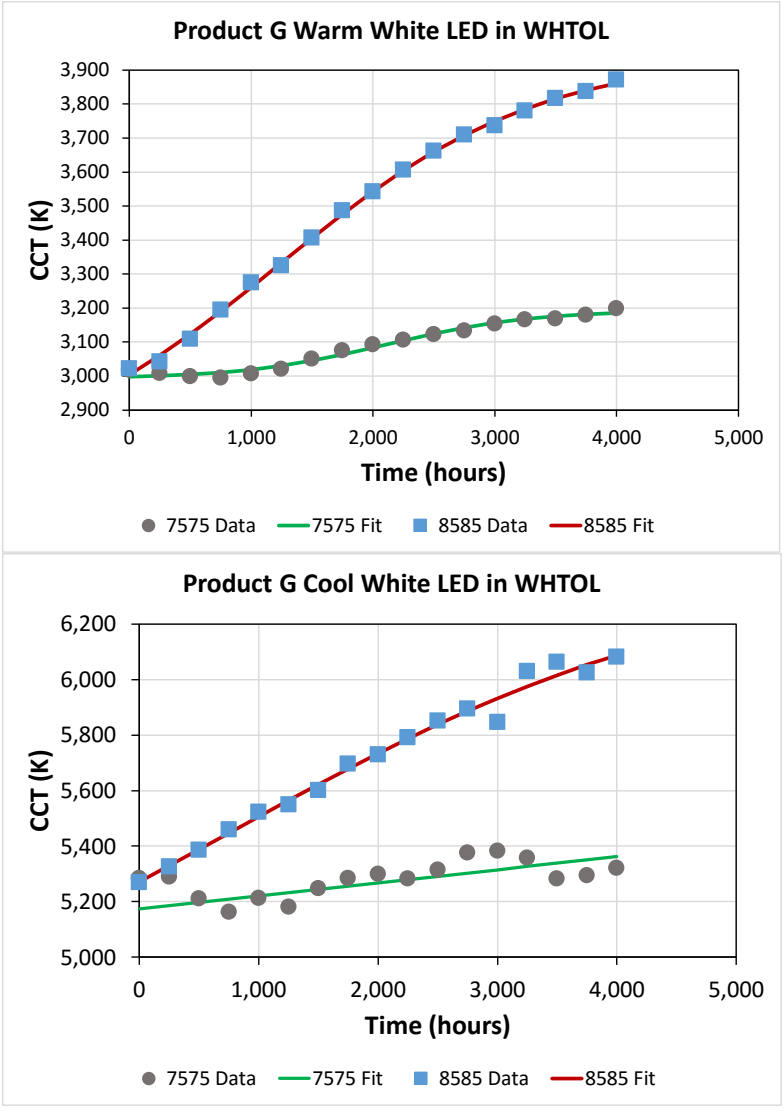

Table 4B-6. Logistic Fit Parameters for CCT Values of LEDs in WHTOL Testing

Color	Test	*k*	C	Max CCT	R^2	Durbin-Watson
Warm white	7575	1.71×10^{-3}	36.8	3,193	0.982	0.75
Cool white	7575	9.85×10^{-5}	1.45	6,320	0.552	0.89
Warm white	8585	9.45×10^{-4}	3.17	3,940	1.00	1.97
Cool white	8585	4.90×10^{-4}	1.45	6,417	0.987	2.52

Auburn University also examined the expansion of the silicone-phosphor layer in Product G, and the results are given in **Figure 4B-25**. Virtually no expansion of the silicone-phosphor layer was found in cross-sectional SEM imaging, which indicates that the silicone did not swell in the presence of moisture. This finding helps to explain the absence of a blue shift, as was observed for the XR-C product. We attribute this finding to the use of higher-durometer silicone encapsulants in the LED die structure. The higher-durometer materials have a lower permeability to moisture, but still allow moisture transport through the material. In addition, the higher-durometer matrix is less able to accommodate the hygroscopic swelling that occurred with Product XR-C, and this mechanism for blue chromaticity shifts has been essentially eliminated in modern surface-emitting LEDs.

Figure 4B-25. Cross-Section SEM Image of the Interface Between the Die and the Silicone-Phosphor Layer for a Control Sample of Product G (Left) and a Sample Subjected to 5,352 Hours of 8585 (Right)

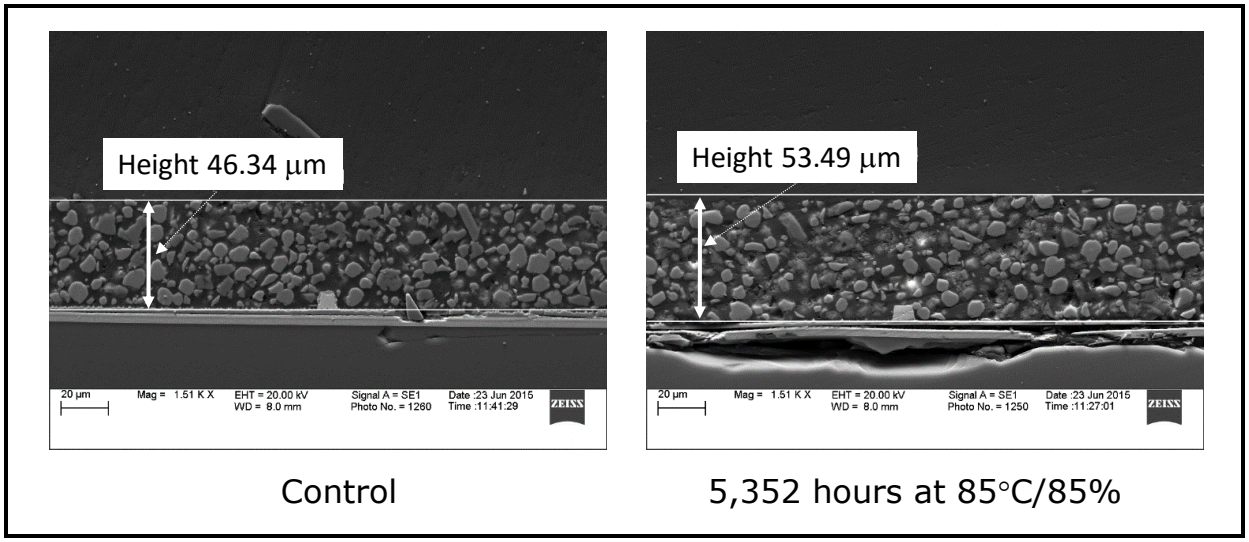

Note: Virtually no change in the thickness of the phosphor-binder layer was found. The images were taken at a magnification of 1,500X and a working distance of 8.0 mm.

Surface-Emitting HP-LEDs with Phosphor-Ceramic Plate Conversion Layers in WHTOL

Product LR represents an alternative approach to fabricating HP-LEDs and was evaluated during our testing for this reason. This LED structure was very commonly used in many early SSL products and was a direct competitor to Product G when it was first introduced. This type of structure is still used in some HP-LEDs and elements of this structure will likely be used in higher-power devices, such as laser-based emitters. A picture of the general package structure used in Product LR is given in **Figure 4B-26**. The distinguishing feature of this LED package is the use of a ceramic binder as a matrix for the phosphor to create a "phosphor plate." This phosphor plate is placed on top of the LED and held in place with a thin silicone adhesive. A silicone lens is then molded over the LED to promote light extraction. Lumileds was an early leader in this technology, which was also used by other LED manufacturers, including Osram. The primary advantages of this LED package structure are that the phosphor plate has better thermal conductivity and lower permeability than a phosphor layer made with silicone binder. Therefore, this package is better able to dissipate any heat that builds up in the phosphor layer and is better at preventing degradation of the phosphor by atmospheric contaminants such as water. As a result, the LEDs with this structure exhibited significantly better stability in WHTOL and temperature shock stress tests than did LEDs made with silicone binders [48-51].

Figure 4B-26. Schematic Cutaway of the General Package Structure of HP-LED Devices, Such as Product LR, That Use the Phosphor Plate Structure

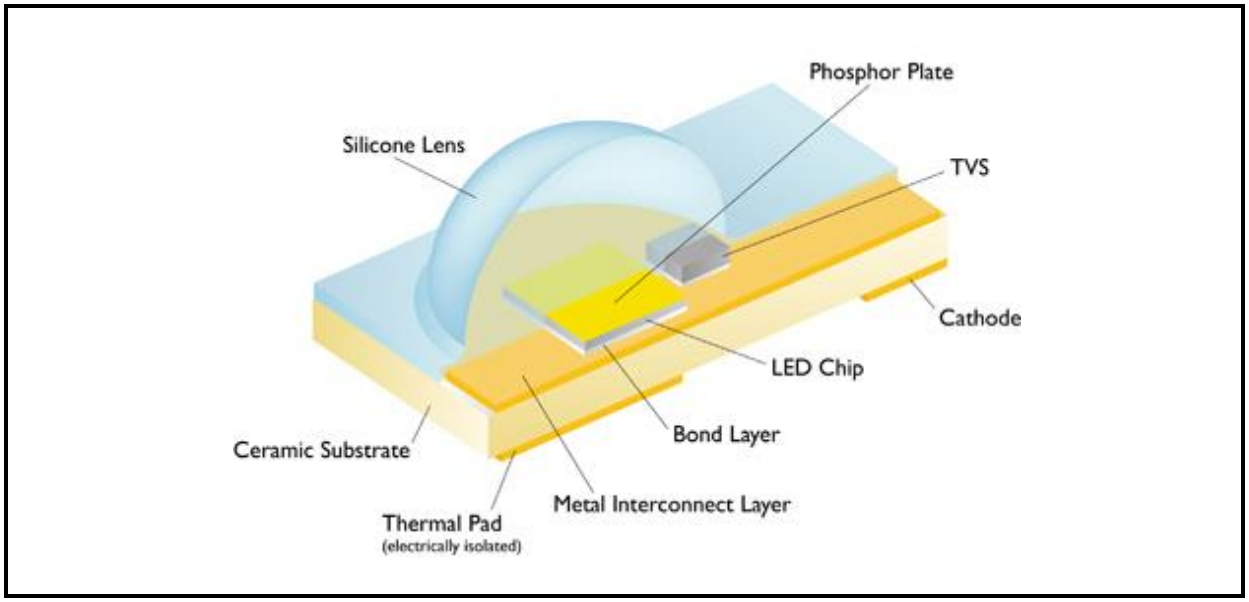

Testing of Product LR devices was conducted at RTI, and both cool white and warm white products were examined during this study under WHTOL environments of 8585 and 7575.

The devices were operated at 700 mA, and power was supplied to the devices on a 1-hour duty cycle.

The lumen maintenance behavior of the Product LR devices is given in **Figure 4B-27**, and the value of the α parameter depended upon the WHTOL test that was used and the CCT value of the LED. In contrast to the findings with the Product G devices, the luminous flux decayed throughout the WHTOL testing period for both cool white and warm white products. The decay rates for the different test conditions of cool white and warm white products are given in **Table 4B-7**.

Figure 4B-27. Average Luminous Flux Maintenance for the Test Samples of Product LR Devices

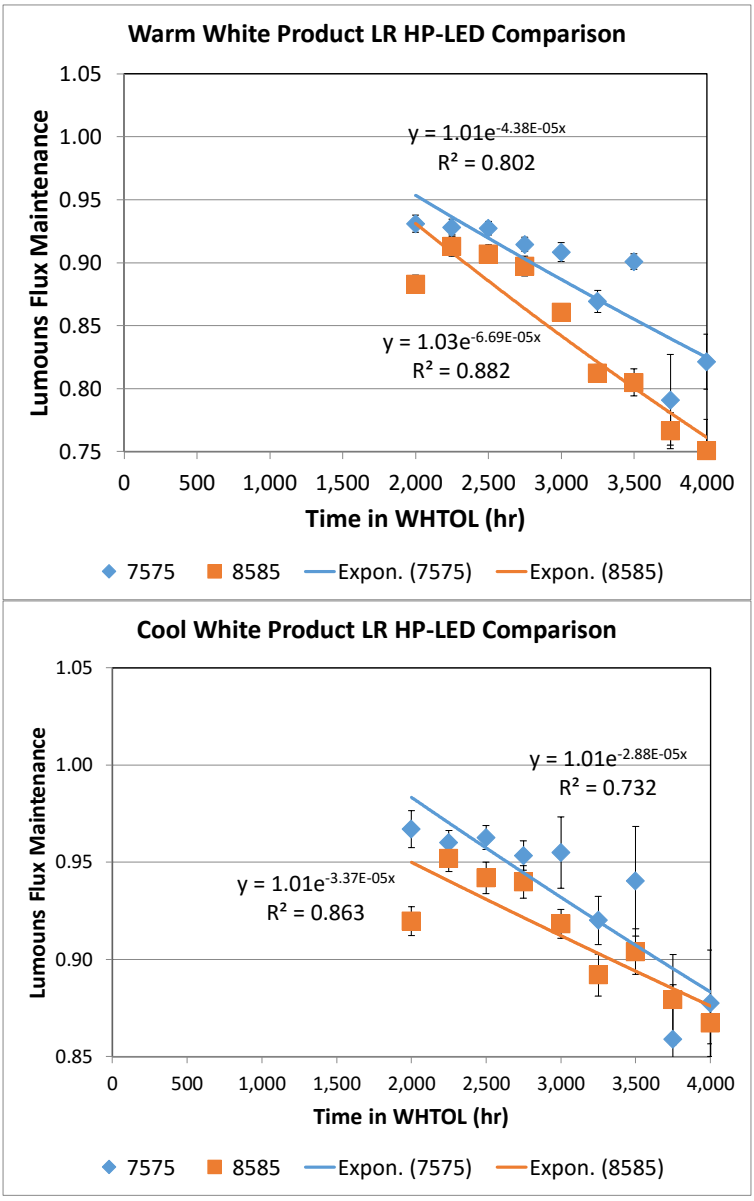

Note: The results for warm white LEDs are shown on the top, and the results for cool white LEDs are shown on the bottom. The error bars represent one standard deviation about the average.

Table 4B-7. Rates of Exponential Decay for WHTOL Test of Product LR LEDs Compared with Temperature Alone

LED Color	WHTOL Test	Exponential Decay Rate
Warm white	7575	4.38×10^{-5}
Warm white	8585	6.69×10^{-5}
Cool white	7575	2.88×10^{-5}
Cool white	8585	3.37×10^{-5}
Warm white	85°C and 500 mA	4.31×10^{-6}
Cool white	85°C and 500 mA	1.63×10^{-6}

The time-dependent SPD measurements obtained from the warm white version of Product LR exposed to 8585 and 7575 are shown in **Figure 4B-28**, and the corresponding SPD measurements for the cool white package are shown in **Figure 4B-29**. For both the warm white and cool white spectra, emissions did not significantly shift for either the LEDs or the phosphor layer. This finding suggests that the glass/ceramic binder used in the phosphor plate produces a more stable secondary emitter, even in oxidizing environments such as WHTOL. In addition, the magnitude of the blue LED emission peak consistently decreased over time for both warm white and cool white, indicating that there is virtually no expansion of the phosphor plate in high-temperature and high-humidity environments. There are some clear advantages to this package type from a chromaticity stability standpoint; however, the lumen maintenance of this package was not equal to that of Product G in this testing. In addition, the manufacturing processes required to make the phosphor plate and to attach it the die are potentially costlier than those associated with the phosphor-silicone composite. Consequently, this type of package is mostly used for very high-power devices, such as laser-pumped emitters, and most LED packages made today use the phosphor-silicone composite layer.

Figure 4B-28. SPD Measurements for Warm White Version of Product LR in 7575 (Top) and 8585 (Bottom) as a Function of Exposure to the WHTOL Environment

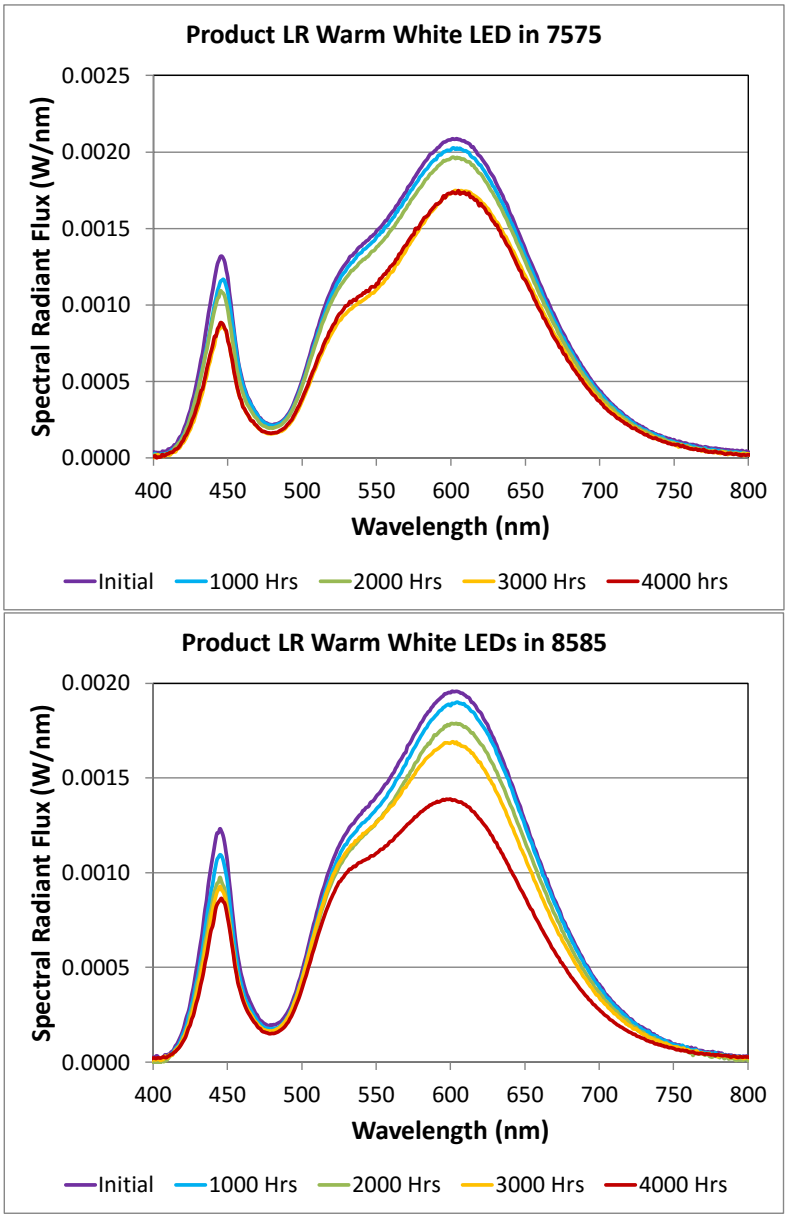

Figure 4B-29. SPD Measurements for Cool White LEDs in the Product LR Package Exposed to 7575 (Top) and 8585 (Bottom) as a Function of Exposure to the WHTOL Environment

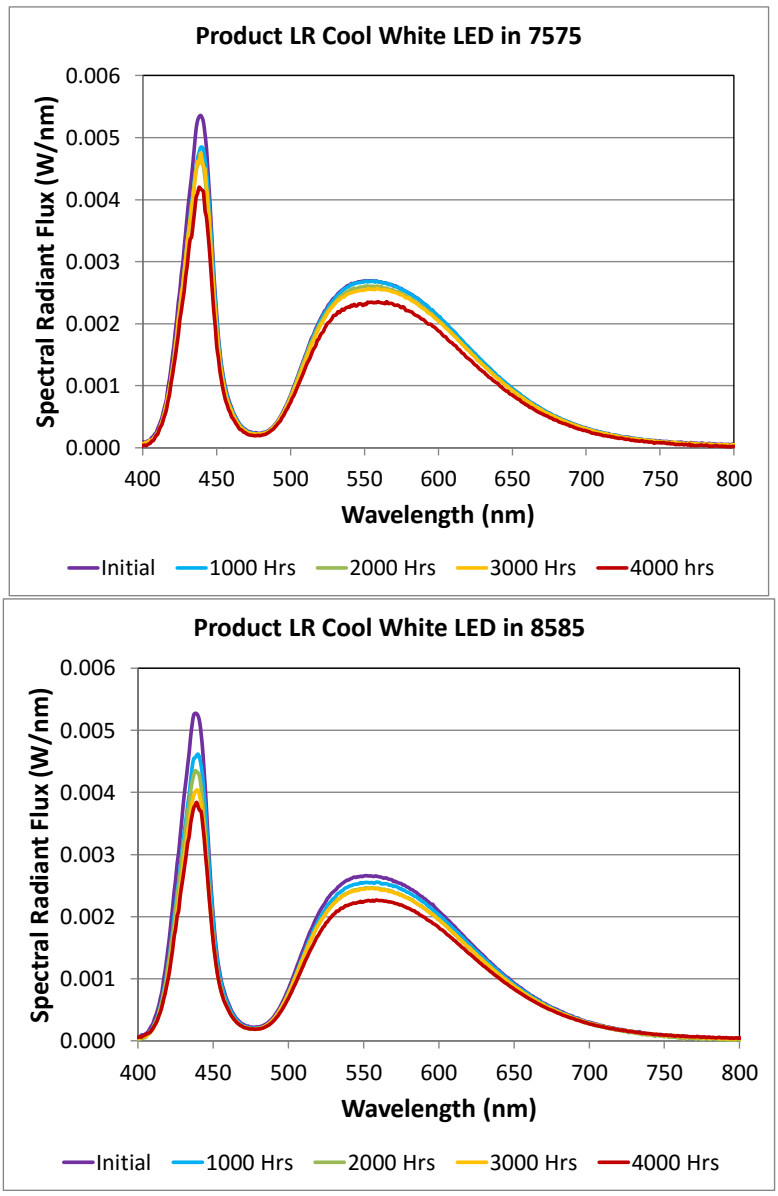

Bulk-Emitting, Shaped Chips HP-LEDs with Silicon-Phosphor Conversion Layers in WHTOL

A recent advance in LED technology for lighting applications is the use of shaped chips to increase the light extraction efficiency of bulk LED emitters [52; 53]. Bulk emitters are attractive because of their better droop performance, but the limited escape cones have restricted their use until recently. In a white light-emitting shaped chip, a phosphor-silicone

conversion layer is applied around the shaped chip in a three-dimensional structure, as shown in **Figure 4B-30**.

Figure 4B-30. Pictures of Three-Dimensional, Shaped LED Chips Used for Lighting

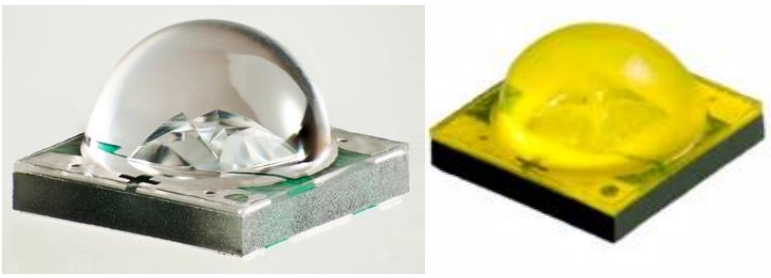

Note: The chip on the left is a direct-emitting blue LED, and the chip on the right is a pcLED device in which a phosphor-silicone composites surrounds the three-dimensional structure and provides secondary conversion of blue photons.

We have previously provided comprehensive reports on the performance of bulk LED emitters with shaped chips in WHTOL testing [46; 54; 55]. For simplicity, the results will be summarized here. Product T, which uses the bulk-emitter shaped LED described in these reports, exhibits behavior like that discussed above for Product G. In particular, the phosphor emission peak shifted to significantly lower wavelengths, resulting in an increase in luminous flux after 6,000 hours of 8585. The net result was a large chromaticity shift in the green direction (CSM-2 behavior with a negative $\Delta u'$), and the magnitude of this shift was generally larger than that reported above for Product G. It is not known whether the larger chromaticity shift observed for Product T is a consequence of the shaped-chip structure or whether different phosphor blends are used in this device than in Product G. In 7575 test, the rate of chromaticity shift was again higher for the warm white version of Product T (bulk LED with shaped chip) compared with Product G (surface emitter with phosphor-silicone conversion layer); however, for the cool white version of each product, the rate of chromaticity shift was lower for Product T and for Product G. These findings suggest that there are potential differences in the phosphor mixes used in the two products, which may account for some of the differences in observed behavior.

A multichip version of Product T is also available on the market, and a picture of this device is shown in **Figure 4B-31**. The small "bumps" visible in Figure 4B-31 are individual LEDs that are connected in series. Tests were conducted at RTI on the multichip version of this device, and some accommodations to the test procedures described above were made to facilitate the study. First, the LEDs were tested in the commercial luminaire shown in **Figure 4B-32**. To examine only the changes in the LEDs, the lenses were removed from the luminaire, and the driver was placed outside the environmental chamber but connected to the LED board through insulated wiring. In addition, the performance of the five LEDs in

the luminaire light source was measured ensemble at the luminaire level. The tight spacing of the LEDs makes it virtually impossible to measure the light emissions from a single device without modifying the LED board. The LEDs that were tested consisted of 16 small LEDs in series with five LED packages in series. This resulted in 80 LEDs total in series. A voltage of roughly 250 V was required to operate the luminaire. We decided to pursue testing on this product to mimic behavior that would be found in COB-LEDs.

Figure 4B-31. Picture of the High-Voltage Version of Product T, Which Contained Multiple Small LEDs in the Same Footprint

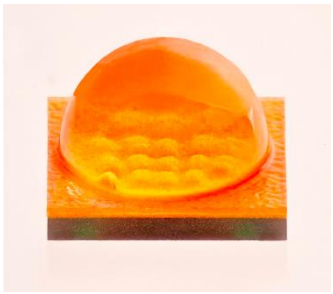

Figure 4B-32. Picture of the Luminaire Used to Test the High Voltage, Multichip Version of Product T

Separate experiments were conducted on the high-voltage version of Product T using the procedures described above, and the behavior of this product was found to be similar to the behavior of the single-chip version of Product T. An example of this data in shown in **Figure 4B-33**, which gives the change in $\Delta u'v'$ as a function of time in 7575. The total chromaticity shift, ($\Delta u'v'$), increased rapidly and exceeded the parametric limit of 0.007, set by Energy Star®, in less than 1,250 hours of testing in 7575. An examination of the individual chromaticity coordinates revealed that the chromaticity shift is accounted for almost entirely

by a negative shift in the u' component, which is characteristic of CSM-2 behavior and a green chromaticity shift. The magnitude of the luminous flux maintenance, chromaticity shift, and increase in CCT for the high-voltage version of Product T was similar to that of the corresponding warm white single-chip version of Product T and largely aligned with that discussed above for Product G.

Figure 4B-33. Chromaticity Shift, as Measured by $\Delta u'v'$, for the High-Voltage Version of LED Product T

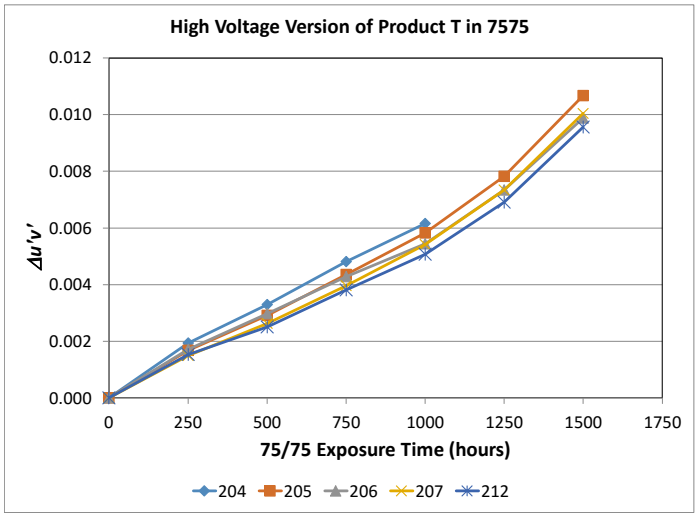

Note: The samples were tested in groups of five mounted in a luminaire with the lens removed and a driver external to the environmental chamber.

Testing of MP-LED Modules in Elevated Ambient Temperatures

Finally, as part of DOE Award DE-EE0007081, RTI conducted elevated ambient testing on a series of LED modules composed of separate assemblies of 40 warm white MP-LEDs and 40 cool white MP-LEDs. Each LED assembly consisted of four LEDs in series in each string and 10 LED strings in parallel. There were two LED assemblies, warm white and cool white, per LED module. A picture of the LED module is shown in **Figure 4B-34.** The CCT values of the MP-LEDs in the module are distinguishable by their color: the warm white LEDs have an orange color (due to a higher content of red-emitting phosphors), and the cool white LEDs have a yellow color (due to the large concentration of cerium-doped yttrium aluminum garnet [Ce:YAG] in the phosphor mix). Additional details on the LED modules and their testing can be found in a paper by Davis et al. [40].

Figure 4B-34. Picture of the LED Modules Tested as Part of DOE Project DE-EE0007081 and Included Here for Completeness

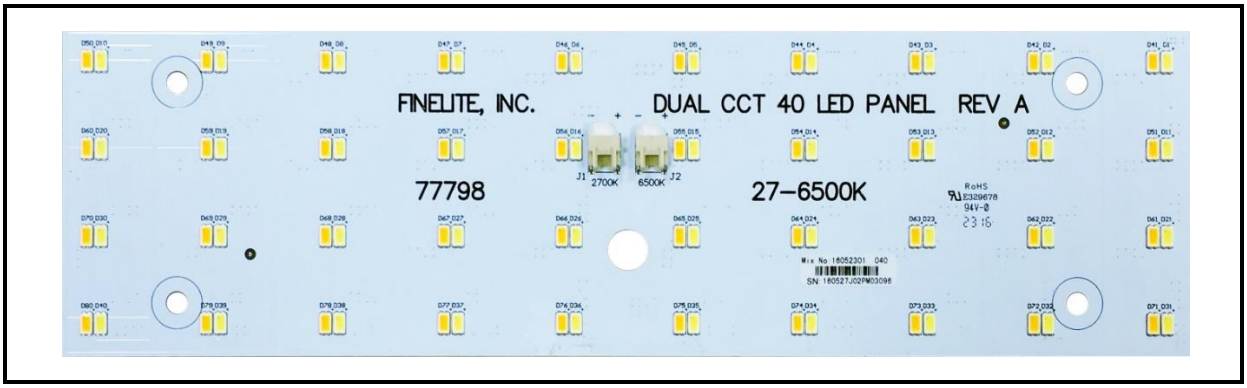

Note: The modules consist of separate assemblies of 40 warm white MP-LEDs (the orange modules in the image) and 40 cool white MP-LEDs (the yellow modules).

During elevated ambient testing, a group of LED modules was placed in an oven with the temperature set to either 75°C or 95°C. No humidity was intentionally introduced during these HTOL tests. The LED modules were hung vertically from metal racks using metal clips, and no additional heat sinks were applied to the boards. Four boards were hung from each metal rack, and each board irradiated the backside of its neighboring board, which was covered with white solder mask. The spacing between adjacent boards was approximately 4 inches to allow sufficient air flow to maintain thermal equilibrium during test.

The LED assemblies on each module were operated separately at preselected currents of 350 mA, 700 mA, 1,000 mA, and 1,500 mA. Because the LED modules were configured with 10 parallel strings of LEDs, the actual current delivered to each LED was 1/10th of the total drive current. Both LEDs on the board were operated simultaneously at the preset current level when in the oven, and separate electronics were used to provide power to each assembly. The LED assemblies set to 350, 700, and 1,000 mA were operated by individual single-channel LED drivers programmed to a specific, constant current level. The LED assemblies operated at 1,500 mA were controlled by two-channel laboratory power supplies. The modules were switched on a 1-hour on and 1-hour off cycle, with the 700 mA and 1,000 mA samples switching together and the 350 mA and 1,500 mA samples switching together.

This configuration exposes the LED boards to both elevated ambient temperatures and elevated irradiation levels from both warm white and cool white LEDs. This approach was used to accelerate aging by maximizing the amount of environmental stress on the LED modules. In general, we found that the board temperature increased by 12–14°C above the elevated ambient temperature on boards when both LED assemblies operated with a forward current of 1,500 mA (i.e., 150 mA per LED).

Photometric measurements were taken at regular intervals on these boards, and 8,000 hours of data have been recorded to date. Each LED assembly was measured separately. During photometric testing, a forward current of 700 mA was applied to the LED assembly on the LED module, corresponding to 70 mA per LED, regardless of the forward current used in the HTOL tests. This approach allowed the calculation of TM-21-11 values, including the decay constant α, using the Energy Star® TM-21-11 calculator [56]. The α values calculated for both warm white and cool white LED assemblies at the various currents and temperatures are given in **Table 4B-9**.

There were some differences in performance between the LED module and the manufacturer's data for the LED alone. For a LED module operated at a forward current of 1000 mA in HTOL, the measured luminous flux value was 0.98 after 8,000 hours of testing, in agreement with the value reported by the LED manufacturer for LM-80-08 test conditions of 100 mA and 85˚C. After 8,000 hours of testing at a forward current of 1,500 mA for the LED module in HTOL, the luminous flux maintenance of the LED module was actually better than that given by the LED manufacturer (0.963 for the LED module compared with 0.867 for the LED using LM-80). Nonetheless, the measured α values for the LED assemblies are higher than the reported α value of 3.48×10^{-6} given in the LM-80 data sheet for this LED.

We attribute this difference to three factors. The first factor is the natural errors and uncertainties associated with these measurements, including the likely differences in case temperatures between the two measurements. Second, the test results given here were taken at the LED module level (i.e., LEDs plus printed circuit board plus solder mask), whereas the manufacturer's LM-80-08 report is for LEDs only. This difference can be important, as we have found that the solder mask on these LEDs turns brown at high temperatures and photon flux, as occurred in these tests. Third, the reported LM-80 results are for warm white LEDs with a CCT value of 3,000 K. The warm white LEDs that were incorporated into the modules tested here had a CCT value of 2,700 K, which may be expected to have a higher α value due to the greater use of red nitride phosphors.

Table 4B-8. α Values Calculated with the Energy Star® TM-21-11 Calculator for the MP-LED Modules Under Different Ambient Temperatures and Forward Currents

	75˚C Elevated Ambient		95˚C Elevated Ambient	
Current	**Warm White**	**Cool White**	**Warm White**	**Cool White**
350 mA	2.82×10^{-6}	2.61×10^{-6}	3.98×10^{-6}	3.63×10^{-6}
700 mA	1.57×10^{-6}	3.29×10^{-6}	5.01×10^{-6}	2.34×10^{-6}
1,000 mA	6.69×10^{-6}	4.38×10^{-6}	5.49×10^{-6}	3.45×10^{-6}
1,500 mA	8.16×10^{-6}	6.44×10^{-6}	9.94×10^{-6}	8.29×10^{-6}

The degradation of the solder mask on these LED modules during elevated ambient exposure is shown in **Figure 4B-35**, and the processes involved in the degradation reaction are initiated by both temperature and light. The amount of change depends on both temperature and current because light flux is related to current. If temperature is constant, higher currents will still produce a greater change in solder mask reflectance than lower currents. However, the level of degradation appears to reach a limiting value such that all reflectance profiles of the LED boards were equivalent to those shown in Figure 4B-35. Clearly, as the solder masks age in the accelerated environment, the reflectance drops at all visible wavelengths, which will affect luminous flux output due to self-absorption. In performing photometric measurements of these parts, we used the auxiliary lamp and self-absorption correction factors determined when the modules were new. To more closely follow the behavior that would be observed in a luminaire, we did not add additional corrections as the solder mask started to turn brown. Therefore, there is an uncompensated self-absorption during photometric measurement of the parts that will lower luminous flux values in aged samples; however, we expect this difference to be minimal, especially because the luminous flux maintenance values that are measured at the module level are equal to or greater than the reported values at the LED level. We attribute the observed degradation in the reflectance properties of the solder mask to oxidation of the epoxy in the solder mask, which caused the brownish tint to the solder mask.

Figure 4B-35. Reflectance Spectra of the Solder Mask from an Unexposed Board and Boards Following 8,000 Hours of Exposure of Separate Populations to 75˚C and 95˚C Elevated Ambient Environments

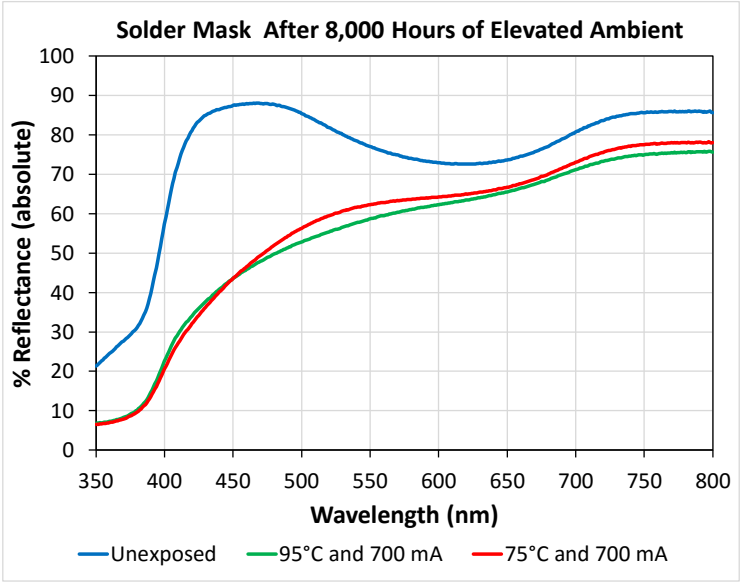

An examination of the photometric properties of these LED modules also reveals differences in the chromaticity stability of warm white and cool white LEDs. The chromaticity changes for the cool white and warm white LEDs are shown in **Figure 4B-36** and **Figure 4B-37**, respectively, for forward currents of 350 mA and 1,500 mA.

Figure 4B-36. Chromaticity Shifts Measured for Cool White LEDs from the Tested MP-LED Modules

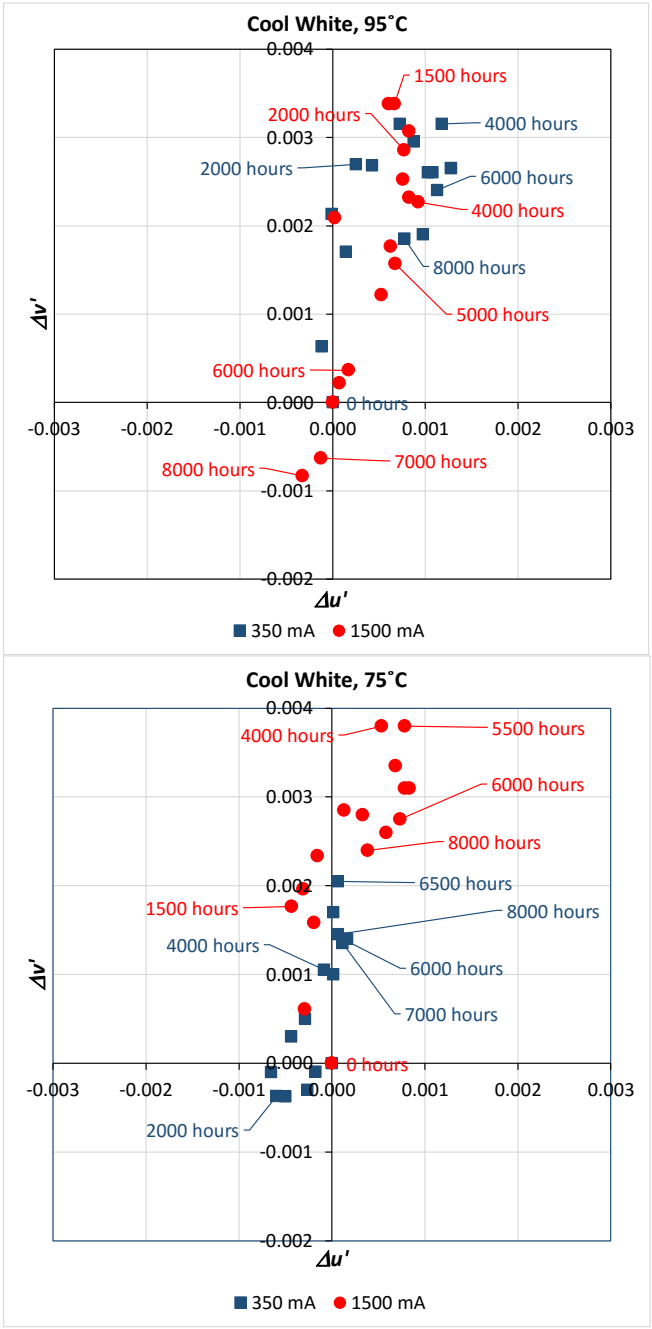

Note: The graph on top shows the performance at the 95˚C elevated ambient temperature ($T_{substrate}$ ~ 107˚C), and the graph on the bottom shows the behavior in the 75˚C elevated ambient temperature ($T_{substrate}$ ~ 88˚C). For both graphs, red circles represent forward current of 1,500 mA

per module and blue squares represent 350 mA per module. Measurement times are indicated for select data points.

Figure 4B-37. Chromaticity Shifts Measured for Warm White LEDs from the Tested MP-LED Modules

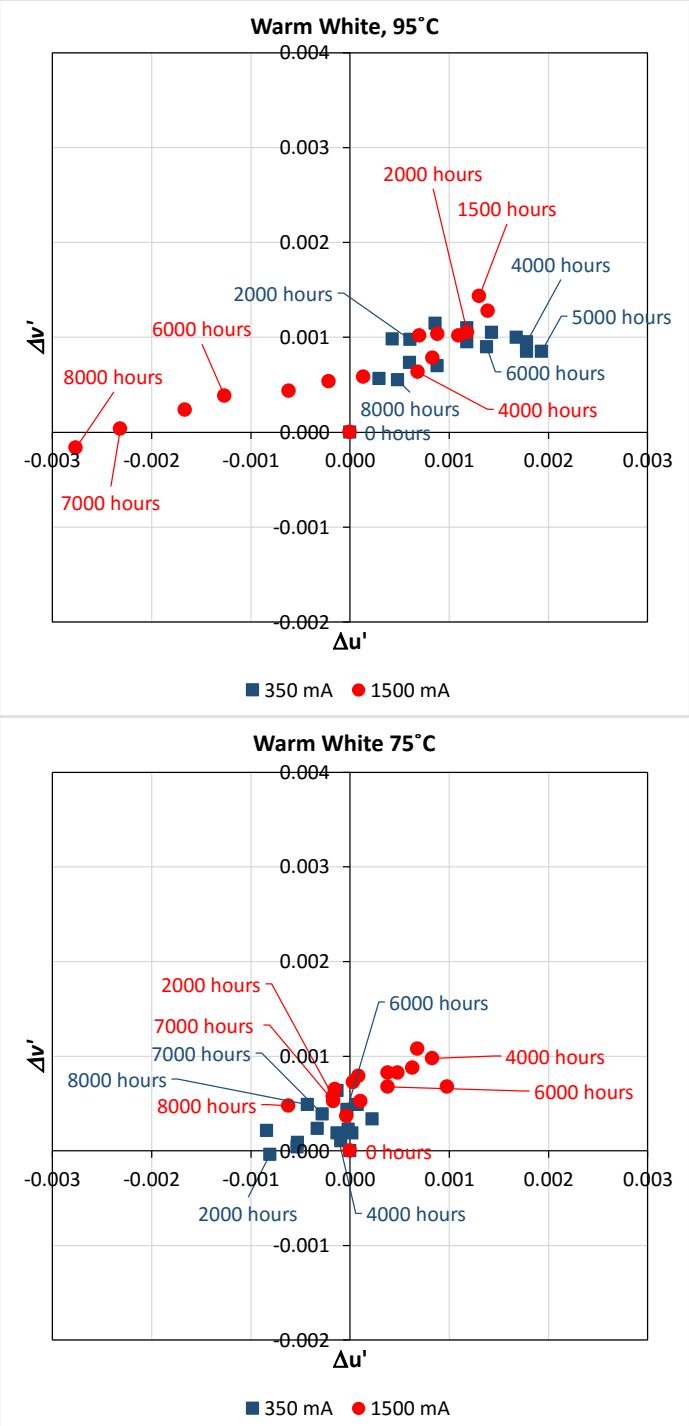

Note: The graph on the top shows the performance at the 95°C elevated ambient temperature ($T_{substrate}$ ~ 107°C), and the graph on the bottom shows the behavior in the 75°C elevated ambient temperature ($T_{substrate}$ ~ 88°C). For both graphs, red circles represent forward current of 1,500 mA per module and blue squares represent 350 mA per module. Measurement times are indicated for select data points.

For the cool white LEDs in the 95°C elevated ambient environment, the general trends observed for the 350 mA and 1,500 mA samples were the same, but the timing and extent of the chromaticity shifts were different after 8,000 hours of exposure to the HTOL conditions. For the 1,500 mA samples, the chromaticity shift initially proceeded in the yellow direction (i.e., primarily along the positive v' axis) for the first 1,500 hours of testing. Then the chromaticity reversed and shifted toward the blue direction. The chromaticity point after 8,000 hours of testing was bluer than the starting point (i.e., both $\Delta u'$ and $\Delta v'$ were negative relative to the starting point). At the end of 8,000 hours of HTOL testing at an elevated ambient temperature of 95°C ($T_{substrate}$ ~ 107°C) and 1,500 mA, the total amount of chromaticity shift for the LED modules, as measured by $\Delta u'v'$, was 0.0009, which is less than the value given in the LM-80-08 report for 105°C and 150 mA (0.0022). This type of chromaticity shift has been observed in other MP-LED packages and has been assigned as a CSM-4 shift [27]. The same basic pattern was observed for the samples operated at 350 mA in the 95°C elevated ambient temperature, although the timing and extent of reaction were different. Most notably, the lower operating current slowed the chromaticity shift process so that the maximum yellow shift occurred after 4,000 hours. In addition, the ending chromaticity point was in a more yellow direction relative to the starting point (i.e., both $\Delta u'$ and $\Delta v'$ were positive relative to the starting point), although the chromaticity shift was trending toward the blue direction. Consequently, the $\Delta u'v'$ value for the LED modules operated at 350 mA in the 95°C HTOL test was 0.0020; however, this value is trending downward because of the blue shift. There is no reported LM-80-08 value for this LED at a forward current of 35 mA.

The same basic trends were found for the cool white LEDs in the 75°C elevated ambient, as shown in the bottom graphic in Figure 4B-36. At an operational current of 1,500 mA, the chromaticity of the LED modules initially shifted in the yellow direction and reached a maximum value at roughly 5,500 hours of testing. At this point, the chromaticity reversed and began to move toward the blue direction, which is characteristic of CSM-4 behavior. For the 350 mA operating current in the 75°C elevated ambient, the initial chromaticity shift was in the blue direction (i.e., both $\Delta u'$ and $\Delta v'$ were negative relative to the starting point) for roughly 2,500 hours. The chromaticity then proceeded in a generally yellow direction until 6,500 hours, when it reversed and again shifted in the blue direction. This behavior is a textbook CSM-4 shift, and the absence of the initial blue shift in the other three measurements may be the result of the higher stress conditions and the time between measurements. In other words, the first blue shift happened so fast in these tests that it was not measured, given the measurement frequency. In general, the CSM-4 behavior of

the cool white LED can be attributed to the photo-oxidation of the molding resin used in the device. This reaction can be expected to proceed at the interface between the molding resin and the silicone encapsulant and require the presence of both an oxidant (i.e., water or air) and blue photons. A bulk photo-oxidation process would be expected to be slower because (1) the oxygen has to diffuse through the already-oxidized material to reach an interior reaction site and (2) the blue photon flux will be attenuated by absorption from the surface layers. There is undoubtedly some impact from the yellowing of the solder mask of the LED modules, but we believe this is a secondary influence, with the behavior of the warm white LEDs being the dominant influence.

For the warm white LEDs in the 95°C elevated ambient temperature, a significantly different chromaticity behavior was observed. At an operating current of 1,500 mA, the initial chromaticity shift of these LEDs was generally in the red direction (i.e., both $\Delta u'$ and $\Delta v'$ increased relative to the starting point and $\Delta u'$ was generally larger than $\Delta v'$). After 1,500 hours, the chromaticity reversed and proceeded in a green direction until 6,000 hours. This shift was parallel to the $\Delta u'$ axis. The chromaticity coordinates then drifted in the cyan direction. At the end of 6,000 hours of exposure to HTOL conditions of 95°C ($T_{substrate}$ ~ 107°C) and 1,500 mA, the $\Delta u'v'$ value for the warm white LED modules was 0.0017, which is better than the LM-80-08 reported value at a LED case temperature of 105°C and drive current of 150 mA. The larger change in the u' component, compared with the smaller change in v', indicates that a significant green shift is occurring, possibly because of phosphor oxidation. The same basic trend was found for the 350 mA operational current in the 95°C elevated ambient except that the chromaticity reversal did not happen until 5,000 hours. In the 75°C elevated ambient test, the chromaticity shift occurred along a similar trajectory, although the rate of change was slower than observed in 95°C testing. At both 1,500 mA and 350 mA, the reversal in chromaticity shift occurred after 5,000 hours, and the change was less distinctive than found at 95°C.

With this insight into the chromaticity shifts occurring in both the cool white and warm white LED assemblies in the MP-LED modules, models can be constructed to project chromaticity at future times. In building these models, it is advantageous to start with the most stressful condition, which is 95°C and 1500 mA for these samples. Although both u' and v' should be modeled for the most accurate estimation, for brevity, only $\Delta v'$ is shown for the cool white assembly because the chromaticity change is primarily in the v' direction. As shown in **Figure 4B-38**, the chromaticity change of the cool white LEDs can be modeled with a bounded exponential function for the initial yellow shift and a logistic function for the blue shift. Least squares fits were used to determine the parameters for all models. All models had R^2 values in excess of 0.85 (R^2 was greater than 0.95 on most), and the autocorrelation of the model residuals was minimal, as judged by the Durbin-Watson statistic. The use of a bounded logistic function for the blue chromaticity shift is significant because it indicates that there is a limit to the mechanism responsible for this reaction. We believe that this limit

is the finite area available at the surface of the MP-LED molding for the photo-oxidation reaction to occur. There is some indication from the 95°C and 1,500 mA cool white data that the rate of change is indeed slowing between 6,500 and 8,000 hours, supporting a lower bound at roughly $\Delta v' = -0.005$. This is equivalent to a 9-step MacAdam ellipse chromaticity change from the maximum yellow shift ($\Delta u'v' = 0.0034$), but is well within the 0.007 total chromaticity shift ($\Delta u'v'$). However, additional testing is needed to confirm the location of this lower bound, and this testing is underway. There is no evidence of what the chromaticity shift will be after the limit of the blue shift is reached. The LED modules may continue to shift in the blue direction, but likely at a slower rate, which could indicate bulk oxidation of the molding resin.

Figure 4B-38. Chromaticity Shift Models for the Cool White Assemblies in the MP-LED Modules

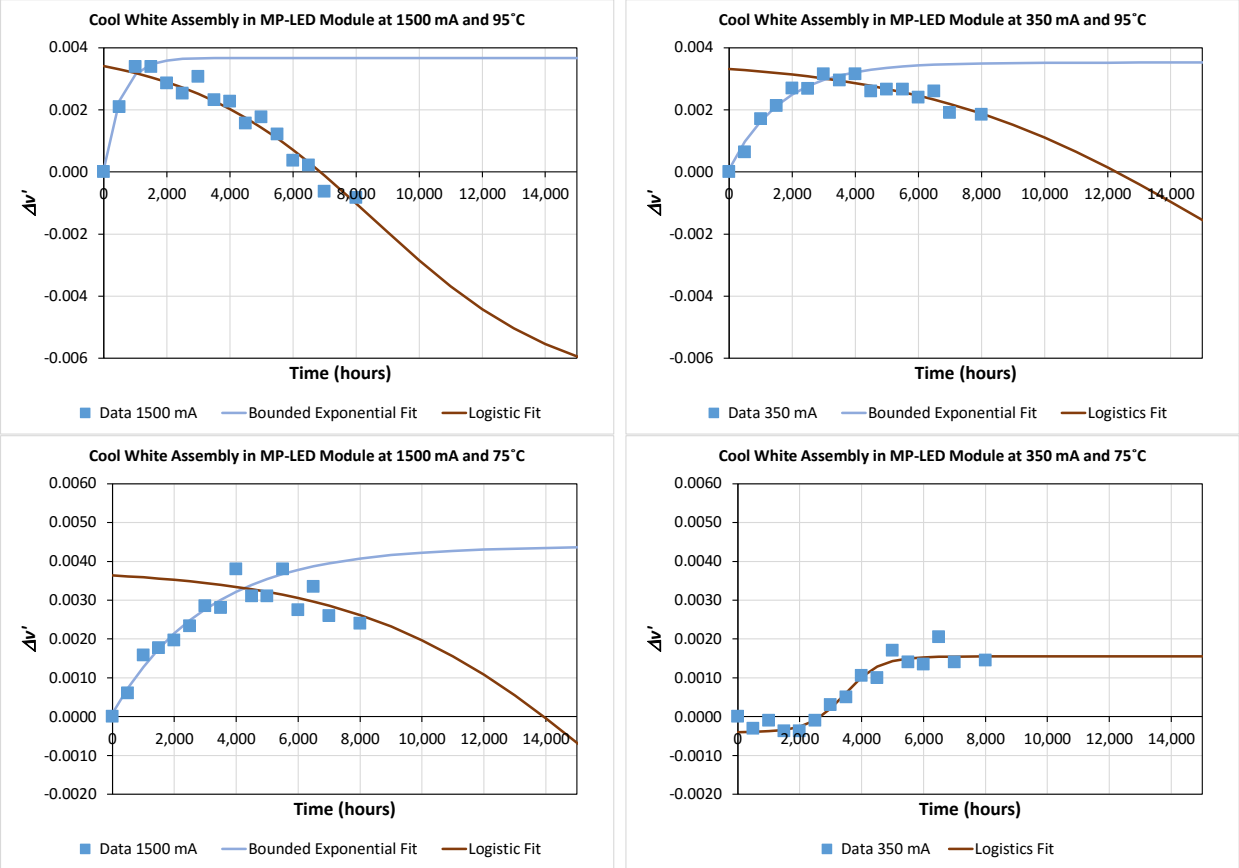

The chromaticity projections for the cool white LEDs demonstrate that the rate of decrease in the v' coordinate slows as the temperature and current decrease. At the lower stress condition of 350 mA and 75°C, the initial shift is in the blue direction (which was not modeled), followed by the expected shift in the yellow direction (i.e., $\Delta v'$ increases). In this

instance, the yellow shift is best modeled by a logistic function because there appears to be an incubation period when the initial blue shift is dominant. At 8,000 hours, there was not sufficient data to model the second blue shift, so it is not included in this analysis.

For the warm white LED, the $\Delta u'$ coordinate models are shown for brevity because this coordinate exhibited the largest change in HTOL testing. However, for the best accuracy, both chromaticity coordinates should be modeled. As shown in **Figure 4B-39**, the shift in the green direction (i.e., the region where $\Delta u'$ is decreasing) appears to be slowing around 8,000 hours, according to the data acquired at 1,500 mA and 95°C. This is a significant finding because it indicates that a lower bound may exist for the green shift as well. Because a green shift is caused primarily by oxidation around the surface dopant in a doped-nitride phosphor, the existence of a lower limit of this process is consistent with the surface concentration of rare-earth dopants being finite, as suggested by Yeh et al. [30]. Because the oxidation of the green phosphor is a surface process, the reaction will become resource-limited as the surface reaction sites are consumed. As this happens, the rate of reaction decreases and the process approaches an asymptote. However, additional testing is required to confirm the exact location of this asymptote. It is possible that additional chromaticity shifts occur after 8,000 hours of elevated ambient temperatures, but there is no indication in the available data. For example, the green shift could continue but at a lower rate, as reported elsewhere [41], or the blue shift found in the cool white packages could emerge as the dominate chromaticity shift mechanism.

Figure 4B-39. Chromaticity Shift Models for the Warm White Assemblies in the MP-LED Modules

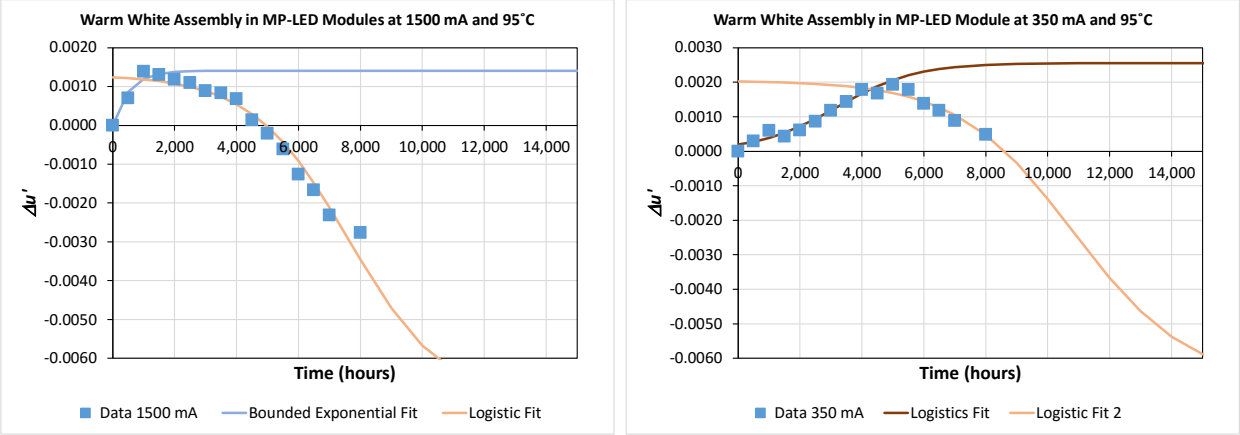

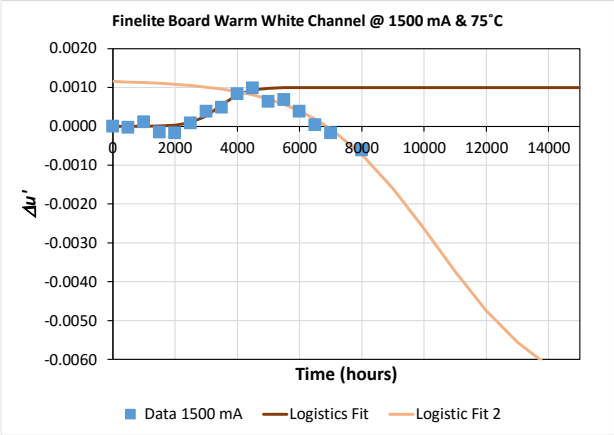
Finelite Board Warm White Channel @ 1500 mA & 75˚C
0.0020
0.0010
0.0000
-0.0010
-0.0020
-0.0030
-0.0040
-0.0050
-0.0060
Δu'
0
2000
4000
6000
8000
10000
12000
14000
Time (hours)
Data 1500 mA
Logistics Fit
Logistic Fit 2

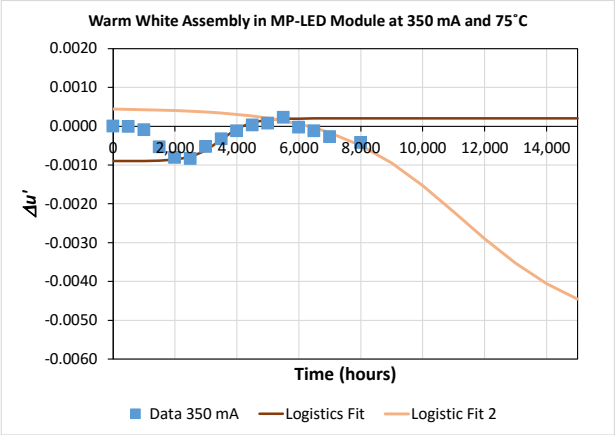
Warm White Assembly in MP-LED Module at 350 mA and 75˚C
0.0020
0.0010
0.0000
-0.0010
-0.0020
-0.0030
-0.0040
-0.0050
-0.0060
Δu'
0
2,000
4,000
6,000
8,000
10,000
12,000
14,000
Time (hours)
Data 350 mA
Logistics Fit
Logistic Fit 2

4.C LED Lamp Behavior

Although data acquired using the LM-80-08 method is not readily available to the general lighting public, information about reliability of LED devices can be gathered by examining public sources of information about specific lamp and luminaire types. Individual LEDs are incorporated into LED lamps and luminaires to make SSL devices. Some of the first products that appeared on the market were LED lamps, but the actual lifetimes of these products deviated widely from users' expectations, which created a potential credibility issue for this nascent technology.

To lend clarity to the situation, Pacific Northwest National Laboratory (PNNL), through funding from DOE, conducted a series of benchmarks and an evaluation of various LED lamps, including PAR38 lamps [57-60], A19 lamps [61-63], and the L-prize lamps [64; 65]. Several different tests were performed as part of this evaluation, including initial performance characterizations [57; 61; 65], operation at elevated ambient environments [60; 63; 27], and highly accelerated stress testing (HAST) [59; 64]. In many cases, the performance of LED-based products was directly compared with that of traditional lighting technologies such as incandescent, halogen, and compact fluorescent lamps (CFL). A general finding from PNNL's work is that the luminous efficacy of LED lamp products has improved considerably over the last 5 years, and now LED lamps are generally more efficacious than products that rely on other lamp technologies. In addition, LED products were found to have better lumen and chromaticity maintenance than conventional lamp technologies and are more robust.

During this project, RTI partnered with PNNL to expand on their initial benchmarking studies on the performance of LED lamps. This effort was motivated in part by the availability and thoroughness of the data that PNNL collected during its tests. In some PNNL datasets, full SPD measurements were taken on a weekly basis using the lab's automated long-term test apparatus (ALTA) facility. An additional motivation was to fill in gaps in the data about LED performance. As noted above, LED manufacturers are hesitant to provide information on their products, especially spectra data and chromaticity maintenance information, and the PNNL data helped to fill this gap.

Originally, because of limited resources, this project did not intend to look at LED lamps due to the limited design features in many lamps and the wide-ranging quality of lamp products. However, as the project progressed, we decided to include LED lamps on a limited basis to broaden the data and fill in the knowledge gaps regarding the behavior of LED products. As such, this section will focus only on our findings, and is not intended to be a broad survey of the reliability of all LED lamps.

4.C.1 Elevated Ambient Testing of PAR38 Lamps

Using one of its ALTA facilities, PNNL conducted lumen and chromaticity maintenance testing of PAR38 lamps for nearly 14,000 hours in a mildly elevated environment of 45°C. The lamps were continuously operated during the test (i.e., they were not switched on and off), except during power outages [60]. This work examined 32 commercial LED-based PAR38 products, 2 equivalent CFL-based commercial PAR38 products, 3 equivalent halogen-based PAR38 products, and 1 equivalent ceramic metal halide-based PAR38 product. Five samples of each product were tested, providing a means to assess the reproducibility of results [60].

RTI and PNNL performed a deep dive into the reliability of the test products, including additional analyses of the 160 LED-based PAR38 samples. The analyses performed by RTI included a detailed examination of the chromaticity changes across the different LED lamp models [27]. Given that the PAR38 lamps were operated at a mildly elevated ambient temperature of 45°C, minimal changes in the lenses and other optical materials in the lamps were seen in the test samples, with one exception. Because of the design of PAR38 LED lamps and the minimal changes in optical materials, virtually all chromaticity shifts observed in this study were attributed to changes in the LEDs [27]. Consequently, RTI used these data to fill the gaps in the limited amount of information shared by LED manufacturers, and obtained a fuller picture of LED performance.

Another advantage of the collaboration between RTI and PNNL is that the 32 different LED-based PAR38 lamps used a variety of LED packages (as shown in **Table 4C-1**), including HP-LEDs, plastic leaded chip carriers (PLCCs), COB-LEDs, and hybrid LEDs. HP-LEDs generally consist of a ceramic base that is soldered to a printed circuit board (PCB), and the maximum operational power of these devices is greater than 2 W. PLCCs consist of one or more LED dies in the base of a molded plastic chip carrier with the LED attached to a silver-plated lead frame overmolded with a polymer resin such as PPA, PCT, EMC, or SMC. The operational power range of PLCCs can vary widely depending on the number of LEDs in the package. MP-LEDs are a special class of PLCCs that often contain a single die and are operated at power levels below 0.5 W. COB-LEDs consist of multiple LEDs mounted on a common substrate (often ceramic) and covered with a common phosphor layer. Hybrid LEDs consist of LEDs with different emission wavelengths that are mounted on a common PCB and mixed together in an optical cavity to produce white light. In this case, the hybrid LED package consisted of three slightly greenish pc-LEDs and a single red direct-emitter in the same package.

Table 4C-1. Breakout of the LED Package Types Found in the 32 Different LED PAR38 Lamps Examined in CALiPER 20.5 [27]

LED Package Types	Number of PAR38 Lamps in CALiPER 20.5 [27]
HP-LEDs	18
PLCCs	7
COB-LEDs	6
Hybrid LEDs	1
Total	**32**

Based on the analyses that were performed jointly with Michael Royer of PNNL and summarized in DOE CALiPER 20.5, five primary chromaticity shift modes (CSMs) were identified in the PAR38 lamps [27; 66]. The primary CSMs are presented in **Table 4C-2**, and examples of each CSM are found in **Figure 4C-1**. In addition, for a given product, the similarity of the $\Delta v'$ versus $\Delta u'$ graphs in **Figure 4C-1** demonstrates that the chromaticity shift variation across a given product line may be quite similar, even if the initial chromaticity points of each product are slightly different.

Table 4C-2. Primary CSMs Observed in PAR38 Samples [27; 66]

CSM	Direction of Terminal Chromaticity Shift	Changes in u' and v'
CSM-1	Blue	During the blue shift, both u' and v' decrease
CSM-2	Green	During the green shift, u' decreases, but v' changes little or may increase slightly
CSM-3	Yellow	Both u' and v' increase during the yellow shift
CSM-4	A complex shift consisting of first blue, then yellow, then a second blue shift	During both blue shifts, both u' and v' decrease; during the yellow shift, both u' and v' increase.
CSM-5	Red	During the red shift, u' increases, but v' changes little or may increase slightly.

Figure 4C-1. Plots of Chromaticity Changes, as Measured by $\Delta v'$ Versus $\Delta u'$ for Five PAR38 LED Lamp Products, with Five Samples for Each Product [27]

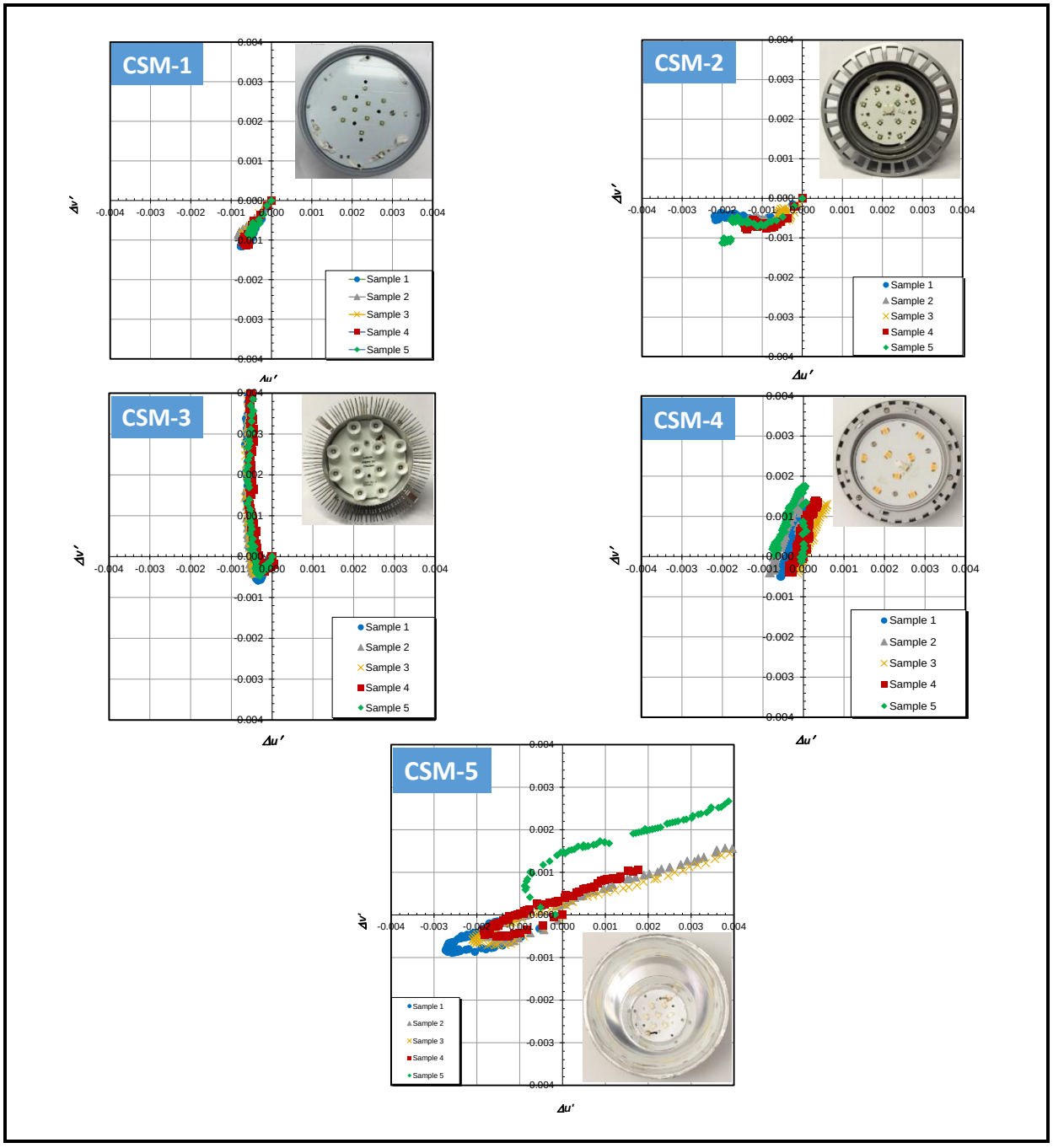

Several published reviews on the causes of chromaticity shift in LED packages have drawn extensively on the findings of this work, and this information will not be repeated here [27; 66-68]. However, as shown in **Figure 4C-2**, one of the key findings from our analysis is that there is a clear difference in CSM behavior between the different LED packages. PAR38

lamps with HP-LEDs predominantly demonstrated CSM-3 behavior, with 72% of the sample population changing chromaticity via this mode or the closely affiliated CSM-5 mode during the test period (approximately 14,000 hours). If testing for these lamp models were terminated sooner, then the terminal mode of chromaticity shift might not have been observed and either CSM-1 or CSM-2 behavior may have been found. This is a constraint of the experimental design more than an indication of the long-term behavior of the LED package. Indeed, there were five PAR38 lamp models with HP-LED packages representing 28% of the lamp samples with HP-LEDs that demonstrated either CSM-1 or CSM-2 population during the test period. These lamp models contained HP-LEDs that were operated at low-stress conditions as indicated by the LED board temperature and power per LED in the device. This finding suggests that low- stress operating conditions using low LED junction temperatures and forward currents can delay the onset of the terminal chromaticity shift and extend chromaticity maintenance. This information is beneficial to LED-device designers, especially when considering the costs of operating more LEDs at lower current levels or driving fewer LEDs harder.

Figure 4C-2. CSMs Observed in PAR38 Lamps Categorized by the LED Package Types Used in the Lamps [27]

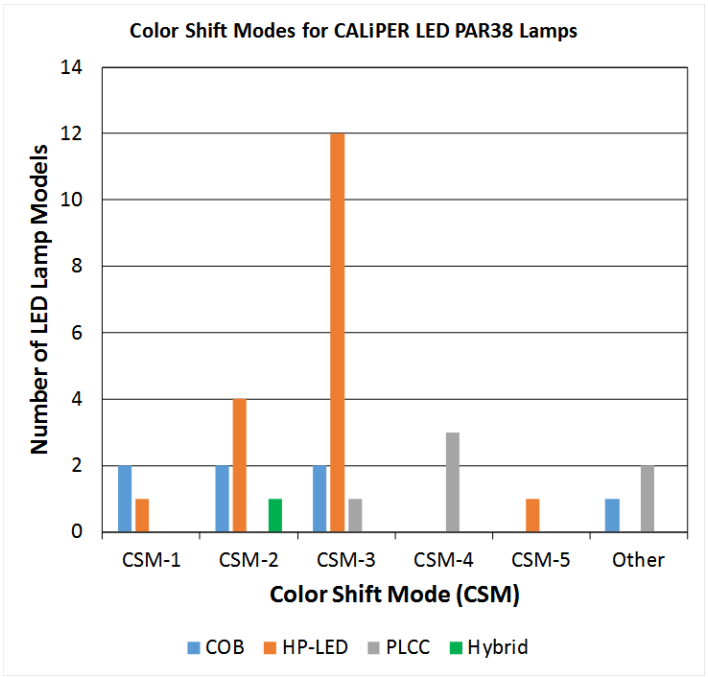

A significant portion of the PAR38 lamps containing PLCC LEDs exhibited CSM-4 behavior, which was the dominant shift mode found for this package type in this study [27]. CSM-4 chromaticity shifts have been attributed to the degradation of the molding resin (i.e., especially PPA and PCT) used in plastic packages [67; 69].

The chromaticity shift for the PAR38 lamps studied in CALiPER 20.5 can be modeled using the methods described in Section 4.B. Models for Sample 12-97, which was previously identified as a parametric failure for exhibiting excessive chromaticity shift, are shown in ***Figure 4C-3***. This device was identified to exhibit the CSM-4 mode in which the initial chromaticity shift is in the blue direction, followed by a shift in the yellow direction, and then by a prolonged and terminal shift in the blue direction. As shown in Figure 4C-3, the initial blue shift is very short (lasting approximately 500 hours) and can be modeled with a bounded exponential function. The R^2 value of this model is 1.000 and the Durbin-Watson statistic of the model is 1.01. The yellow shift lasted from about 500 hours to about 4,500 hours, and can be modeled with a generalized logistic function. The R^2 value of this model was also 1.000, and the Durbin-Watson statistic was only 0.46, which suggests some degree of autocorrelation of the residuals. The maximum change in $\Delta u'v'$ was calculated to be 0.002 during the yellow shift under the operational conditions of the lamp. The final chromaticity shift can also be modeled with a generalized logistic function. The least-squares fit of this model calculated that the maximum shift with this mode will be 0.0124. The R^2 value of this model was 0.999, and the Durbin-Watson statistic was calculated to be only 0.408, which also suggests some degree of autocorrelation among the model residuals.

Figure 4C-3. Model of the Chromaticity Shift for Sample 12-97 [27]

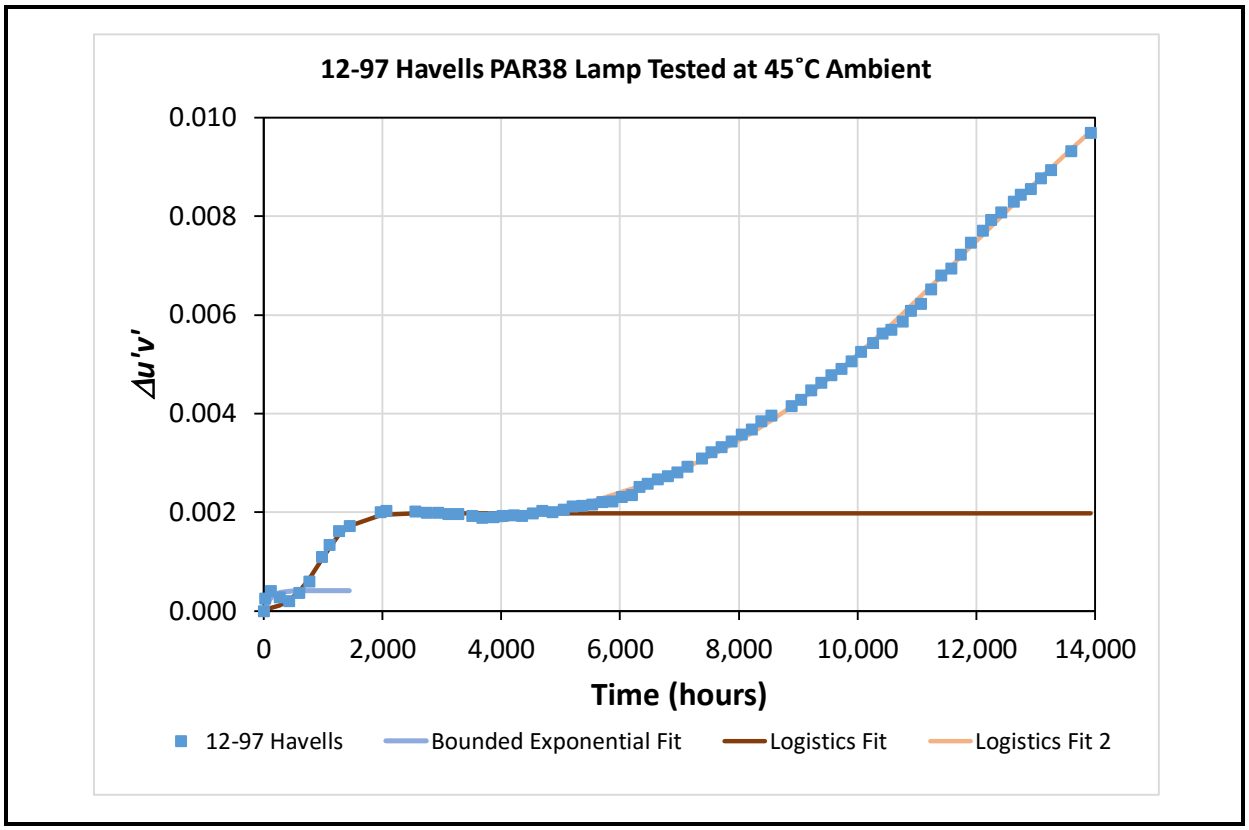

4.C.2 Elevated Ambient Testing of A19 Lamps

Leveraging the experimental findings from PNNL captured in CALiPER 3.2 [63], RTI conducted a similar analysis of chromaticity shifts for 60-watt equivalent A19 lamps. The breakout of observed CSMs by LED package types is given in ***Figure 4C-4***. The duration of the tests on the A19 lamps was 7,660 hours, more than 6,000 hours shorter than the PAR38 lamp study. Thus, we anticipated that some samples would not reach their terminal chromaticity shift mode during the test period.

In this study, the dominant CSM was CSM-1, but CSM-3 was also significant. Contributing factors to this finding are the shorter duration of this test and the lower power requirements of A19 lamps compared with PAR38 lamps. For PLCC packages, the dominant CSM was CSM-4, in agreement with findings from the PAR38 study. Only one example of hybrid and remote phosphor structures was included in these data, and there were no products that contained COB-LEDs.

The chromaticity shifts observed for these lamps can be modeled using the kinetic model as described above, and an example is shown in ***Figure 4C-5*** for product 13RT-08 [63]. The selected product is a hybrid-LED A19 lamp manufactured by LEDnovation. As shown by these models, the chromaticity of this product initially shifts in the green direction, as $\Delta u'$ initially decreases rapidly and then approaches the asymptotic value of -0.006. This behavior is best modeled with a bounded exponential function, and good statistical measures (R^2 = 0.991 and Durbin-Watson statistic = 1.481) were calculated for this fit. Near the 2,000 hour mark, the $\Delta u'$ component enters the emergent stage and the chromaticity rises slowly. In this case, a logistic model provides the best fit, and the least-squared determined model was found to be statistically significant (R^2 = 0.988 and Durbin-Watson statistic = 1.726). As shown in Figure 4C-5, the $\Delta v'$ component can best be modeled with a logistic function starting at time zero, although this model gives modest statistical merit and there is some indication of autocorrelation between the residuals (R^2 = 0.883 and Durbin-Watson statistic = 0.649). These results demonstrate that the kinetic-based chromaticity model can be applied to LED and lamps. In Section 4.D, we will demonstrate that the same model also applies to luminaires.

Figure 4C-4. CSMs Observed in A19 60-watt Equivalent Lamps Sorted According to LED Package Types (Data from [63]).

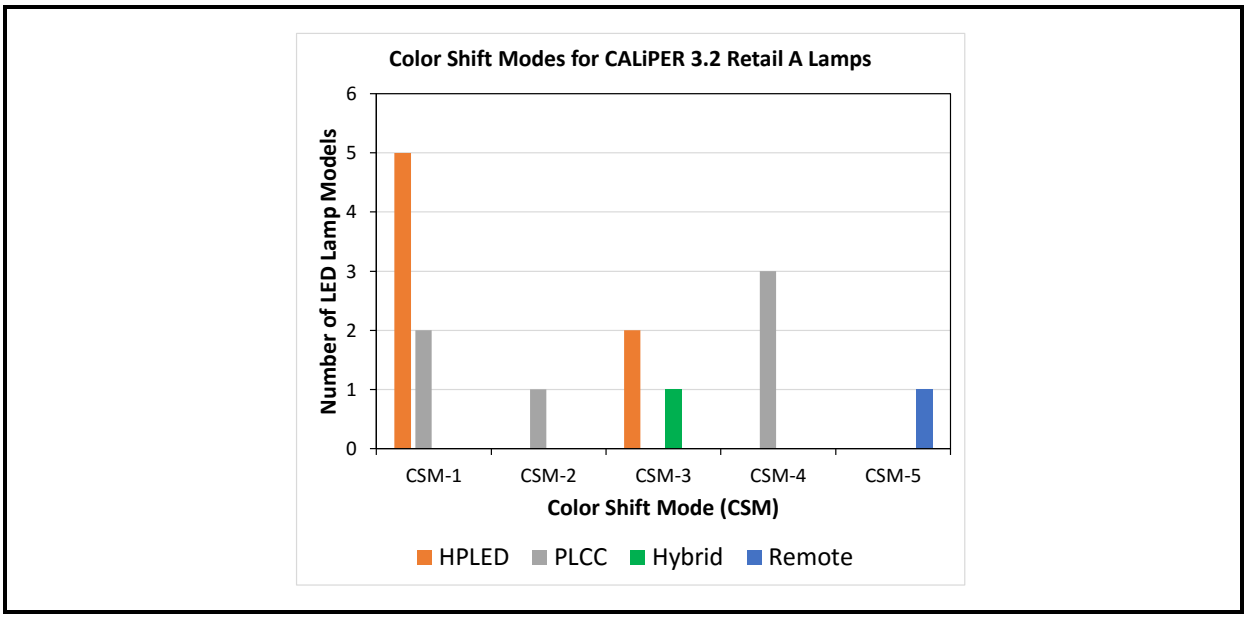

Figure 4C-5. Models of Time Dependence of Changes in $\Delta u'$ and $\Delta v'$ for PNNL Sample 13RT-08

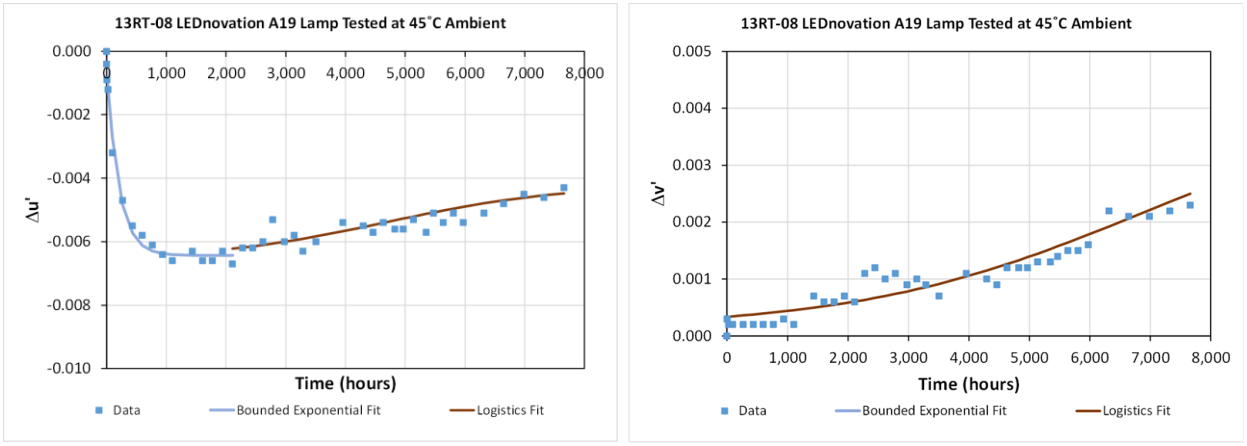

Note: This sample is a hybrid-led A19 60-watt equivalent lamp made by LEDnovation.

4.C.3 Accelerated Stress Testing of A19 Lamps

As part of this project, Auburn University took the lead on investigating the long-term reliability of LED lamps in accelerated stress testing. Auburn created a large sample set of commercial SSL lamp products and tested various populations of these products under different accelerating aging conditions and test durations. All testing was performed on LED-based A19 lamps that produced luminous emissions similar to those of a 60-watt incandescent lamp. A list of the products examined in these tests is given in ***Table 4C-3***,

and a photo of the lamps examined in this study is shown in ***Figure 4C-6***. Similar lamp products to those tested by Auburn with the codes CCW, CWW, PCW, and PWW were tested by PNNL as part of CALiPER 3.2 [63] with the exception that CALiPER 3.2 only examined warm white samples. The PLP product has been extensively tested by PNNL as part of the L-Prize® evaluation [64; 65].

Table 4C-3. Physical, Electrical, and Photometric Characteristics of the A19 60-watt Equivalent Lamps Studied by Auburn University during This Work

SSL Lamp	CCW	ChWW	CWW	PCW	PLP	PSL	PWW
Manufacturer	Cree		Cree	Philips	Philips	Philips	Philips
Product	BA-19		BA-19	BC11A19	L-Prize	Slim-Line	BC11A19
Luminous Flux (lm)	800	800	800	830	800	800	830
CCT (K)	5,000	3,000	2,700	5000	2,700	2,700	2,700
Power (W)	9	9	9.5	12	12.5	10.5	11
Power Factor	1.0	0.63	0.9	0.9	0.7	0.9	0.7

(continued)

Table 4C-3. Physical, Electrical, and Photometric Characteristics of the A19 60-watt Equivalent Lamps Studied by Auburn University during this Work (continued)

SSL Lamp	CCW	ChWW	CWW	PCW	PLP	PSL	PWW
Luminous Efficacy (lm/W)	88.9	88.9	84.2	69.1	64	76.2	75
LED Type	HP-LED	MP-LED	HP-LED	Remote phosphor	Remote phosphor	MP-LED	Remote phosphor
Lamp Length (mm)	111.1	125	112.7	104.6	106.7	111.7	105
Lamp Diameter (mm)	60.3	69.6	60.3	61.2	58.4	68.9	60
Lamp Weight (g)	113	148	113	132	176	56	1132

Figure 4C-6. Photo of the A19 Lamps Examined in This Study and the Configuration of These Lamps for the Room Temperature Operational Life Test (protocol SSL3)

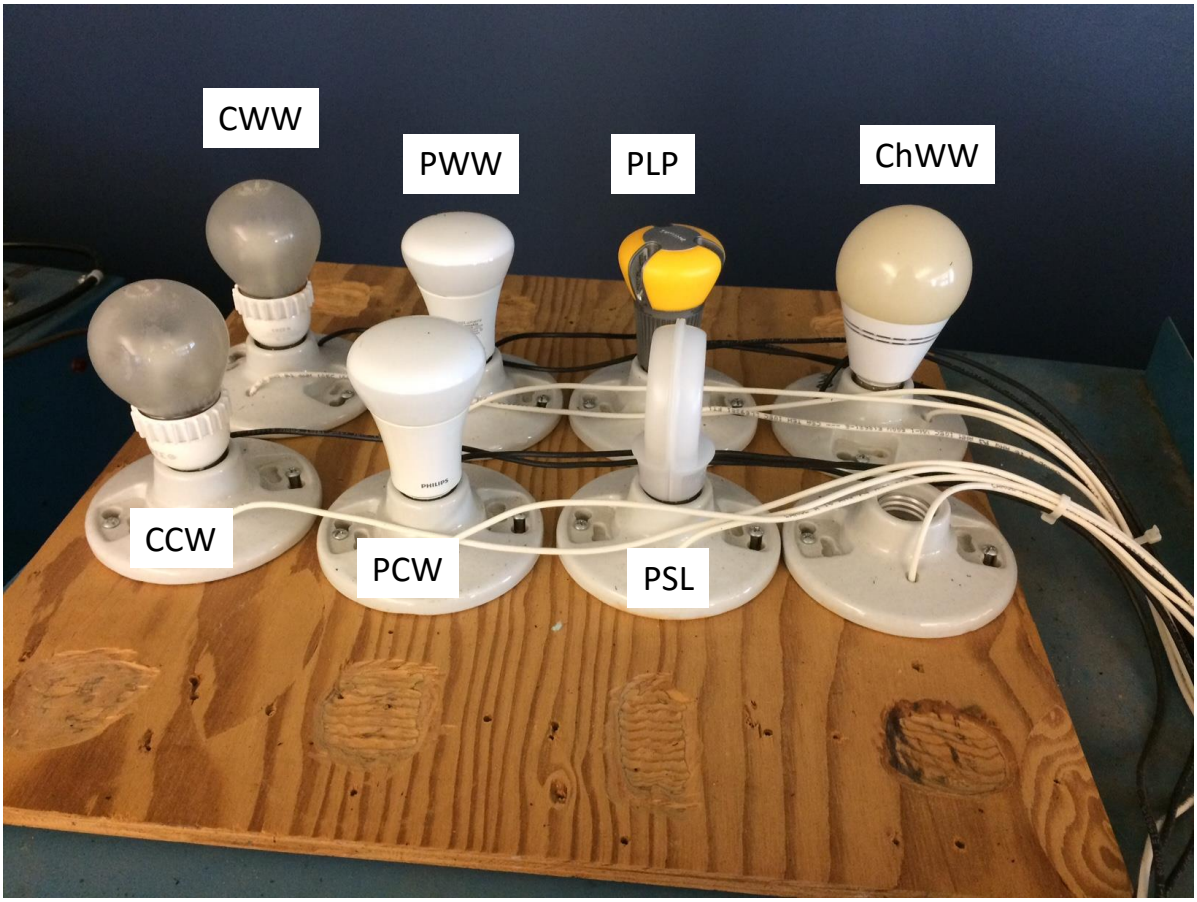

During this study, Auburn University investigated the accelerated aging of the lamps using several testing protocols consisting of different combinations of temperature, humidity, and electrical bias. These protocols are referred to as G1, G2, and G3 throughout this discussion, and the details of each are given in ***Table 4C-4***. Essentially, protocol G1 is a steady-state temperature and humidity soak (SSTHS) conducted at 85°C and 85% relative humidity (RH) with the lamps unpowered; protocol G2 is a HTOL test conducted at 85°C with no humidity control; and protocol G3 is a WHTOL test conducted at 85°C and 85% RH (hereafter termed 8585). For both operational life tests (i.e., protocols G2 and G3), electrical power to the lamps was cycled with a 1-hour on and 1-hour off profile.

Table 4C-4. AST Protocols Used by Auburn University for Initial Testing of A19 Lamps

Protocol	Temperature Control Level	Humidity Control Level	Electrical Bias
G1	85°C	85% RH	None
G2	85°C	None	Cyclic at 1 hour on and 1 hour off
G3	85°C	85% RH	Cyclic at 1 hour on and 1 hour off

Five sampling periods of 168 hours each, for a total of 840 hours (5 weeks) of accelerated aging, were conducted on PLP lamp samples for each AST condition listed in Table 4C-4. The impact of these environments on luminous flux maintenance is shown in ***Figure 4C-7***. Operation of the lamps in 85/85 (i.e., protocol G3) produces the greatest luminous flux decay and higher levels of accelerated aging than either an HTOL or SSTHS.

Figure 4C-7. Comparison of the Luminous Flux Maintenance of A19 Lamps under AST Conditions G1, G2, and G3

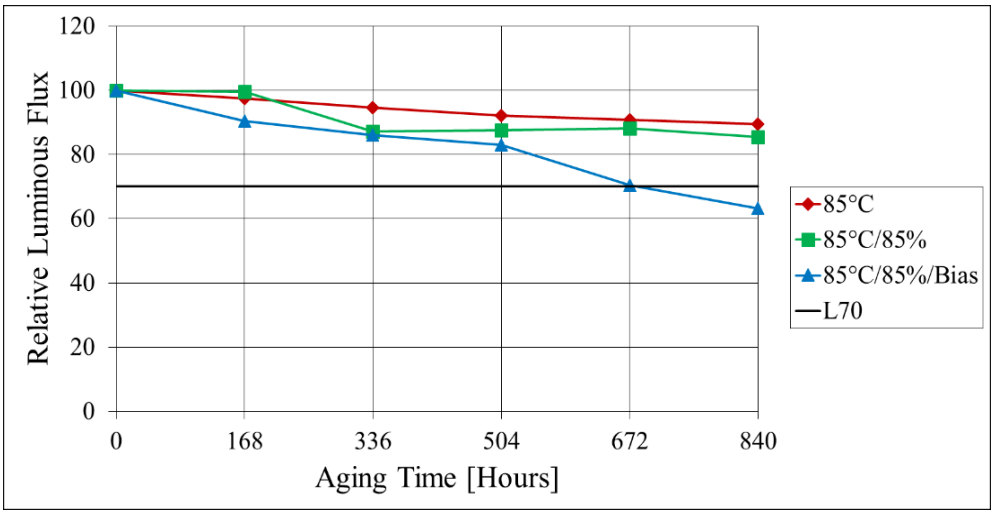

Based on the finding that temperature and humidity produce greater acceleration rates than temperature alone, a new series of AST protocols was developed around variations of the WHTOL procedure. Details on these three test protocols are provided in ***Table 4C-5***. One sample of each A19 lamp examined in this study was tested in the room temperature operational life (RTOL) test (i.e., protocol SSL3). A selection of products drawn from Table 4C-3 were tested under the other conditions, and 10 samples of each product were typically tested. In performing these tests in environmental chambers using protocols SSL1 and

SSL2, the lamps were mounted on a wooden board configured as shown in ***Figure 4C-8***, which accommodates the samples in the test chamber. The sample center-to-center distances are shorter than that used by PNNL in CALiPER 3.2 [63] presenting the possibility of some effects from neighboring radiation influencing the results. However, this configuration is aimed at allowing sufficient air flow around the lamps for convective cooling in addition to conductive cooling through the socket.

Table 4C-5. AST Protocols Used by Auburn University for Extended Testing of A19 Lamps

Protocol	Temperature Control Level	Humidity Control Level	Electrical Bias	Measurement Interval
SSL1	85°C	85% RH	Cyclic at 1 hour on and 1 hour off	Every 1,000 hours
SSL2	55°C	65% RH	Cyclic at 1 hour on and 1 hour off	Every 1,000 hours
SSL3	25°C	25% RH	Cyclic at 1 hour on and 1 hour off	Every 1,000 hours

Figure 4C-8. Photo of the Configuration of A19 Lamps during the SSL1 and SSL2 Testing Protocols

The luminous flux maintenance of the A19 lamps examined during the RTOL test (i.e., protocol SSL3) are shown in ***Figure 4C-9***, and the configuration of the lamps during the room temperature operational life test is shown in ***Table 4C-6****.* Since the testing protocol involved power cycling of the lamps, the results are different that those reported by PNNL in

CALiPER 3.2. Most notably, there were two catastrophic failures during the RTOL testing, sample CWW (between 4,000 and 5,000 hours) and CCW (between 5,000 and 6,000 hours), whereas no catastrophic failures were found during the CALiPER 3.2 testing. In addition, the luminous flux decay for samples PWW and PLP was found to be higher than that of the steady state tests performed by PNNL. These findings suggest that cycling of the lamps shortens their lifetime from both catastrophic and parametric failure standpoints.

Figure 4C-9. Luminous Flux Maintenance of A19 Lamp Samples Examined by Auburn University in the Room Temperature Operational Life Test (Protocol SSL3)

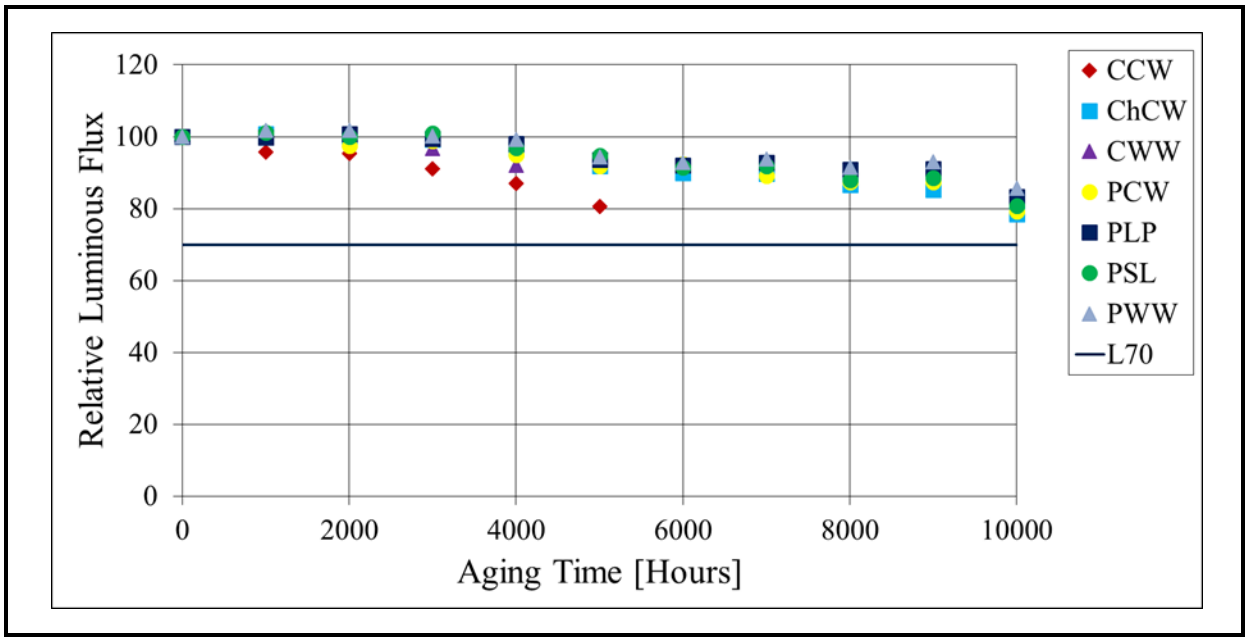

Note: The solid blue line represents the L70 threshold.

The change in chromaticity coordinates of the lamps in the room temperature operational life test (protocol SSL3) is given in ***Table 4C-6***. This change is measured as the difference between the last and first measurements. For most samples, the last measurement was taken after 10,000 hours of operation, except for the catastrophic failures (i.e., CCW and CWW). Many of the samples exhibited excellent chromaticity stability, although sample ChWW can be considered a parametric failure after 10,000 hours of testing.

Table 4C-6. Chromaticity Properties of Individual A19 Lamps in the Room Temperature Operational Life Test[a]

Property	ChWW	CCW	CWW	PSL	PLP	PCW	PWW
$\Delta u'$	−0.0027	−0.0007 (5,000 hr)	−0.0019 (4,000 hr)	−0.0001	0.0006	0.0006	0.0011
$\Delta v'$	−0.0064	−0.0057 (5,000 hr)	−0.0010 (4,000 hr)	0.0011	0.0011	−0.0008	0.0010

$\Delta u'v'$	0.0070	−0.0057 (5,000 hr)	−0.0022 (4,000 hr)	0.0011	0.0013	0.0010	0.0015
CSM	CSM-3	CSM-1	CSM-2	TBD	CSM-5	CSM-5	CSM-5

[a] Measurement time for chromaticity shift properties is between the initial measurement and after 10,000 hours of operation, except for samples CCW and CWW. For these samples, the measurement time is shown in parentheses below the property value.

The same procedures for modeling chromaticity shift as discussed in Section 4.B can be applied to these lamps, and an example is given in ***Figure 4C-10*** for the ChWW sample operated for 10,000 hours at room temperature. Initially, this device shifts in a predominantly green direction, and then begins shifting primarily in the yellow direction. The total chromaticity shift, as measured by $\Delta u'v'$, can be broken into two components: a fast-acting component that is responsible for the initial chromaticity shift that is primarily in the green direction, and a slower-acting component in the yellow direction that is mainly responsible for the terminal chromaticity shift resulting in parametric failure. The fast-acting component lasted to about 5,000 hours of room temperature operation, and this process can be modeled with a bounded exponential function (R^2 = 0.995 and Durbin-Watson statistic = 1.211). The slow-acting chromaticity shift process is best modeled with a logistic function that rises slowly (R^2 = 0.959 and Durbin-Watson statistic = 1.584). The maximum shift with the later mechanism was calculated to be 0.013.

Figure 4C-10. Model of the Chromaticity Shift for A19 Lamp Sample ChWW in the Room Temperature Operational Lamp Study Performed by Auburn University, in Which the Lamp Was Operated for 10,000 Hours in Protocol SSL3 Testing

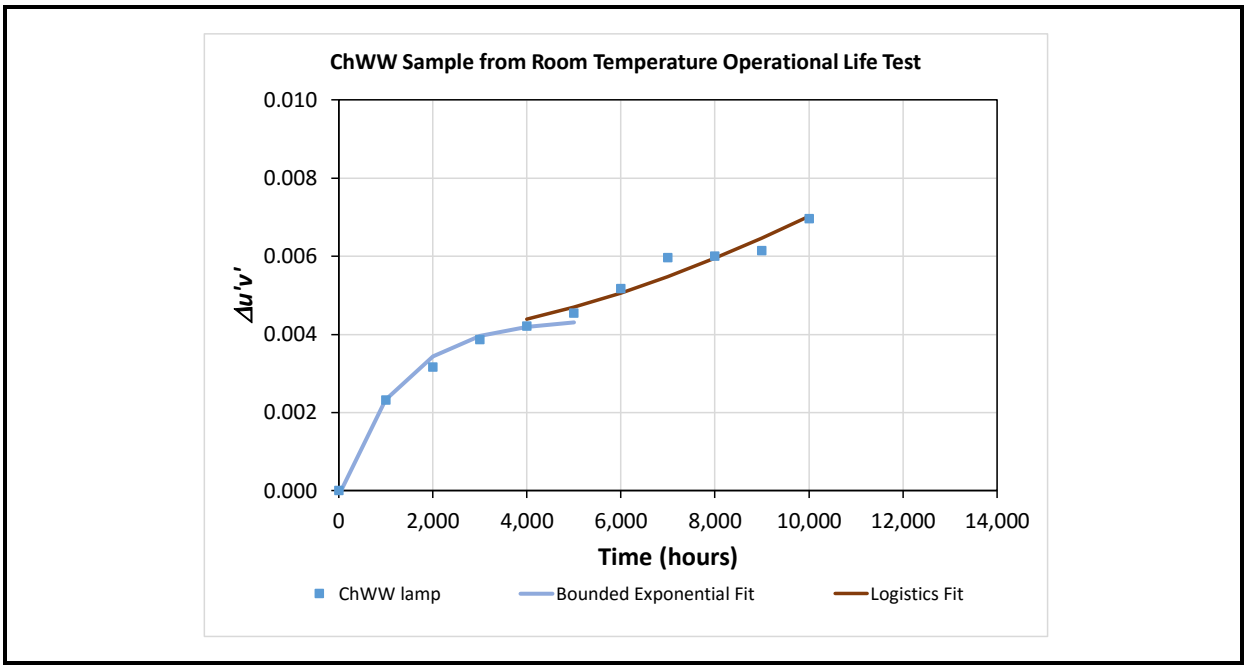

Note: Protocol SSL3 (RTOL testing) was used in this test and the lamp was operated for 10,000 hours.

Based on the experimental findings for luminous flux maintenance of the RTOL test samples, Auburn University calculated the decay rate constants using a modified procedure described in TM-28-14 [70]. The decay rate for the RTOL test was calculated using data acquired from 1,000 hours forward, and these decay rate constants are shown in ***Table 4C-7***.

Table 4C-7. Decay Rate Constant of A19 Lamps in Room Temperature Operational Life Test (Protocol SSL3)

Lamp Product	Testing Protocol	Decay Rate Constant
CWW	SSL3	3.12×10^{-5}
CCW	SSL3	4.37×10^{-5}
ChWW	SSL3	2.30×10^{-5}
PWW	SSL3	1.71×10^{-5}
PCW	SSL3	1.99×10^{-5}
PSL	SSL3	2.04×10^{-5}

Similar studies were performed with testing protocols SSL1 and SSL2, but only select products were tested under each condition. The luminous flux maintenance profiles for CWW, ChWW, and PWW products in testing protocol SSL1 (85/85) are shown in ***Figure 4C-11***, ***Figure 4C-12***, and ***Figure 4C-13***, respectively. The corresponding luminous flux maintenance profiles for CCW, PCW, and PSL products in testing protocol SSL2 (55/65) are shown in ***Figure 4C-14, Figure 4C-15,*** and ***Figure 4C-16***, respectively. Each sample in these figures is operated until catastrophic failure occurs, and they are dropped from the graph at that point because no luminous flux is being produced.

Figure 4C-11. Luminous Flux Maintenance Profiles for the 10 CWW Samples Exposed to SSL1 Testing Protocol

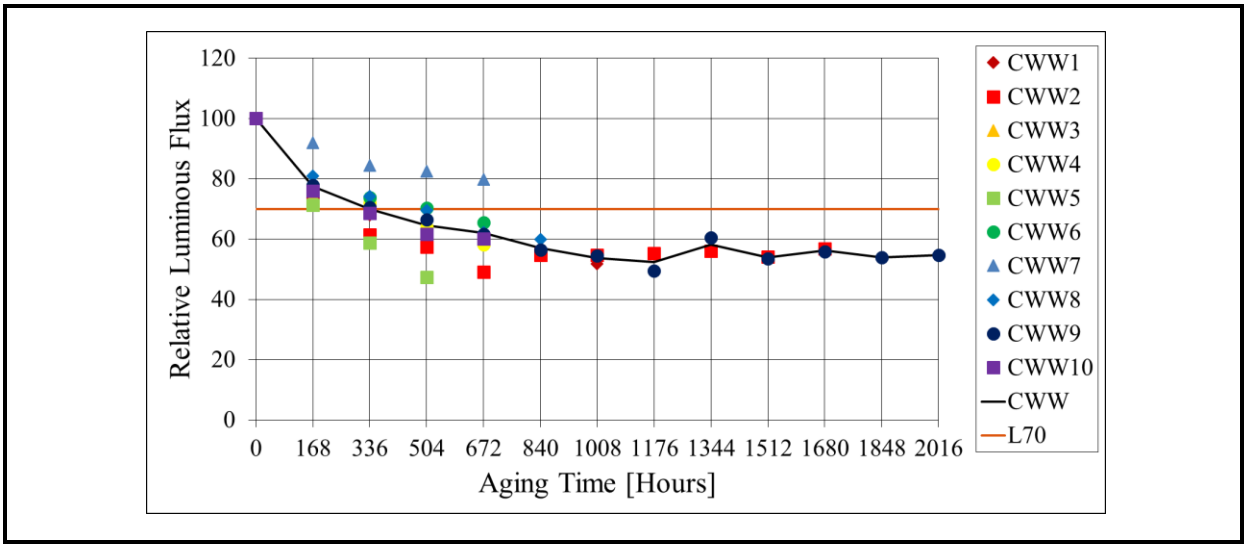

Note: The black line is the lamp average and the solid orange line is the L70 threshold.

Figure 4C-12. Luminous Flux Maintenance Profiles for the 10 ChWW Samples Exposed to SSL1 Testing Protocol

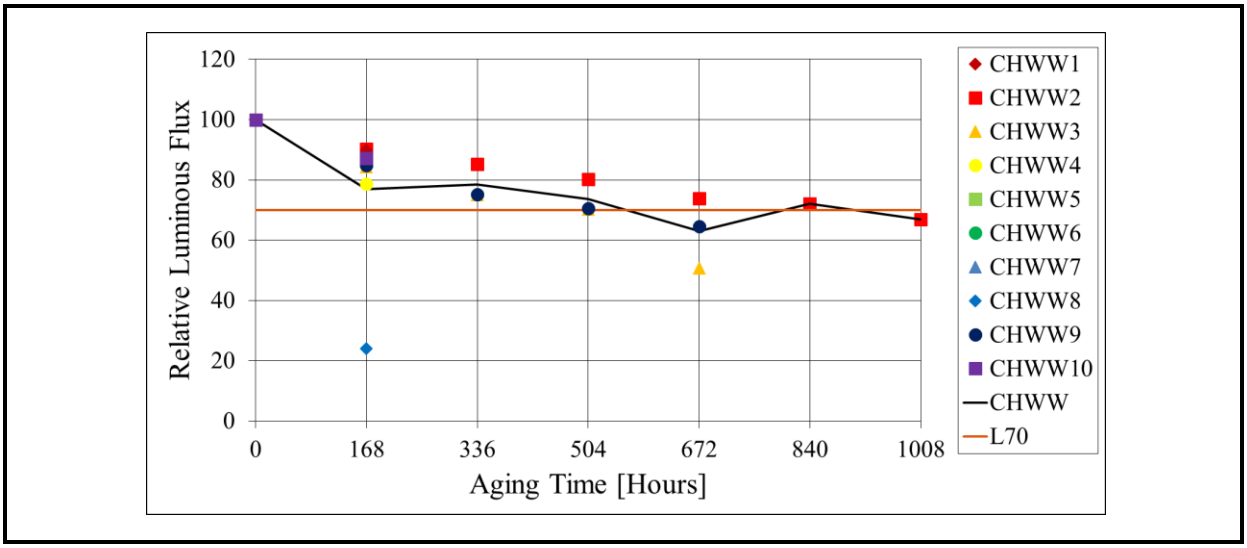

Note: The black line is the lamp average and the solid orange line is the L70 threshold.

Figure 4C-13 Luminous Flux Maintenance Profiles for the 10 PWW Samples Exposed to SSL1 Testing Protocol

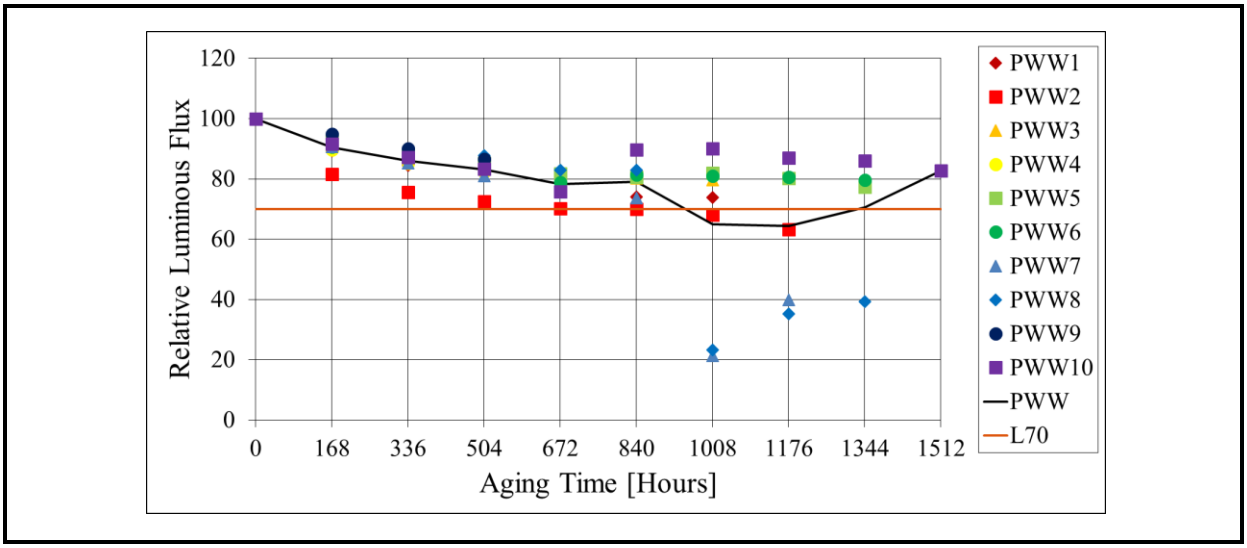

Note: The black line is the lamp average and the solid orange line is the L70 threshold.

Figure 4C-14. Luminous Flux Maintenance Profiles for the 10 CCW Samples Exposed to SSL2 Testing Protocol

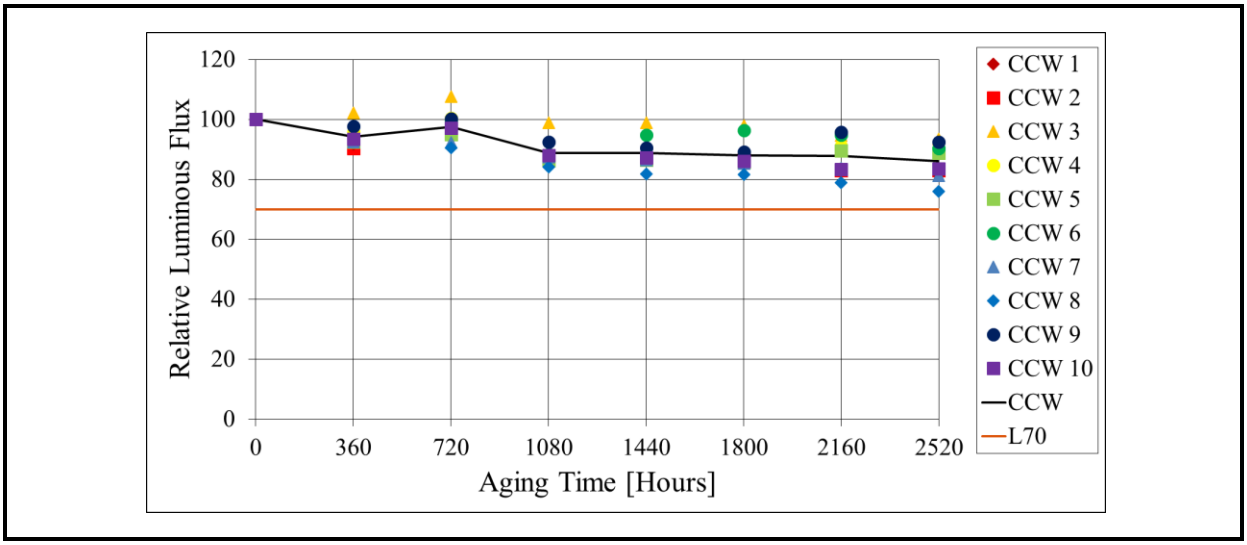

Note: The black line is the lamp average and the solid orange line is the L70 threshold.

Figure 4C-15. Luminous Flux Maintenance Profiles for the 10 PCW Samples Exposed to SSL2 Testing Protocol

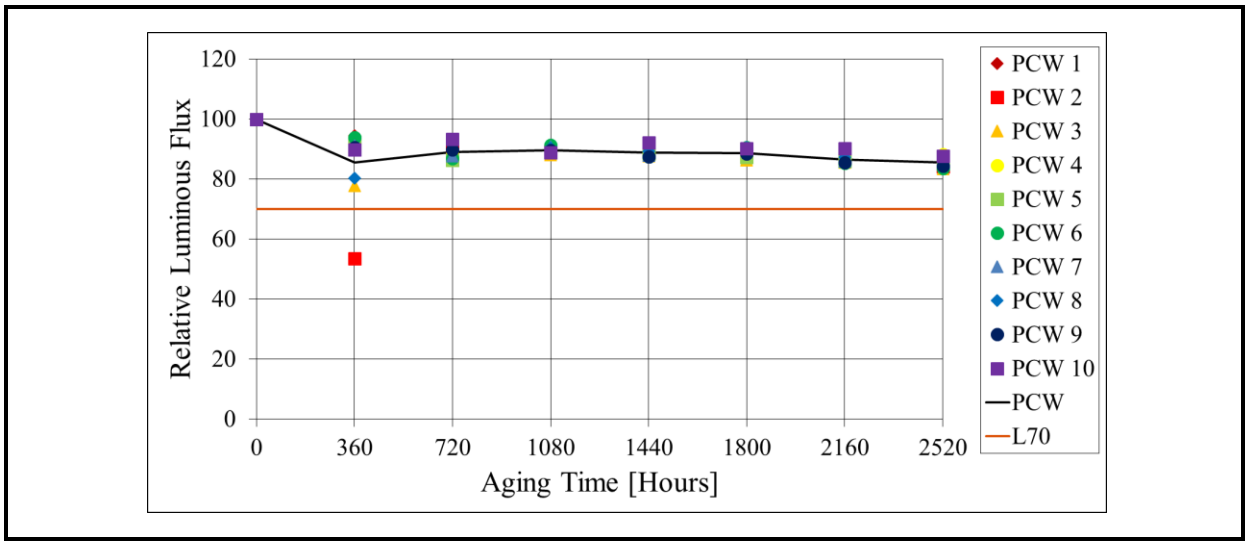

Note: The black line is the lamp average and the solid orange line is the L70 threshold.

Figure 4C-16. Luminous Flux Maintenance Profiles for the 10 PSL Samples Exposed to SSL2 Testing Protocol

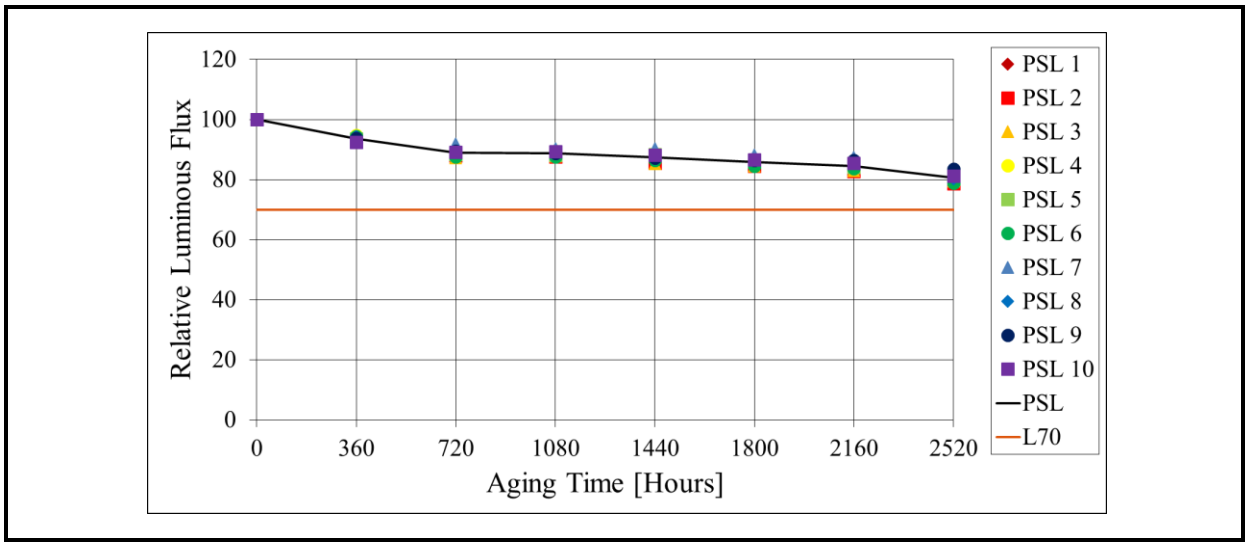

Note: The black line is the lamp average and the solid orange line is the L70 threshold.

The SSL1 protocol resulted in rapid degradation in luminous flux for the tested products. The luminous flux from all samples of the CWW dropped below the L70 value in less than 600 hours of testing, as shown in ***Figure 4C-11***, and the samples can be considered parametric failures. All 10 samples were still operational when they dropped below the L70 threshold, but they continued in testing until electrical failure occurred. Consequently, they can be classified as parametric failures but remained in operation until catastrophic failure (i.e., "lights out") occurred. 90% (9/10) of the CWW products failed electrically before the test was terminated at 2,016 hours. The lone CWW product surviving at the end of the test

produced 55% of its initial luminous flux. In contrast, the dominant failure mode for the ChWW product was catastrophic failure, with only two products surviving long enough to become parametric failures. For the PWW product, there was a mix of parametric (3 units) and catastrophic (7 units) failures.

For test protocol SSL2, neither parametric nor catastrophic failures were observed during the 10,000 test hours. In addition, the luminous flux decay was slightly higher in SSL2 (55/65) than in SSL3 (room temperature) testing. This finding illustrates the highly accelerating nature of test protocol SSL1 (85/85) versus the milder operational stress conditions, such as SSL2. The time to failure for the lamps from protocol SSL1 were plotted in a Weibull chart, and the result is shown in ***Figure 4C-17.***

An excellent fit to the Weibull equation was obtained after the first 30% had failed. Some other factor, such as design flaws, may have been responsible for the first 30% of the failures, whereas the remaining failures closely follow the Weibull equation. The Weibull parameters were calculated to be 1.52 (β or shape parameter) and 976 hours (η or characteristic life). The calculated value for β indicates that the test was accelerating failure rates, but this β value is lower than that found for SSL luminaires during the Hammer test [37]. However, the characteristic life, η, which is the time to failure required for 63.2% of the population, is similar for the two tests.

Figure 4C-17. Weibull Chart Showing the Failure Time of A19 Lamps Subjected to the SSL1 Test Protocol (8585)

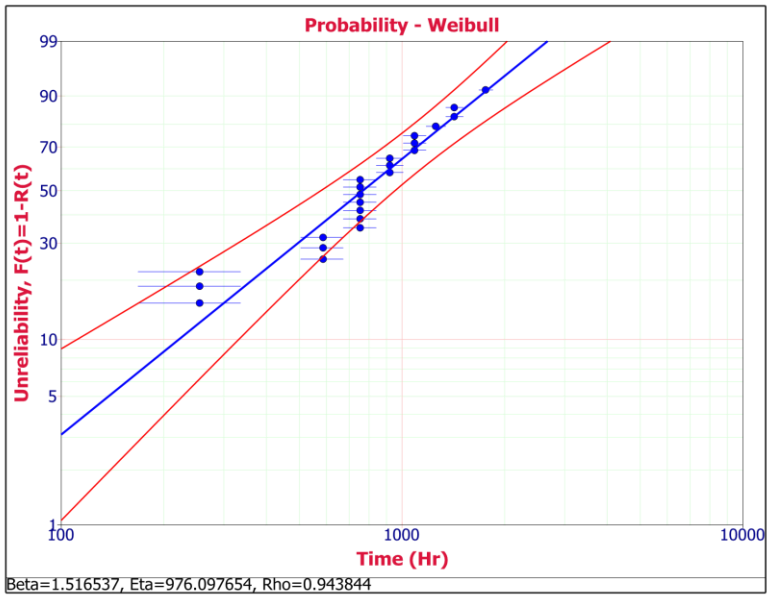

Note: The solid blue line gives the average probability and the red lines show the 90% confidence intervals.

Except for one CWW sample, each SSL lamp from test protocol SSL1 catastrophically failed at some point during testing. Continuity and diode testing was performed on the electrical drivers of each lamp in this test population to investigate potential causes of failure.

Many of the early failures captured in the Weibull plot arise from the ChWW products, and a photo of the driver board for this product is shown in ***Figure 4C-18***. The key components of the driver are highlighted in Figure 4C-18, in which U1 is the controller integrated circuit (IC), D1—D7 are diodes, and Q1 is the switching metal-oxide-semiconducting field-effect transistor (MOSFET). The results from the continuity test indicate that the controller IC is the component most likely to fail, with short circuiting being the dominant failure mechanism. In addition to this mechanism, degradation of some surface mount components was also observed, but their impact on circuit performance was not investigated.

Figure 4C-18. Electrical Driver Used in ChWW with Key Components Identified

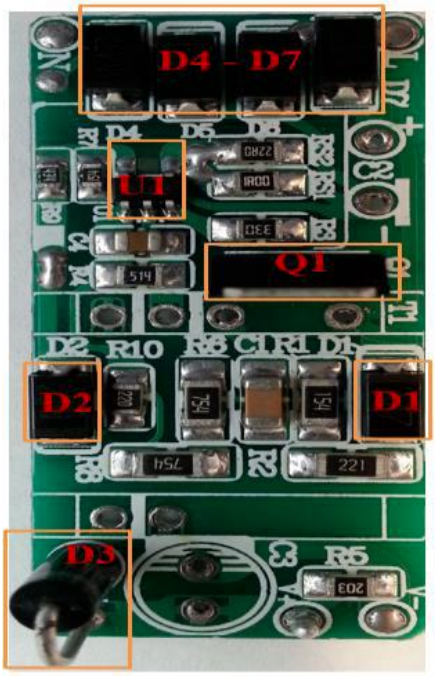

Different failure modes were found in the continuity testing of the other lamps that failed during test protocol SSL1 (8585). For example, 40% of the CWW products had an open fuse, which suggests a current surge in the device, possibly from component shorting. For the PWW samples in test protocol SSL1, continuity and diode testing indicated that catastrophic failure occurred in multiple components (including electrolytic capacitors and discrete components), with the device switching transistors being a common failure site. With the PWW samples, multiple components were often found to fail, including the fuses, which suggests a failure cascade possibly started by a shorted MOSFET.

4.D LED Luminaire Behavior

From the beginning, this project was designed around performing accelerated aging studies on 6" downlights. By analogy to field of genetics, where fruit flies are widely used in studies because they share 75% of the genes that cause human diseases, 6" downlights are the "fruit flies" of the lighting industry because

- LED downlights are widely used in most lighting markets around the world and accounted for more revenue in 2014 than any one single luminaire type [71];
- global revenue from LED downlights totaled more than $4 billion in 2014 (21% of sales), which is almost as large as total LED sales in lighting (~$5 billion) [71];
- downlights incorporate a wide range of LED technologies including HP-LEDs, MP-LEDs, COB-LEDs, remote phosphor devices, and hybrid LEDs;
- a wide variety of design features are available with downlights, including various sizes of optical mixing cavities and indirect lighting;
- materials used in downlights are similar to those used in other luminaire designs;
- downlights can use either integrated or stand-alone drivers;
- downlight products are regularly refreshed by lighting manufacturers and product developments closely track those in LEDs;
- downlights are inexpensive and in most instances were purchased for under $30 per sample; and
- downlights are small and easy to handle; they occupy minimal space in environmental chambers.

Consequently, the bulk of this project was spent studying the behavior of 6" downlights under accelerating stress conditions, and this section reports the major findings from this work. The findings for downlights are believed to be applicable for nearly every luminaire design, as long as proper consideration is given to the impact of device design on luminous flux and chromaticity maintenance as discussed in Section 4.A.

4.D.1 Luminaire Operation at Room Temperature

Throughout this project, a series of 6" downlights has been maintained in the ceiling of the office area where the research staff is located. These downlights have been operated continuously since May 2012 except for brief periods when they were removed from the ceiling for LM-79 testing with a 65" integrating sphere. This RTOL test (i.e., room temperature and normal office environment operation) used 6" downlight luminaires from a variety of manufacturers and included multiple products and design features. Originally, these devices were intended to be control samples for the Hammer Test (described in Section 4.D.4), but the experiment continued after the conclusion of the Hammer Test. This section summarizes the sample behavior in the multiyear RTOL.

Five different commercial 6” downlight products, covering examples of different LED packages, were installed in a hallway at RTI’s facility and wired to remain constantly illuminated. The downlights were installed by qualified electricians and according to manufacturers’ specifications, including the installation of the downlights into recessed housing and the use of junction boxes and greenfield whips in the installation. A picture of the installation is given in **Figure 4D-1**, and some details on luminaire design and performance properties are provided in **Table 4D-1**. The 12 samples were evaluated for lumen maintenance, chromaticity shift, and photometric flicker (in later years) approximately every 6 months of this project and were removed from the ceiling for spectrometer testing each time and then reinstalled. The samples discussed in this section have reached between 18,000 and 41,500 hours of illumination as of January 2017.

Figure 4D-1. Picture of the Downlights Used in the RTOL Test After Installation in a Ceiling in a Common Area in RTI Offices

Table 4D-1. Specifications for the 6" Downlight Luminaire Models Used in RTI's RTOL Test

Designation	Cree LR6	Lighting Science Group Glimpse	Sylvania RT6	Philips Lightolier Calculite	Cree CR6
Manufacturing date	Nov-09	Feb-12	Mar-12	Aug-12	Apr-11
Optical mixing cavity	Yes	No	Yes	Yes	Yes
Line voltage nominal [V]	120	120	120	120	120
Light engine configuration	Hybrid LED	pcLED	pcLED	Remote phosphor	Hybrid LED
LED type	HP-LED	MP-LED	COB-LED	HP-LED	HP-LED
Number of LEDs/luminaire	34	36	1	22	5–7
Specified maximum LED junction temp	150°C	125°C	150°C	150°C	150°C
Specified maximum LED current [A]	1.0	0.16	1.08	1.0	1.0
LED PCB type	Metal core	Laminate	Ceramic	Metal core	Metal core
Thermal interface material LED to PCB	Thermally conductive pad	Thermally conductive pad	Thermal grease	Thermally conductive pad	Thermally conductive pad
Heat sink type	Finned block	Housing	Housing	Finned block	Housing
Power specified [W]	12.5	15	14	28	9.5
Initial luminous flux measured [lumens]	962	719	884	1,295	562
Measured CCT [K]	3,387	3,019	3,010	3,015	2,725
Optical reflector material	MCPET	None	MCPET	Metallized film	WhiteOptics
Lens composition	Polycarbonate	Acrylic	Acrylic	Polycarbonate	Polycarbonate

The average lumen maintenance data across the products examined in the RTOL test is shown in **Figure 4D-2**. Testing of the Cree CR6 products was started later than testing for the rest, and those products have reached only 18,600 hours of testing at this point. Although several products maintained high luminous flux output levels for much of the test, the Philips Lightolier and Cree LR6 experienced noticeable lumen depreciation over time. Both of these luminaires can be considered architectural- or specification-grade luminaires, whereas the Sylvania RT6, Lighting Science Group (LSG) Glimpse, and Cree CR6 are intended more for the residential market.

Figure 4D-2. Average Luminous Flux Maintenance for Each Luminaire Product in This Normal Operational Life Test

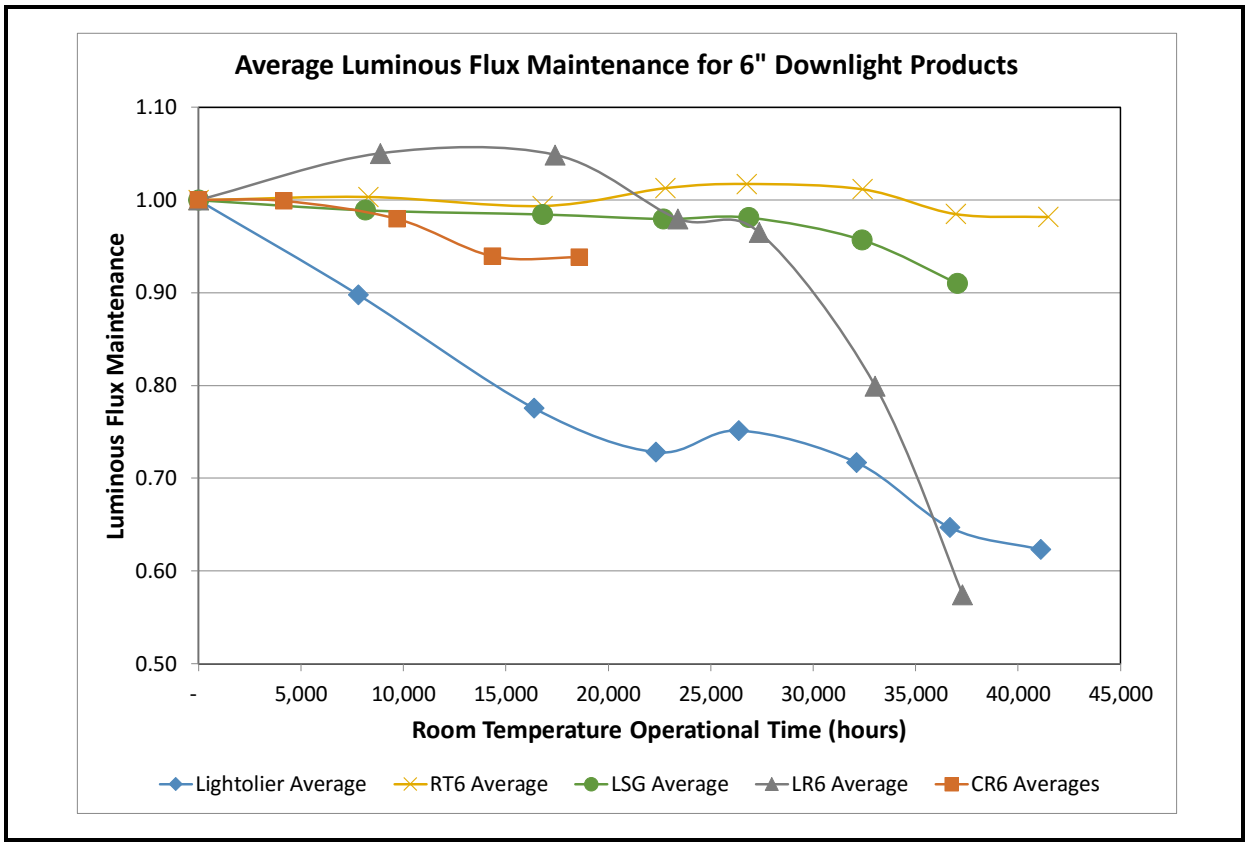

As shown in Figure 4D-2, the average luminous flux maintenance of the three Philips Lightolier luminaires decreased rapidly from the beginning. This behavior is indicative of an unusual event in the luminaires, as will be discussed below. In contrast, the luminous flux maintenance of both Cree LR6 samples increased to above 1.0, indicating that they became more efficient with time and remained at that level for roughly 20,000 hours. At that point, both samples began experiencing a rapid decrease in luminous flux.

In contrast, the luminous flux maintenance of the Sylvania RT6 and LSG Glimpse products was relatively constant throughout the test. The Sylvania RT6 samples were still producing more than 95% of their initial luminous flux after more than 40,000 hours of continuous use. The LSG Glimpse luminaires were removed from testing after 37,000 hours because of lens breakage with the regular handling. At the time of their removal from testing, these luminaires were still delivering more than 90% of the initial luminous flux, but the rate of luminous flux decay appeared to be increasing. Detailed analyses of these luminaires as well as specific findings for each product are discussed below.

The performance of each of the 12 luminaires in RTOL test is shown in **Figure 4D-3**. In general, the overall behaviors of the samples within product lines were similar. For example,

even though one CR6 device (#01) had a slightly lower luminous flux maintenance, its output change over time was very similar to that of the other two CR6 devices. Likewise, Lightolier device #30, after a significant initial drop in output, carried on with a profile similar to those of its population counterparts. The average values shown in Figure 4D-2 demonstrate that the Sylvania RT6 and LSG Glimpse performed much better than other products, up to 35,000 hours. Both RT6 samples continue to maintain their luminous flux output and have experienced more than 42,000 hours of operation with minimal change in luminous flux. All three of the Lightolier samples can be considered parametric failures, because the lumen maintenance of each dropped below 70% in less than ~35,000 hours. Significant photometric flicker began to occur on the LR6 devices after ~30,000 hours of testing, which explains the quick drop in lumen maintenance from the previous measurement.

Figure 4D-3. Luminous Flux Maintenance for Each of the 12 Samples in the Normal Operational Life Test

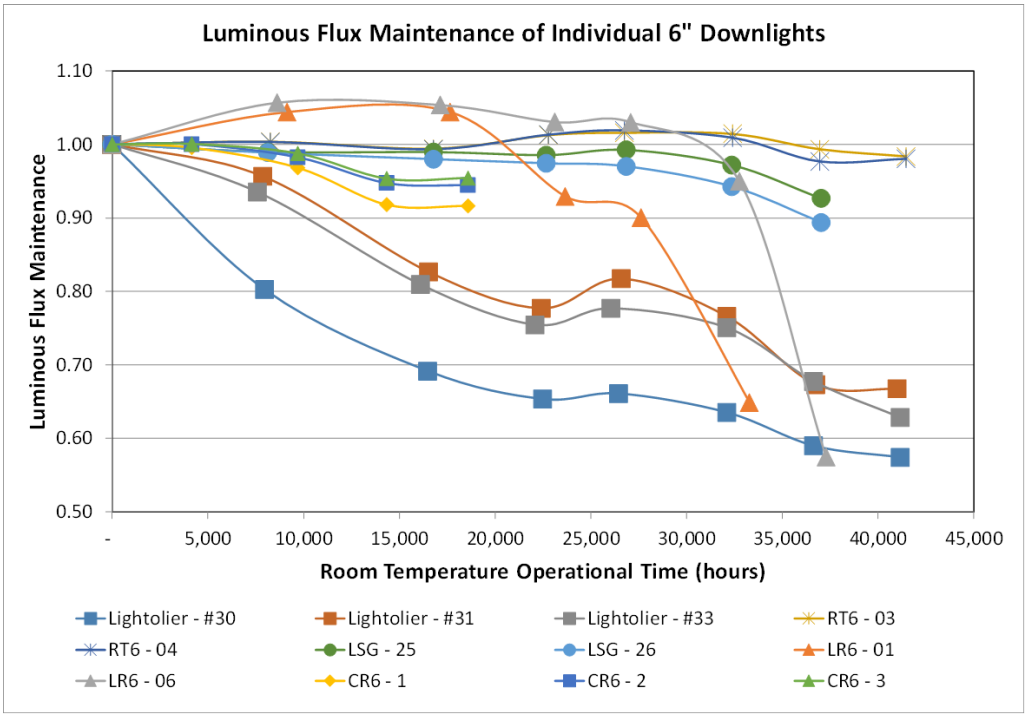

RTOL Test Results for Philips Lightolier Calculite

The Philips Lightolier Calculite luminaire is an architectural specification-grade luminaire that uses a remote phosphor architecture in which 22 royal blue HP-LEDs (emission wavelength ~ 450 nm) at the base of an optical cavity irradiate a remote phosphor disc. The LED board is shown in **Figure 4D-4**, and a cutaway view of this luminaire is shown in **Figure 4D-5**.

The PCB containing the LEDs is covered with a metallized plastic reflector with holes to accommodate the LEDs, and the walls of the optical cavity are covered with a specular-reflecting, metallized film that is glued to the cavity sidewalls. A glass lens sits on top of the remote phosphor disk. This light engine sits at the base of a 6”-long aluminum extruded can, and the primary emissions (from the blue LED) and the secondary emissions (from the remote phosphor) are mixed in the aluminum can to produce white light. The device is operated by an external driver that is connected to the luminaire through a greenfield whip.

Figure 4D-4. Picture of the LED Board Used with the Philips Lightolier Calculite Downlight Examined in This Study

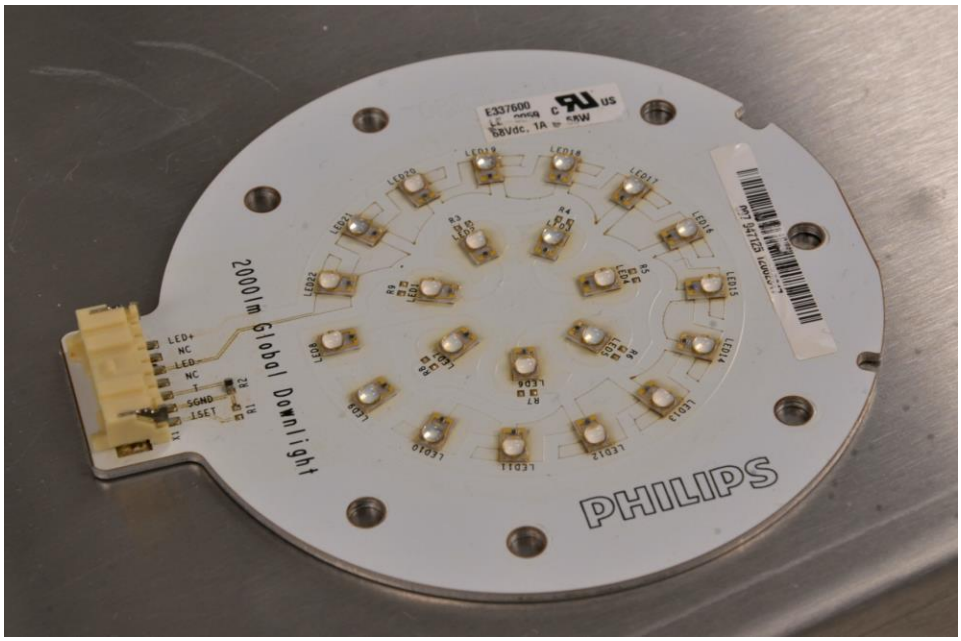

Figure 4D-5. Cutaway View Showing the Components of the Philips Lightolier Calculite Luminaire

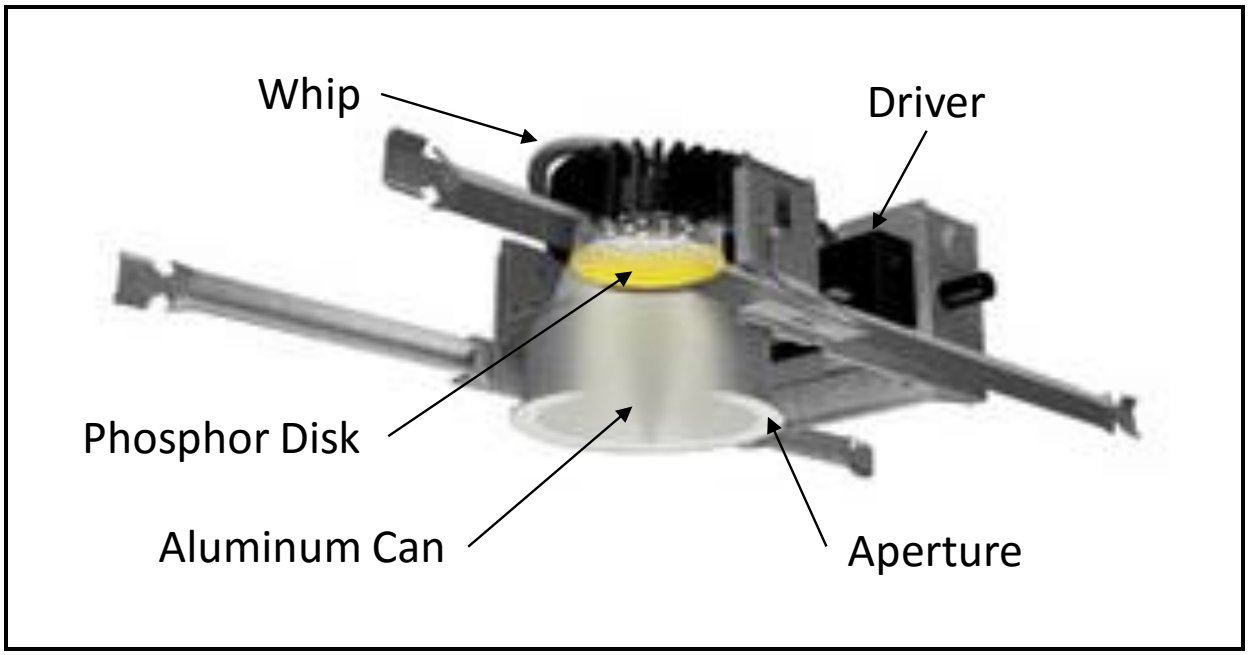

The luminous flux produced by these luminaires began depreciating almost immediately. They are now producing on average close to 60% of their initial luminous flux readings and are considered parametric failures for falling below the 70% luminous flux maintenance threshold. During year 2 of this project, the RTI team conducted an analysis as to why there was such a significant lumen depreciation in these products, particularly because these lights were meant to be control luminaires for the Hammer Test experiments. **Figure 4D-6** shows a comparison between the Philips Lightolier Calculite RTOL samples (DUTs number 30, 31, 33) and equivalent samples in the Hammer Test (DUTs number 22, 23, and 32) [37]. Minimal degradation in luminous flux was found for these products in the Hammer Test, in sharp contrast to the findings from the RTOL tests.

Figure 4D-6. Luminous Flux of Philips Lightolier Calculite Luminaires

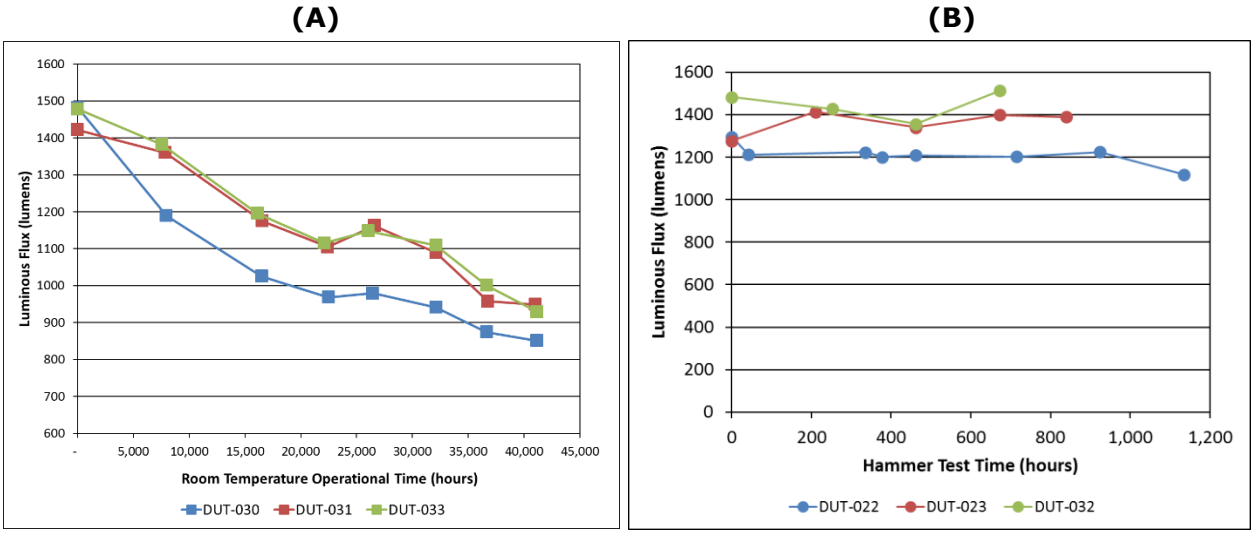

Notes: (A) from the RTOL test and operated constantly at room temperature and humidity, and (B) exposed to the Hammer Test procedure [37]. Testing on each luminaire was stopped in graph B after the last data point was taken and the devices were still functional at that time.

In an effort to rule out driver failure as the cause for reduced luminous flux, we replaced the driver on DUT #33 with a fully functional driver from the Hammer Test. Unfortunately, replacing the driver did not improve lumen output; so we concluded that the depreciation was caused by a phenomenon inside the luminaire housing. The RTI team then disassembled the housing of two of the three Calculite samples in RTOL testing and discovered that a residue was coating the metalized plastic reflector that sits at the base of the optical cavity and surrounds the blue LEDs. The residue can be seen as small liquid dots in **Figure 4D-7** and is readily apparent if the surface is wiped with a cotton swab. It is unknown whether, but believed to be highly likely that, this residue covers other surfaces in the optical cavity. On the basis of Fourier transform infrared spectroscopy (FTIR) results, we concluded that this residue was dioctyl phthalate, a common plasticizer. We have not investigated why this phenomenon was seen in the real-time samples and not the Hammer Test samples.

Figure 4D-7. Picture of the Reflector From a Philips Lightolier Calculite 6" Downlight Sample That Exhibited Excessive Lumen Maintenance Loss

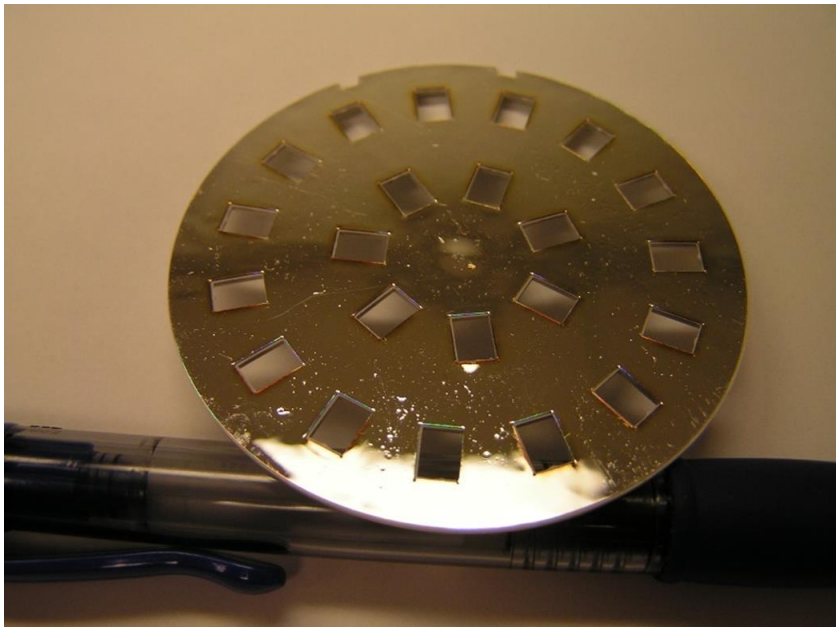

The emission color of the Calculite samples shifted over time in the blue direction of the spectrum, and the same shift was found for all samples, as shown in **Figure 4D-8**. The value of v' decreased by nearly a 7-step MacAdam ellipse, whereas the value of u' decreased only slightly. The SPD profiles of these samples are shown in **Figure 4D-9**, and the same data normalized to maximum of the blue emission peak are shown in **Figure 4D-10**. These data provide a deeper understanding of the causes of the observed color shift. The relative drop in phosphor emissions shown in Figure 4D-10 provides clear evidence that less phosphor emissions are produced by the luminaire and that the phosphor conversion process is being affected by the plasticizer residue. This effect could be due to either a drop in the quantum efficiency of the phosphors used in this device or a dissolution/loss of phosphor particles. As a result, proportionally more blue photons are emitted from the device and the chromaticity shifts to the blue.

Figure 4D-8. Values Over Time for *u'* and *v'* of the Three Philips Lightolier Calculite Luminaries in Normal Operational Life Tests

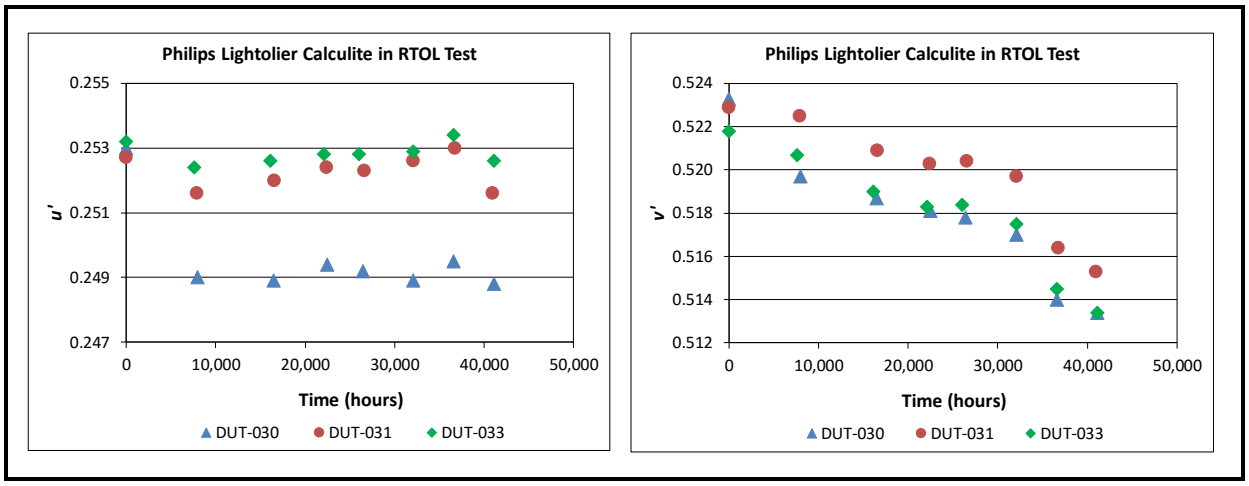

Figure 4D-9. SPD of Lightolier DUT-030 During RTOL Test

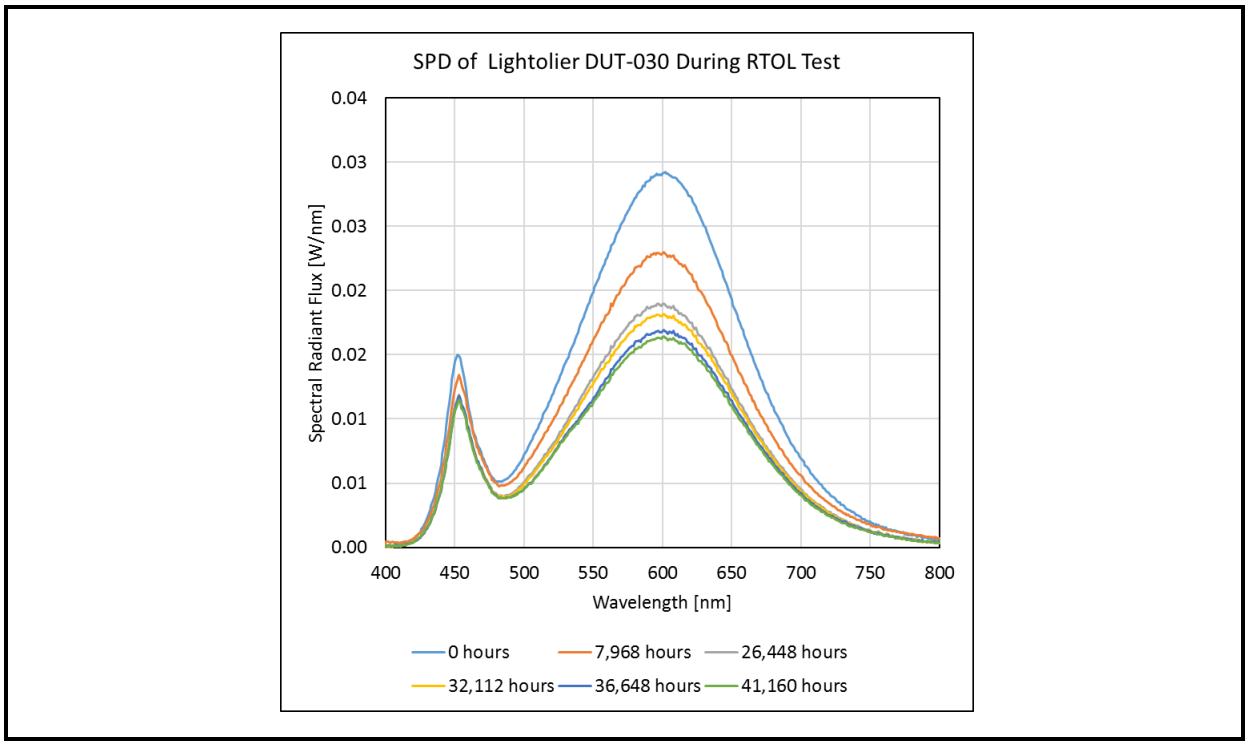

Figure 4D-10. The SPDs Over Time Shown in Figure 4D-9 for Calculite Sample #30 Normalized to the Maximum of the Blue Emission Peak at ~450 nm for Each Measurement

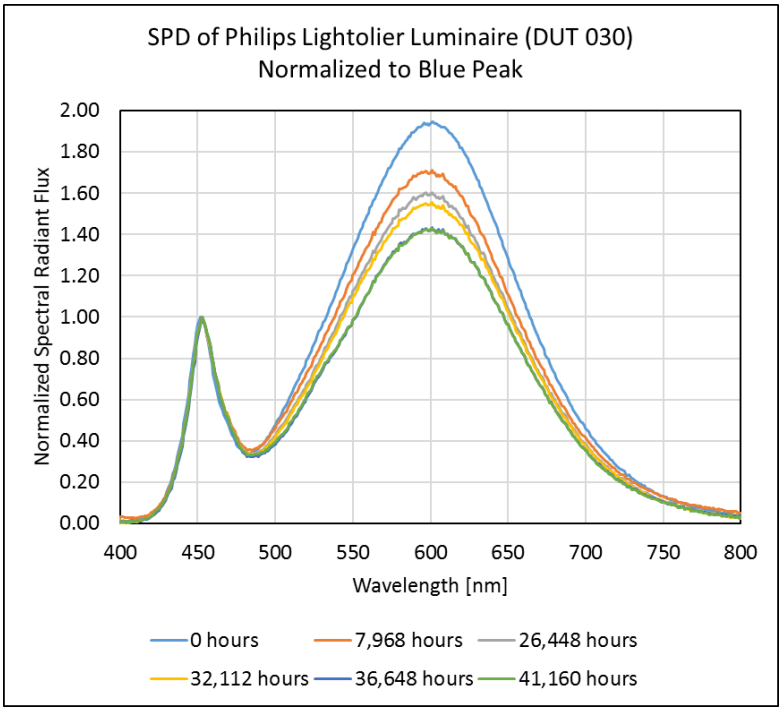

RTOL Test Results for Cree LR6

The Cree LR6 was one of the first high-CRI downlight products available on the market and was sold primarily by distributors as a specification-grade luminaire. The product contains an integrated driver, hybrid LED light engine, and controls; pictures of these luminaire components are shown in **Figure 4D-11**. The light engine is a hybrid LED device in which multiple LEDs are blended in an optical cavity to produce white light. Two versions of the hybrid LED light engine used in this product were included in our RTOL testing, a two-LED version consisting of pcLED green LEDs and direct-emitting red LEDs and a three-LED version in which a direct-emitting cyan LED is added to the two-LED version. The light engine shown in Figure 4D-11 is the three-LED version, and the red, green, and cyan chips are clearly observable. The SPDs for both samples are shown in **Figure 4D-12**, and the addition of the cyan chip can be seen to produce the direct LED emission centered around 470 nm. Both versions of the light engine contained a photometric sensor (which is visible as the device on the small green PCB in Figure 4D-11), and the current feed to the different LEDs is adjusted in an effort to achieve greater luminous flux and chromaticity stability.

Figure 4D-11. Picture of the Housing and Driver of the Cree LR6 (left) and the Hybrid Light Engine (right)

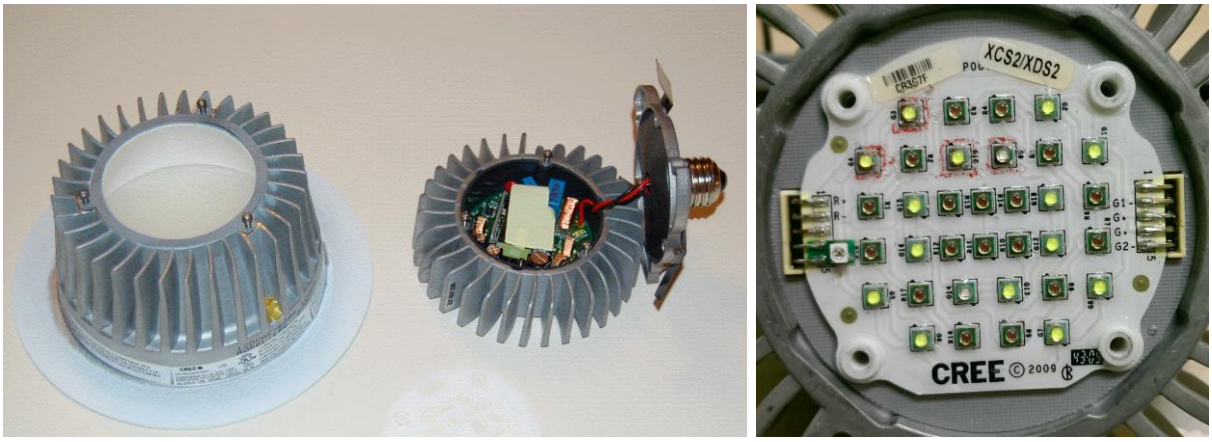

Figure 4D-12. SPDs for Cree CR6 Luminaires in the RTOL Tests

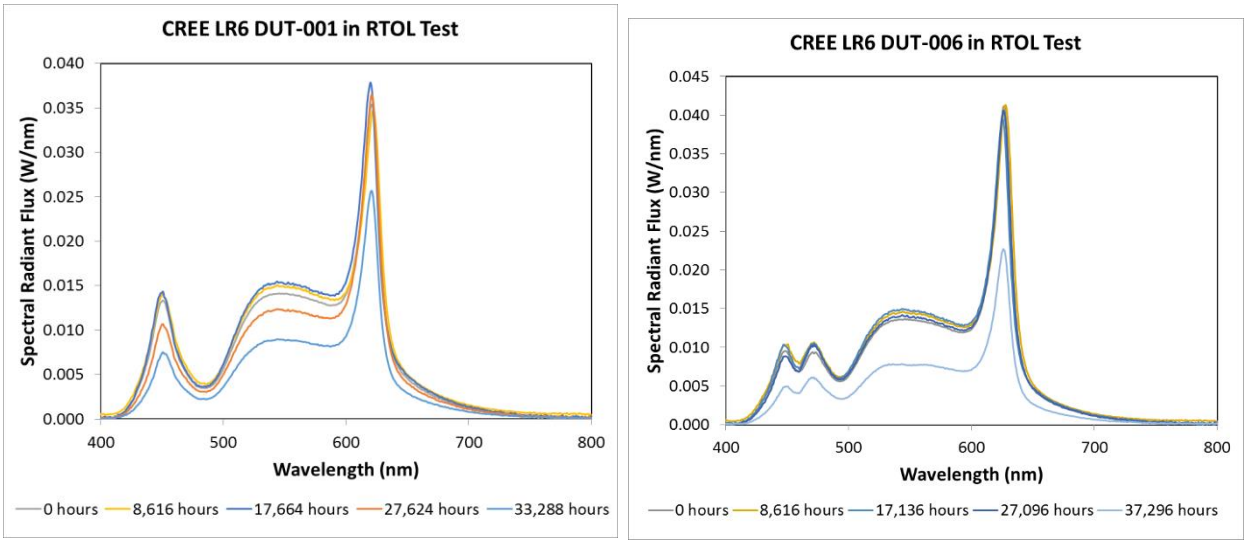

Notes: DUT-001 used a two-LED light engine, whereas DUT-006 added a cyan direct emitter.

The two test samples that composed the Cree LR6 population maintained their luminous flux output for approximately 20,000 hours but then deteriorated quickly over the next year (**Figure 4D-13**). The primary cause of this deterioration is the rise of photometric flicker, which will be discussed further below. During the test, the chromaticity can be seen to shift initially in the blue direction, followed by a shift toward the red (CSM-5), as shown in **Figure 4D-14**). The red shift is likely caused by a decrease in emission from the red direct-emitting LED. When photometric flickers rise in the device, the chromaticity point becomes less stable and there appears to be a shift toward the green direction, likely due to deterioration of the red emitter.

Figure 4D-13. Luminous Flux of Cree LR6 Luminaires in Real-Time Life Tests

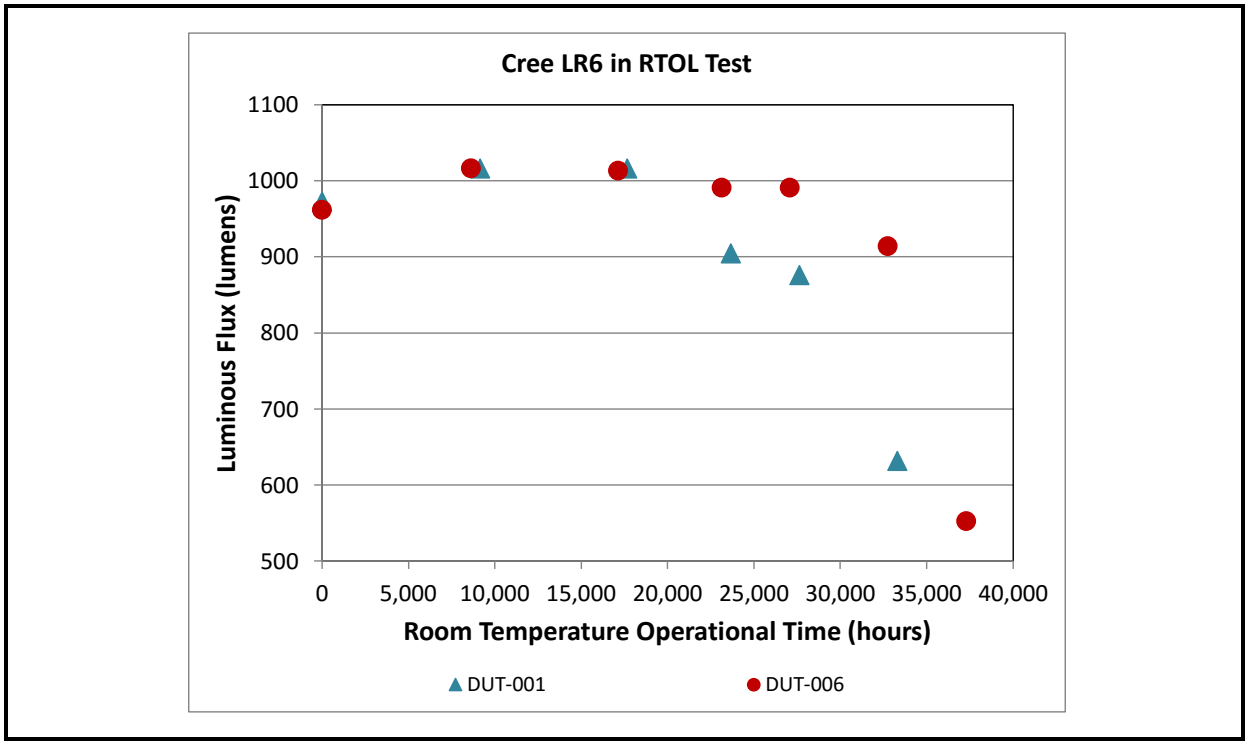

Note: Output held relatively steady through approximately 20,000 hours of continuous operation, but then it began to decrease.

Figure 4D-14. Values for *u'* and *v'* of Cree LR6 Luminaires in RTOL Tests Show Complex Changes Over Time

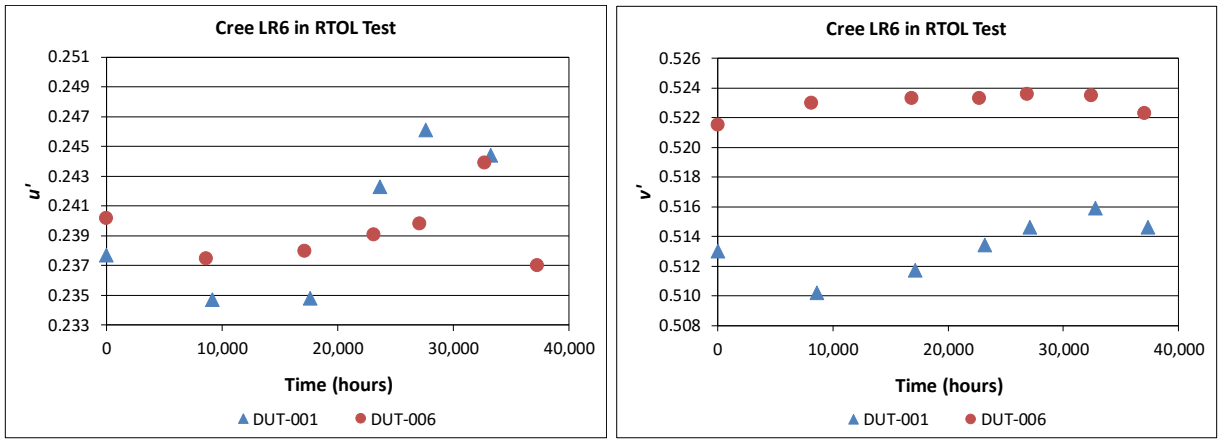

Notes: (A) An inflection point for the entire population occurs around the 20,000-hour mark, which roughly corresponds to the time at which these samples began to decrease in luminous flux.

Both LR6 samples began to exhibit uncomfortable levels of photometric flicker after roughly 3 years of continuous operation in the RTOL tests. The measured flicker frequency of DUT-006 was 60% and the % Flicker valuer was measured at 99.6%, well above acceptable standards [72; 73]. The measured flicker waveform from DUT-006 is shown in

Figure 4D-15. Because of the excess amount of visible flicker, these luminaires were removed from testing at ~33,000 hours (DUT-001) and ~38,000 hours (DUT-006). An electrical analysis of DUT-006 by Dr. Praneet Athalye of Buck-Boost, Ltd., also showed an increase in total harmonic distortion (THD) for these devices, from 9% to >20% during device flicker. A close inspection of the light engine revealed that several LEDs were shorted together, which could be alleviated by probing the board and removing the conformal coating on the board. The affected LEDs are indicated by hand-drawn red squares in Figure 4D-11. Consequently, we assign this failure mode to issues with the printed circuit board that may include solder joint fatigue and component shorting due to dendritic growth underneath the board's conformal coating.

Figure 4D-15. Flicker Waveform of Cree LR6 DUT-006

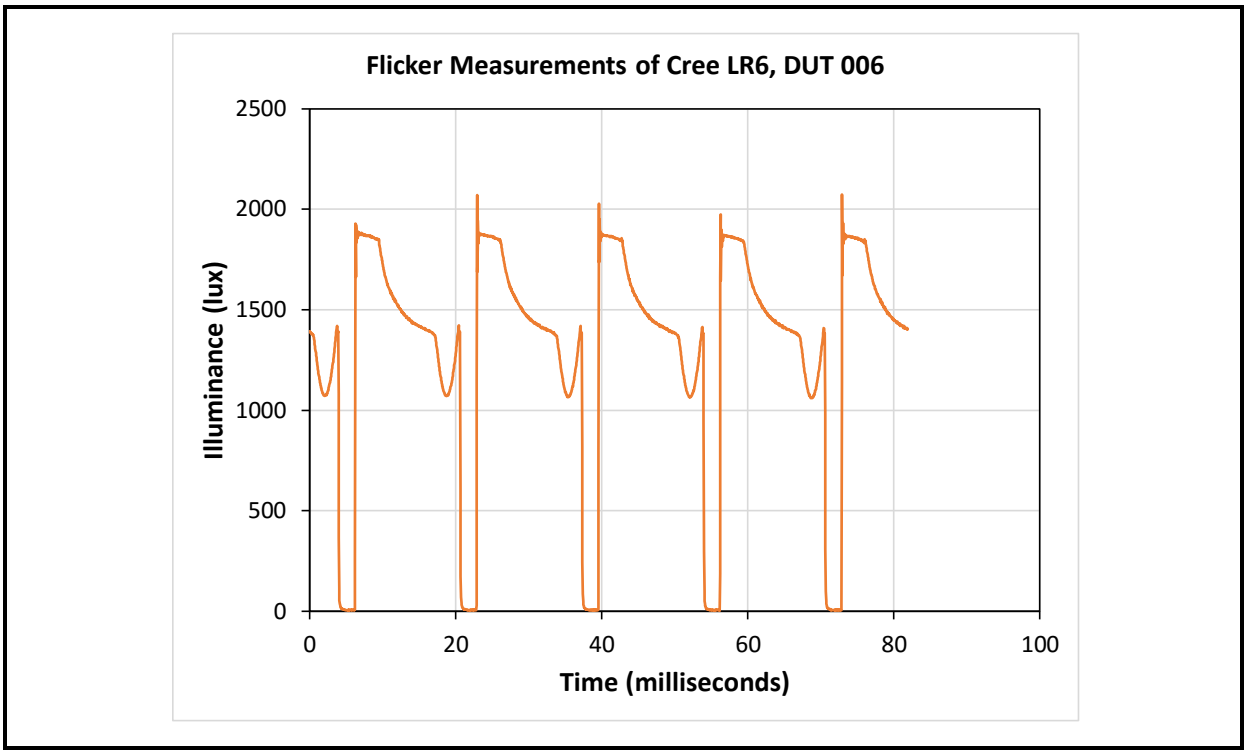

Note: This device began to exhibit visual levels of photometric flicker after 37,000 hours of operation.

RTOL Test Results of Lighting Science Group (LSG) Glimpse

The LSG Glimpse is a downlight designed for the residential market and sold primarily through big box retailers. As shown in Table 4D-1, the device contains MP-LEDs and virtually no optical mixing cavity. An opaque acrylic lens is used to eliminate a pixelated appearance and to diffuse the light as it emerges from the luminaire. The unit is powered by an external driver that is integrated into the device and directly connected to the light engine through soldered interconnects. The light engine and the device are pictured in **Figure 4D-16**.

Figure 4D-16. Pictures of the LSG Glimpse Luminaire Showing the Back of the Housing and the Potted Driver (left) and the Light Engine (right)

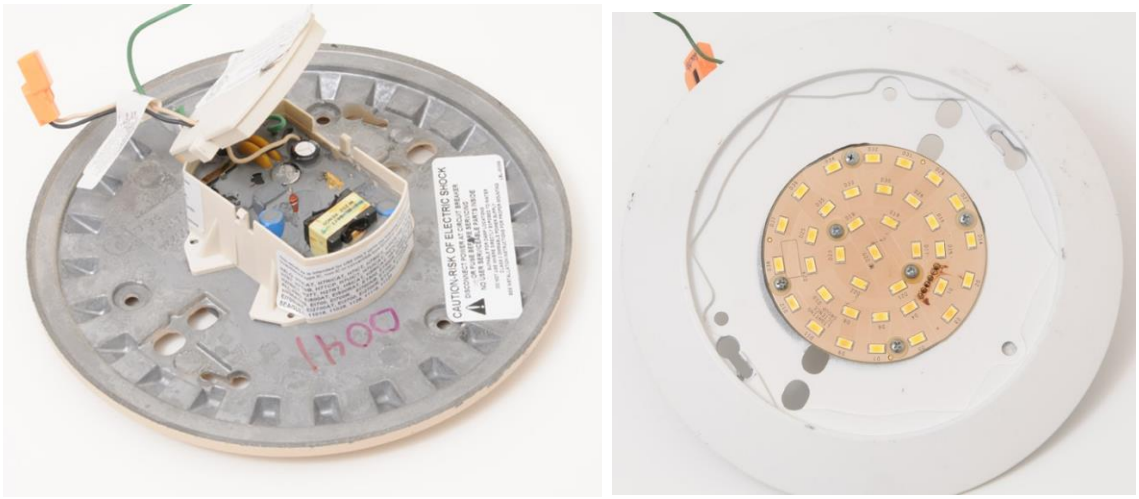

The LSG Glimpse devices performed well during RTOL tests, dropping by only about 65 lumens (9% drop) in 37,000 hours of continuous illumination (**Figure 4D-17**). However, the rate of luminous flux decay began to increase after 30,000 hours of testing, suggesting that faster LED decay would likely have occurred if the tests continued. Because the device lenses were broken during removal from the ceilings for testing, the devices were removed from testing to make room for new samples.

Figure 4D-17. Luminous Flux Over Time of the LSG Glimpse Luminaires in Real-Time Life Tests

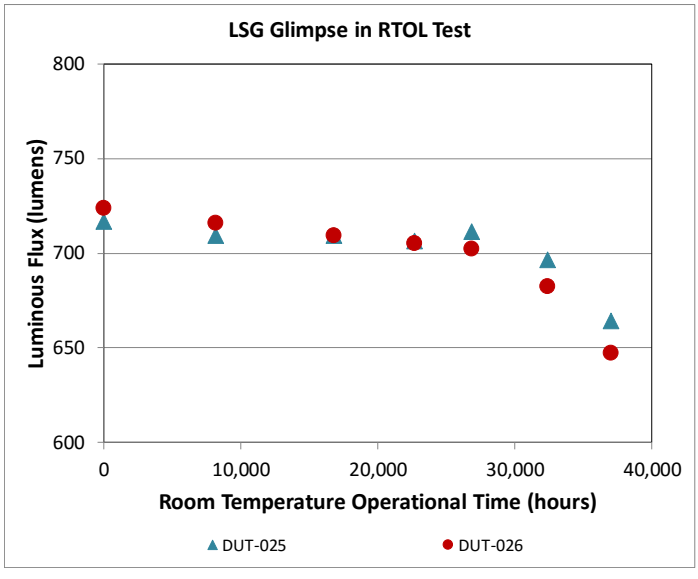

Note: Both devices performed well over time, only dropping about 50 lumens over 37,000 hours of continuous operation.

Figure 4D-18 shows the change in *u′* and *v′* over time that was measured for the two devices in RTOL tests. After a small initial drop, the *u′* chromaticity coordinate increased steadily, whereas the *v′* chromaticity coordinate initially rose quickly and then leveled out. Taken together, these behaviors are indicative of CSM-5 behavior (*u′* is increasing and *v′* changes little) after the first year (i.e., 8,766 hours) of operation. In confirmation of a red shift, the CCT values of these luminaires decreased by roughly 50 K during this test. There was also a noticeable change in the chromaticity between the 32,000-hour measurement (taken on January 13, 2016) and the 37,000-hour measurement (taken on July 25, 2016). We ran additional control luminaires that were stored separately to confirm that the calibration of the integrating sphere was correct. On the basis of confirmation of correct sphere calibration, we concluded that some physical change happened in these luminaires between the two test periods. As will be shown below, a similar effect was also observed for other test samples.

Figure 4D-18. Change Over Time for *u′* and *v′* for the Two LSG Glimpse Luminaires in Normal Operational Life Tests

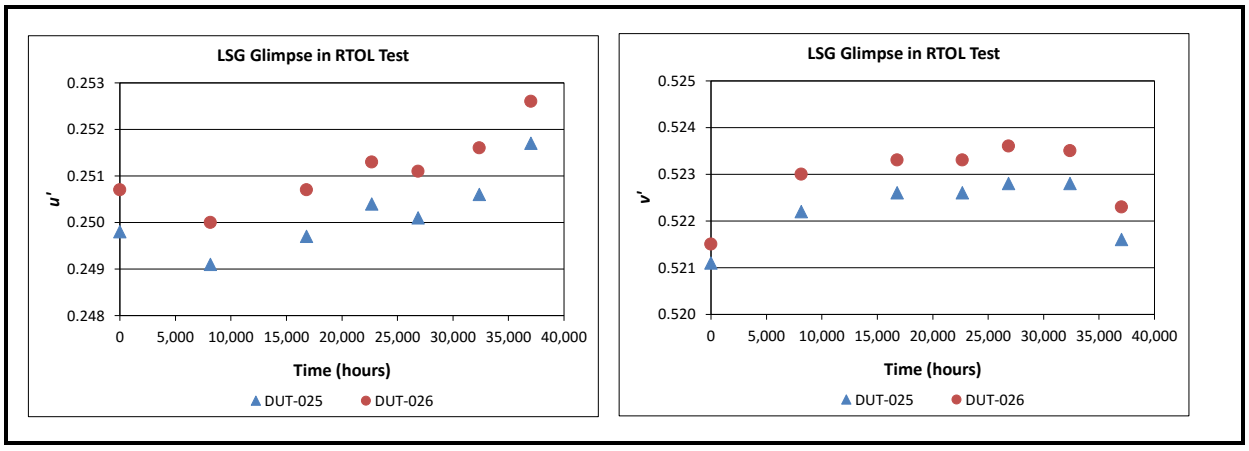

During the time between these two measurements in the RTOL, two events happened to the building that may have affected the photometric properties of the luminaires: the installation of a new roof on the single-story building where the fixtures were housed and the repaving of the building's parking lot. The roof installation is particularly notable because the luminaires are mounted roughly 10 feet below the building's roof and this process produced volatile organic carbons (VOCs) that could be smelled for several days. Although there is no definitive proof, we speculate that VOCs may have caused these photometric shifts, because the reroofing and repaving projects both happened in the intervening time between these two measurements.

RTOL Test Results for Sylvania RT6

Multiple versions of the Sylvania RT6 were tested during this study, but the same version was used in both RTOL and Hammer Tests. This product's first version, which was designed primarily for the residential market, uses a single COB-LED as the light source at the base of an optical cavity, and an optical mixing cavity is formed above the LED using an MCPET® reflector. The assembly is housed in a metal casing, which acts as a heat sink. The integrated driver for the unit sits on the opposite side of the LED board and the two are connected by a pair of wires. The downlight, the driver, and the LED board are pictured in **Figure 4D-19**.

Figure 4D-19. Picture of the Sylvania RT-6 Downlight Examined in RTOL Tests, Along With the Driver and LED Boards

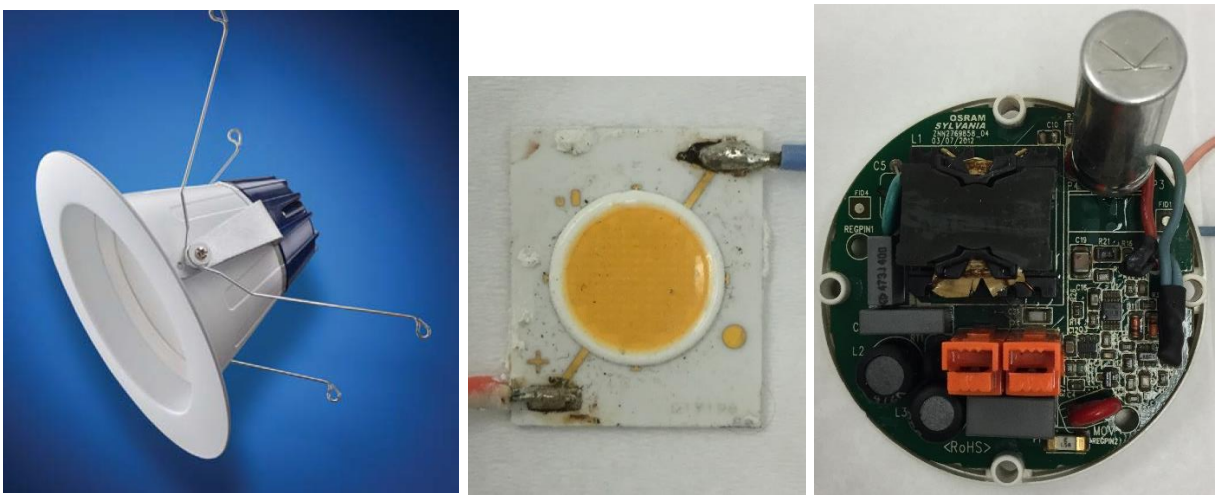

The Sylvania RT6 devices also performed well through the RTOL tests, dropping by less than 20 lumens in 41,000 hours of continuous illumination. **Figure 4D-20** shows the luminous flux of these samples over time, and **Figure 4D-21** shows the change in chromaticity coordinates change over time. Initially, both u' and v' decrease, which is indicative of a blue shift. At about 15,000 hours, v' begins to increase for both samples, whereas u' changes little until after 25,000 hours. This behavior is characteristic of a yellow (CSM-3) shift. Between 32,000 and 37,000 hours of testing, large changes were observed in both u' and v' coordinates in a manner very close to that observed for the LSG Glimpse product (see Figure 4D-18). This finding provides additional corroboration for the impact of a contaminant on the chromaticity point of these devices.

Figure 4D-20. Luminous Flux Over Time of the Sylvania RT6 Luminaires in RTOL Tests

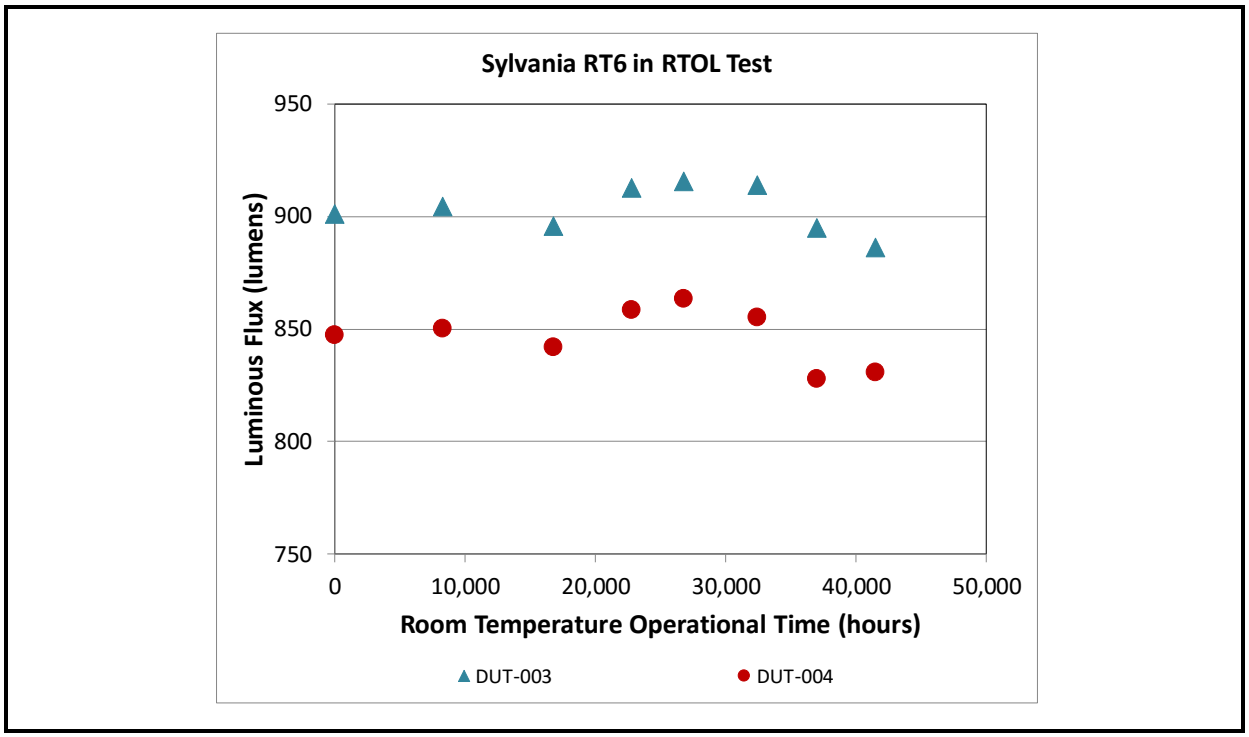

Note: Both devices performed well over time, dropping less than 20 lumens over 41,000 hours of continuous operation.

Figure 4D-21. Changes With Time for *u'* and *v'* for the Two Sylvania RT6 Luminaires in Normal Operational Life Tests

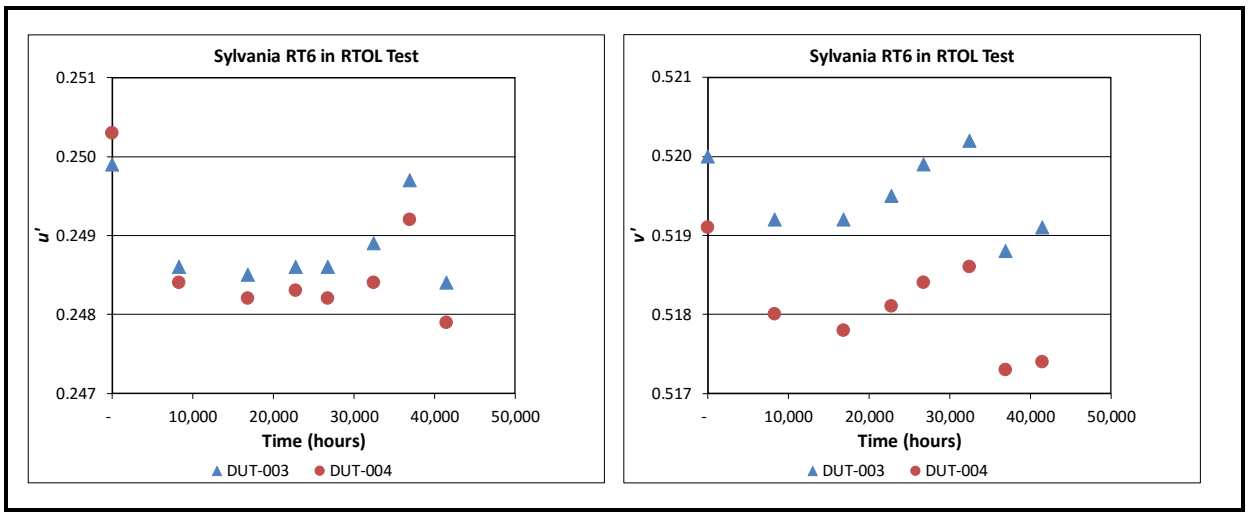

Figure 4D-22. The Spectral Radiant Flux of the Sylvania RT6 luminaire.

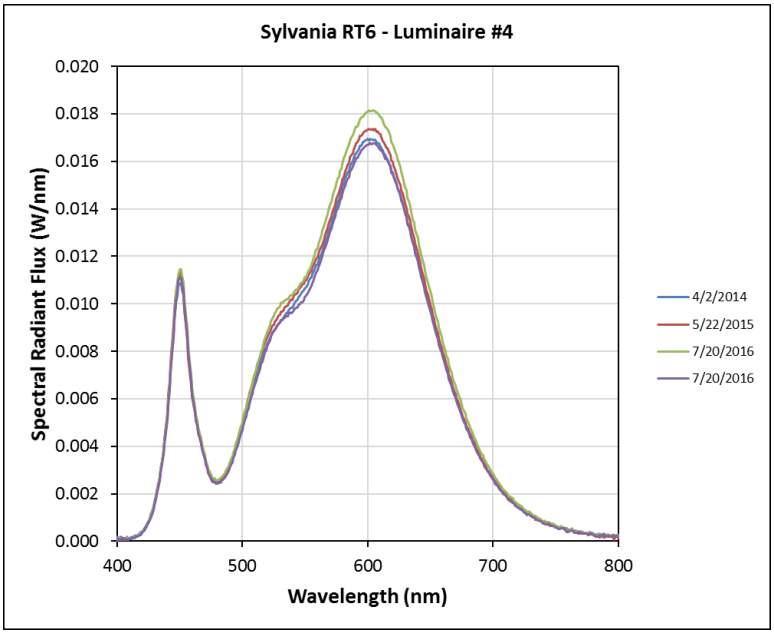

Note that the bump in the Green Peak and the Green Peak itself change maximum intensity as well as wavelength over time.

RTOL Test Results for Cree CR6

A derivative of the LR6, the Cree CR6 appeared on the market several years later, designed primarily for residential use and available from big box retailers. The CR6 also uses a hybrid LED light engine that mixes phosphor-converted, green HP-LEDs with red direct-emitting LEDs, as shown in **Figure 4D-23**. Both the CR6 and LR6 use a hybrid LED light source, but there are significant differences between the products. First, the CR6 does not have a photometric sensor, so the driver circuit for the hybrid LEDs is simpler and much smaller. The device also has significantly fewer LEDs than the LR6 does, which simplifies the driver design. The optical cavity has been simplified as well, with the MCPET used as the reflector in the LR6 being replaced with the WhiteOptics reflector sheet. The finned housing of the LR6 has also been replaced with an aluminum housing that serves as the heat sink. The integrated driver is mounted on the opposite side of the heat sink from the LEDs and the two are connected by soldered wires. A picture of the downlight and the LED board is shown in Figure 4D-23.

Figure 4D-23. Picture of the Cree CR6 Downlight and Driver (left) and Hybrid LED Light Engine (right)

Several Cree CR6 luminaires were added to the test matrix more than 2 years after testing started. To date, the three Cree CR6 luminaires in the RTOL test matrix have achieved 18,000 hours of use during this project; each has shown a 55- to 65-lumen decrease over that time (6–8% drop) (**Figure 4D-24**). Although the luminous flux delivered by the CR6 luminaires held fairly steady through early measurements, it has since decreased more than the RT6 luminaires did in their 42,000-hour test time (see Figure 4D-20).

Figure 4D-24. Luminous Flux Over Time of Cree CR6 Luminaires in RTOL testing.

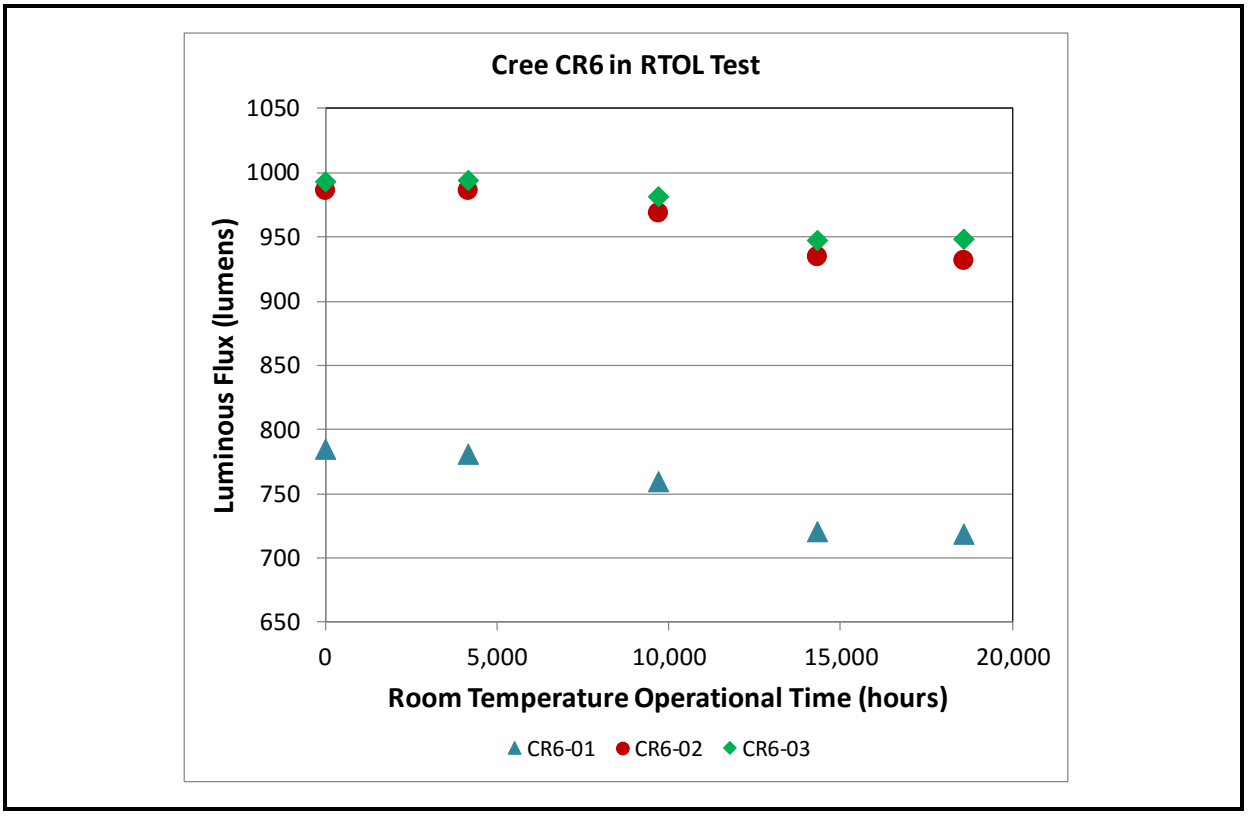

The chromaticity change over time for the CR6 luminaires is dominated by an increase in *v'* whereeas the change in *u'* is much smaller. This chromaticity shift behavior can be categorized as CSM-3. These luminaires did not show the large change in chromaticity between the January 2016 and July 2016 readings that was observed in the RT6 and Glimpse samples. The reason for this difference is unknown, but the discrepancy provides an additional indication that the sphere was functioning properly because these samples were measured at the same time as the RT6 and Glimpse samples.

Figure 4D-25. Values for *u'* and *v'* Over Time of Three Cree CR6 Luminaires in RTOL Tests Show a Dominance by *v'* and a Yellow Shift Over Time, Which Can Be Categorized as CSM-3

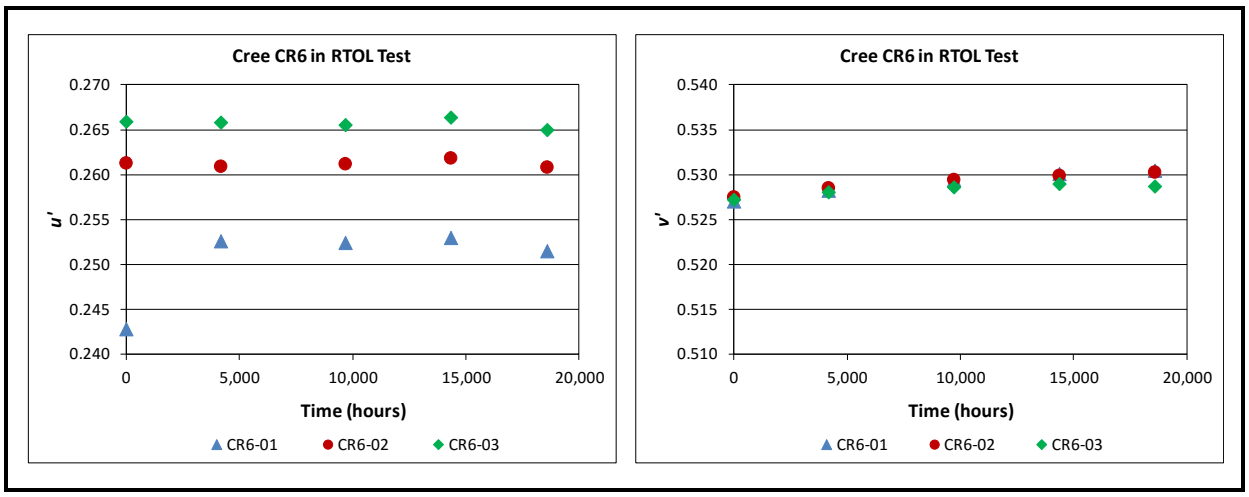

4.D.2 Guidance Document for SSL Luminaire and Lamp Use

As part of the cost-share contribution to this effort, RTI worked with the state of North Carolina to produce a guidance document for the use of SSL technologies in buildings and facilities owned by the state of North Carolina. State-owned facilities include office buildings, educational and residential buildings in the state universities, roadway lighting along the state's major highways, and prisons. Public schools in the state tend to be owned by local school districts. However, the guidance document will be visible to engineers and professionals throughout the state and its use will likely extend to county and municipal buildings, which likely include similar lighting installations. The guidance document is available online [74], along with a webinar discussing it [75].

A primary motivation for creating this document was to provide general guidance to state-employed engineers on the use of SSL technologies in public lighting installations. The document was originally created by a panel of electrical and lighting engineers from different state agencies. The first draft of the guidance document was circulated to major lighting companies for additional comments, which were incorporated into the document if appropriate. The guidance document provides best practices for new construction and major renovations using LED lighting as well as retrofits of existing lighting installations with LED lamps. With SSL lighting being a new technology, both the state construction office (SCO) and the general population of state-employed lighting engineers lacked sufficient knowledge to write appropriate specifications for bidding on a job. As a result, there were numerous examples of poor LED lighting installations, which created a hesitancy to use the technology [76]. The problems that were observed in these early installations included high failure

rates rapid discoloration of LED lamps, and excessive flicker due to transformer and other system issues. The interested reader is encouraged to review this document.

4.D.3 Accelerated Stress Testing

Developing an understanding of SSL luminaire lifetime requires building a knowledge base of likely failure modes and their impact on luminaire lifetime. Because field failure data are generally not widely available, these failures must be created through accelerated tests. The goal of accelerated testing is to accelerate the degradation of device performance to a short enough time scale that failure can be measured in laboratory experiments [77]. Device degradation is typically achieved by elevating the environment stress conditions slightly above those that the product would experience during normal operation. Examples of environmental stresses that can be used to accelerate device degradation include temperature (both high and low temperatures), humidity, pollutants, vibration, and electrical stresses.

It is essential that the accelerated stress test (AST) methodology used for SSL luminaires and lamps faithfully reproduce the cumulative exposure of LED–based products and be completed in a short period of time without introducing new failure modes. Often this can be achieved with an environmental stressor level slightly above the maximum operating temperature; however, setting the environmental stress level too high can introduce new failure modes, which is undesirable. For example, higher temperature settings can increase the rate of most degradation processes, because degradation is usually a chemical process that increases as temperature increases. However, setting the temperature level too high can produce undesirable side effects such as the melting of plastic lenses, which—although not a failure mode that is likely to occur during normal operation—may affect the lumen and chromaticity maintenance of the device.

Guidelines for typical maximum operating conditions of SSL luminaires can be determined by examining several industry documents, including the Energy Star requirements for luminaires [34]. It may be necessary to further delineate the AST methods by whether the luminaire is intended for indoor or outdoor use. For instance, temperature shock performance may be more important in outdoor luminaires than in indoor ones. Among the environments outlined in the Energy Star luminaire requirements are outdoor luminaires with minimal operating temperatures of at least −20°C and operation in wet (e.g., rain) environments. This could represent conditions found in environmental extremes such as Fairbanks, Alaska, and Miami, Florida, respectively. The maximum operating temperature of both indoor and outdoor luminaires is often dictated by the maximum allowable junction temperature of the LED as listed on the manufacturers' specifications. This value is determined in part by the ambient temperature, the drive current, and the cumulative thermal resistance from the LED junction to ambient. For indoor lighting, an extreme case

may be recessed luminaires mounted in ceilings or high bays where ambient temperatures can exceed 80°C, especially in hot climates such as in Phoenix, Arizona.

For LEDs, the limits of elevated thermal stresses can be determined from the LM-80 data and the LED specification sheet. Most manufacturers provide data at substrate temperatures of 55°C, 85°C, and 105°C, which provides an indication of how the LED will perform at those temperatures. In addition, many LEDs have limitations on T_j in the range of 105°C–150°C, depending on the design of the LED. Because T_j depends on the operational forward current, the temperature of the ambient environment, and the thermal resistance between the LED and the substrate, maintaining the LED junction temperatures below the maximum operational temperature is important to preserving normal operating performance in accelerated tests. Temperatures much above the maximum temperature specification may introduce additional failure modes, such as damage to the epitaxial layer or electrical contacts, which can change the I-V profile of the LED [54].

For SSL luminaires and components, thermal-aging experiments are mandatory to reproduce the environment experienced by the luminaire components during operation, storage, and shipping. Literature results have indicated that annealing LED packages at temperatures of 150°C and higher provides an accurate representation of the influence of the high junction temperatures experienced in SSL die [78-80]. However, testing for luminaires may not be able to be conducted at such elevated temperatures because the plastics used in lenses and reflectors will melt.

LED packages are often not hermetically sealed, and common encapsulants, such as silicones, have high permeability to moisture [16]. Consequently, the incorporation of humidity exposure is also a likely environmental stressor to be used in AST, and protocols are already established for steady-state humidity testing. For example, a cyclic bias (i.e., 1 hour on and 1 hour off) at fixed steady-state humidity levels is recommended by JEDEC JESD22-A101-C [81]. This test is performed to evaluate the reliability of non-hermetically packaged electronics. The cyclic electrical bias allows sufficient cooling during the off-cycle for moisture to collect inside the LED package and other surfaces. This will likely intensify the impact of any moisture-related failure mechanisms such as poor gasketing in outdoor luminaires or moisture ingress into the luminaire and critical components such as LEDs.

Another accelerating factor to be considered is the impact of radiation from the LED light emitter and other sources. Typically, prolonged exposure to blue and ultraviolet (UV) radiation may change the reflectance and transmittance properties of the materials used to fabricate reflectors, optics, and painted surfaces [82-84]. For LED devices, UV radiation is less of an issue unless the device is used outdoors. Typically, blue LED exposure is more important to monitor and can cause changes in LEDs, encapsulants, lenses, and reflectors, especially in conjunction with one or more additional environmental stressors, such as heat and humidity. Such radiation-induced changes in optical properties will increase light losses

occurring in the luminaire over time, either through absorption or scattering, and reduce overall luminaire efficiency, as discussed in Section 4.A.

Consequently, a significant amount of thought needs to be given to the testing protocols used for AST. The desired protocol will help to accelerate a potential failure mode under normal operation conditions but will not create new failure modes. A variety of ASTs have already been institutionalized in the electronics industry, and RTI selected from these established methods in building our AST protocols. **Table 4D-2** summarizes the protocols used for AST studies in this work.

Table 4D-2. Summary of the Standards for Thermal and Biased Humidity Test Procedures Used in This Work

Test	Standard Test Methods	Procedures	Minimum Test Durations
Thermal aging	JEDEC JESD22-A103C	Continuous storage at 150°C (Condition B) or 180°C (Condition C) with possible storage at other temperatures	1,000 hours
Biased humidity	JEDEC JESD22-A101-B	Operation of the device at 85°C and 85% relative humidity under a cyclical bias (typically 1-hour duty cycle)	1,000 hours
Temperature shock	MIL-STD-202G Method 107G	Cycle temperature between −40°C and 125°C with a 15-minute dwell time at each extreme	200 cycles
Lumen maintenance	IES LM-80-08	Operation of the LED light source at a minimum of three case temperatures (i.e., 55°C, 85°C, and a manufacturer-recommended temperature) at the same drive current	6,000 hours minimum, with 10,000 hours preferred

4.D.4 Hammer Test Results

Before the beginning of this project, DOE had established the LED Systems Reliability Consortium (LSRC), which comprised members of the Next Generation Lighting Industry Alliance (NGLIA) and other interested luminaire manufacturers. Although this group had been meeting for several years before the start of this project, virtually no information on failure modes for LED luminaires was publicly available. To gain new insights into potential LED failure modes, RTI began working with the LSRC, and this collaboration produced important documents for the industry on LED luminaire lifetime testing [85] and the impact of chromaticity shift on LED luminaire reliability [86].

In addition, the LSRC and RTI jointly designed a highly accelerated stress test (HAST) to induce failures in LED devices in less than 2,000 hours of testing. In addition to the core members of the LSRC, Dr. Abhijit Dasgupta of the University of Maryland, Dr. Xuejun Fan of

Lamar University, and Dr. Willem van Driel of Philips contributed their experience and insights into designing the HAST.

The intent of this collaboration was to develop a Hammer Test and a HAST testing method that would produce failures in SSL luminaires in a reasonable test period (defined as less than 2,000 hours of testing). This test was not intended to be a universal accelerated life test (ALT) for luminaires, but instead was designed solely to provide insights into potential failure modes. Once identified, these failure modes could be studied in a more quantitative fashion than is possible with a rapid screening protocol such as the Hammer Test. In conducting the Hammer Test, RTI used luminaires donated by many major manufacturers. The properties of some of these luminaires are listed in Table 4D-1 and the properties of the remaining luminaires examined in this test are shown in **Table 4D-3**. A report on the major findings was published on the DOE Web site [37].

Table 4D-3. Remaining Luminaires Examined in the Hammer Test [37]

Designation	BetaLED (Cree) Essentia	Lunera 2x2 Troffer
Manufacturing date	Jun-2012	Apr-12
Optical mixing cavity	No	Yes
Line voltage nominal [V]	120	120-277
Light engine configuration	pcLED	pcLED
LED type	HP-LED	MP-LED
Number of LEDs/luminaire	28	256
Specified maximum LED junction temp	150°C	150°C
Specified maximum LED current [A]	1.0	0.15
LED PCB type	Metal core	Laminate
Thermal interface material LED to PCB	Thermally conductive pad	None
Heat sink type	Finned block & heat exchanger	Housing
Power specified [W]	55	40
Initial luminous flux measured [lumens]	2,488	3,144
Measured CCT [K]	2,70	3,400
Optical reflector material	None	Paint
Lens composition	PMMA	Acrylic

The Hammer Test developed by the LSRC and RTI is actually a composite of four separate ASTs, drawn from those listed in Table 4D-2, that are performed sequentially. The detailed protocol for Hammer Testing is provided below, and a graphical representation of the temperature, humidity, and electrical stress levels is provided in **Figure 4D-26**.

Figure 4D-26. Temperature, Relative Humidity, and Electrical Bias Profile of Each Loop of the Hammer Test

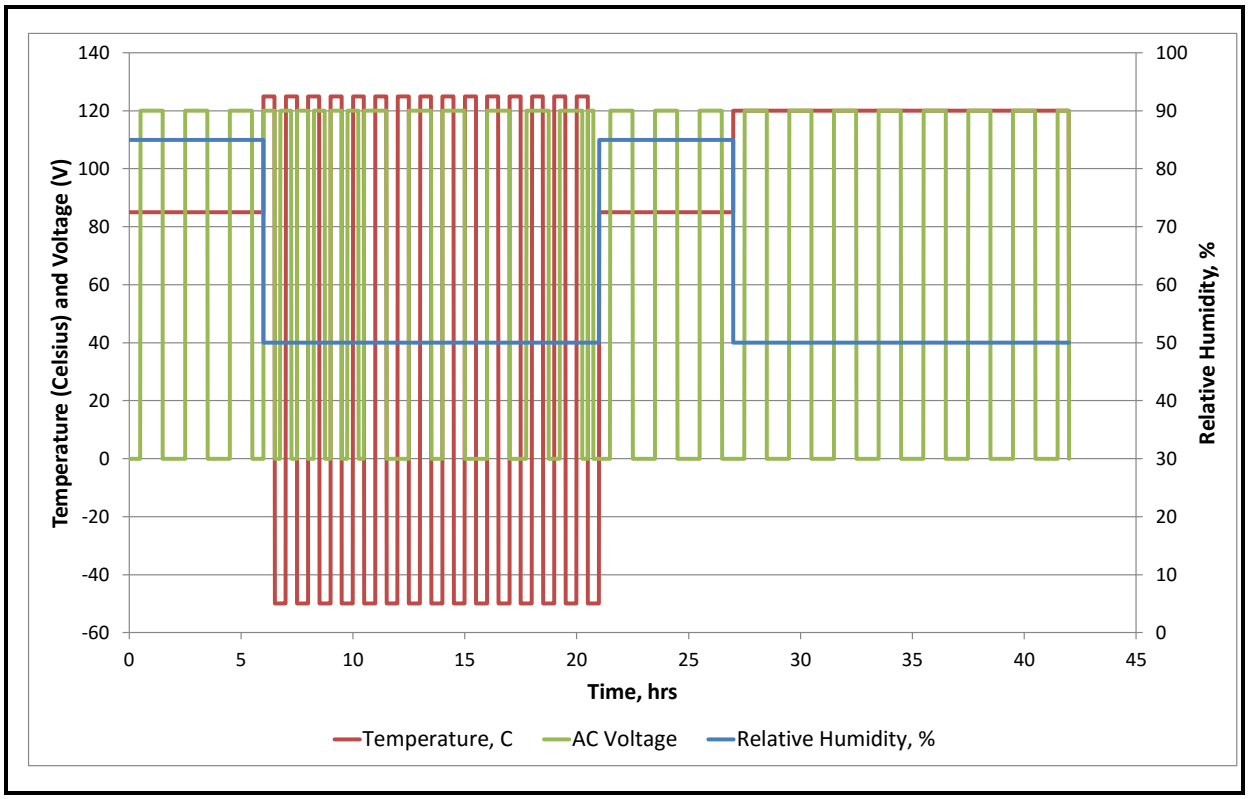

One loop of the Hammer Test consists of four stages of different environmental stresses, with each stage modeled after common stress tests used in the electronics industry. Cumulatively, one loop of the Hammer Test lasts for 42 hours, with each stage presenting a stress comprising variations in heat and humidity.

Stage 1: Steady-state temperature, humidity-biased life test consisting of 6 hours at 85°C and 85% relative humidity (RH).

> This testing stage was modeled after JEDEC standard EIA/JESD22-A101-C [81]. During Stage 1, the devices under test (DUTs) are placed in an environmental chamber set to a constant environment of 85°C and 85% RH. Power is applied to the devices on a 1-hour cycle—the devices are switched on for an hour and then off for an hour for a total of 6 hours.

Stage 2: Temperature shock consisting of 15 hours cycling at –50°C to +125°C (air-to-air). Hold time at each extreme was 30 minutes.

> This testing stage was modeled after JEDEC standard JESD22-A104D [87]. For the temperature shock stage, the DUTs are moved to a thermal shock chamber that rapidly cycles between −50°C and +125°C. The chamber recovery time during the temperature excursion is less than 5 minutes. The DUTs are held at each temperature extreme for 30 minutes before being switched to the next setting.

Power is applied to the devices asynchronously with the temperature cycle—they are powered on for varying lengths of time not concurrent with the temperature cycling. This stage lasts for a total of 15 hours.

Stage 3: Steady-state temperature, humidity-biased life test consisting of 6 hours at 85°C and 85% RH.

During the second humidity exposure stage, the DUTs are placed in an environmental chamber set to 85°C and 85% RH. Power is applied to the devices on a 1-hour cycle—the devices are switched on for an hour and then off for an hour for a total of 6 hours.

Stage 4: High-temperature operational lifetime consisting of 15 hours at 120°C.

This testing stage was modeled after JEDEC standard JESD22-A108C [88], although the test time used was shorter than the 1,000-hour minimum specified by the standard. In this stage, the bake stage involves holding the devices at a constant temperature of 120°C for 15 hours in the same environmental chamber used for humidity exposure. During Stage 4, power is cycled on and off hourly.

The Hammer Test provides an extreme stress environment for the luminaires, and the testing protocol is intended to create failures in a reasonable period of time. These failures can provide qualitative information on potential field failure modes in SSL luminaires that can be studied in more depth using more quantitative ALTs.

Seventeen samples chosen from the luminaires described in Table 4D-1 and Table 4D-3 were placed in the Hammer Test, and the test was conducted for a total of 40 loops (1,680 hours). Because of the need to perform air-to-air shock, the tests were performed at C&C Technologies in Apex, North Carolina. Because of the different insertion times of the luminaires, the longest test time for any luminaire was 1,470 hours (35 loops) when the test was terminated. Units that were received late in the testing period had experienced fewer test hours when the procedure was stopped. Of the units tested, 12 luminaires (71%) failed during the test, with the remaining 5 units still operating at test termination. The failure time of each unit is given in **Figure 4D-27**. For simplicity, the failure time is equated to the total Hammer Test time when the failure was first observed. In other words, interval censoring was not used on the data; rather, the failure time was assumed to be the end time of the cycle when failure occurred.

Figure 4D-27. Failure Times of the Luminaires in the Hammer Test

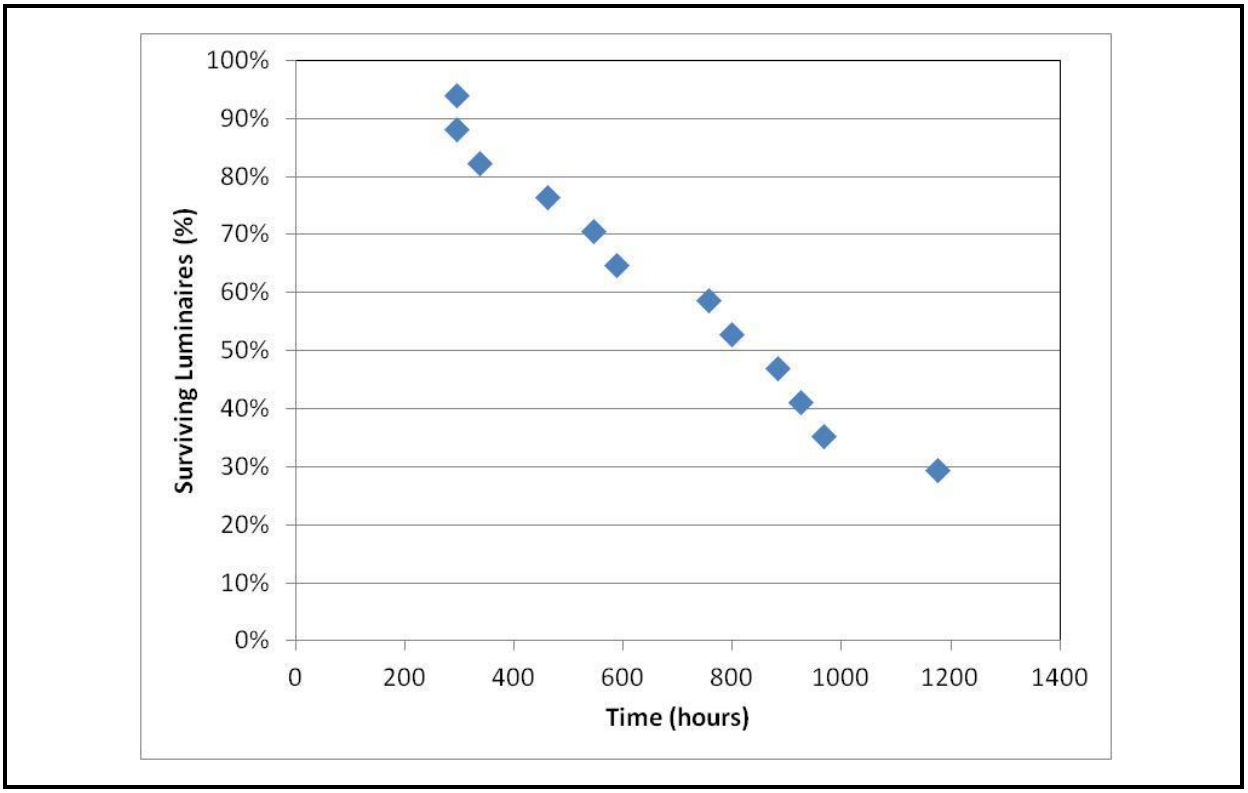

For this test, luminaire failure was defined as either (1) catastrophic failure when the unit produced no light or (2) parametric failure for lumen maintenance when the unit produced light but at a level less than 70% of the initial luminous flux (i.e., L_{70} value). Color shift was monitored during testing but was not used as a failure criterion. Ten of the failed units exhibited catastrophic failure when examined after testing, and the cause of these catastrophic failures was generally found to be associated with either the driver circuit, the LED board, or the connection between the two. Two failures were initially thought to be potential lumen maintenance failures due to a reduction in luminous flux below L_{70}. However, these failures were eventually assigned to board- and component-level issues that adversely affected LED drive voltages. Although two failures were eventually assigned to solder interconnects on the LED boards, the LEDs by themselves were not found to be a source of failure in the Hammer Test.

The data provided in Figure 4D-27 can also be recast as a Weibull probability plot, as shown in **Figure 4D-28.** A two-parameter Weibull model was used to fit the data, and MLE methods were used to account for right-censored data, with median rank methods applied to the censored data. This treatment of the data resulted in the following parameters for the Weibull model:

Shape parameter (β) = 2.027

Scale parameter (η) = 1,008.8 hours

Because the β value was greater than 1, wearout phenomena are responsible for the failure of the luminaires. In addition, because each loop of the Hammer Test includes 12 hours (29%) of 8585, the value of the shape parameter can be compared to 8585 tests. As discussed in Section 4.C, the β value of the Hammer Test was higher than that for the 8585 test alone on LED lamps, indicating a higher degree of acceleration in the Hammer Test. We speculate that the higher degree of acceleration is likely the result of the incorporation of the temperature shock test (i.e., Stage 2) into the Hammer Test protocol.

Figure 4D-28. Weibull Probability Plot for the Luminaires Subjected to the Hammer Test

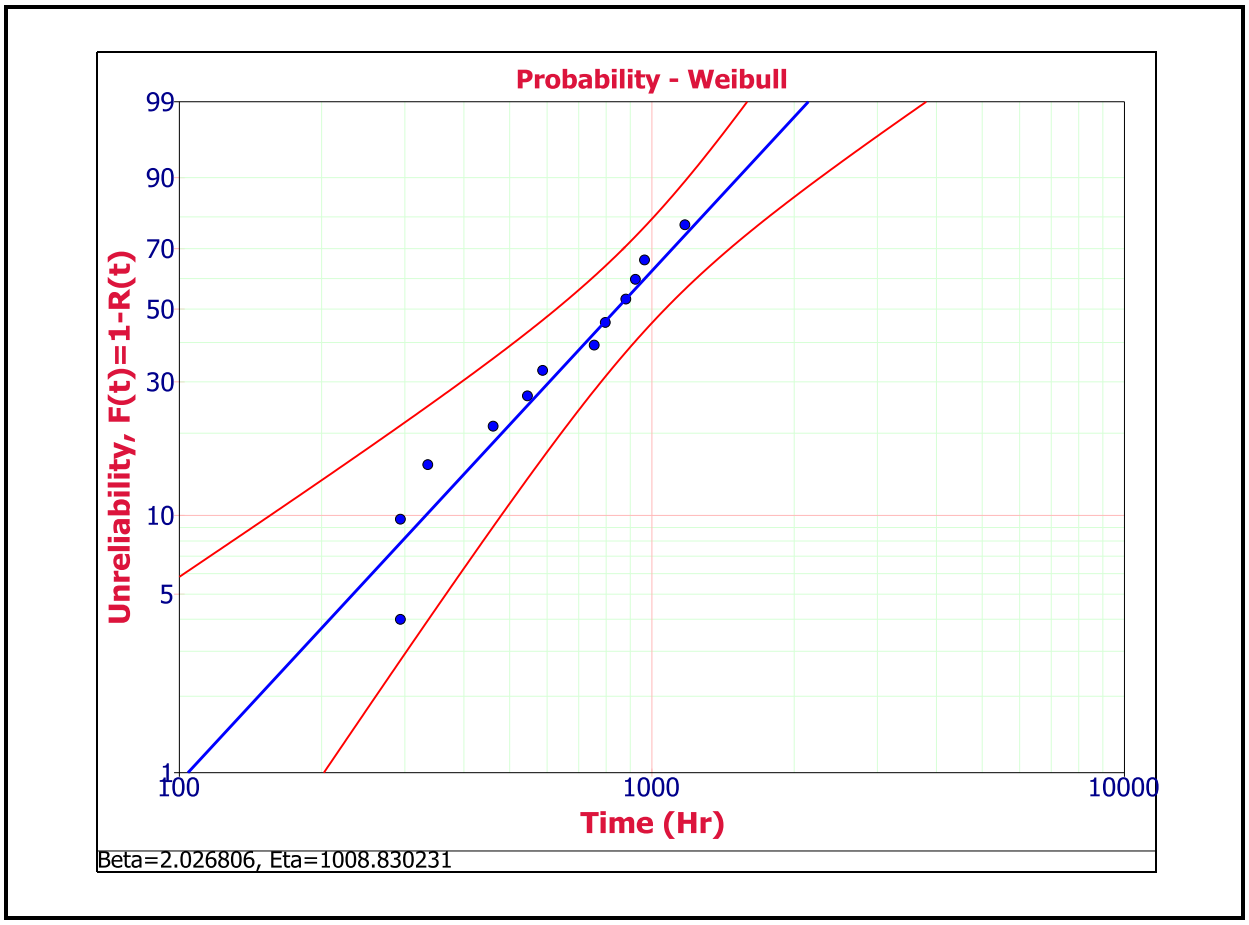

To understand the failures that were created by the Hammer Test, we conducted failure analysis of these products in conjunction with the luminaire manufacturers. A high-level distribution of the failure modes is given in **Figure 4D-29**. Board-level failure in the driver

was the most common failure mode in this test, and the six failures that were classified as PCB failures occurred in the Cree LR6 and the LSG Glimpse. This finding is not surprising because (1) all of the tested luminaires were designed for indoor operation; (2) the temperature shock cycle of the Hammer Test places severe stresses on PCBs; and (3) the fixed nature of the LED board and driver connections in these devices will likely increase strain on the bond pads, resulting in failure. Although the temperature shock endpoints used in the Hammer Test may be outside the common operational range of these indoor luminaires, several recent studies have demonstrated that temperature cycling can occur in LED devices and result in component failure [89; 90].

Figure 4D-29. Distribution of Failure Modes for Luminaires Examined During the Hammer Test

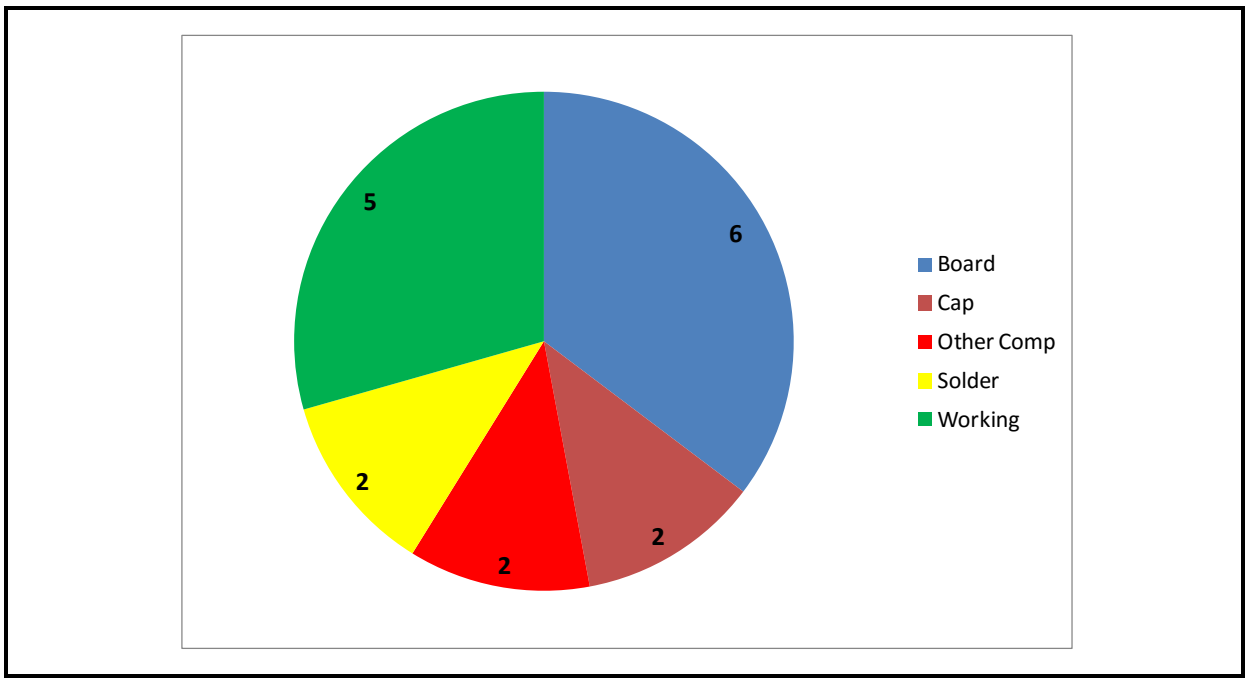

The Cree LR6 and the LSG Glimpse luminaires were the only products in the Hammer Test in which the LED board was rigidly fixed to the driver board. For the other products, a flexible wire soldered at both ends connects the two boards, and this type of interconnect may be better able to accommodate expansion and contraction cycles during the temperature shock stage. Board-level issues were also observed after 30,000 hours of operation of the Cree LR6 in RTOL experiments, indicating that the Hammer Test identified a potential reliability issue with the luminaire. However, no board-level failures were observed through 36,000 hours of RTOL testing for the LSG Glimpse. One of the failed LSG Glimpse devices was returned to the manufacturer, which confirmed that (1) there were no issues with the LEDs and (2) some bond pads had separated from the board, resulting in a break

in the circuit. After repairing these pads, the manufacturer was able to demonstrate that the rest of the device was fully operational. Therefore, it was concluded that the failure mode of the LSG Glimpse (i.e., bond pad lifting) that was identified in Hammer Test is not likely to occur during normal use.

Several other failure modes were observed in the remaining devices during the Hammer Test. A Sylvania RT6 device failed because of issues with the controller IC and the MOSFET. As will be discussed later, this failure mode is consistently repeated throughout our additional studies on luminaire reliability and is thought to be a common field failure. In addition, film capacitors were observed to fail in the Cree CR6 during the Hammer Test, and this failure mode is also consistently repeated in additional tests performed during this work. Finally, two Philips Lightolier Calculite downlights failed because of apparent solder joint reliability issues. Solder joint failure was rarely observed during our testing protocols, except for the Hammer Test, but it has been reported in other SSL devices when large temperature excursions are taking place [89]. The Calculite luminaires that were involved in RTOL testing all were parametric failures due to excessive loss of luminous flux. As discussed above, this mechanism was not repeated in the Hammer Test.

In conclusion, although the Hammer Text was performed using extreme settings of environmental stresses, it identified many of the failure modes that occur in SSL luminaires. However, the test did occasionally introduce a new failure mode, as occurred with the LSG Glimpse, or a failure mode did not occur in the Hammer Test but did in normal use, as occurred with the Calculite downlights. Consequently, the true value of the Hammer Test is in identifying potential failure modes with minimal testing burden. These failure modes can be investigated further with additional testing protocols to determine their overall impact on product reliability.

4.D.5 Remote Phosphor Disk Studies

In an effort to understand the behavior of remote phosphor materials, such as those used in the Philips Lightolier Calculite downlight, we studied the characteristics of such remote phosphor materials in 7575 and 8585 environments. Our work built on previous studies in two important ways. First, the work performed by the RTI team examined both warm white and cool white remote phosphors disks. Second, our experimental conditions were intentionally chosen to minimize the impact of photo-oxidation of the polycarbonate material on which the remote phosphor is deposited.

Previous studies of accelerated aging of remote phosphors have typically concentrated on cooler CCT materials with higher Ce:YAG content. Dal Lago and colleagues examined the performance of 4,000-K remote phosphor plates in ASTs carried out at temperature levels between 85°C and 145°C [91]. This study, which also included irradiation of the samples with blue light ranging from 40 mW/cm^2 to 350 mW/cm^2, found a degradation mechanism that significantly reduced luminous flux and produced a color shift. The primary degradation

mechanism identified in this study was photo-oxidation of the polycarbonate substrates used for the remote phosphor disks. Mehr, van Driel, and Zhang also investigated the optical degradation of remote phosphor plates formed on polycarbonate substrates [92; 93]. This work examined samples with CCT values of 4,000 K and 5,000 K and observed degradation in luminous flux and color point stability when the polycarbonate samples were exposed to temperatures between 100°C and 140°C for prolonged periods. Higher temperatures produced faster degradation kinetics and consequently faster lumen depreciation and color shift.

The findings from RTI's investigation of the binder chemistry of common remote phosphor disks is described elsewhere [94] and will be only summarized here. In short, different phosphor chemistries were deposited using different binder systems, with the warm white remote phosphor disks using a urethane binder and the cool white remote phosphor disks using an acrylic binder. For both remote phosphor formulations, the 8585 environment produced much greater losses in luminous flux, which were tied to increased absorption in the binder layer. For the phosphor materials themselves, the 7575 test exerted minimal impact on the cool white phosphor (presumably Ce:YAG) and minimal impact on the warm white phosphor. These findings suggest that 7575 testing may be more appropriate for LED luminaires because of the less aggressive nature of the environment.

4.D.6 Luminaire Operation in Accelerated Stress Tests

A major focus of this project was to investigate the long-term reliability of SSL luminaires and to build models that describe this behavior. Several different models are necessary to understand the long-term behavior of SSL luminaires, and AST is the best approach for gathering this information in a reasonably short period of time. Among the models that are needed to describe the reliability of SSL luminaries are those that describe

- long-time behavior of LEDs in the luminaire, including luminous flux and chromaticity maintenance;
- aging behavior of the materials used for lenses and reflectors in SSL luminaires; and
- electrical driver long-term performance and the impact of environment and power quality on the driver.

Most of this report has focused on the first two parts of a SSL luminaire system model. The goals of Section 4.D.6 are to present data from AST experiments on complete luminaires and to leverage the models discussed earlier in this report to build a deeper understanding of the lumen and chromaticity maintenance of these devices. This information is important to understand the potential causes of parametric failure such as excessive lumen depreciation or chromaticity shift. Section 4.D.8 will take a deeper look at the reliability of LED drivers and their impact on catastrophic and parametric failures to complete the models for understanding SSL luminaire behavior.

As discussed previously, the vast majority of AST experiments conducted during this work were performed on 6" downlights because of their ubiquitous use in the light industry, relatively low cost, small size, and relatively rapid incorporation of new technologies. The downlight products that were examined in this study ranged from architectural- and specification-grade fixtures provided by manufacturers to residential fixtures that were purchased online and at big-box retailers. The luminous flux of these devices ranged from 600 lumens to almost 2,500 lumens. Although most of the products tested were warm white fixtures, several neutral white (CCT ~ 4,000 K) and cool white (CCT ~ 5,000 K) fixtures were also tested. A list of some of the properties of the luminaires examined in this study is given in **Table 4D-4**.

AST experiments on entire luminaires started at roughly the same time as the Hammer Test. As part of our scope for this study, we chose to perform experiments on entire luminaires, rather than merely on their components, in order to identify any potential interactions between luminaire subsystems that may affect overall reliability. Findings from the Hammer Test helped to inform the methodology and testing protocols used with entire luminaires in several ways. First, the Hammer Test provided an indication that high temperature bakes do not provide a fast-enough acceleration factor to reach our goal of developing a practical test that requires less than 3,000 hours. High-temperature bakes also increase the risk of melting or deforming plastic parts, such as lenses. Second, both temperature cycling and humidity seem to provide high acceleration rates, but they are difficult to do at the same time and were done sequentially in the Hammer Test. Temperature shock experiments typically require a special chamber where the samples are quickly transported between the high and low temperatures. The rapid temperature change is a key component of the temperature shock and would cause excessive moisture condensation if performed in conjunction with elevated humidity. Consequently, it is not practical to do both temperature shock and bias humidity tests in the same chamber, and using multiple chambers in this study would significantly increase the experimental complexity.

As a result of these factors, RTI decided to concentrate our study around temperature and humidity testing of SSL luminaires. The experimental protocols developed by RTI can be broadly classified as WHTOL tests [81]. On the basis of findings from the Hammer Test, we used three different temperature and humidity protocols were used: (1) 85°C and 85% RH (8585), (2) 75°C and 75% RH (7575), and (3) 65°C and 90% RH (6590). This work is believed to be the first public evaluation of LED luminaires in temperature and humidity environments.

Table 4D-4. Photometric, Electrical, and Physical Properties of Luminaires Examined in this Study

Designation	Cree CR6	Cree T67	Cree Essentia	Commercial Electric T65	Sylvania RT6	Sylvania RT6 HO	LSG Glimpse	LSG Glimpse Indirect	LSG ECS DN6 W27	OptiLED Round 150	Acuity Security Lamp
Optical mixing cavity	Yes	No	No	Yes	Yes	Yes	No	Yes	Yes	Yes	No
Line voltage nominal [V]	120	120	120	120	120	120	120	120	120	120	120
Light engine configuration	Hybrid LED	pcLED	pcLED	pcLED	pcLED	pcLED	pcLED	pcLED	pcLED	pcLED	pcLED
LED type	HP-LED	HP-LED	HP-LED	MP-LED	PLCC 2 LEDs/package	HP-LED	MP-LED	MP-LED		HP-LED (cool white) MP-LED (warm white)	COB-LED
Number of LED packages/luminaire	4	5	28	28	8	24	36	32	12	12 (cool white) 156 (warm white)	2
Initial luminous flux measured [lumens]	599 (warm white) 601 (cool white)	727	2,482	800	755	1,312	892	639	610	768 (natural white) 662 (warm white)	1,341
Measured CCT [K]	2,721 (warm white) 4,844 (cool white)	2,809	2,755	2,756	2,720	3,352	3,033	2,741	2,751	4,032 (natural white) 2,883 (warm white)	3,957
LED PCB type	Metal core	Metal Core		FR-4			FR-4			Metal core	
Thermal interface material LED to PCB	Thermal pad										
Heat sink type	Housing	Housing		Housing	Housing	Finned housing	Housing	Housing	Housing	Finned housing	
Power specified [W]											
Optical reflector material	WhiteOptics	—	—	PET film	Molded PC		—	Painted aluminum dome		Paint	
Lens composition	PC	PMMA	PMMA	PMMA	PMMA	Glass	PMMA	PMMA		PMMA	PMMA
Average initial power consumption (w)	8.5	11.1	54.7	10.3	9.2	19.1	13.9	11.2	10.2	15.3 (warm white) 15.0 (cool white)	17.2
Driver type	Buck	Boost	2-stage	2-stage	Buck	Flyback	Buck	Buck	Buck	Flyback	Flyback

The temperature humidity experiments on SSL luminaires were conducted in three different environmental chambers at RTI: wa Tenney TC10RS-2, a T20RC-2, and a C20RS. All chambers can be set to a given temperature and humidity level, which is controlled through sensors in the chamber and heat exchangers and evaporators in the chamber control system. A thermocouple was attached to the exterior housing of each DUT to permit examination of the sample temperature during experiments. To understand the temperature changes that occur in the DUTs during experiments, we first measured the temperature rise of the DUTs when the electrical bias was switched on in a closed environmental chamber, but with all chamber controls turned off. For these experiments, large two-stage drivers were used. As shown in **Figure 4D-30**, the temperature of the DUTs increased when the power was applied to the devices, and the measured temperature increase varied between 10°C and 35°C.

Figure 4D-30. Temperature Change of LED Drivers in Environmental Chamber With the Chamber Controls Turned Off

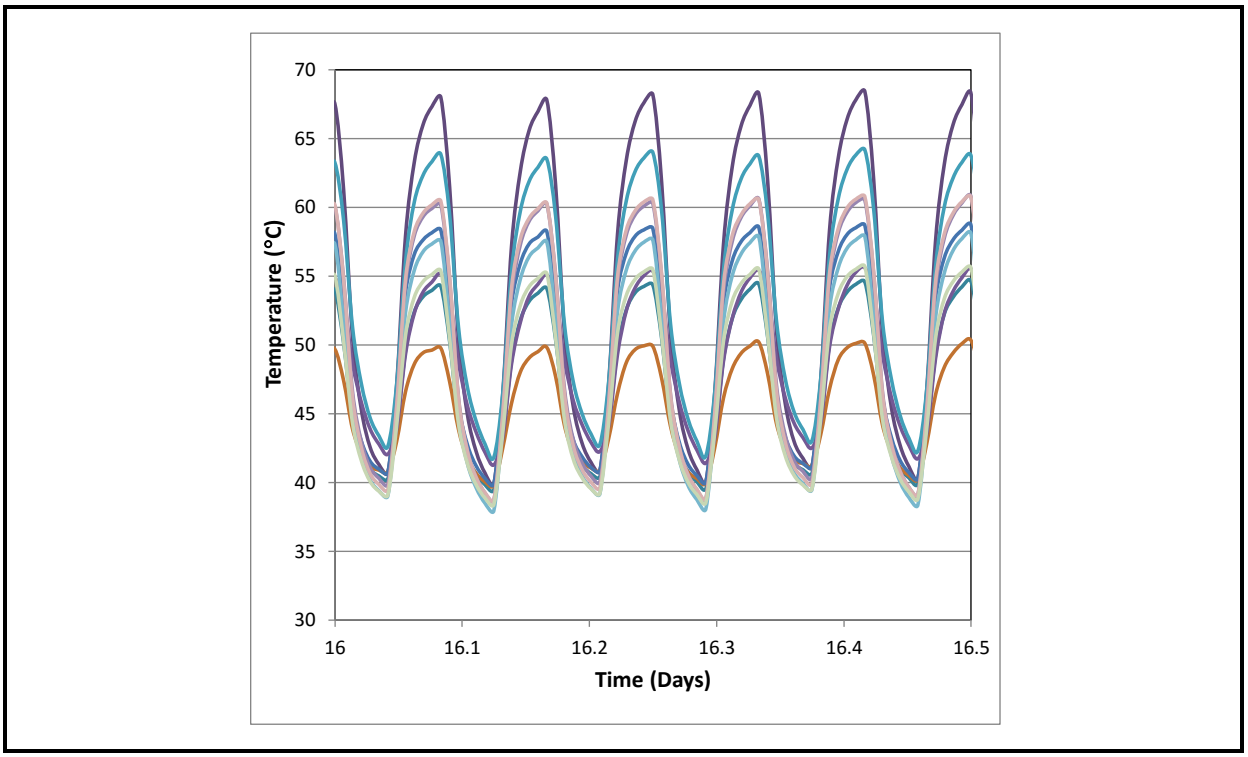

Note: The DUTs in this test were large two-stage drivers and the thermocouple was placed on the external case of the DUTs.

When the environmental chamber is turned on and the controls engage, the temperature and humidity controls of the chamber will also affect the temperature rise in the samples. As shown in **Figure 4D-31**, the same rapid temperature rise occurs when the device is turned on in the WHTOL environment; however, the total temperature rise is less than that with the chamber controls off. For the drivers shown in Figure 4D-31, the temperature rise

when the DUT is powered is between 4°C and 10°C, which is significantly smaller than in the uncontrolled chamber. In addition, the thermal profiles of the DUTs are different in the WHTOL environment, and this difference may be due to the lower temperature rise that occurs in these experiments. It can be seen that the DUTs achieve near thermal equilibrium in Figure 4D-31 early during the 1-hour time period when the bias is applied, whereas the temperature appears to still be rising, albeit at a slower rate, in the uncontrolled experiment (Figure 4D-30). When the bias is removed, the temperature of the DUTs in WHTOL quickly returns to the ambient setting in the WHTOL experiment. The reason that a larger temperature rise is not found in our WHTOL tests is that the chamber's control systems help to manage the heat pumped into the chamber background by the luminaires, and this influence controls the rise in surface temperature of the DUTs. In this type of test, it is likely that the thermal shock of the rapid temperature rise and fall will have a bigger impact on reliability than the absolute temperature increase will.

Figure 4D-31. Example of the DUT Temperature Change During 7575 WHTOL Experiments With the Chamber Controls Fully Engaged

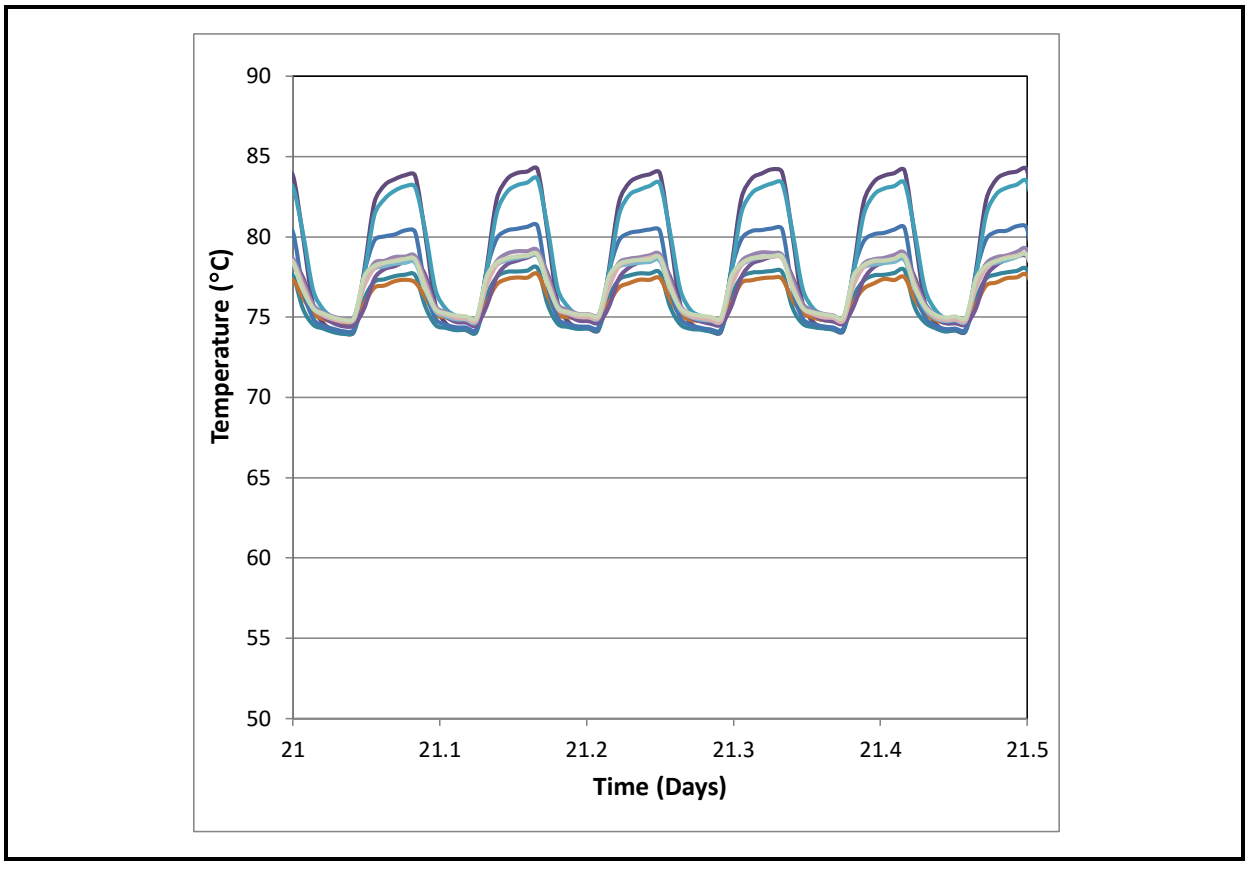

Note: The DUTs are the same drivers are shown in Figure 4D-30 and the thermocouples were in the same locations.

However, significant temperature rises can still occur in LED luminaires under the right conditions. We have seen temperature excursions of up to 15°C in the external case temperatures of luminaires being tested. In addition, the temperatures of some components such as MOSFETs and transformers can be even higher, with temperature increases of more than 20°C above ambient being observed in many cases. The thermocouples attached to the luminaire case also provide a means to monitor device failure during temperature-humidity testing, as shown in **Figure 4D-32**. When a catastrophic device failure occurs, the temperature does not rise as much as when the luminaire is operating normally. However, there is still some small background temperature increase due to the impact of the other luminaires in the environmental chamber. It should also be noted that the periods of the last three cycles before failure are the same. However, when the unit is energized, failure occurs before the rapid temperature rise can happen. This finding suggests that for this DUT, catastrophic failure occurred nearly instantaneously with the device being turned on.

Figure 4D-32. Example of Device Failure During 7575 Experiments

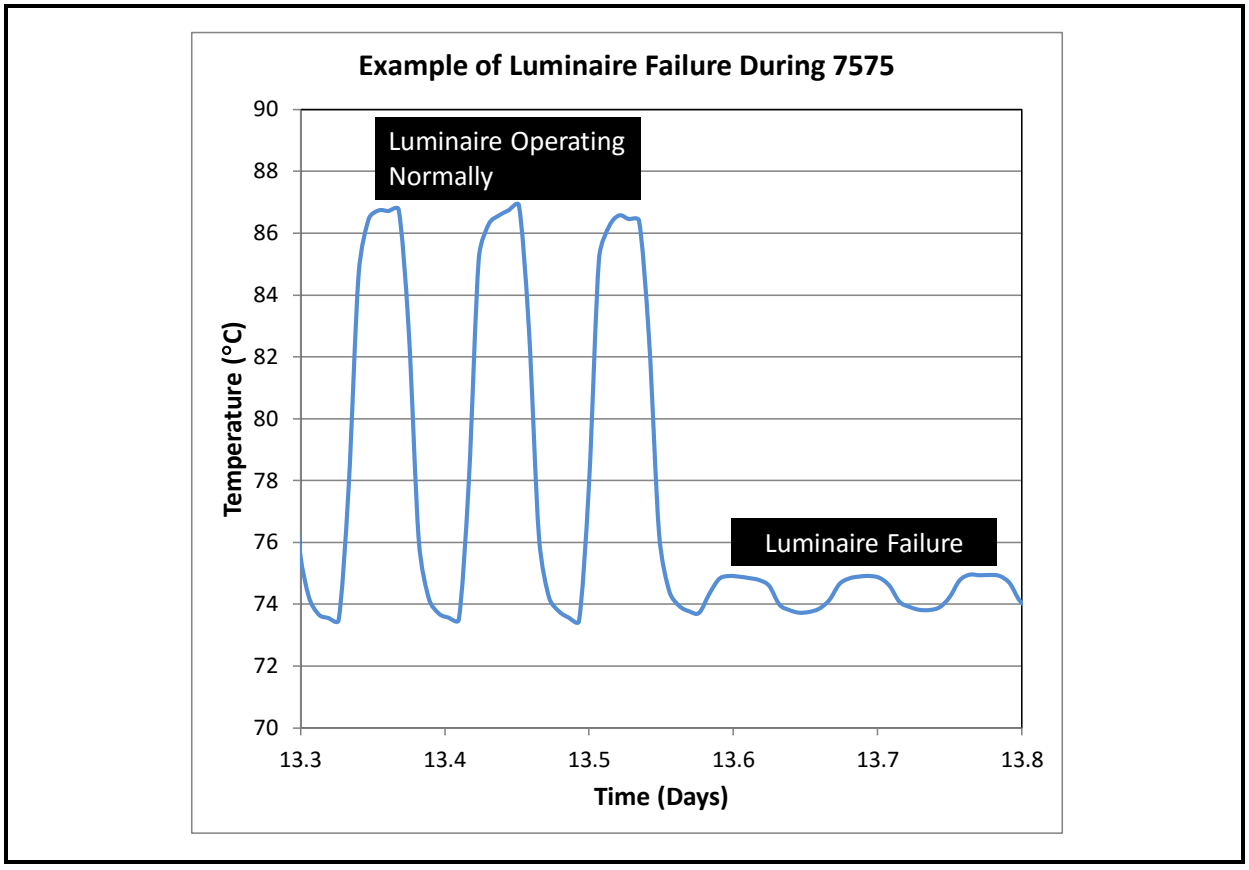

Lithonia Security Lamp

The Lithonia Security Lamp is a pole-mounted SSL light fixture intended for outdoor use. The unit also has a photocell for activation at night. There is no gasketing between the lens and the device house and between parts of the housing to prevent moisture ingress. Samples of this luminaire were purchased from online sites, so the device can be considered an outdoor residential luminaire. Pictures of the device are shown in **Figure 4D-33**. This device was chosen for testing because it is a luminaire designed for outdoor use, it has low cost, and it has a footprint similar to that of 6" downlights. However, the device does not have the ingress protections of higher-end outdoor luminaire and would represent a worst-case scenario for this type of product.

Figure 4D-33. Pictures of Lithonia Security Lamp

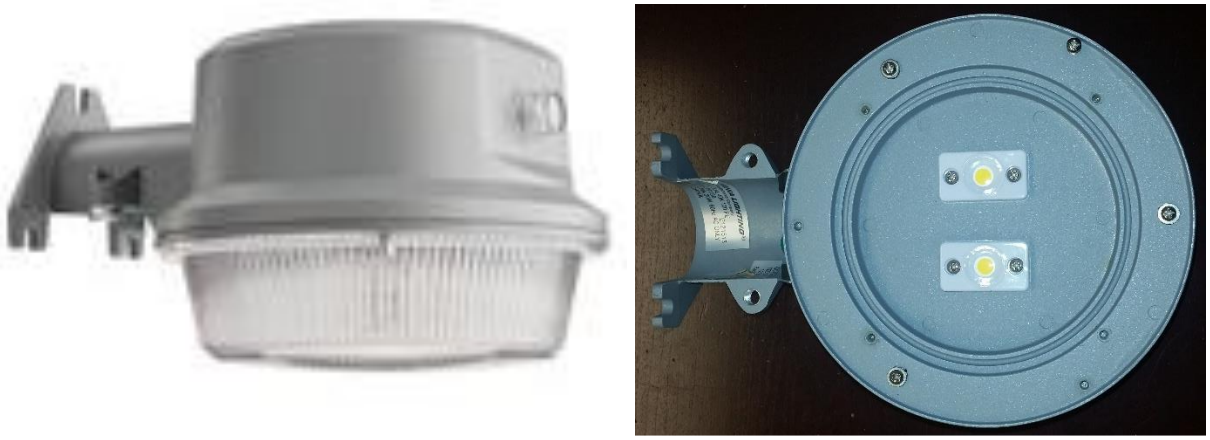

Samples of this security lamp were tested in both 7575 and 8585 environments and were generally found to exhibit strong performance under WHTOL testing conditions, despite the absence of ingress protection. During 2,500 hours of testing in 8585, one unit exhibited a catastrophic failure (at between 750 and 1,000 hours), but the other two units were still operational at the end of the test. The average luminous flux maintenance of these two devices was 0.998 at the end of testing. However, the test was stopped after 2,500 hours since both surviving units had chromaticity shifts ($\Delta u'v'$) in excess of 0.012.

As shown in **Figure 4D-34**, the chromaticity shift is 8585 is predominantly in the negative $\Delta u'$ direction with a much smaller $\Delta v'$ component. This behavior can be best modeled using the generalized logistic function for both $\Delta u'$ and $\Delta v'$. The experimental results and the associated models provide a clear indication that the $\Delta v'$ shift is bounded, and the upper limit was $\Delta v' = 0.0028$. The least-squares fit to a generalize logistic model also determined that there was an upper bound to the $\Delta u'$ shift as well, but the bound on this shift was determined to be −0.018, which will produce a parametric failure for chromaticity shift. The value of the upper limit on $\Delta u'$ was also supported by the finding that there was an inflection

point in the derivate of $\Delta u'$ with time near 2,000 hours. There were some signs that another shift may have been occurring in the first 500 hours of testing, but this shift, if it did occur, could not be teased out from the data. The observed chromaticity shift is characteristic of a CSM-2 shift in the green direction under 8585, and the magnitude of the shift indicates that this mechanism is the terminal chromaticity shift in these tests.

Figure 4D-34. $\Delta u'$ and $\Delta v'$ Data and Chromaticity Shift Models for Lithonia Security Lamp in 8585

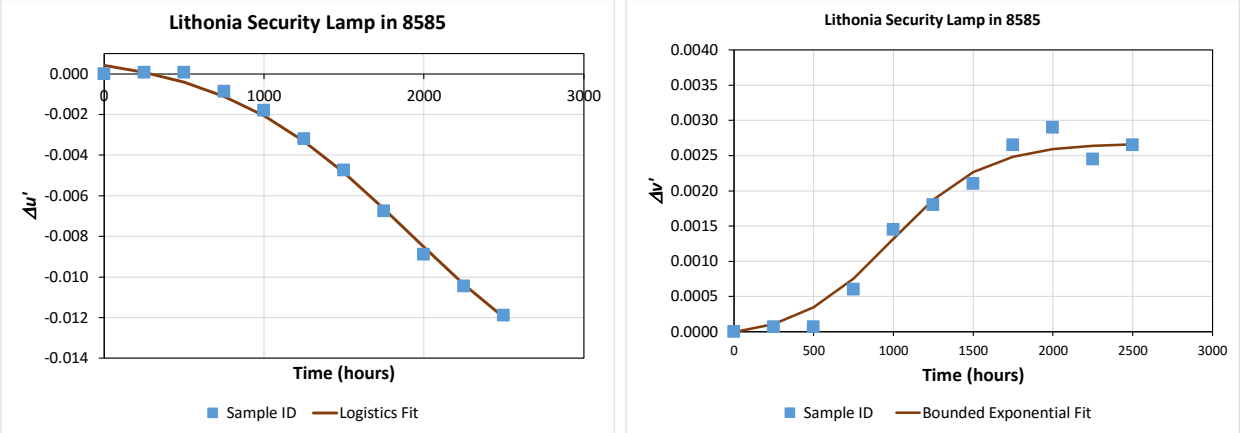

The Lithonia Security Lamp was also tested in 7575 and the findings were similar, although the rate of change was slower. Because the magnitude of the measured chromaticity shift was much smaller in 7575, the DUTs were operated for 7,000 hours in this environment. During this test period, two out of three DUTs failed catastrophically, one after 4,500 hours of testing and one after 5,500.

The information from the chromaticity shift model of the Lithonia Security Lamp in 8585 can be used to inform the model of the same product in 7575. However, as shown in **Figure 4D-35**, these are slightly different behaviors between the two test environments. In the more aggressive 8585 condition, the test results showed a quick jump to the terminal chromaticity shift, which is best modeled with a generalized logistic function. In contrast, the lower acceleration factor of the 7575 test enabled another shift to be detected during the burn-in stage, and this shift can be best modeled with a bounded exponential function. The terminal chromaticity shift can be seen to begin around 2,000 hours. The same bounded behavior occurs with $\Delta v'$, which provides some consistency in the data, but the onset of the limiting $\Delta v'$ shift occurs roughly 3,000 hours later in 7575 than in 8585.

Figure 4D-35. $\Delta u'$ and $\Delta v'$ Data and Chromaticity Shift Models for Lithonia Security Lamp in 7575

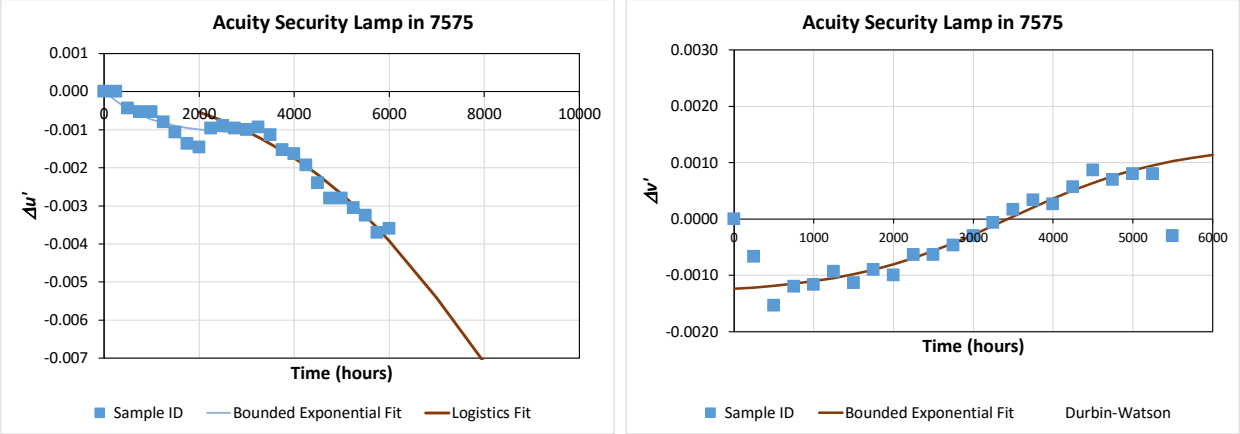

The generalized logistic models for the terminal chromaticity shift of the Lithonia Security Lamp product are given in **Table 4D-5**. A key finding from this analysis is that the chromaticity shift process is the same in 8585 and 7575, but the rates are different. This finding is supported by the fact that the models for the two test conditions have similar values for *C*, *A*, and the x-offset and y-offset. In particular, the values for the parameter *A* are very similar for each coordinate, indicating that the maximum shift of this chromaticity process is similar in both test conditions. However, the value for *k* is different for the two models, with the *k* value for 8585 testing being roughly 4.1x larger than that of 7575. The value of *k* in these models gives the rate of chromaticity change, and the ratio of the two can be thought of as the acceleration factor for 8585 relative to 7575 (i.e., chromaticity shift degradation is happening 4x faster in 8585 than in 7575 for this device).

Table 4D-5. Parameters for the Chromaticity Shift Models of Lithonia Security Lamp in 8585 and 7575

	k	C	A	X-Offset	Y-Offset	SSE	R^2	DW
$\Delta u'$ in 8585	1.68×10^{-3}	25.1	−0.018	0.00	0.0011	1.66×10^{-8}	0.996	0.976
$\Delta u'$ in 7575	4.06×10^{-4}	25.2	−0.018	751	0.0006	4.54×10^{-7}	0.976	1.056
$\Delta v'$ in 8585	3.41×10^{-3}	29.0	0.0020	0.00	−0.0001	3.11×10^{-7}	0.976	1.975
$\Delta v'$ in 7575	9.79×10^{-4}	29.0	0.0027	0.00	−0.0013	2.18×10^{-7}	0.965	2.052

DW = Durbin-Watson statistic.

The Cree Essentia downlight is an architectural specification-grade light fixture intended for use in high ceilings in both indoor and outdoor environments. The version of this product that was tested by RTI is shown in **Figure 4D-36**, and its properties are given in

Table 4D-3. Each LED is protected by a secondary lens that is housed in a metal plate, and the entire lens assembly is gasketed to the main housing to provide some level of moisture ingress protection. The device is operated by an external driver (Philips Advance Part Number: Xitanium LED-INTA-10000C-60-DB) connected to the LED board through the greenfield whip.

Figure 4D-36. Picture of Cree Essentia Luminaire Subjected to 8585 Testing by RTI

This device was tested only in the more aggressive 8585 environment, and two out of three samples were able to survive more than 4,000 hours under these conditions. One device failed at 2,000 hours and the driver was replaced, allowing the unit to continue being tested. At 4,000 hours of the aggressive 8585 test, the average lumen maintenance was 0.80, and the average chromaticity shift was 0.018. By comparison with the performance of the Lithonia Security Lamp and other results discussed below, this level of performance is excellent in the aggressive 8585 test that was conducted.

The chromaticity shift of the warm white LEDs in this product was dominant by a CSM-2 shift in the green direction. The models for $\Delta u'$ and $\Delta u'v'$ are shown in **Figure 4D-37.** The model for $\Delta v'$ is not shown for brevity, because the shift in this direction is minimal. The total chromaticity shift $(\Delta u'v')$ is dominated by $\Delta u'$, and a key finding from these experiments and the associated modeling is that the chromaticity shift in the $-\Delta u'$ direction is bounded with a limiting value of around -0.015 for $-\Delta u'$. A second key finding is that

there are potentially two different bounded chromaticity shift processes that can be modeled with generalized logistic functions. These two shifts can be seen to occur sequentially, and together they are responsible for the overall chromaticity shift. In a similar manner, this type of behavior has been overserved in some of our studies on individual LEDs (see Section 4.3 or [54]). On the basis of the observed spectral shifts shown in **Figure 4D-38**, the terminal chromaticity shift for this device in 8585 testing is a shift in the phosphor emission peak to lower wavelength, consistent with oxidation of the red nitride phosphor. This reaction has been shown to be primarily a surface process [30]. The mechanism for the second, smaller chromaticity shift that appears after the terminal shift has concluded is unknown, but it could be due to a secondary process such as oxidation of bulk phosphor dopant sites.

Figure 4D-37. Models of the Shift in *Δu′* and *Δu v′* for the Cree Essentia Downlight in 8585

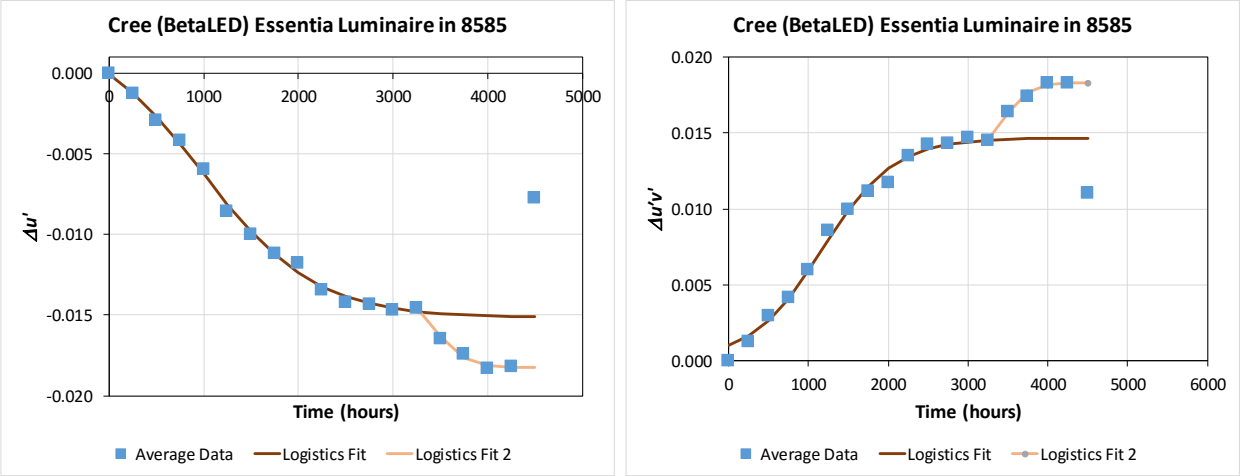

NOTE: The statistics for the first generalized logistic model for $\Delta u'$ are $R^2 = 0.997$, SSE = 1.07×10^{-6}, and Durbin-Watson statistic = 2.07, whereas those for first generalized logistic model for $\Delta u'v'$ are $R^2 = 0.993$, SSE = 2.84×10^{-6}, and Durbin-Watson statistic = 1.16.

Figure 4D-38. Radiant Flux Spectra Measured for the Same Cree Essentia Luminaires in 8585 Testing at Different Exposure Times

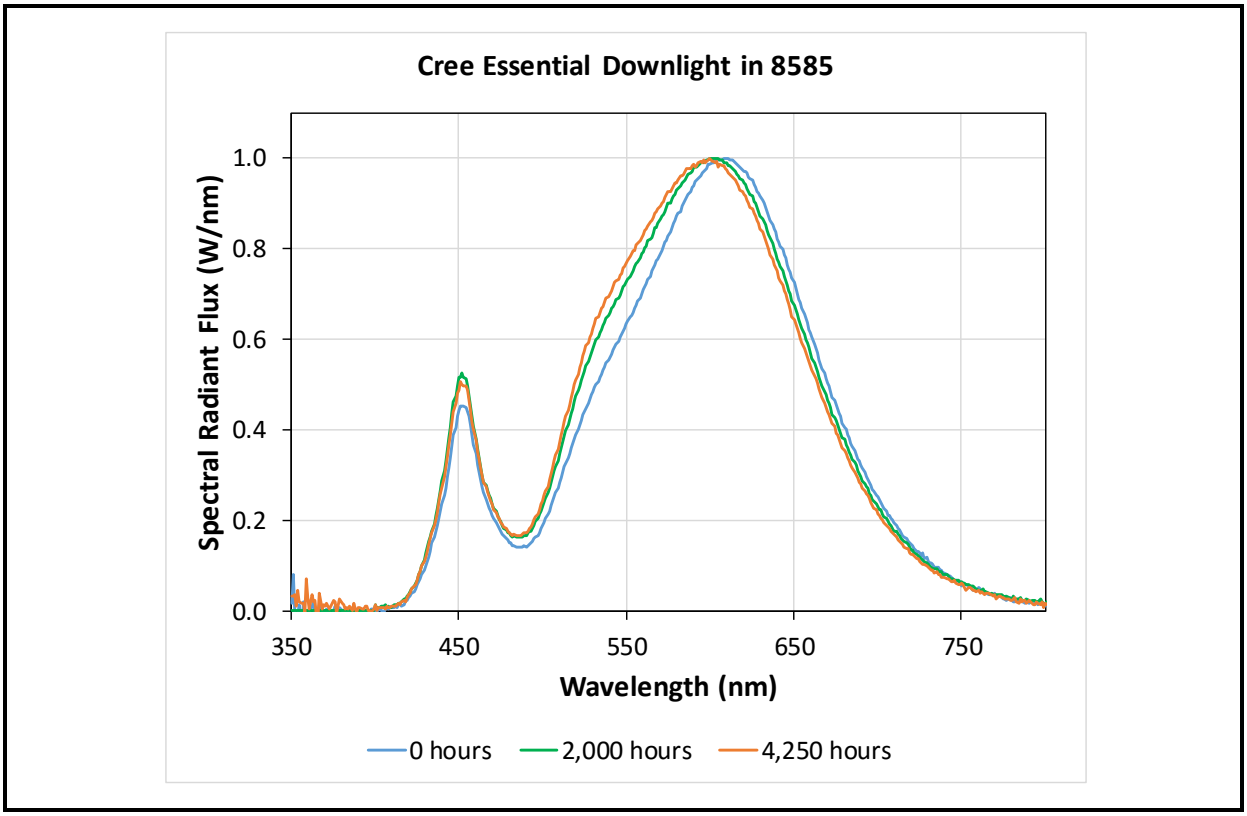

OptiLED Round150 6" Downlight Luminaire

The OptiLED Round150 is a 6" downlight primarily for the commercial market. This device was tested extensively during this project; both neutral white (CCT ~ 4000 K) and warm white (CCT ~ 2750 K) versions of the device were examined in 8585, 7575, and 6590. Although both CCT values of this device used the same integrated driver structure, the light engines of the two were quite different. As shown in **Figure 4D-39** and summarized in **Table 4D-**4, the neutral white light engine is comprised of 12 HP-LEDs (connected in series), whereas the warm white light engine consisted of 156 MP-LEDs (connected as 12 strings in series with 13 LEDs in parallel).

Four samples of each CCT value of the Round150 6" downlight were placed in 8585 testing. This luminaire did not fare well in the testing, with all of the samples exhibiting catastrophic failure in relatively short test times. Only one sample lasted for more than 1,000 hours in the test, with most failing before 750 hours of testing. The short lifetime of this product that was measured in 8585 was insufficient to collect meaningful information on lumen maintenance and chromaticity shift.

Figure 4D-39. Pictures of the Light Engines Used in the OptiLED 6" Downlight— Neutral White (Left) and Warm White (Right)

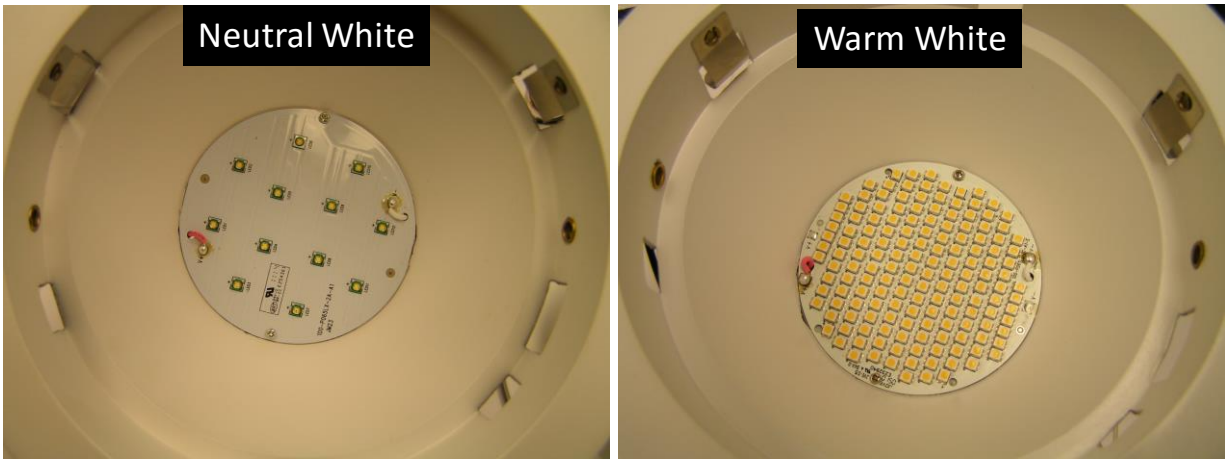

Ten samples (5 warm white and 5 cool white) were also tested in 7575, and the product performed much better in this environment, and only two samples (one warm white and one cool white) exhibited catastrophic failure. Most of the samples survived to the end of the test (3,000 hours); however, two of the warm white samples displayed a sharp reduction in luminous flex output at 2,000 hours.

As might be expected, the behaviors of the two CCTs populations were different from each other in the 7575 test. As shown in **Figure 4D-40**, the total chromaticity shift, as measured by $\Delta u'v'$, exhibits behavior that can be best modeled with a bounded exponential function. This type of behavior has an upper bound at $\Delta u'v' \sim 0.006$ for both neutral white and warm white products, which means that if this were the only chromaticity shift mechanism, then a device would not exceed the parametric threshold of $\Delta u'v' > 0.007$ for this test. However, at roughly 1,000 hours of 7575 exposure, a second chromaticity shift process appears (but only in the warm white LED), and this mechanism produces a continuous chromaticity shift in the green direction that ultimately results in a parametric failure.

Figure 4D-40. Chromaticity Shift Data and Associated Models for Total Chromaticity Shifts for Warm White OptiLED Round150 Luminaire (left) and Neutral White Luminaire (right)

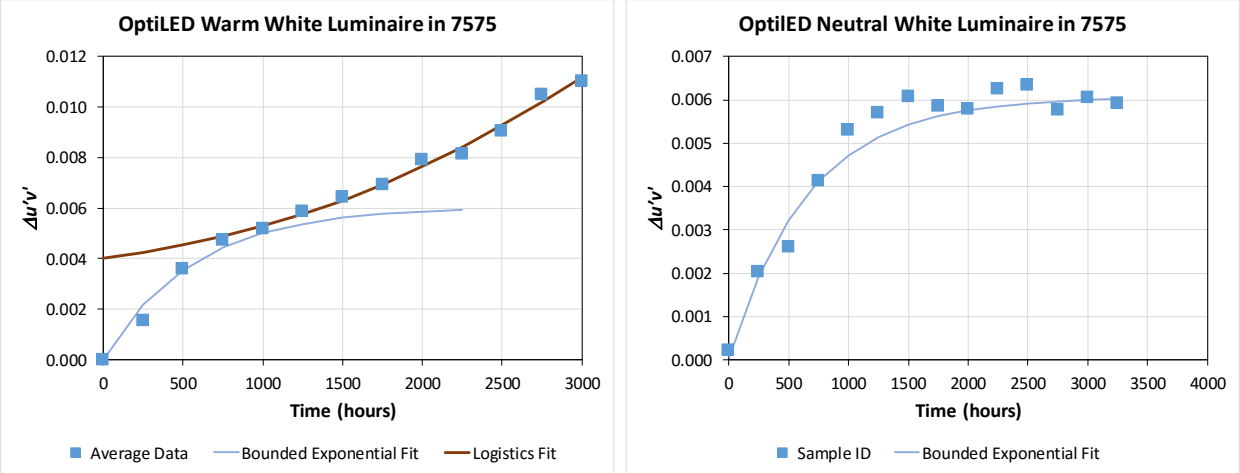

Note: The statistics for the generalized logistic model of warm white product are R^2 = 0.994, SSE = 3.30 x 10^{-7}, and Durbin-Watson statistic = 2.63, whereas those for the bounded exponential model of the neutral white product are R^2 = 0.959, SSE = 7.58 x 10^{-7}, and Durbin-Watson statistic = 1.08.

The nature of this shift can be determined by examining the change in the individual chromaticity coordinates, $\Delta u'$ and $\Delta v'$, for the warm white version of the OptiLED Round150. The experimental data and associated models for this product produced by this study are given in **Figure 4D-41**. Whereas the $\Delta v'$ component can be seen to reach a limiting shift at 0.0028 for the warm white product, the behavior of the $\Delta u'$ component is more complicated. Our model of the chromaticity change in the $\Delta u'$ component shows that two sequential mechanisms occur. First there is a mechanism that coincides with the $\Delta v'$ changes and can be modeled with a bounded exponential. Second, there is the terminal chromaticity shift, which begins around 1,000 hours and can be modeled with a generalized logistic function. Consequently, the chromaticity can be seen to shift in the greenish yellow direction for the first 1,000 hours, followed by a prolonged shift in the green direction (i.e., $\Delta u'$ is negative and $\Delta v'$ changes little during this time). This model provides a clear indication that the terminal chromaticity shift is a CSM-2 shift.

In contrast with the behavior with the warm white sample, the chromaticity shift of the neutral white version of the OptiLED Round150 luminaire is driven entirely by the $\Delta v'$ component. The models and associated data for the neutral white product are given in **Figure 4D-42**. The chromaticity shift is in the yellow direction (i.e., $\Delta v'$ is positive and $\Delta u'$ changes little), in contrast to the behavior found for the warm white product. This finding once again illustrates the difference in stability of the phosphors used in cool white LEDs compared with that of the warm white phosphors and the factor that LED package plays a role in chromaticity shift.

Figure 4D-41. Chromaticity Shift Data (*Δu′* and *Δv′*) and Associated Models for the Warm White Version of the OptiLED Round150 Product

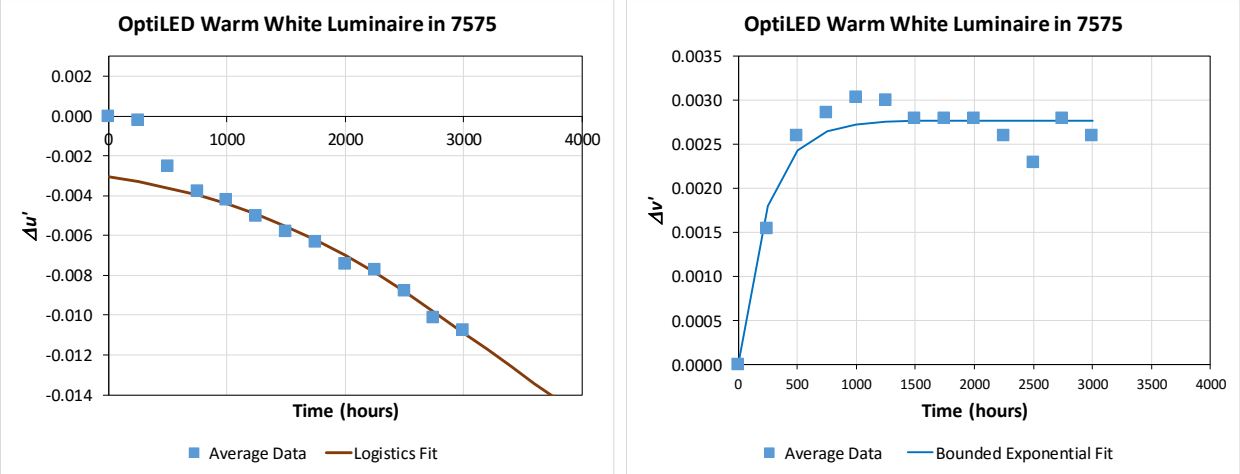

Note: The statistics for the generalized logistic mode of $\Delta u'$ are R^2 = 0.994, SSE = 4.48 x 10^{-7}, and Durbin-Watson statistic = 1.83, whereas those for the bounded exponential model of the $\Delta v'$ component are R^2 = 0.930, SSE = 5.79 x 10^{-7}, and Durbin-Watson statistic = 1.26.

Figure 4D-42. Chromaticity Shift Data (*Δu′* and *Δv′*) and Associated Models for the Neutral White Version of the OptiLED Round150 Product

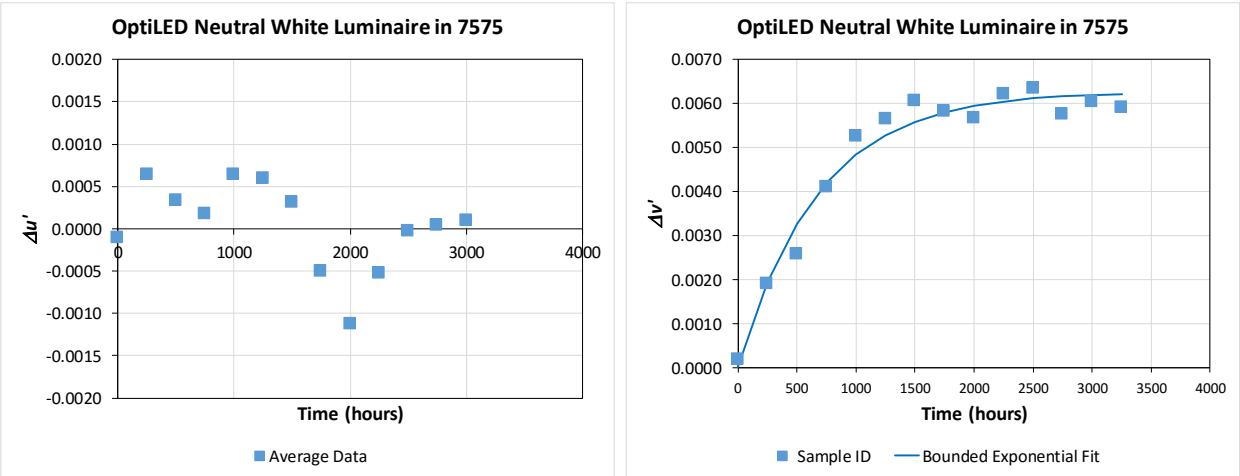

Note: The statistics for the bounded exponential model of the $\Delta v'$ component are R^2 = 0.968, SSE = 1.49 x 10^{-6}, and Durbin-Watson statistic = 1.41.

The behavior of these luminaires in 6590 was similar to that in 7575, but the catastrophic failure rate was higher. Of the 10 samples in 6590 testing, 6 failed in fewer than 2,250 hours of testing. The failure rate was highest for the neutral white luminaires (4 of 5 catastrophic failures). The chromaticity shift ($\Delta u'v'$) data and associated models for the 6590 samples are shown in **Figure 4D-43** and can be seen to be similar to those of the same products in 7575, although the rate of the terminal chromaticity shift was 1.75x higher (k = 8.20 x 10^{-4} in 7575 and k = 4.6 x 10^{-4} in 6590) in 7575 than in 6590. Thus, although 6590

produced higher catastrophic failure rates in the electronics than did 7575, the impact of the LEDs and the photopic properties of the luminaires was less in 6590.

Figure 4D-43. Total Chromaticity Shift Data and Associated Models for Chromaticity Shifts for Warm White OptiLED Round150 Luminaire (left) and Neutral White Luminaire (right)

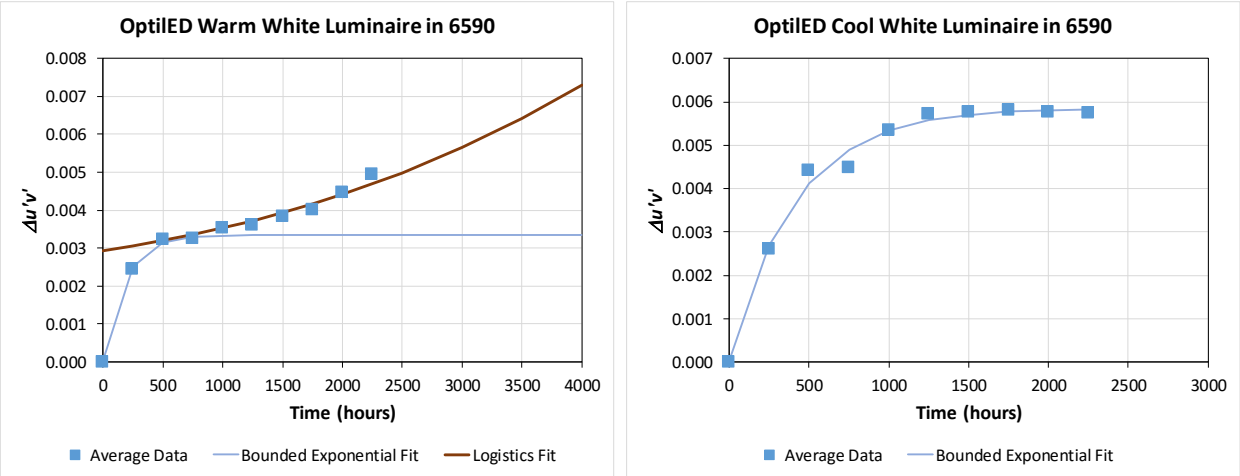

Note: The statistics for the generalized logistic model of warm white product are R^2 = 0.997, SSE = 1.27 x 10^{-7}, and Durbin-Watson statistic = 9.95, whereas those for the bounded exponential model of the neutral white product behavior are R^2 = 0.991, SSE = 3.02 x 10^{-7}, and Durbin-Watson statistic = 2.80.

LSG Glimpse Indirect 6" Downlight Luminaire

The LSG Glimpse Indirect downlight was one of the downlights that was tested the longest in WHTOL, having been tested for 7,000 hours in 7575. The downlight was found to perform well in WHTOL, with all samples surviving 6,000 hours of 7575 and two devices still operating after 7,000 hours of testing in 7575. In addition, the average lumen maintenance of this device was 0.83 after 6,000 hours of 7575 testing, suggesting excellent luminous flux maintenance performance. The Glimpse Indirect luminaires use the output of 32 MP-LEDs projected onto a diffuse reflecting dome to produce white light through an aperture in the house. A picture of the device and the associated LED board is shown in **Figure 4D-**44, and additional characteristics are listed in Table 4D-4.

Figure 4D-44. Picture of the LSG Glimpse Indirect Luminaire (left) and Its LED Board (right)

The overall chromaticity shift for the LSG Glimpse lamp in 7575 is in the red direction; the data and associated models are shown in **Figure 4D-45**. The chromaticity shift can be deconvoluted into two sequential shift mechanisms. The first shift is a rapid change in chromaticity when the luminaire is first turned on. The first shift mechanism produces a two-step change in chromaticity ($\Delta u'v'$ = 0.002), and this process is best modeled with a bounded exponential function. As will be shown later, this shift is mainly in the yellow direction ($\Delta v' > \Delta u'$). Eventually, a second chromaticity shift mechanism appears and enters the emergent stage at around 2,000 hours of 7575 exposure. This shift mechanism produces a steady increase in chromaticity, resulting in the $\Delta u'v'$ threshold being exceeded at around 5,000 hours. As discussed above, this shift can be modeled with a logistic function with parameters of A = 0.031, k = 5.34 x 10-4, and C = 29.58.

Figure 4D-45. Average Chromaticity Shift ($\Delta u'v'$) of the LSG Glimpse Indirect Lamps During 7575

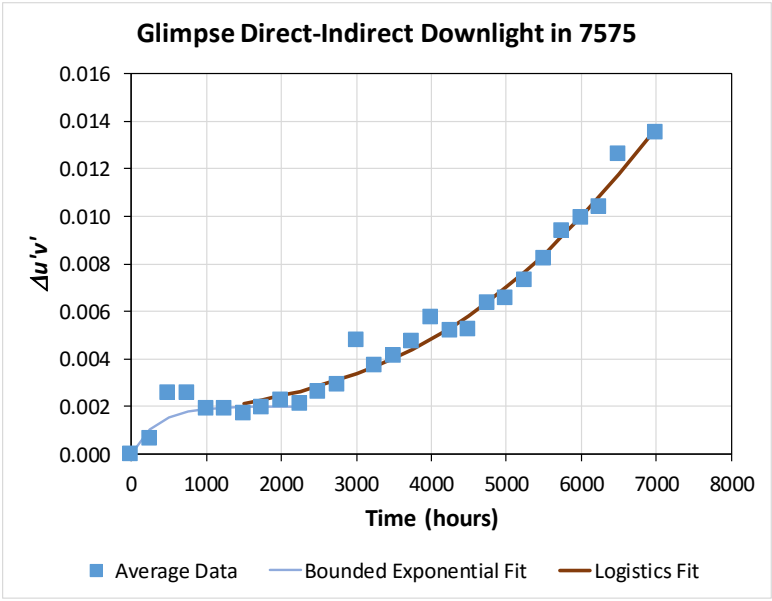

Note: The statistics for the bounded exponent model of $\Delta u'v'$ for the first 2,000 hours are R^2 = 0.963, SSE = 1.99 x 10^{-6}, and Durbin-Watson statistic = 1.44, whereas those for generalized logistic of $\Delta u'v'$ for after 2,000 hours are R^2 = 0.965, SSE = 5.07 x 10^{-6}, and Durbin-Watson statistic = 1.52.

By leveraging the $\Delta u'v'$ model as the starting point, models can be built for the individual chromaticity coordinates, and these models are shown in **Figure 4D-46**. Both $\Delta u'$ and $\Delta v'$ can be seen to be shifting by similar positive amounts, which is indicative of a red shift and CSM-5 behavior. The coefficients for these three models are summarized in **Table 4D-6**.

Table 4D-6. Coefficients for the Generalized Logistic Models of the Chromaticity Coordinates of the LSG Glimpse Indirect Luminaire

Coordinate	*k*	C	A	X-Offset	Y-Offset
$\Delta u'v'$	5.34 x 10^{-4}	29.6	0.0306	1,300	0.0010
$\Delta u'$	4.28 x 10^{-4}	27.2	0.0250	0	−0.0013
$\Delta v'$	4.85 x 10^{-4}	21.8	0.0196	1,050	0.0008

Figure 4D-46. Average Change in $\Delta u'$ and $\Delta v'$ for the LSG Glimpse Indirect Luminaire During 7575

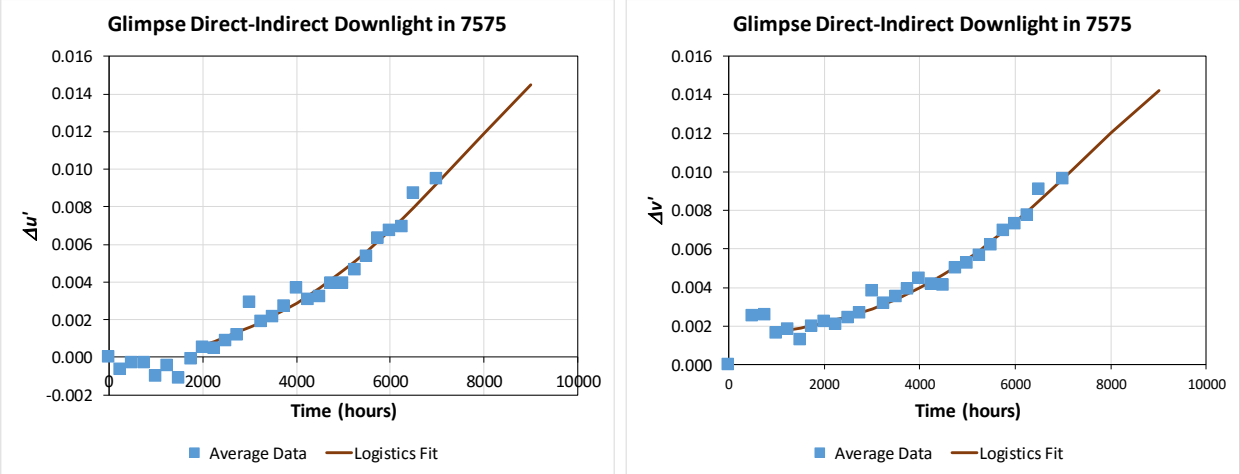

Note: The statistics for the generalized logistic model of $\Delta u'$ component are R^2 = 0.972, SSE = 4.51 x 10^{-6}, and Durbin-Watson statistic = 1.74, whereas those for the generalized logistic model of $\Delta v'$ component are R^2 = 0.982, SSE = 2.44 x 10^{-6}, and Durbin-Watson statistic = 1.82.

The SPD observed for the LSG Glimpse Indirect product is shown in **Figure 4D-47** for the initial measurement, after 4,000 hours of exposure to 7575, and after termination of the experiment after 7,000 hours of 7575 exposure. The same spectra normalized to the phosphor emission maximum is shown in **Figure 4D-48**. The radiant flux SPD intensity for the LSG Glimpse Indirect luminaire decreases over time, and **Figure 4D-48** demonstrates that this decrease is proportionately higher over the wavelength range of 475 nm to 600 nm than in other parts of the spectra. In addition, the SPD remained relative constant above 600 nm, and no new peaks appeared in this region of the spectrum. This finding indicates that the observed red shift is due to a loss of a portion of the green emissions relative to the starting point, not to the emergence of new red emitters. Because a reduction in green emissions relative to red produces a red shift, the observed spectral changes are consistent with the observed red shift found in the chromaticity coordinates.

Figure 4D-47. SPD of DUT-B Equipped With Warm White MP-LEDs as Initially Recorded and After 4,000 and 7,000 Hours of Exposure to 7575

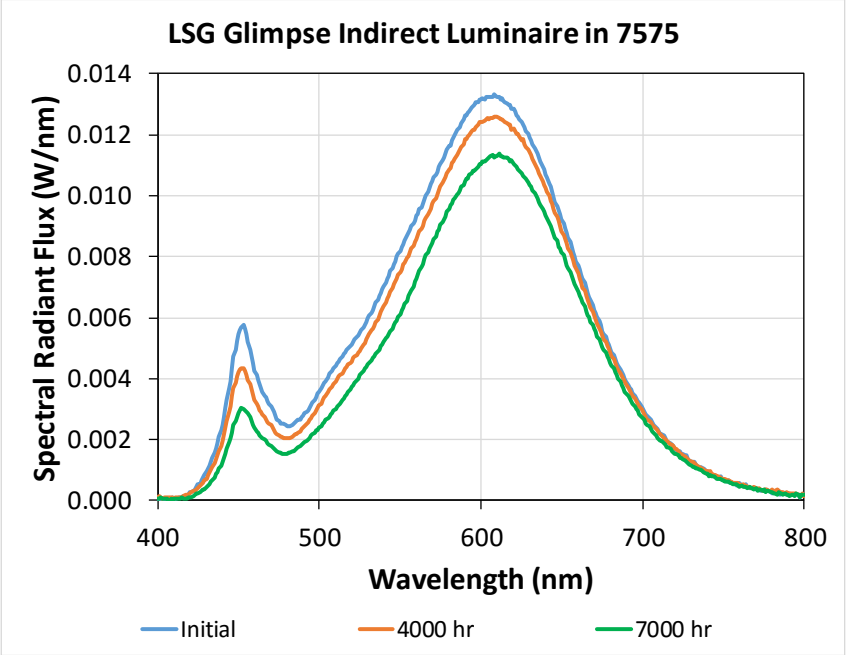

Figure 4D-48. SPD Normalized to the Phosphor Emission Maximum for Both the Initial Measurement of DUT-B and After 4,000 and 7,000 Hours of Exposure to 7575

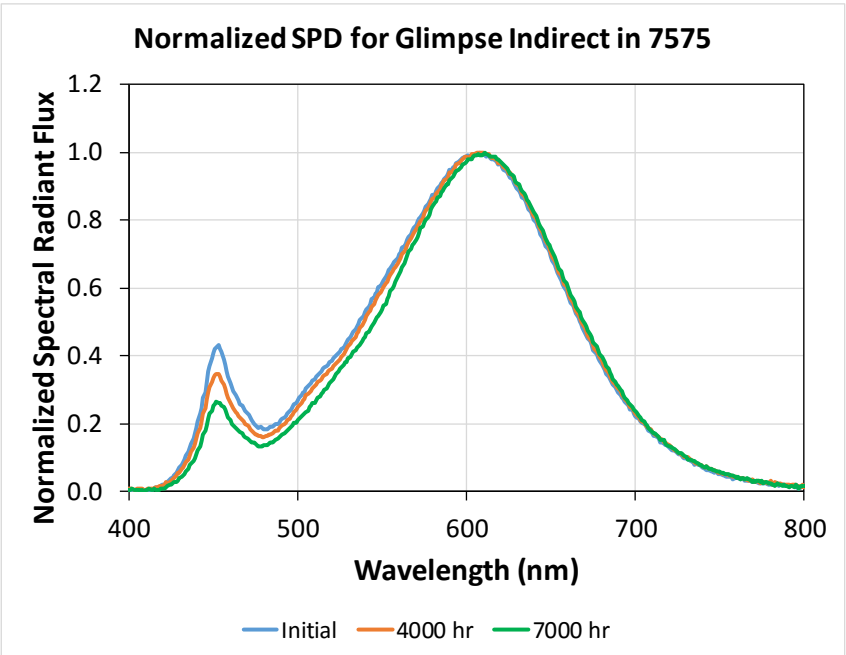

Commercial Electric T-65 Downlight

The Commercial Electric T-65 downlight, a house-branded downlight device available from a big-box retailer, is intended for residential use. The downlight is designed and manufactured by Cordelia Lighting but privately branded as Commercial Electric. The device is pictured in **Figure 4D-49**, and additional properties are listed in Table 4D-4. Different populations of the Commercial Electric T-65 product were examined in this study at all three WHTOL settings. As can be expected, the catastrophic failure rate was highest in 8585, with all failures assigned to the driver. More information on the catastrophic failures will be discussed in the next section. However, there were no parametric failures in 8585, possibly due to the short test time. Catastrophic driver failure was less of an issue in 7575, but it did happen on occasion, usually after more than 2,000 hours of exposure. It was not unusual for this luminaire to survive for more than 4,000 hours in 7575 testing, although luminous flux maintenance typically fell below the 70% threshold for such long test times. The 6590 test was performed for only 2,250 hours and no catastrophic failures were found with the device.

Figure 4D-49. Picture of the Commercial Electric T-65 6" Luminaire With the Front Lens Removed

An outcome for exposure in 7575 is a physical darkening of the LEDs as testing progressed. A closer of the effect by Auburn University determined that the metal leadframe that is LED is attached to is not completely covered by resin during the overmolding operation. Instead, parts of the leadframe remain exposed after LED assembly. During WHTOL, the exposed lead begins to react with moisture and becomes dark. This chemical change will have adverse impacts on both lumen maintenance and chromaticity stability.

A comparison of the total chromaticity change of the Commercial Electric T-65 luminaire under the three WHTOL test conditions is shown in **Figure 4D-50**. In 8585, the total chromaticity shift rises to a maximum value in 1,000 hours. This increase is produced by a decrease in both the u' and v' coordinates, indicative of a blue shift. After a short stabilization period, the total chromaticity shifts begin to decrease after 1,500 hours in 8585, but this change is not observed during the testing period for either 7575 or 6590. The total chromaticity shift decrease is driven by an increase in both the u' and v' coordinates. As discussed previously, $\Delta u'v'$ is a measure of the Euclidean distance from the starting point. So, when u' and v' first shift away from the initial chromaticity point and then shift back toward it, the total chromaticity shift will increase and then begin to decrease until the point of closest approach to the initial chromaticity occurs. After that point, the total chromaticity shift will begin to increase again. Unfortunately, the 8585 exposure experiments could not be run long enough to see the full cycle of the chromaticity shift because of driver failures in the aggressive 8585 environment. Although the chromaticity shift processes occurring with the Commercial Electric T-65 lamp could be modeled with a combination of bounded exponential and generalized logistic functions, no attempt has been made to do so because of the limited 8585 data set.

Figure 4D-50. Comparison of the Chromaticity Change, as Measured by $\Delta u'v'$, for the Commercial Electric T-65 Luminaire in Various WHTOL Tests

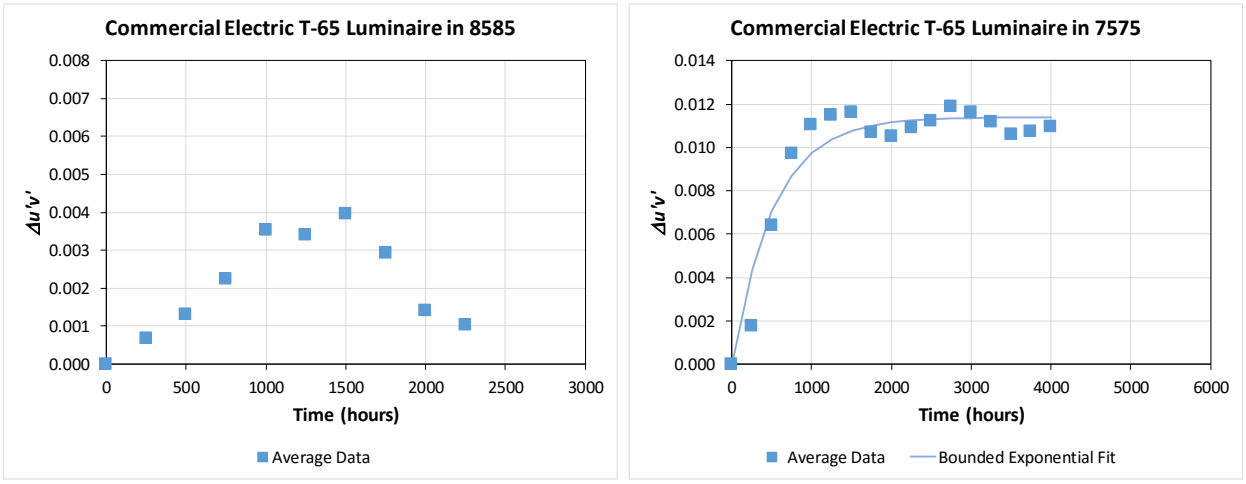

(continued)

Figure 4D-50. Comparison of the Chromaticity Change, as Measured by $\Delta u'v'$, for the Commercial Electric T-65 Luminaire in Various WHTOL Tests (continued)

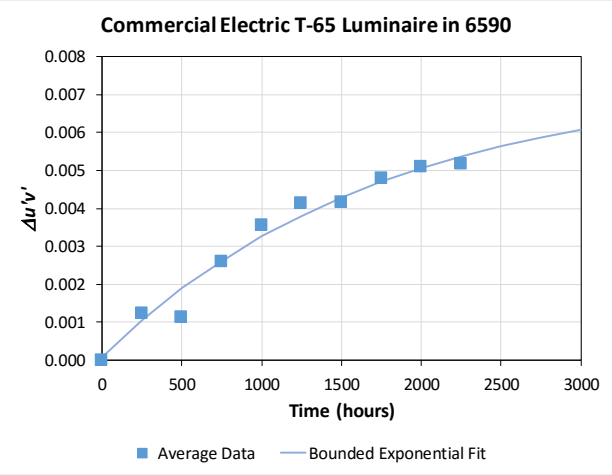

As shown in **Figure 4D-50**, the total chromaticity shift of the Commercial Electric T-65 luminaires in 7575 can be modeled with a bounded exponential with an asymptotic limit of $\Delta u'v'$ = 0.0114. Breaking this shift into its constituents, **Figure 4D-51** shows that both $\Delta u'$ and $\Delta v'$ shift in the negative direction, with the $\Delta v'$ shift having a larger asymptotic value. Similar behavior was also observed in 6590, as shown in **Figure 4D-52**, except that the rate was slower. This chromaticity shift process is attributed to the oxidation of the exposed metal lead frame which resulted in the absorption of light are high wavelengths. A comparison of the least-squares fit coefficients for the chromaticity shift models of the Commercial Electric T-65 mode is given in **Table 4D-7**. When we compared the *k*-values for $\Delta u'v'$ in 7575 and 6590, the 7575 test was found to have an acceleration factor of 3.4 over the 6590 test.

Figure 4D-51. Data and Associated Models for $\Delta u'$ and $\Delta v'$ of a Population of Commercial Electric T-65 6" Downlights Exposed to the 7575 Environment

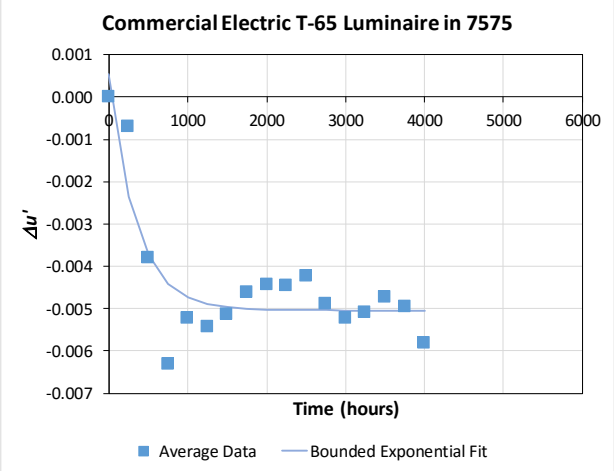

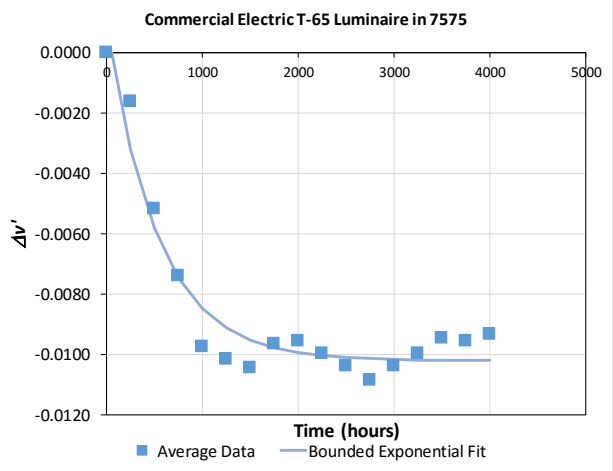

Figure 4D-52. Data and Associated Models for $\Delta u'$ and $\Delta v'$ of a Population of Commercial Electric T-65 6" Downlights Exposed to the 6590 Environment

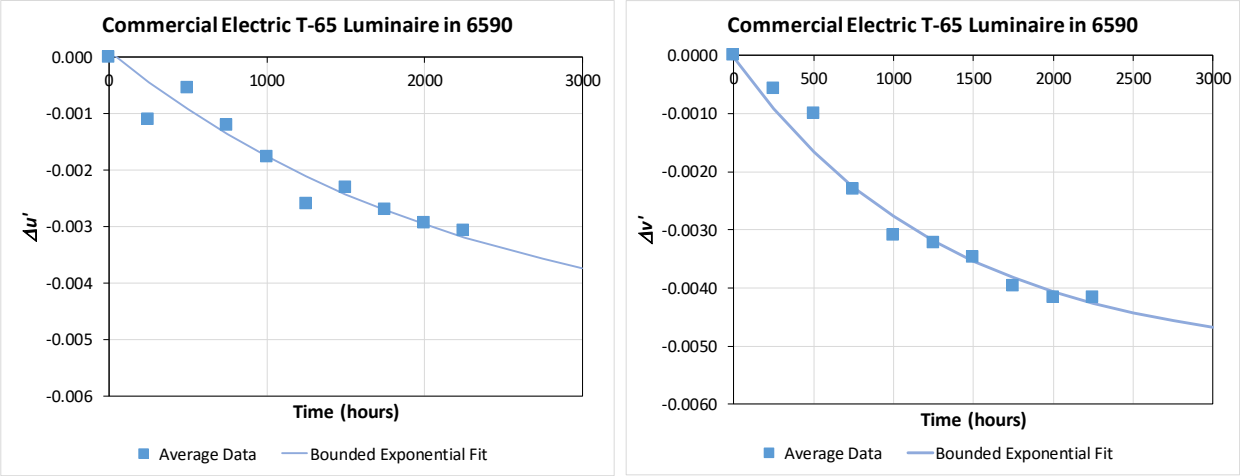

Table 4D-7. Least-Squares Fit Coefficients of Bounded Exponential Models From the Chromaticity Shift of the Commercial Electric T-65 Population

Shift Component	*k*	A	C	SSE	R^2	Durbin-Watson
$\Delta u'$ in 7575	2.92×10^{-3}	−0.0056	0.0005	9.38×10^{-6}	0.782	1.602
$\Delta v'$ in 7575	1.86×10^{-3}	−0.0112	0.0009	9.98×10^{-6}	0.939	1.190
$\Delta u'v'$ in 7575	1.93×10^{-3}	0.0114	0.00	1.43×10^{-6}	0.925	1.153
$\Delta u'$ in 6590	4.42×10^{-4}	−0.0052	0.0001	1.93×10^{-3}	0.912	2.368
$\Delta v'$ in 6590	7.46×10^{-4}	−0.0052	0.00	7.14×10^{-7}	0.967	1.312
$\Delta u'v'$ in 6590	5.71×10^{-4}	0.0073	0.0001	8.96×10^{-7}	0.971	2.168

4.D.7 Organic Light Emitting Diodes (OLEDs)

OLEDs are an emerging class of lighting devices. Upon the guidance of DOE, RTI performed AST and failure analysis of the leading commercial OLED luminaire, the Acuity Chalina. A report on this analysis was jointly written with PNNL and is available on the DOE web site and should be consulted for full details on the testing [95].

The Acuity Chalina luminaire is available by mail order from a big-box retailer. One of the best-selling OLED luminaires, it incorporates the latest OLED panel technology and provides a good benchmark of the status of this technology. The device is pictured in **Figure 4D-53**.

Figure 4D-53. Picture of the Acuity Chalina OLED Luminaire (left) and an Individual OLED Panel With Light Diffuser Film Applied to the Top Surface (right)

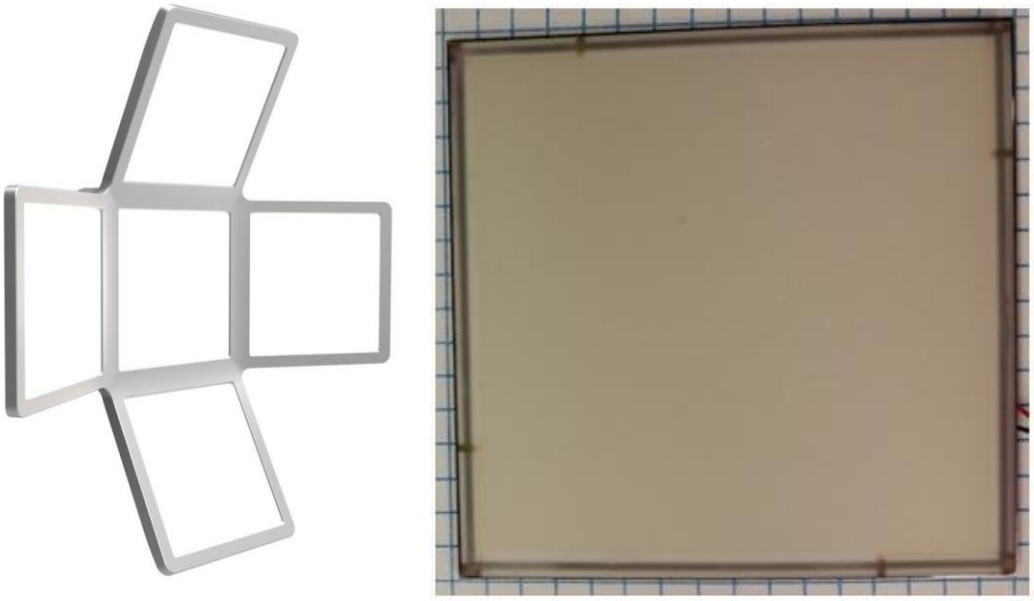

Testing was performed on both entire luminaires, which consist of five 10 cm-by-10 cm OLED panels and a driver, and individual panels (dimensions of 10 cm x 10 cm) operated by an external power supply. Four AST protocols have been used to date:

1. 45°C bake of luminaires operated at 150 mA
2. 75°C bake of individual panels operated at 150 mA
3. Exposure of luminaires to 75°C and 75% relative humidity (75/75) while operating at 150 mA
4. High current (200 mA) operation of an OLED panel in 45°C bake

The 45°C elevated ambient was chosen as an AST protocol because of its use in previous CALiPER testing of LED products. Thus, performance in this test environment can provide some comparison to the performance of conventional LED products from the 2012 to 2013 time frame. Consequently, updating the 45°C elevated ambient test will be the focus of this briefing. Additional AST protocols were chosen to examine the behavior of the devices under higher stress levels, and further details on the findings from this analysis are given in the CALiPER 24 report [95].

For simplicity, all DUTs were operated continuously during the 45°C elevated ambient test. In addition, equivalent samples were operated at room temperature as controls. The light engines of whole luminaires were exposed to elevated ambient conditions of 45°C, but the drivers were placed outside the AST chambers. The luminaire light engines were mounted on riser brackets to allow air contact on the majority of the luminaire surfaces while baking, as shown in **Figure 4D-54**.

Figure 4D-54. Picture of Two Acuity Chalina OLED Luminaires in Elevated Ambient Temperature Bake Test of 45°C

Notes: The device drivers were placed outside of the chamber. One OLED panel on the bottom luminaire DUT is not functioning.

After completion of each AST cycle, photometric measurements were performed on each DUT in a calibrated 65” integrating sphere, and photometric properties such as luminous flux, SPD, and chromaticity were recorded at regular intervals. In addition, electrical properties of the individual panels were checked with an Agilent handheld LCR meter (Model U1733).

Four OLED luminaires (DUTs 224–227) were tested in the 45°C bake for more than 6,000 hours. One luminaire (DUT 224) exhibited the complete failure of one panel between 125 and 250 hours of testing, as shown in Figure 4D-54. The loss of this panel resulted in a reduction of power consumption, as shown in **Figure 4D-55**. However, the device

continued to produce illumination, albeit at a reduced level, suggesting that the nonoperable panel failed as an electrical short circuit. This was later confirmed in subsequent testing.

Figure 4D-55. Power Consumption of the Control Luminaire and Four DUTs (#224, #225, #226, and #227) Subjected to Elevated Ambient Conditions of 45°C for Extended Periods of Time

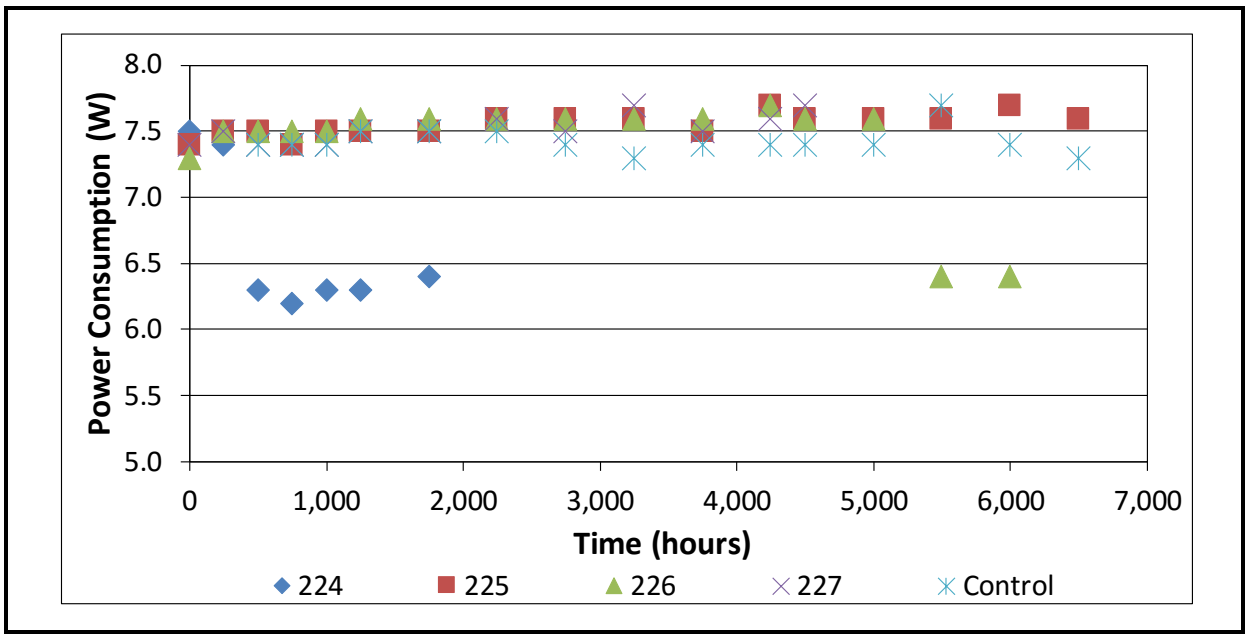

DUT #224 remained in testing until it exhibited abrupt failure sometime between 1,750 and 2,250 hours. The abrupt failure of the driver was traced to the MOSFET that serves as the power switch in the SMPS driver. Because the driver for this luminaire was outside the chamber, it was subject to milder conditions than the luminaires were, so failure was not caused by the direct impact of the elevated ambient temperature on the driver. Further examination of DUT #224 revealed that a second OLED panel had stopped working between 1,750 and 2,250 hours of testing. It is unknown whether the driver failure was due to the loss of two OLED panels and the change in the electrical load experienced by the driver or to a latent defect in the MOSFET or other circuit components.

DUT #226 also experienced a panel failure between 5,000 and 5,500 hours. It was put through an additional bake cycle and did not change between the last two measurements. One luminaire, DUT #225, remains in testing.

As part of the characterization of the OLED luminaires, the impedance of the five panels in the control luminaire was compared with that of the 18 operating panels from DUTs 224–227. The impedance of each panel was measured at three frequencies—100 Hz, 1,000 Hz, and 10,000 Hz—as shown in **Table 4D-8**. A close inspection of the data reveals several

main trends. First, the impedance of the failed panels is much lower than that of the operational panels, indicating the presence of an electrical short in the panel. This was confirmed by a visual inspection of the panels, where a dark spot on the OLED can be observed. Second, the mean impedance of the panels from luminaires subjected to the 45°C elevated ambient is higher than that of the control sample at all measured frequencies, and this difference was found to be statistically significant using the t-test. Third, the measured standard deviations of the DUTs subjected to the 45°C elevated ambient is larger than the control. This last observation indicates an increase in variation in panel impedance for the DUTs subjected to the elevated ambient, which is consistent with aging of the DUTs. The finding that these panels fail as electrical shorts explains why the device still operated with two panels not functioning.

Table 4D-8. Average Impedance of Individual OLED Panels From the Control Luminaires, Fully Operational Panels from 45°C Tests, and Failed Panels from 45°C Tests

Frequency	100 Hertz	1000 Hertz	10,000 Hertz
Panels from control	2,375 ± 10 ohms	248 ± 1 ohms	25.9 ± 0.1 ohms
Operational panels from 45°C bake	2,579 ± 48 ohms	272 ± 6 ohms	28.1 ± 0.6 ohms
Failed panel #1 from 45°C bake	7.1 ohms	7.1 ohms	6.8 ohms
Failed panel #2 from 45°C bake	3.3 ohms	3.3 ohms	3.3 ohms

Note: The report uncertainties represent one standard deviation.

Through 6,500 hours of exposure to 45°C, the average luminous flux maintenance of three luminaires (DUTs 225–227) had decreased to below 85%. **Figure 4D-56** shows that this decrease occurred steadily over time, with a calculated decay rate constant of 3.28×10^{-5}. DUT #227 has been exposed for only 4,500 hours, however, and is not in the averages after this. DUT #226 was removed at 5,500 hours because of a panel failure.

Figure 4D-56. Luminous Flux Maintenance of Commercial OLED Products in an Elevated Ambient Environment of 45°C

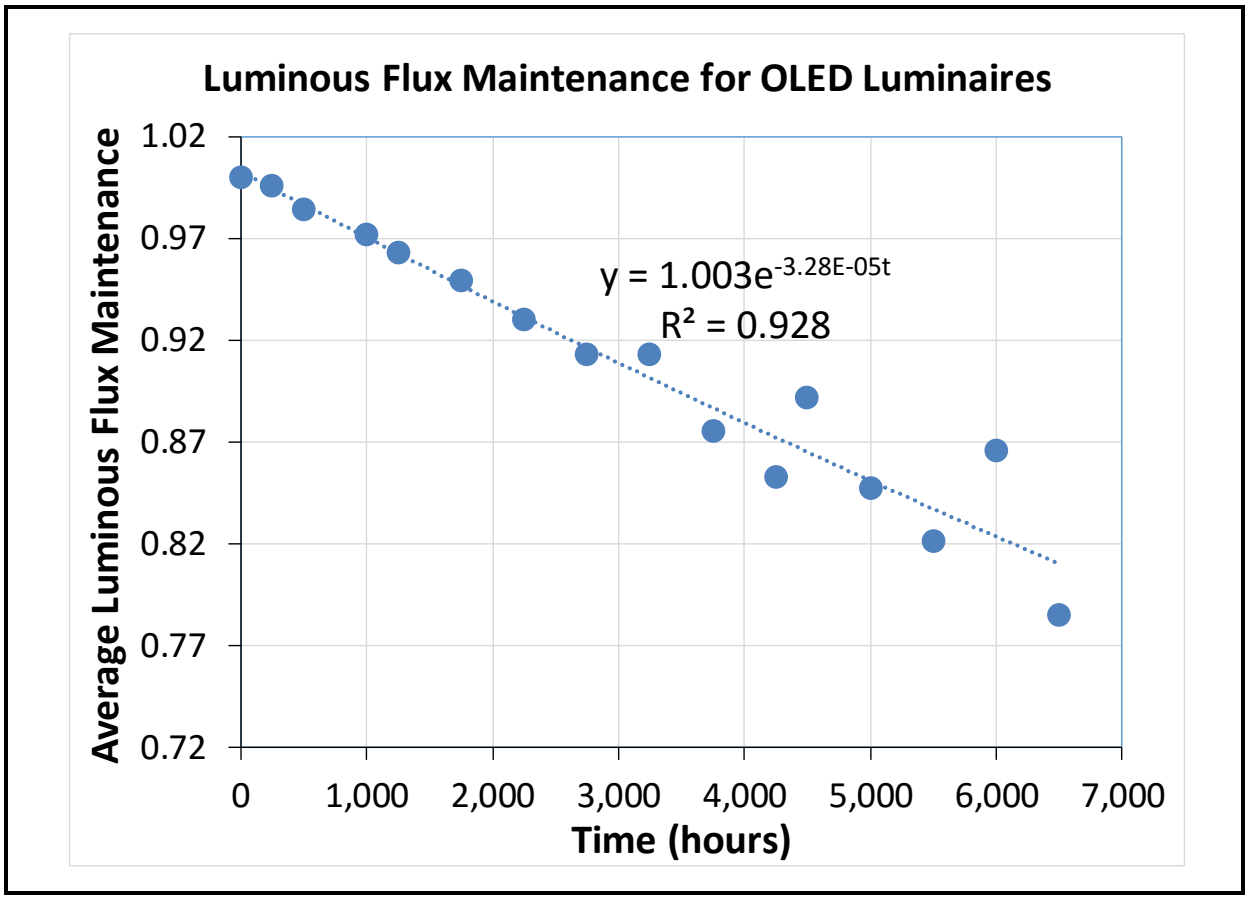

Chromaticity shift in the OLED luminaires during the 45°C AST is proceeding in the blue direction with both u' and v' decreasing at approximately a linear rate, as shown in **Figure 4D-57**. This behavior is analogous to the CSM-1 behavior that was observed for PAR38 lamps containing inorganic LEDs [27]. A representative SPD from DUT #226 is given in **Figure 4D-58**, and similar measurements were made for the other DUTs. The observed chromaticity shift can be explained by a reduction in emission from red and green sources while the blue emitter remains roughly constant. The lower stability of the red and green emitters is characteristic of phosphorescent sources, which have higher initial efficiencies but lower stability than fluorescent emitters. In contrast, the higher stability of the blue source suggests that it is a fluorescent emitter.

Figure 4D-57. Graph of *Δv'* vs. *Δu'* for OLED Luminaires Subjected to Elevated Ambient Conditions of 45°C

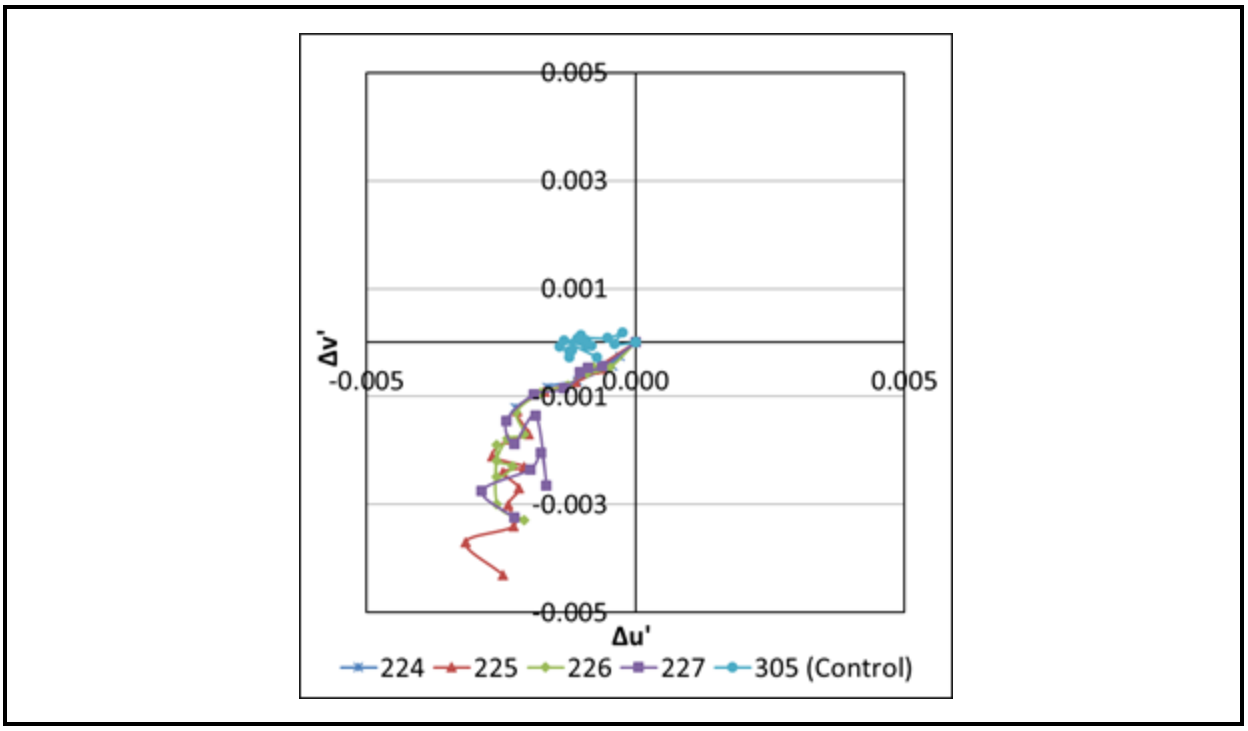

Figure 4D-58. SPD Measurements for DUT 226 at Different Stages of Elevated Ambient Exposure at 45°C

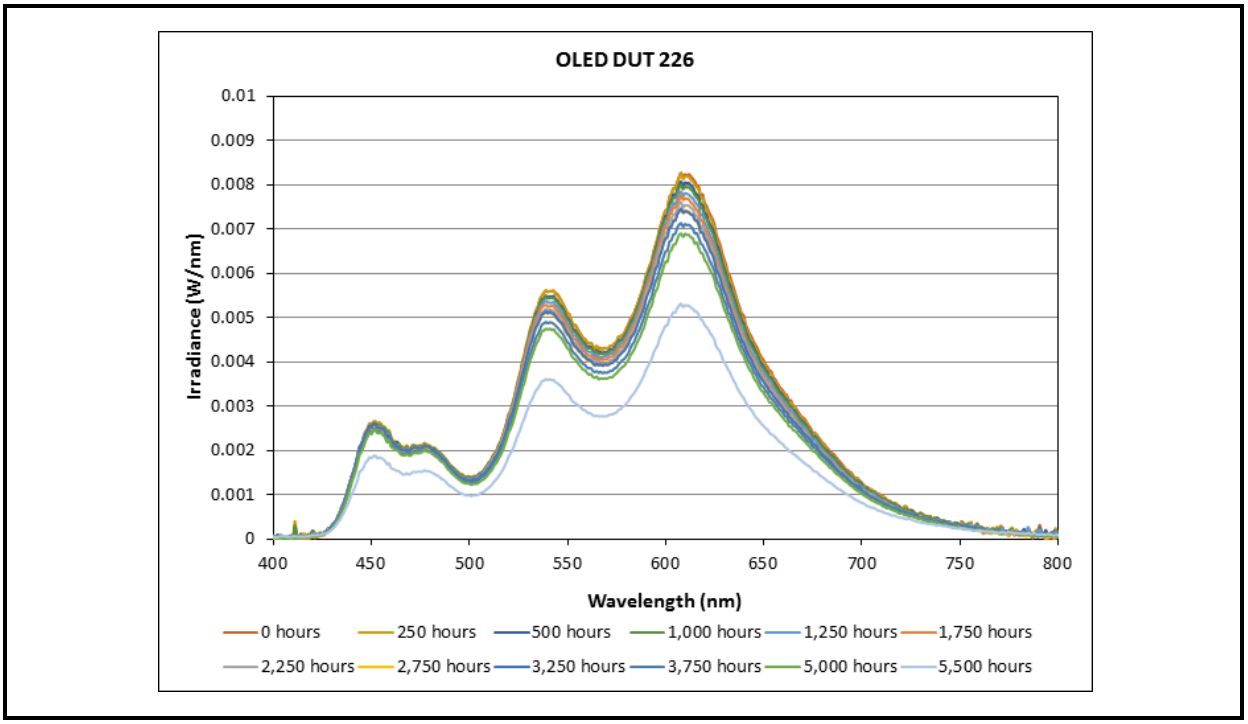

4.D.8 Luminaire Driver Behavior

So far, the focus of this report has been primarily on parametric failures due to excessive luminous flux loss or chromaticity shift. This is due in part to the fact that SSL devices may be expected to survive longer in the field than conventional lighting technologies, so greater emphasis has been placed on building models for parametric failures in this report. Catastrophic failures of LEDs have been found to be rare even under extreme circumstances [37], and we have conducted more than 25 million cumulative hours of testing, with minimal catastrophic failures found in LEDs.

In addition to parametric failures, SSL devices can also undergo catastrophic failure (also called abrupt failure), in which a device produces little to no light at all. This situation is analogous to a blown filament with an incandescent light bulb. Due to the similarity in construction and purpose, comparisons can be drawn between the reliability of general power supplies (e.g., for computers) and the expected behavior of SSL devices. A survey of the general power electronics industry found that the most likely failure sites on power electronics were the power handling semiconductor devices (e.g., switching transistors and power diodes). These devices were listed by 31% of the respondents, while capacitors (17%) and gate drivers (15%) were judged to be the next most fragile [96]. This same study also identified three roughly equally likely causes of failure in power electronic devices: environment, transients, and overload.

The LED Systems Reliability Consortium (LSRC) was formed by DOE and the Next-Generation Lighting Industry Alliance (NGLIA) to provide an industry perspective on the reliability of SSL devices. As part of its work, the LSRC published a document for the industry that provided information on likely failure modes in SSL luminaires. This information, summarized in **Figure 4D-59**, is based on the findings from one manufacturer (Appalachian Lighting Systems) and covers 212 million operational hours [97]. This data, combined with data from the power supply industry survey, provides clear evidence that the reliability of SSL drivers is a potentially limiting factor in the overall device lifetime. To study the reliability of potentially long-lived LED drivers, the LSRC has recommended the use of accelerated testing protocols to reduce test times to manageable lengths [97]. Fortunately, we were able to utilize the same AST protocols to study both changes in luminous flux and chromaticity and to investigate the reliability and robustness of electronic drivers powering these devices. Unfortunately, project the reliability of LED drivers is very complicated since each luminaire seemingly has a different driver design with different characteristics.

Figure 4D-59. Locations of Catastrophic Failure in SSL Luminaires

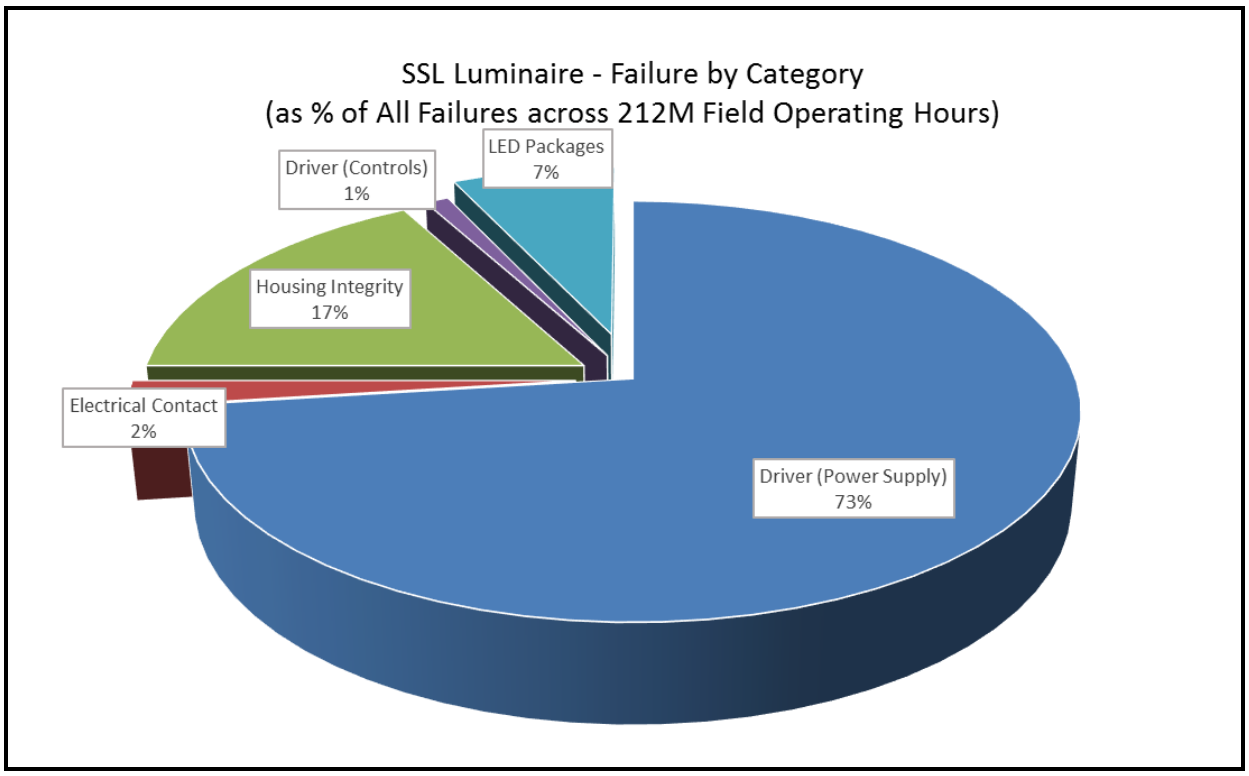

NOTE: Information is based on 212 million operating hours for luminaires and was provided to the LSRC by Appalachian Lighting Systems, Inc. Source: Reference [97].

Common Driver Circuits

The function of the electronic driver used in LED lighting devices is to provide consistent electrical power to the LEDs in the device. Typically, an alternating current (AC) source serves as the electrical power source (i.e., mains) and provides the input energy for the device, although drivers with direct current (DC) mains can also be found. Within the driver, the mains voltage is converted to a regulated output that is set to either a constant current or a constant voltage. Constant current drivers are the most common because the luminous flux of LEDs is proportional to current; however, constant voltage drivers, in which a series resistor sets the current level, can also be found. Failure to provide a steady electrical power supply to the LEDs can result in a variety of undesirable lighting effects, including flicker (i.e., time-dependent variation in light output) and poor device reliability.

Some of the first power supplies used in lighting devices were linear power supplies that presented a linear (i.e., purely resistive or dissipative) load to the electrical grid, which is preferred by electrical utility companies. Linear power supplies offer the advantages of minimal electromagnetic interference (EMI) emissions and low cost. However, they are also relatively low in efficiency and dissipate a lot of energy as heat in the driver.

To achieve high electrical efficiency, the most common drivers used with LED devices are SMPS [98]. Even though they present a non-linear load to the electrical grid, the efficiency of SMPS devices has led to their rapid adoption in applications such as LED drivers and computer power supplies. SMPS devices can readily achieve efficiencies greater than 80% in most designs, and it is even practical to achieve efficiencies above 90% in some custom designs. SMPS devices are not without their drawbacks, one of the biggest of which is their non-linear loads, which can result in large inrush currents and reflected power returned to the grid. Inrush current occur when a non-linear device is first turned on and are the result of the initial charging of capacitors and inductors. Fortunately, SMPS designs allow for compensating this effect to a degree, so that SMPS devices can behave more like a linear resistive load to the grid and inrush can be controlled. As a result, the power factor of LED drivers employing SMPS typologies is typically above 0.80 in nearly all SSL applications and is often above 0.95 in many LED lighting systems. Another potential drawback of SMPS power supplies is increased EMI emissions due to the rapid switching. A key element of the SMPS is an IC controller that operates a power transistor, typically a MOSFET. The transistor continually switches at a high frequency between the on and off state, and voltage regulation for the entire device is achieved by controlling the ratio of on to off time for the switching transistor.

Most drivers used for converting power from the AC main electrical supply to the DC drive current required for LED-device operation are composed of five or more electronic circuits, as shown in **Figure 4D-60**. If the driver is used for DC-DC conversion, some of the front-end circuits can be eliminated, but the back-end components such as switched mode control and DC voltage output filter are still required and similar components are used. The primary electrical circuits in an AC-to-DC driver include circuits for:

- Filtering and conditioning the input AC power
- Rectifying the input AC power to DC power
- Shaping the DC power to reduce ripple and to provide power factor correction (PFC)
- Operating the switching transistor in the SMPS and regulating output power
- Filtering the DC output power supplied to the LEDs.

Figure 4D-60. Generalized Schematic of the Electrical Circuits Commonly Used in SMPS Drivers for SSL Devices

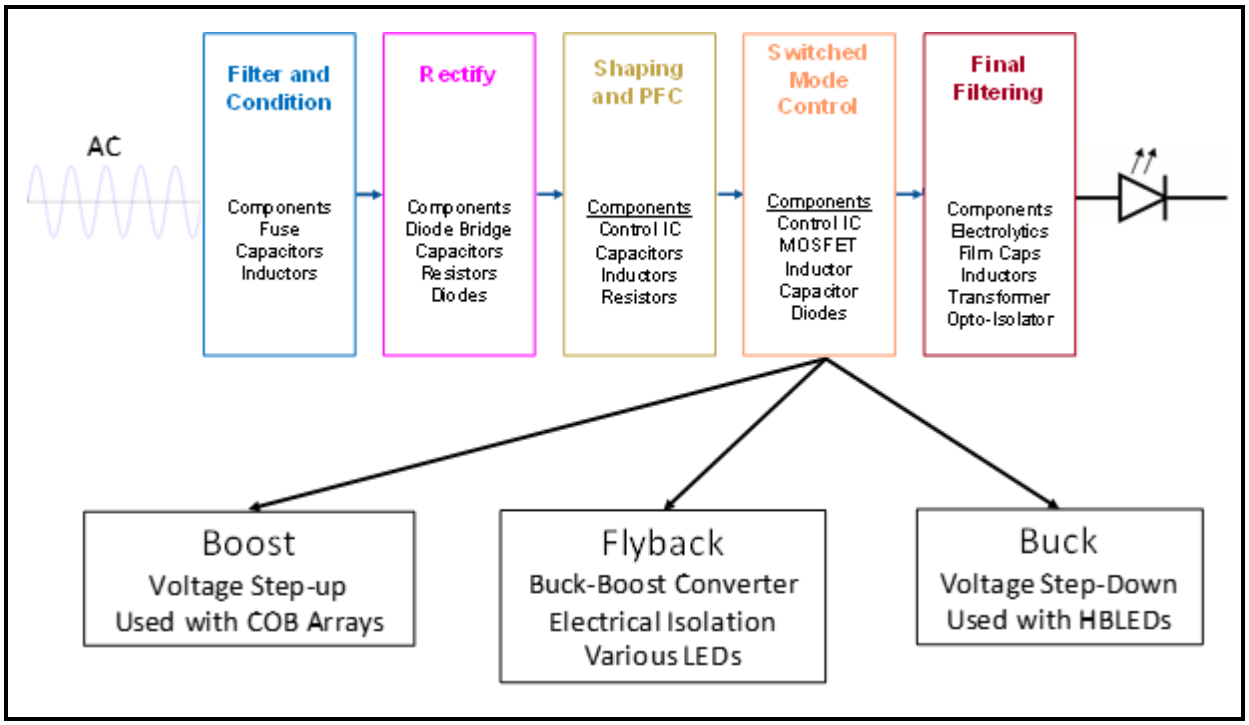

The AC filtering and conditioning circuit is the initial electrical interface between the lighting system and the electrical power mains. The principal job of this circuit is to remove any transients, surges, or swells that may be present in the electrical power supply so that the remainder of the circuit has relatively clean power to operate from. A secondary function of this circuit is to act as an electromagnetic interference (EMI) filter to reduce harmonics transferred from the SMPS device back onto the grid. The AC filtering and conditioning circuit usually consists of several main components, including a fuse, a metal oxide varistor (MOV), and a resonant filtering element composed of capacitors, resistors, and inductors. The fuse is the first line of defense for the circuit and provides protection if the current flow exceeds the device's specification. Failure of a fuse will render the driver inoperable, but will hopefully preserve other parts of the circuit if quick triggering. The failure of fuses can be determined by a simple continuity check or by checking that there is no current flowing to the device. The MOV is a fast-acting, non-linear device that shunts excessive transient currents to ground and provides a measure of surge suppression. Transient suppression will result in accumulated damage for MOVs, but the component will continue to operate until a threshold damage level is reached. Unfortunately, it is difficult to tell if these components have failed without specialized equipment, so the health of aged MOVs is often unknown [99-101]. Resonant filtering circuits consist of energy storage devices such as capacitors and inductors and energy dissipative devices such as resistors. These components are

generally placed after the MOV in the electrical circuit and provide the primary clean-up of the electrical signal. Ideally, the output of a properly designed AC filtering and conditioning circuit is a clean AC waveform with very low ripple. Although the capacitors on the AC filter circuit help to reduce the impact of voltage transients and sags, they also cause large inrush currents when the device is first turned on. These inrush currents can be as much as 40-times larger than the steady state current according to guidelines published by the National Electrical Manufacturers Association (NEMA) [102] and may affect components later in the device, unless the inrush current level is limited by a resistor.

The second circuit in the common driver provides the rectification stage, which begins the process of converting the AC power into DC power. At the heart of the rectification stage is a diode bridge, which generates DC power from the AC input, albeit usually with some ripple. The ripple is usually removed as part of the rectification stage or incorporated into the next stage, DC peak shaping and PFC.

The DC peak shaping and PFC circuit not only acts to smooth the ripple on the rectified DC wavelength, but also helps to minimize the amount of unused power reflected by the driver back on to the grid. Such reflected power can produce total harmonic distortion (THD) or create issues with supply voltage stability in the branch circuit, which increases voltage transients. A critical part of this circuit is the EMI filter, which helps to eliminate harmonics and reduce ripple in the DC supply. In many designs that we encountered in this study, a passive PFC circuit such as a valley-fill is used to filter harmonics and reduce ripple. A resistor can also be incorporated into the valley-fill circuit to limit in-rush currents. The output from the DC peak shaping and PFC circuit is fed to the IC that serves as the controller for the MOSFET switch. Consequently, if the voltages and waveforms of this section of the circuit change or become distorted as the device ages, the switched mode control circuit will not function properly, which could affect the LEDs.

The switched mode control circuit is the current regulation stage for the entire driver. This stage is operated by an IC that controls and adjusts signals in the PFC and MOSFET switching circuits. In addition, the control IC can adjust the waveforms to maintain compatibility with certain dimmers. An output from the control IC is usually fed directly to the gate of the switching MOSFET, which controls current delivered to the LED array by the MOSFET switching time. Distortion of the waveform applied to the gate of the MOSFET or degradation within the MOSFET can increase flicker in the device output and reduce efficiency. In this work, we have found that any major issue in the driver often shows up in one or more of these circuits.

The final circuit of a typical driver is the DC filtering stage, which acts as a temporary energy storage device to continue LED operation when the MOSFET is switched off and also acts to reduce ripple in the output DC waveform. Common components used in this stage include inductors (e.g., buck circuits) and capacitors (e.g., boost circuits). Degradation of

these components can also allow ripple to remain in the DC waveform applied to the LEDs and produce excessive photometric flicker in the LEDs.

The drivers used in LED lighting devices consist of many components, any of which can fail during operation to produce complete device failure (i.e., catastrophic, abrupt, or "lights out" failure), reduced performance (e.g., reduction in luminous flux), or intermittent failure (e.g., flicker). Since the drivers must blend in with the SSL device, a variety of driver shapes and sizes are used in the industry, dependent in large part upon the available space in the SSL device. Basic, single-stage drivers, such as those shown in **Figure 4D-61**, are used in SSL lamps. Since space is at a premium in LED lamps, the simple design with low parts count and minimal magnetics (i.e., transformers and inductors) helps to keep size and price low. SSL devices such as 6" downlights often can accommodate drivers with more capabilities such as flexible dimming or multi-stage typologies with higher power factors. As shown in **Figure 4D-62**, these designs are often less size-constrained, so the parts density can be lower on the board, improving thermal management. Finally, advanced lighting systems such as tuning white light (TWL) luminaires require drivers that combine both multi-stage typologies (for higher power factors) and separate channels for each LED type being controlled. These multi-stage and multi-channel devices often have two or more controller ICs and a relatively high number of passive and active components, as shown in **Figure 4D-63**.

Figure 4D-61. Simple Drivers Used in SSL Lamps

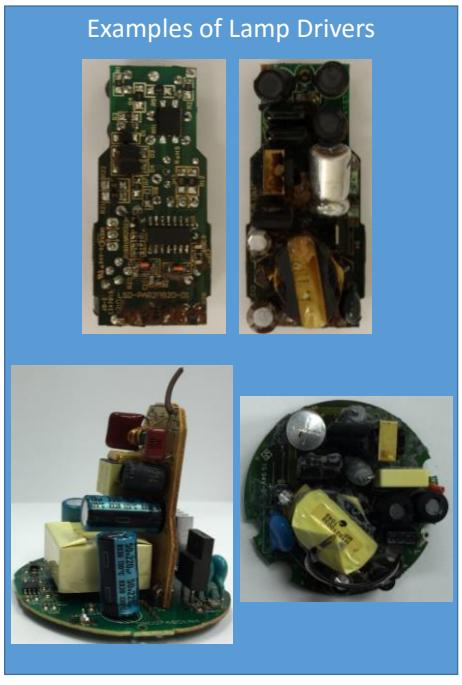

Figure 4D-62. Drivers Used in More Complex SSL Devices, Such as Downlights

Figure 4D-63. Multi-stage and Multi-channel Drivers Used with TWL Luminaires

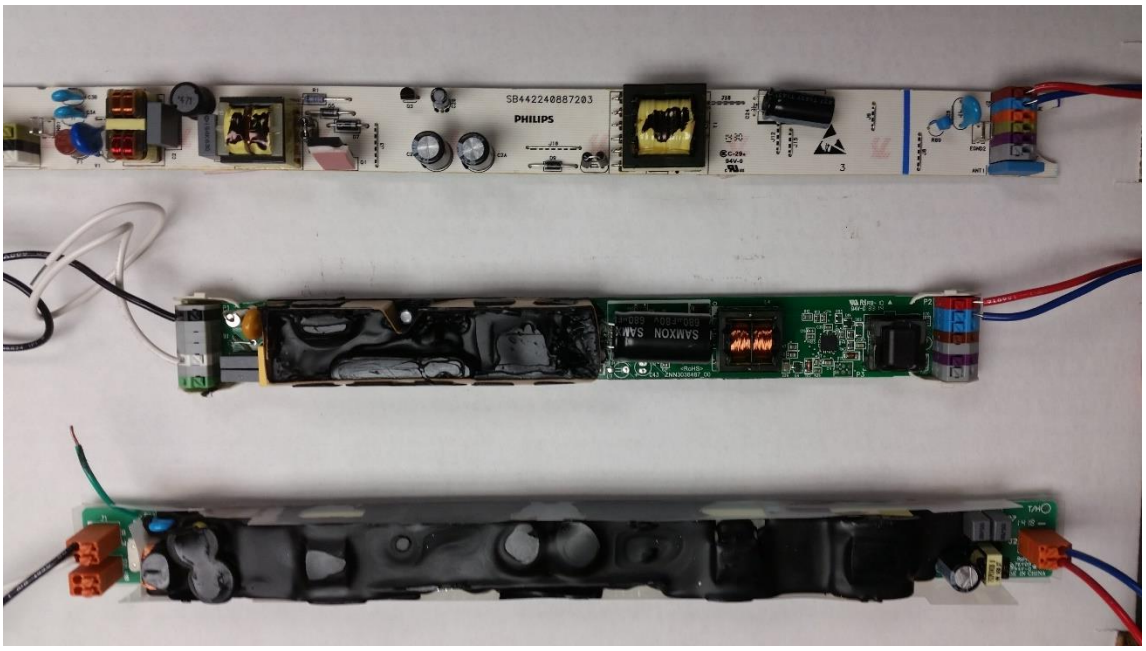

Common Failure Modes of Electrical Components Used in SSL Drivers

From a reliability and operational perspective, five common driver components deserve special attention, because they have been shown to be potential failure sites [96; 103; 104]. These components are switching transistors such as MOSFETs, capacitors, inductors, diode bridges and diodes, and resistors.

One of the most common failure mechanisms of LED drivers is failure or degradation of the MOSFET, and the consequence of this failure mode can range from loss of control in illuminance levels to excessive flicker [105]. The most common failure mode in MOSFET devices is shorting between the collector and emitter terminals, due to several failure mechanisms, including gate dielectric breakdown [106; 107], hot carrier injection [108; 109], and increased junction temperatures caused by delamination of the transistor from the lead frame [110; 111]. The primary causes of these failures are either improper thermal management or voltage transients. Consequently, having good thermal management, including adequate heat sinking, and the choice of MOSFET package architectures with low thermal impedance are critical to reliable operation [104]. In addition, because MOSFETs are sensitive to electrical overstress, choosing components with high forward breakdown voltages, applying sufficient derating factors, and adding additional filtering on the terminal inputs can increase reliability [112].

Failure in MOSFET is often are not readily apparent upon a visual inspection; however, an electrical inspection can usually identify a failed MOSFET, especially if the device failed as the result of an electrical short. A simple continuity or diode check with a digital multimeter (DMM) will confirm whether the MOSFET is operating correctly. In addition, if a characteristic I-V test is performed, a failed device can be readily detected by the high leakage current as shown in **Figure 4D-64**. The graph shows the MOSFETs removed from two equivalent luminaires that were simultaneously exposed to 7575. DUT-144 failed after 4,250 hours of testing, and the high leakage current of this device is apparent when compared to DUT-147, which is still operational.

Figure 4D-64. Comparison of the Characteristic I-V Curves from Two MOSFETs from Equivalent Downlights

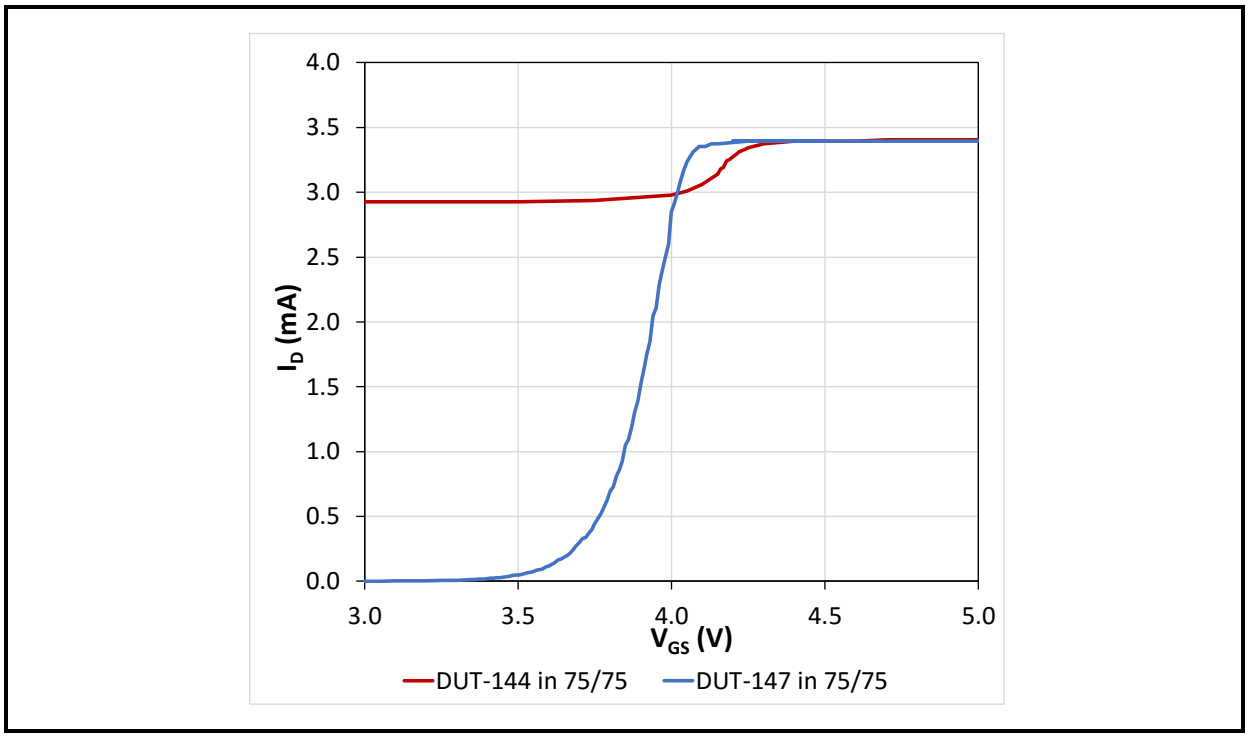

NOTE: Both devices were subjected to more than 4,000 hours of testing in 7575. The drain voltage (V_{DD}) was set at 5 V in this test.

On occasions, the damage caused by overheating of a MOSFET is so extensive that it can be observed from outside the package. An example where MOSFET failure produced a visible detect in the device package is shown in **Figure 4D-65**. This sample was taken from a 6" downlight that exhibited catastrophic failure, and shorting of the MOSFET resulted in a large current flow through the device, which melted and distorted the epoxy overmolding material. Since the MOSFET was integrated into the same package as the controller IC, the thermal management capabilities of the package was not as good as a common discrete MOSFET, so the impact of the heat buildup are more apparent. Even though device failure is not often visible from the outside, the shorting that occurs during MOSFET failure produces severe damage to the interior of the device, which can often be detected in scanning acoustical microscopy (SAM), as shown in **Figure 4D-66**. In this image, red indicates delamination of the epoxy in the package from the LED die, whereas gray indicates intimate contact between the die and the epoxy overmolding compound. The devices shown in Figure 4D-66 are also the same ones whose characteristic I-V curves are shown in Figure 4D-64.

Figure 4D-65. Failed MOSFET from a 6" Downlight

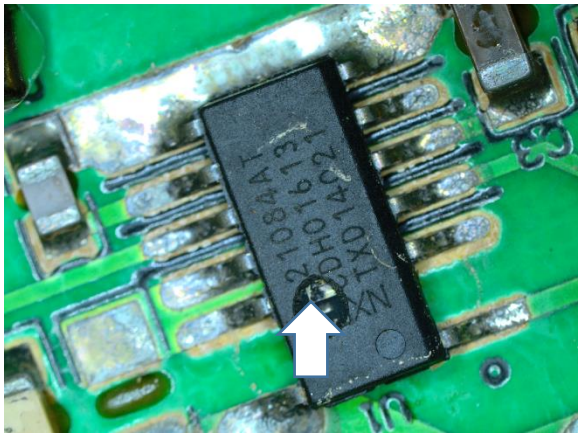

Note: The corner of the MOSFET die is visible near the tip the arrow.

Figure 4D-66. SAM Images of MOSFETs from Equivalent Luminaires Subjected to 7575

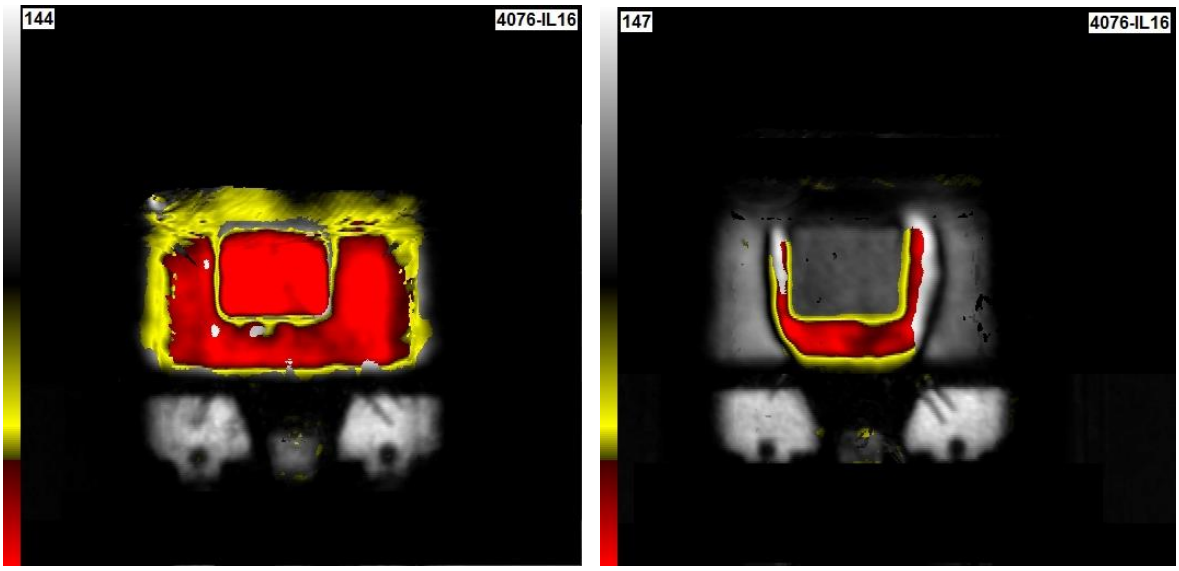

Note: The device on the left is from a failed part (DUT-144) while the device on the right (DUT-147) is from a downlight that was still operating after 4,500 hours of testing.

In addition to semiconducting devices like MOSFETs, a number of passive components populate most LED driver boards. An example is given is given in **Figure 4D-67**, with the major discrete components identified. One of the most common components in an LED driver is the capacitor, which can be present in LED drivers either as surface-mount technology (SMT) chip capacitors or through hole film capacitors and electrolytic capacitors. Usually multiple capacitors and a mix of capacitor types are found in each driver, as shown in Figure 4D-67. Capacitors typically serve several functions in electrical systems, including

filtering out transients and voltage ripple and serving as temporary energy storage sources during voltage sags or during MOSFET switching. However, the high-charging currents that capacitors draw when a device is first energized cause the short-duration, large inrush currents that are often observed with LED drivers and other non-linear electronic devices and can affect product reliability [102].

Figure 4D-67. One-side of a Driver Board for a 6" LED Downlight with the Parts Labeled

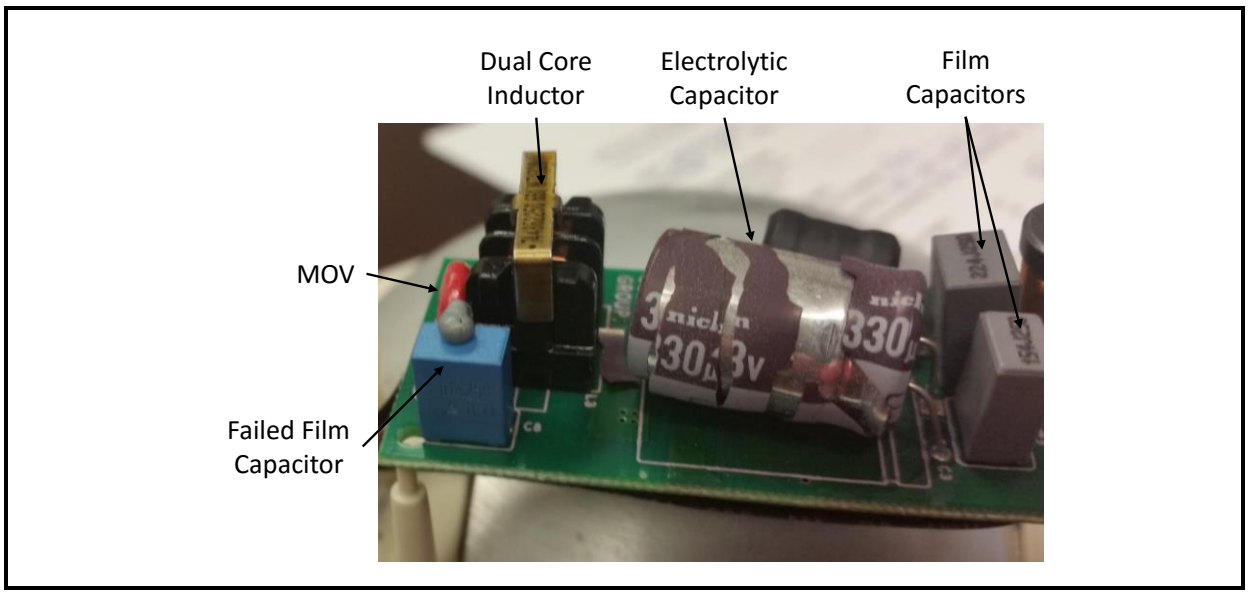

Electrolytic capacitors often consist of wound aluminum electrodes, anodized on one side, immersed in a liquid electrolyte (typically a sodium hydroxide solution) with aluminum dioxide (Al_2O_3) and a separator serving as the dielectric. A picture of a typical electrolytic capacitor after disassembly is shown in **Figure 4D-68**. Electrolytic capacitors are often used in LED drivers to filter out transients and ripple voltages, especially on the DC output and sometimes to serve a similar function on the AC input. While electrolytic capacitors have the highest energy storage capabilities of the three common capacitor types, their reliability and performance is affected by temperature, voltage spikes, and other stress [113]. To overcome this limitation, manufacturers will typically derate electrolytic capacitors by a factor of two or higher, and minimize the exposure of the component to transients by placing them in areas of the circuit where electrical and thermal stresses are minimized [114].

Figure 4D-68. Typical Structure of an Electrolytic Capacitor after Disassembly

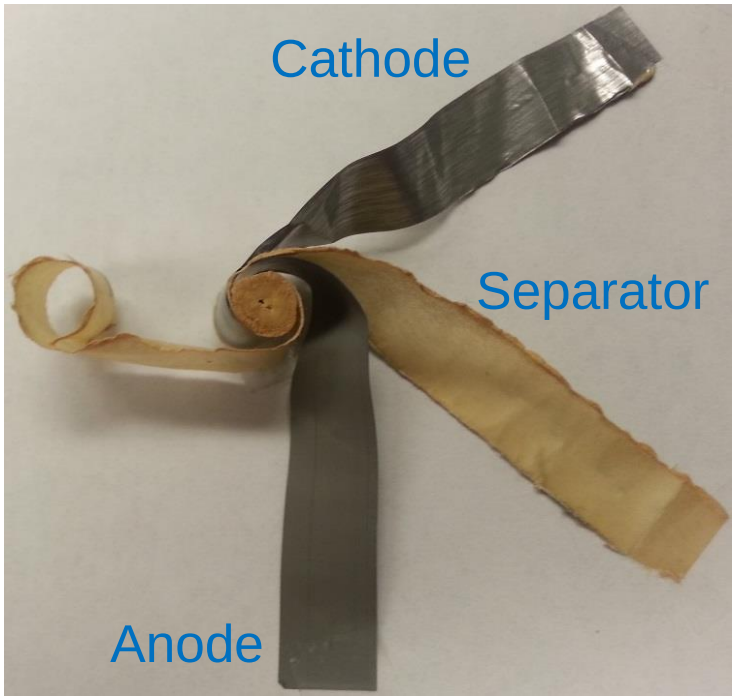

The failure rate of electrolytic capacitors is usually one or more orders of magnitude higher than film capacitors [115]. A common wearout mechanism in electrolytic capacitors is the loss of electrolyte either through leakage, degradation, or vaporization, leading to an increase in equivalent series resistance (ESR) and a decrease in capacitance [114; 116]. In extreme cases, the pressure inside the electrolytic capacitor can increase to a high enough level to cause rupture of the device, as shown in **Figure 4D-69**. In addition, transient voltage spikes that exceed the voltage rating of a capacitor, even for a few milliseconds, can produce hot spots within the component that greatly accelerate time to failure [114; 117]. The design of an electrolytic capacitor is also known to impact its reliability, with larger capacitors generally having better heat dissipation ability and higher reliability than smaller ones. Although the lifetime of electrolytic capacitors is known to have a strong dependence on temperature, simple AST protocols, such as high temperature storage testing, often have minimal impact on the ESR and capacitance of properly chosen components [118; 119]. Instead, operational lifetime tests, in which the device is operated either continuously or on a power cycle, generally accelerate wearout failure mechanisms faster due to internal heating from the electrical power. Experiments examining this difference were performed at Auburn University as part of this project and will be discussed further below.

Figure 4D-69. Driver for 6” Downlight that Exhibited Multi-component Failure

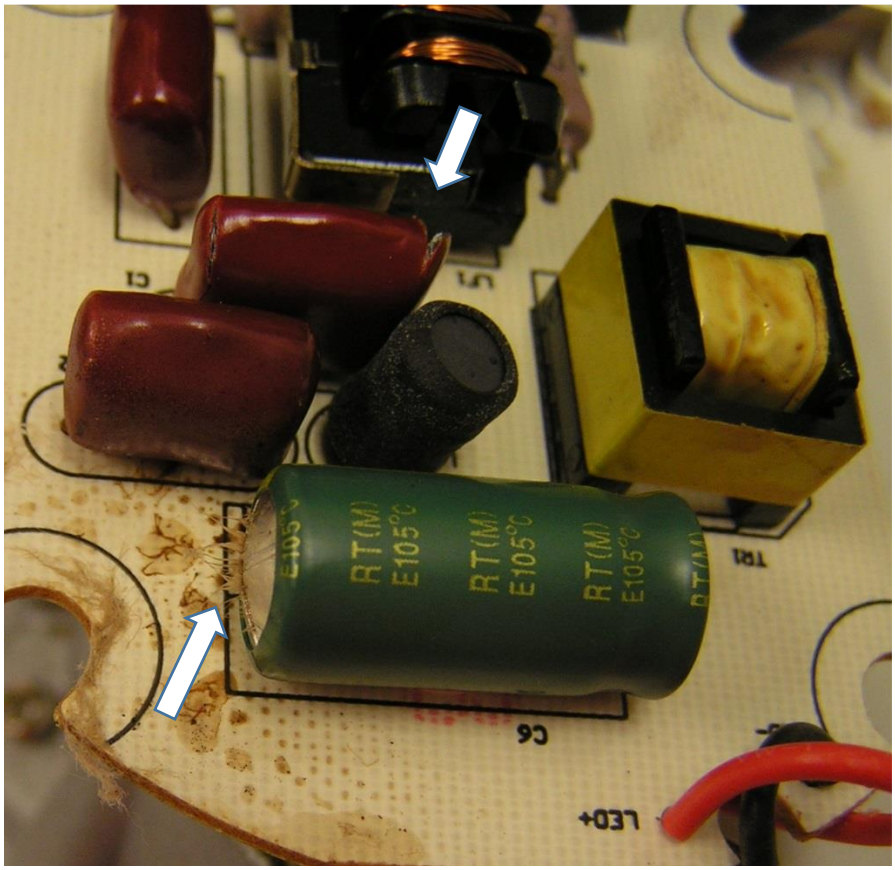

Note: Failure of the electrolytic capacitor (C6) and film capacitor (C1) is indicated by arrows.

Film capacitors are compact and highly reliable devices that are increasingly being used in more LED driver designs, especially in filtering the AC mains supply, where transients can be an issue. The common film capacitor consists of a wound thin-film aluminum layer on a polymer substrate that acts as a separator. After the attachment of the leads with a Schoop metallization process, the entire jelly roll structure is encapsulated in an epoxy coating. Film capacitors exhibit the ability to “self heal” if defects form. Essentially, the area of the electrode where the short is formed is ablated when shorted, which restores operation to the device but at a loss of capacitance [119]. As a result, film capacitors exhibit a number of desirable characteristics compared to electrolytic capacitors, including lower ESR, higher surge voltage tolerance, and no polarization [120]. Film capacitors also tend to fail open due to degradation of the metal interconnects within the capacitor. Although failure of film capacitors is less common than electrolytic capacitors, they will fail under instances of high temperature, humidity, electrical stress, and mechanical stress [121; 122]. Examples of failed film capacitors are shown in Figure 4D-67, Figure 4D-69, **Figure 4D-70**, and **Figure 4D-71**. Of special note in these figures is the Schoop metallization, which is visible in all

four pictures and has apparently melted and oozed through a hole in the case in Figure 4D-67.

Figure 4D-70. Side View of a Failed Film Capacitor from LED Drivers

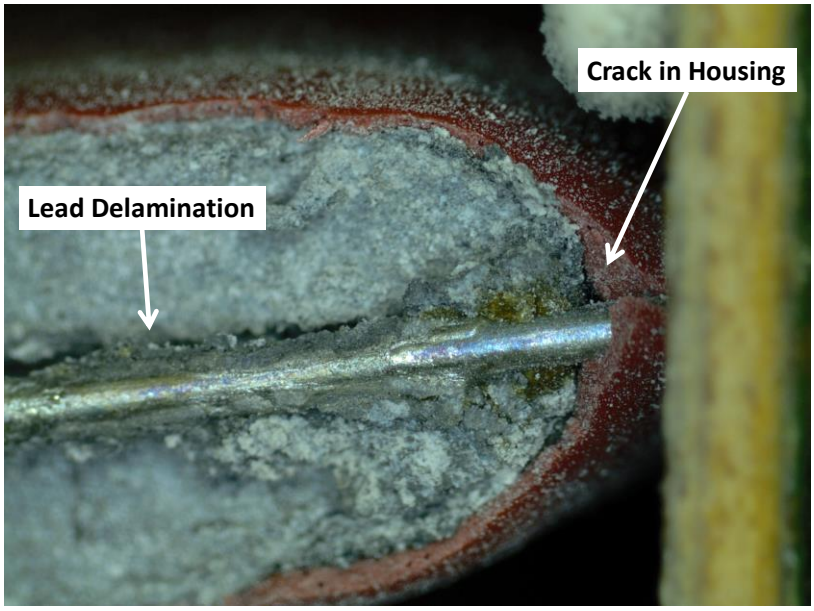

Figure 4D-71. Top View of a Failed Film Capacitor Showing the Schoop Metallization and the Winding

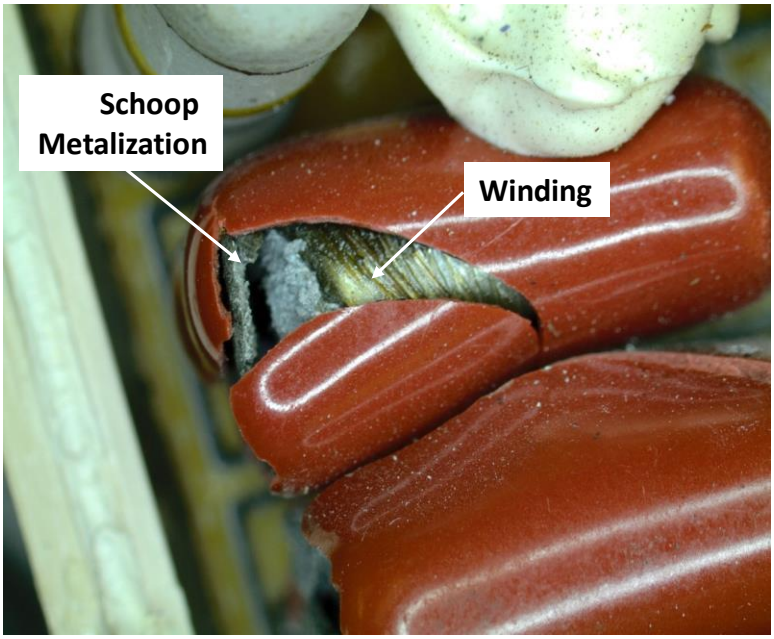

Inductors and transformers are other common electrical components found in LED device drivers. These components serve several functions, including combining with capacitors to form LC filters on the driver front end and providing energy storage to power the LEDs in SMPS (e.g., buck typology). In addition, transformers are used in Flyback driver topologies to electrically isolate the input AC power from the output DC line through inductive coupling between the primary and secondary windings on the transformer. Although failures in inductors and transformers are rare, when they occur, such failures can usually be traced to either excessive current loads, breakdown of insulating dielectrics, or broken interconnections.

A variety of resistors are found in SMPS designs, the most common of which are surface-mounted chip resistors, followed by through-hole resistor technologies. Resistors are used in SMPS designs to control voltage and current levels. Generally, resistors will often fail open due to short-term transients that produce current flows through the component in excess of the rated capacity and essentially burns the component out. Examples of resistor failures from both normal operational testing and accelerated life testing are given in **Figure 4D-72**. A variety of root causes can be responsible for resistor failure, including manufacturing defects and failure of regulation components, which can cause cascade failures in which excess current flows through the resistor and other components.

Figure 4D-72. Failed Resistors from WHTOL Testing on 6" Downlights

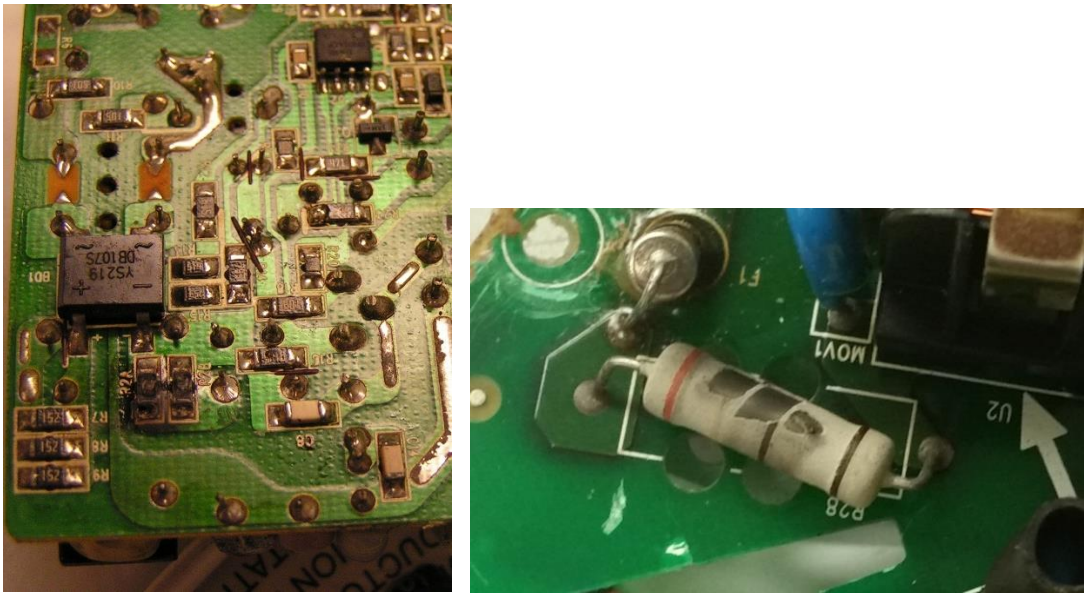

Note: SMT resistors are shown on the left and through-hole resistors are shown on the right.

Semiconductor diodes and diode bridges are essential elements of SMPS designs for AC-powered devices. They provide management of current flow and rectification of the electrical voltage from the input mains. As commonly occurs in power electronic components, the reliability of semiconductor diodes and diode bridges is affected by temperature and electrical overstress. The use of proper thermal management techniques, including minimizing the heat buildup in diode and diode bridge packages and applying proper deratings, is important to achieve reliable products.

Common Driver Topologies

Electronic drivers for SSL applications are available in a variety of topologies that vary depending on whether the voltage supplied to the LEDs is higher or low than the AC mains voltage [98]. The buck driver topology is a common low-cost, step-down driver structure, whereas the boost driver topology is a common step-up driver structure. Other driver topologies, such as the boost-buck and flyback, can be either step-up or step-down, depending on their configuration. Multiple typologies can be combined in a single driver to increase the power factor, and the combination of a flyback typology in the first stage and a buck typology in the second stage is commonly used in two-stage drivers [105]. A comparison of these most common driver topologies is given in **Table 4D-9**, and schematics diagrams of the most common single-stage LED driver topologies are given in **Figure 4D-73**.

Table 4D-9. Common Topologies Found in LED Drivers

Topology	Output Voltage Range	Electrical Isolation of Mains and DC Supply	Mode of Operation
Buck	Output voltage is < 85% of input voltage (i.e., step-down converter).	No	When the switching transistor is closed, energy is stored in the inductor (L1), and the capacitor (C1) powers the LEDs. When the switching transistor is open, L1 in series with LED load provides electrical energy to C1 and LEDs.
Boost	Output voltage is greater than input voltage (i.e., step-up).	No	When the switching transistor is closed, energy is stored in inductor (L1), and LEDs are powered by the charged capacitor (C1). When the switching transistor is open, energy stored in L1 flows through the diode and the parallel combination of the LED string and C1.
Buck-Boost	Can either step-up or step-down the input voltage. Ideal for use with battery.	Capacitive isolation between mains and output	When the switch is closed, voltage ramps up on the inductor (L1), and the capacitor (C1) supplies the LEDs. When the switch is open, L1 provides power to operate the LEDs while C1 charges through L1.

(continued)

Table 4D-9. Common Topologies Found in LED Drivers (continued)

Topology	Output Voltage Range	Electrical Isolation of Mains and DC Supply	Mode of Operation
Flyback	Can either step-up or step-down the input voltage, depending on configuration.	Yes	When the switch is closed, current flows in the primary side of the isolation transformers, and energy is stored in the transformer magnetic field. During this cycle, the LEDs are powered by the capacitor (C1). When the switch is open, the stored energy in the magnetic field charges C1 and supplies the LEDs.

Figure 4D-73. The Most Common Single-stage Driver Topologies Found in SMPS Devices Used in LED Drivers

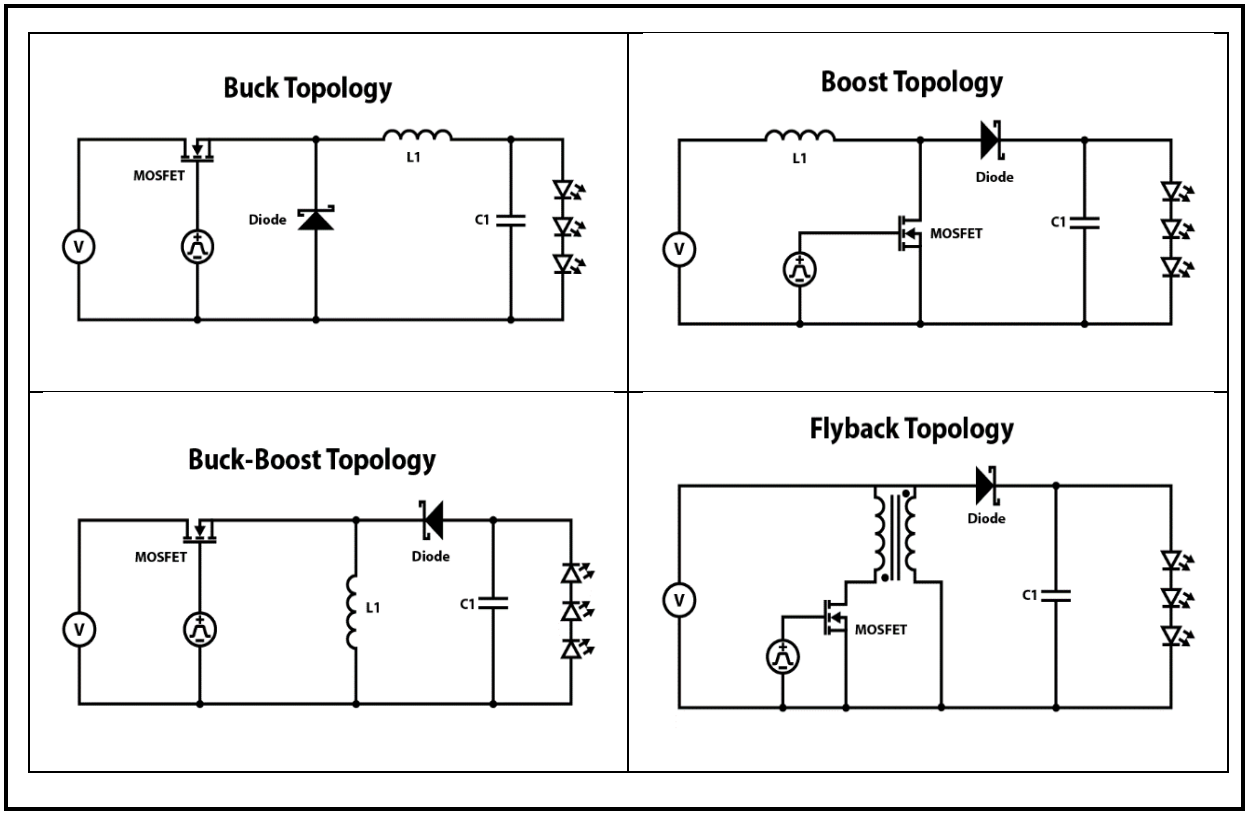

All of these driver typologies contain a MOSFET to provide high frequency, low loss switching. When the MOSFET is switched off, energy stored in capacitors or the magnetic field of inductors and transformers is used to maintain a steady light output by the LEDs. For example, the combination of the buck inductor (L1) in series with the LEDs and a capacitor (C1) in parallel provide power when the MOSFET is switched off in the buck

design. In contrast, a parallel capacitor (C1) is the source power when the MOSFET is switched off in the boost typology. In addition, these driver topologies can also be classified by whether the AC mains and DC output are electrically isolated. Isolated power supplies, such as the flyback typology, typically use an isolation transformer, so that the input and output are inductively coupled but electrically isolated. Non-isolated power supplies have the driver input and output electrically connected.

Single-color LED-based luminaires have made significant market penetration in many demanding lighting applications. With the additional functionality available with LEDs, the next wave of LED lighting technology is likely to be TWL products that can adjust the spectrum of the emitted light between a range of values. This capability allows the light system to produce white light of an appropriate spectrum for the task at hand. For example, a warmer light (i.e., lower CCT) could be used for more relaxed tasks, such as conversations, while a cooler light (i.e., higher CCT) could be used for tasks requiring greater concentration and higher visual acuity [123; 124].

Driver technology is a key enabler for TWL, since the different LED assemblies that form the TWL system must be controlled separately. TWL products can either use separate drivers for each LED assembly or a more complex driver with the controls and switching for all channels, integrated into one unit. In general, a controller IC provides the control signals to operate the LEDs, and this chip supplies a control signal to the gate of the MOSFET.

Since control of the current supplied to each LED assembly is essential for color tuning operation, separate MOSFETs and control signals, one for each assembly, are necessary. Schematically this can be represented by different signals from one controller IC, assuming the integrated multi-channel driver architecture, going to different MOSFETs which, in turn, feed the different LED assemblies, as shown in **Figure 4D-74**. In practice, a single IC with separate channels for each LED assembly is used, and the MOSFETs are either integrated into the same package as the controller IC or are placed on the driver board as separate, discrete devices. Separate energy storage components (e.g., inductors and capacitors) are also part of the DC output for each channel.

Figure 4D-74. Driver Structure for Multi-channel Drivers Such as Those Used in TWL Luminaires

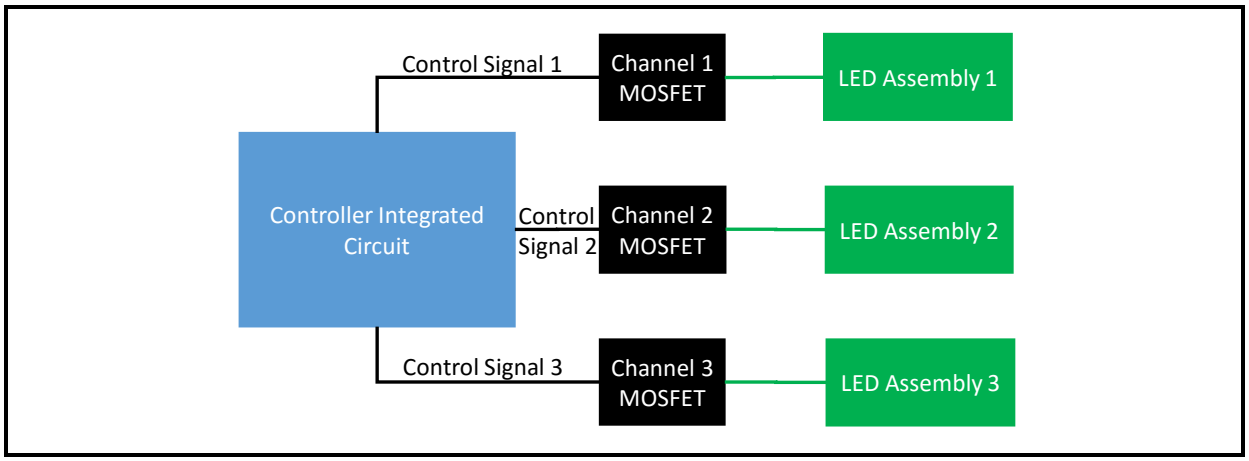

As an additional consideration, it is often desirable to have high power factors in drivers, which is difficult to achieve in a single-stage design. This is less of concern for LED lamps, but is becoming more of a customer expectation in large commercial lighting systems, such as in office buildings. Consequently, two-stage designs are becoming more common. In a typical two-stage driver design, the first stage provides filtering/rectification of the AC input power as well as PFC. The output from the first stage is an intermediate DC signal that feeds the second stage, which consists of the switched mode controller and DC output filtering circuits that provide power to the LEDs. Perhaps the most common multi-stage driver design is a two-stage typology using a flyback circuit in the first stage and a buck circuit in the second, and this structure is shown schematically in **Figure 4D-75**.

Figure 4D-75. Two-stage Driver with a Flyback Typology in Stage 1 and a Buck Typology in Stage 2.

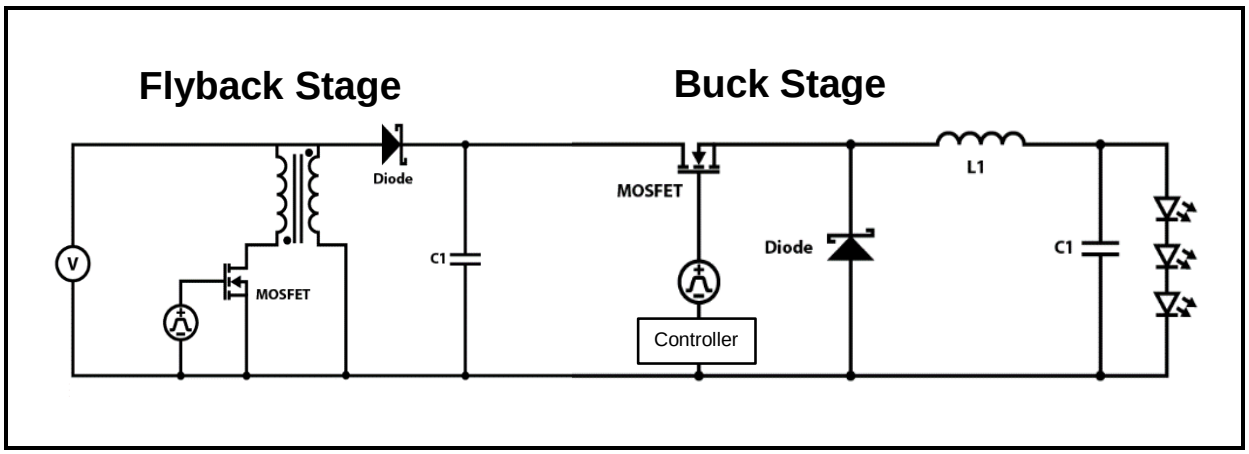

Common Electrical Stresses in LED Device Drivers

The quality of the electrical power supplied to the LED driver has a significant impact on reliability, because electrical components such as MOSFETs and electrolytic capacitors are particularly sensitive to electrical transients. This is especially important for non-linear loads, such as AC-mains powered LED drivers, where large inrush currents can occur when the device is first turned on, and these currents can produce voltage transients, including voltage sags and surges [102]. Likewise, voltage spikes caused by lightning strikes or energizing other non-linear loads on the same branch circuit can create transients that may affect product reliability. Often forms of surge protection, such as MOVs, are incorporated into LED drivers or supply-line branch circuits to minimize the impact of line transients [74]. Another type of transient that can arise is repetitive currents, which are essentially rapid capacitor charge/discharge cycles as part of phase-cut dimming signals [125]. Any of these transients can adversely affect the reliability of the LED driver.

The reliability of LED lighting drivers is impacted by the power quality of the electric source and the system compatibility of the driver with the grid. Power quality is the concept of powering and grounding electronic equipment in a manner that is suitable to the operation of that equipment [126]. System compatibility has been defined by the Electric Power Research Institute (EPRI) as "the ability of a device, equipment, or system, generally a load, to function satisfactorily with respect to its power-supply electrical environment without introducing intolerable electrical disturbances to anything in that environment" [123].

Both the magnitude and duration of electrical transients impact the reliability of SSL lighting drivers, and such transients may arise from the utility side or from other devices on the same branch circuit. In addition, wiring and grounding errors within the lighting infrastructure can magnify the impacts of transients. By studying the impacts of transients on driver reliability, EPRI has demonstrated that driver components such as MOSFET transistors, power diodes, and electrolytic capacitors are particularly susceptible to electrical stress [123]. Surge protection devices such as MOVs are necessary to reduce the transients introduced into the driver.

Accelerated Stress Tests for Electronics

Because the expected lifetime of most LED drivers is long, ASTs must be used to obtain information about the reliability and lifetime of a design in a greatly condensed timeframe. However, it is essential that the AST methodologies used for SSL luminaires reproduce, as accurately as possible, the cumulative exposure of LED–based products. Typically, AST methods involve, at a minimum, a combination of environmental stressors, such as temperature and RH, and electrical stressors, such as variation in supply voltage and the introduction of transients. Depending on the reliability information being sought, other environmental stressors (e.g., chemical contamination, dust) or mechanical stressors (e.g., vibration) can be added to the test matrix [85].

A variety of AST methods have been developed by the electronics industry and can be applied to the LED drivers. Each of these tests provides some insights into potential failure mechanisms; however, lifetime predictions are possible only when the failure rate is appreciable [36; 85]. These methods can be divided into three broad classifications:

- Rapid tests (or highly accelerated stress tests [HASTs]) that provide information on possible failure modes in a minimal test period are generally conducted under highly overstressed conditions. Because these tests are often conducted under conditions well beyond the normal operational regime of the device, failure typically occurs much sooner than under normal conditions. Due to the short testing duration, HAST protocols can be a quick and relatively inexpensive approach to obtaining basic information about failure modes. However, establishing a correlation between the findings from these tests and lifetime predictions is difficult, and there is a danger of introducing new failure modes due to the highly overstressed test conditions.
- Screening tests can be used to compare the performance of different products, provided an evaluation metric is available for the comparison. Screening tests often use established industry accelerating tests (e.g., elevated ambient, temperature cycling), and the tests are conducted for a predetermined period (e.g., 1,000 hours at 150°C or 1,000 cycles of temperature shock). Changes in measurable parameters that are suggestive of potential failure modes (e.g., increased ripple on output DC voltage, solder joint integrity) can be monitored relative to established pass or fail criteria. Such parameters are evaluated to determine whether they remain within acceptable limits (i.e., devices that pass the test) or are outside acceptable limits (i.e., devices that did not pass the test). Because screening tests are often performed for a finite duration, test costs can be determined in advance. However, because there is no assurance of failure or even a significant change in measured parameters, screening tests typically provide limited information about product lifetime and reliability.
- Test-to-failure methods involve operating a sample population in AST experiments until a significant portion of the population, usually greater than 65%, has failed. The primary advantage of test-to-failure methods is that the lifetime and reliability of the product can be calculated if acceptable acceleration factors are known for the test conditions. The primary disadvantage of this approach is that the test period can be very long, because testing is concluded only when a sufficient number of failures have occurred. Consequently, test-to-fail protocols can be expensive to run and consume significant resources, but they can provide the best information about device lifetime and reliability.

In choosing practical ASTs, it is useful to specify whether the device is intended for indoor or outdoor use. Among the environments to be considered for outdoor luminaires are minimal operating temperatures of at least −20°C and operation in hot and humid environments. For indoor lighting, an extreme case may be recessed luminaires mounted in ceilings or high bays where ambient temperatures can exceed 100°C, especially in hot climates such as in Phoenix, AZ. For outdoor lighting, -20°C during winters in Chicago, IL is not uncommon. **Table 4D-10** summarizes representative accelerated test methods that were first developed for the electronics industry and can be applied to LED drivers with appropriate experimental design and test method modifications. Modifications to these test

methods, such as different temperature and humidity settings, can also be used in AST protocols.

Table 4D-10. Summary of Common AST Methods Used

Test	Standard Test Methods	Representative Procedures	Minimum Test Durations
Thermal aging	JEDEC JESD22-A103C	Continuous storage at 150°C (Condition B) or 180°C (Condition C) with possible storage at other temperatures.	1,000 hours
Biased humidity	JEDEC JESD22-A101B	Operation of the device at 85°C and 85% RH under a cyclical bias (typically 1-hour duty cycle).	1,000 hours
Temperature shock	MIL-STD-202G Method 107G	Cycle temperature between −40°C and 125°C with a 15-minute dwell time at each extreme.	200 cycles
Electrostatic discharge sensitivity	ANSI/ESDA/JEDEC JS-001	A model of electrostatic discharges that mimics discharges from the human body. A capacitor is charged at high voltage and then discharged through a resistor in series with the test device.	

For LED drivers, thermal-aging experiments are mandatory to reproduce the high heat experienced by the device during operation and storage/shipping. Recent results have indicated that the temperature inside an LED driver can get very hot and adversely affect lifetime [89; 90]. This finding is consistent with the extensive literature developed by the electronics industry over the last 30 years that clearly demonstrates that temperature can have a significant impact on the reliability of semiconductor devices and other electrical components used in LED drivers [128]. A thermal annealing test, such as JEDEC's JESD22-A103, will allow the examination of high heat on the performance of the entire driver and its electrical components, including the heat load in semiconductors, degradation of die-attach materials, and the likelihood of interconnect (e.g., wire bonds, ball bumps) failures. To avoid introducing new failure modes, modifications to this method can be made to accommodate parts of the luminaire that will not experience the full heat load.

Semiconductor packages and other electronic components are often not hermetically sealed, and common encapsulants, such as glass-filled epoxies, can be permeable to moisture. Hence, humidity testing, especially combined with elevated temperatures, can be an effective way to study failure modes of LED drivers [103]. A typical WHTOL test, such as JEDEC 22-A101B, can provide significant information about failure rates, often more quickly than by testing at higher temperatures. A key element of JEDEC 22.A101B is testing with a cyclic electrical bias consisting of powering the device on and off at a set duty cycle. Such

cyclic biasing allows sufficient cooling during the off-cycle for moisture to collect in the semiconductor package, other electronic components, and other surfaces. This will likely intensify the impact of any moisture-related failures mode such as moisture ingress. Because this test is performed with the electrical components energized, it provides a measure of many potential failure modes, including heat, electromigration effects, corrosion, and a chemical attack. However, care must be taken in choosing the temperature and humidity conditions, because some components, especially film capacitors, may not be able to withstand high-temperature and high-humidity conditions.

Although there is a significant body of knowledge about the behavior of electronic components (e.g., capacitors, MOSFETs) in accelerated tests, there is much less publicly available information about the reliability of these components when integrated into LED drivers. This is likely due in part to the wide variety of driver designs and the absence of industry standards for acceptable driver-level test methods. This fact also presents an impediment to a simple model of LED driver reliability.

Some of the first published studies of driver reliability focused on the impacts of degradation of electrolytic capacitors upon ripple in the output DC waveform [128; 129]. In these publications, Han and Narendran demonstrated that degradation of the capacitance and increase in the ESR of the output filter electrolytic capacitors was a potential cause of parametric failure in SMPS designs using flyback topologies. The changes in capacitance and ESR that occur as electrolytic capacitors deteriorate produced greater ripple in the output waveform. The net result was a drop in relative efficiency, which resulted in greater power dissipation in the driver. However, the device continued to operate during the test period; therefore, this may not be considered a failure if it is viewed in terms of a lighting installation.

As summarized in Section 4.D.4, one of the first published luminaire-level studies of reliability examined the performance of LED downlights in a HAST. This "Hammer Test" was developed to cause device failure in a few hundred hours to facilitate the investigation of failure modes [37]. The downlights used in this testing were provided by six different manufacturers, and the drivers in these devices consisted of common topologies, including buck and flyback. No effort was made in this study to correlate reliability and driver topologies. In addition, because this test is highly accelerated, it is not possible to establish a correlation of the findings to lifetime prediction. However, the Hammer Test was useful in identifying potential failure modes of luminaires that could be studied further.

Despite the fact that the tested products were designed for indoor use in a constant temperature environment, all samples examined in the Hammer Test survived more than 100 cycles of temperature shock, with nearly half surviving 300 cycles. This finding suggests that the reliability of LED luminaires can be high if they are designed properly and that these devices are robust enough to survive for a period of time under conditions

outside of their expected design range. The dominant failure modes found in the Hammer Test were mechanical failures associated with the expansion and contraction of printed circuit boards and solder joints [37]. However, several component failures in the drivers involving capacitors, ICs, and MOSFETs were found.

Another HAST protocol has been developed by the Pacific Northwest National Laboratory (PNNL) to compare the durability of the Philips L–Prize 60-Watt–equivalent LED lamps with market-proven compact fluorescent lamps (CFLs) [64]. In this study, 10 different stress levels consisting of combinations of electrical, thermal, vibration, and humidity stresses were established, and the stress levels were changed in magnitude in each successive step.

Although the stress level used in portions of this test protocol typically exceeded the intended operational range of the product, these tests provide insights regarding the relative durability of LED and conventional lamps. PNNL found that the electrical performance of all the L-Prize LED lamps was within acceptable limits at the end of testing, whereas none of the CFLs were operational. This finding demonstrated that the LED lamps performed better than the CFL benchmarks and that these products could survive extreme conditions outside of their intended operational range. However, as noted by PNNL, such HAST protocols cannot be used to quantitatively estimate device reliability or lifetime.

This body of knowledge, combined with experimental results to be presented below, provide insights into the type of accelerating environments that are necessary to induce failure in LED drivers in a reasonable period of time without unduly introducing new failure mechanisms. One of our findings is that temperature alone has a low acceleration factor, so non-operational bake test of LED drivers would take a long time to accumulate sufficient failures for statistical analysis. A second finding is that the use of operational lifetime tests, especially with the electrical biased cycled on and off, can promote shorter test times. A third finding is that a second environmental stressor, such as humidity, can be combined with temperature and cyclic electrical biasing to reduce test times to less than 3,000 hours.

4.D.9 AST Results of SSL Drivers and Luminaires

Multi-Stage Single Channel Drivers

At the beginning of this project, there was a strong belief in the lighting industry that the reliability of aluminum electrolytic capacitors was likely the single most important factor in LED driver reliability. To scientifically determine whether the data confirmed this suspicion, Auburn University designed a series of experiments to evaluate the level of degradation that occurred in electrolytic capacitors subjected to high-temperature storage life (HTSL) and wet high-temperature storage life (WHTSL) tests. The HTSL protocol consisted of exposing a population of LED drivers to a constant soak at a temperature of 135°C, and one cycle of this test lasted 168 hours. Likewise, WHTSL testing consisted of exposing a population of LED drivers to a constant soak in an 8585 environment, and this test also lasted for 168

hours. Since these tests are storage life tests, they were conducted without electrical bias but will still provide an indication of the behavior of these devices over time. The same driver product, Philips Xitanium driver (Part number 9137 012 13402), was used for both storage tests. At the end of each 168 hour cycle, the drivers were removed from the oven and the capacitance and ESR of the electrolytic capacitors was measured. In addition, the drivers were attached to a light engine, (Philips Fortimo Downlight Module (DLM) 2000/36W), and photometric measurements were taken. The DLM product is intended to be used in conjunction with the test driver product in 6" and 8" downlights. Therefore, we anticipate that the results of this study will have applicability to other downlights in our study. The same DLM light engine was tested with all drivers. The goal of this study was to look for degradation in the electrical properties of electrolytic capacitors and to determine their impact on the luminous flux produced by the light engine.

The Philips Xitanium driver is a dual-stage single channel device that provides dimming compatibility and can operate an external fan if the preset temperature is exceeded. As a result, this device has additional circuits beyond the five basic ones discussed above. The printed circuit board (PCB) of this product is shown in **Figure 4D-76** along with the electrolytic capacitors. The AC filtering and conditioning stage is indicated by a blue triangle in the bottom left-hand corner of **Figure 4D-76**, and the film capacitor used as the initial post-rectification filter is indicated by the green star. The diode bridge is the black object between these two points. The electrolytic capacitors can be shown to be after the rectification stage with capacitors 2, 3, and 4 (in the right-hand side of Figure 4D-76) involved in the LED circuit, whereas capacitor 3 is part of the fan circuit. To facilitate this study, the electrolytic capacitors were removed from the driver board and placed on a breadboard and the reconnected to the driver board using jumper wires. Placing the electrolytic capacitors on an external breadboard, facilitated testing of the devices and a special testing arrangement was built as shown in **Figure 4D-77**.

Figure 4D-76. PCB of the LED Driver Product Used in this Study and the Associated Electrolytic Capacitors and their Location on the PCB

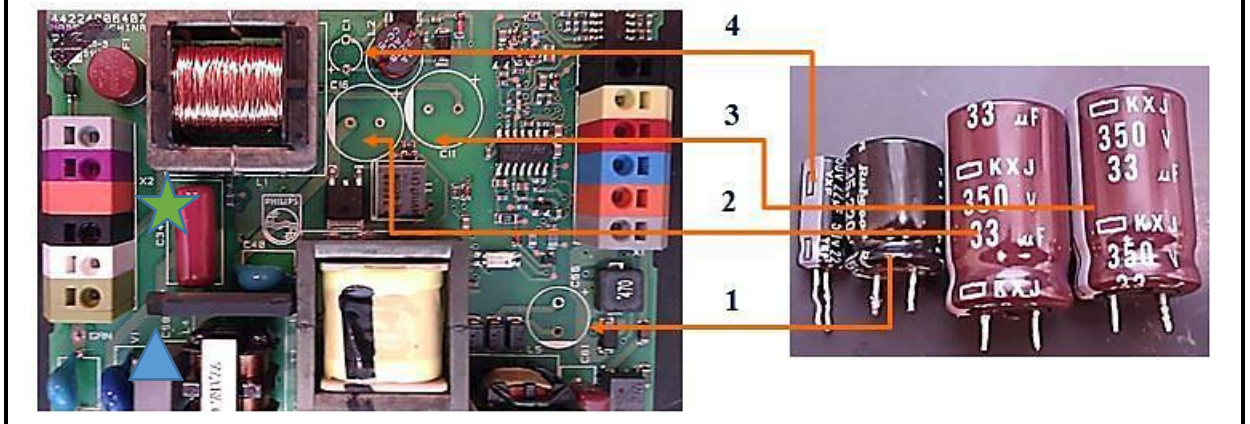

Figure 4D-77. Test Setup Used in this Study

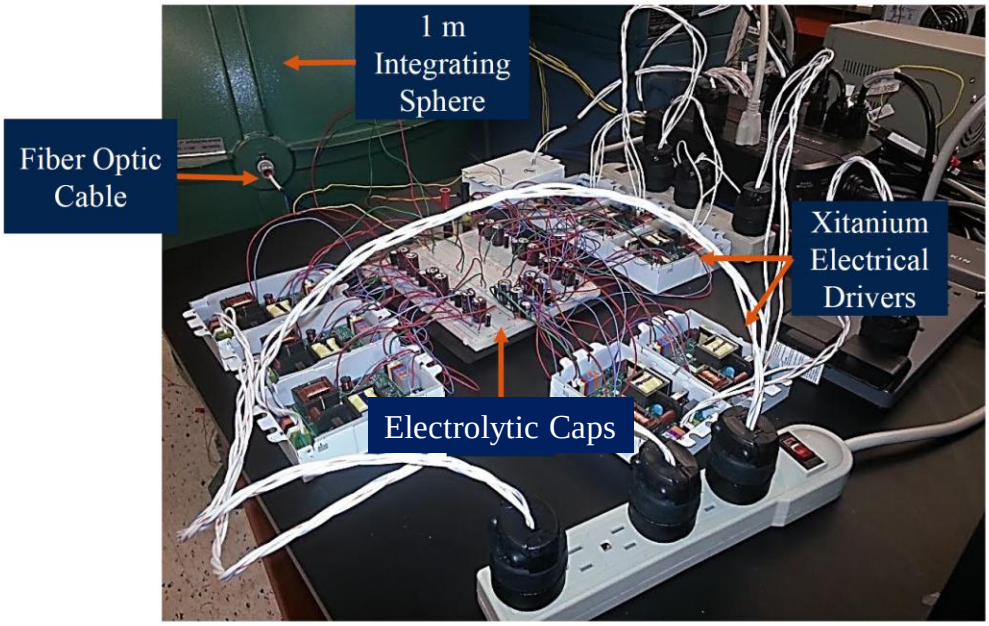

The initial study was conducted on a population of 10 drivers (and their associated electrochemical capacitors) in HTSL testing at 135°C, and the capacitance and ESR of each driver was measured individually. The capacitors were rated for operation at 105°C and the endurance at that temperature ranged from 4000 hours (capacitor number 4) to 10,000 hours (capacitors number 2 and 3). The change in the average capacitance and ESR of the population after 2,120 hours of HTSL testing is shown in **Table 4D-11**. Reduction in device capacitance lowers is ability to filter out ripple, and increases in ESR raises the circuit impedance and can result in a increased voltage drop and greater heat dissipation in the component. In general, the parametric failure threshold of capacitors during storage tests is often taken as a capacitance decrease of more than 10% and an ESR increase of more than 300% [116]. Capacitors #2 and #3 are well below these failure thresholds, while both capacitor #1 and #4 exceed at least one parametric failure threshold. However, despite the large change in capacitance and ESR of the electrolytic capacitors, none of the drivers experienced a decrease in luminous flux during the 2,120 hours of the WHTS test. This finding suggests that significant degradation can occur in some components producing large shifts in component properties, but the impact of the light produced by SSL devices may be minimal. It is also worth noting that the larger capacitors had the highest rated voltages

and the smallest parametric changes in these tests, which provides an indication of the importance of electrolytic capacitor selection in determining reliability.

Table 4D-11. Change in Capacitor Properties during 2,280 Hours of 135°C HTSL Testing

Capacitor Number	Initial Capacitance (μF)	Rated Voltage (V)	Capacitance Change	ESR Change
1	220	35	−5.9%	+318%
2	33	350	−1.5%	+50%
3	33	350	+0.8%	+65%
4	22	50	−11.5%	+364%

After 2,120 hours of testing in conjunction with the LED drivers, Auburn University performed additional tests on just the electrolytic capacitors in HTSL testing at 135°C [132]. These tests, which were terminated after 7,166 hours demonstrated a continued increase in ESR, which is best modeled with an exponential growth function, and continued decrease in capacitance, which is best modeled with an exponential decay function. The change in the capacitance and ESR of electrolytic capacitors can be traced to loss of electrolyte due to thermal effects and degradation in the oxide layer arising from stress cracking. The modeling of capacitance loss with an exponential decay function, as reported here, is supported by previous work [116; 131].

Similar experiments were performed on a different population of 10 LED drivers and electrolytic capacitors in the WHTSL environment of 8585. Full details of these experiments can be found in the literature [118], but will be summarized here. As shown in **Table 4D-12**, the degradation of the electrolytic capacitors was significantly less during WHTSL testing than in HTSL. In addition, there was no change in the luminous flux produced by the drivers after 5,352 hours of testing. However, the drivers exhibited various failure modes during testing ranging from metallization issues in film capacitors to pop-corning of ICs [118]. Based on these results, temperature alone had minimal effect on producing failures in SSL drivers, in agreement with findings discussed in Section 4C for LED lamps, while temperature-humidity studies could be used to identify potential reliability issues in SSL drivers.

Table 4D-12. Change in Capacitor Properties during 5,352 Hours of 8585 WHTSL Testing

Capacitor Number	Initial Capacitance (μF)	Rated Voltage (V)	Capacitance Change	ESR Change
1	220	35	−2.8%	+9%
2	33	350	+0.7%	+5%
3	33	350	+0.4%	+6%
4	22	50	−2.1%	+1%

Multi-State Multi-Channel Drivers

To continue the study of drivers alone, RTI initiated an investigation of two-stage single- and multi-channel drivers in 7575. Unlike the experiments described above, this study was an operational test with the drivers being powered on a one-hour on and on-hour off cycle. In performing these tests, the entire driver was placed inside the environment chamber and connected to an LED load equal to 90% of the rate capacity through external wires. The LED loads were placed outside the environmental chamber to eliminate any influence from LED aging. The properties of the drivers examined in this study are given in **Table 4D-13**. Full details on the results of these tests are available in the literature [105] and will be summarized here.

Table 4D-13. Properties of the Multi-stage Drivers Examined by RTI in a WHTOL Environment of 757

Product Number	Initial Power Consumption and Power Factor	Number of Channels
Driver-B	53.0 W, Power Factor = 0.99	1
Driver-C	42.7 W, Power Factor = 0.99	1
Driver-D	56.2 W, Power Factor = 0.99	1
Driver-E	140 W, Power Factor = 0.99	2
Driver-F	38.2 W, Power Factor = 0.99	4
Driver-G	48.0 W, Power Factor = 0.99	4

As part of this evaluation, three different commercial single-channel, two-stage driver products were tested in 7575. These drivers may be used in conventional luminaires such as troffers and streetlights, and they may also be used in TWL luminaires provided a separate driver is used for each LED channel. The performance of these SSL drivers as a function of exposure time in 7575 was monitored using photometric flicker and power measurements and a summary of findings is given in **Table 4D-14**. In general, minimal changes in both

electrical characteristics and flicker performance were found with these drivers after 2,250 hours of 7575. This finding provides clear evidence that properly designed LED drivers can withstand the harsh environment of 7575 for an extended period without showing any signs of degradation or aging.

Table 4D-14. Change in Electrical and Photometric Properties for Two-stage, One-channel Drivers[a]

	Driver B	Driver C	Driver D
Initial Power	53.0 W	42.7 W	56.2 W
Power after 2,250 hours of 7575	53.0 W	42.6 W	56.8 W
Initial Flicker Percentage	0.6%	0.2%	0.6%
Flicker Percentage after 2,250 hours of 7575	0.6%	0.2%	0.6%
Initial Flicker Frequency	1971 Hz	Not detected	122 Hz
Flicker Frequency after 2,250 hours of 7575	1971 Hz	Not detected	122 Hz

[a] Two samples of each product were tested.

In the final phase of this evaluation, three different commercial multi-channel, two-stage driver products were tested in 7575. Two samples of Driver F and Driver G were tested, but only one sample of Driver E due to its higher output power. For simplicity, only two channels on each driver were tested and approximately equal currents were supplied to each channel. This setting corresponds to roughly a mid-point CCT value in a TWL system. Separate LED assemblies were used for each channel with one driver channel connected to warm white LED assemblies and the second driver connected to cool white LED assemblies. LED modules, consisting of cool white and warm white LED assemblies, were used as electrical loads during testing, and these loads were placed external to the environmental chamber which enabled measurement of the flicker properties of the LEDs during 7575. The performance of these four-channel multi-stage drivers during WHTOL testing was monitored using photometric flicker and power measurements, and a summary of initial and final values of key parameters is given in **Table 4D-15**.

Table 4D-15. Change in Electrical and Photometric Properties for Multi-stage, Four-channel Drivers

	Driver E	Driver F	Driver G
Initial Power	140 W	38.2 W	48.0 W
Power after 2,250 hours of 7575	Failed	40.0 W	48.2 W
Initial Flicker Percentage	0.6%	23.9%	3.9%
Flicker Percentage after 2,250 hours of 7575	Failed	23.9%	3.7%
Initial Flicker Frequency	434 Hz	1440 Hz	300 Hz
Flicker Frequency after 2,250 hours of 7575	Failed	1453 Hz	300 Hz

Note: One sample of Driver E was tested and two samples of both Driver F and Driver G were tested.

In general, the performance of the multi-channel drivers changed more than the single-channel drivers in 7575. The lone sample of Driver-E failed after 1,750 hours of 7575. The temperatures of these drivers were monitored throughout this experiment and the moment of failure of Driver-E is shown in **Figure 4D-78**. Driver-E was the only driver that was on a 2-hour on and 2-hour off electrical cycle due to its thermal mass. The other drivers were switched hourly. When the experiment ended after 1,750 hours of exposures (roughly 73 days), the chamber was opened to cool down, but the devices continued to operate. It was during this time that Driver-E failed, roughly 30 minutes after it was turned on. The point at which failure can be observed in the temperature profile is shown by a black arrow in Figure 4D-78. Beyond this time Driver-E was clearly not working as the temperature did not increase when power was applied. The failure of Driver-E also had a temporarily impact on the temperature profiles of the other DUTs, but they soon returned to normal behavior.

At this point, a rudimentary electrical analysis was performed on Driver-E, and it continued to draw power after failure, albeit at a greatly reduced rate. An electrical examination on a Chroma Test Stand indicated that the first stage of Driver-E was operating correctly (i.e., the stage containing AC filtering). Since the unit was not providing sufficient voltage to turn-on the LED array, the point of failure was likely in the second stage. Unfortunately, the driver was potted so the analysis could not be performed in-house and the assistance of the driver manufacturer had to be enlisted for a more detailed analysis. Based on an analysis of the driver waveforms, the manufacturer traced the failure to film capacitors in the PFC circuit that formed part of the inductor-inductor-capacitor (LLC) resonant filter.

Figure 4D-78. Comparison of the Temperature Profile of Three Drivers during 7575

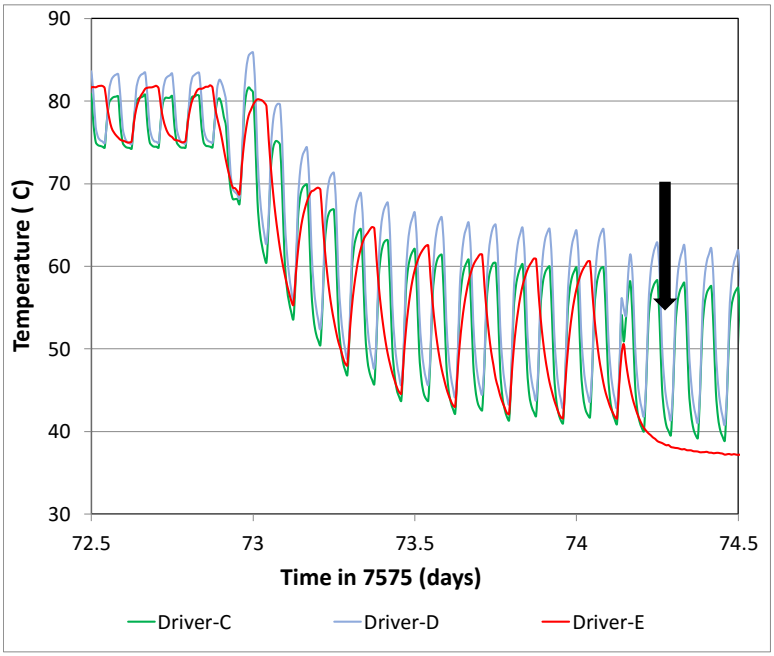

Driver-F and Driver-G exhibited minimal change in photometric flicker performance, in line with the behavior found with the single channel drivers. However, there was an increase in power consumption, especially with the two Driver-F samples, as 7575 exposure progressed. Based on our study on two-stage drivers in 6" downlights (to be discussed below), we believe that this increase in power consumption arises from increased impedance and capacitance in the device, potentially caused in part by parasitic effects in the switching MOSFETs. For Driver-F, there was also some evidence of the driver output being reduced by the controller chip during 7575 testing due to high temperatures. The integration of the switching MOSFETs into the same package as the controller IC resulted in a higher temperature at the controller chip package during 7575 than was found for other parts of the circuit. As a result of the more limited thermal performance of the integrated device, the integrated control chip scaled back the output power during 7575 for Driver-F to avoid overheating. The other driver products utilized separate controller ICs and MOSFETs so the thermal limitations were not a great and the devices operated at full power during 7575 testing.

Accelerated Testing of Drivers for 6" Downlights

A focus of this study was the behavior of 6" downlights in AST environments. Due to their small size, the degradation of both photometric and electric properties of these downlights could be studies simultaneously which helps to consolidate the cost and time necessary to perform these long-running experiments. For example, while some AST studies may only last 1–2 months, other studies may last a year or more. In this work, different populations of 6" downlights were subjected to 8585, 7575, and 6590. The units were powered during testing with AC voltage brought in from outside of the chamber, through a port in the side of the chamber, and connected to each luminaire. During room temperature testing of the downlights with the chamber controls off, the DUT temperature rose by 30°C or more as shown in Figure 4D-30. In contrast, during testing in WHTOL environments with the chamber on, the DUT temperature rise was in the 10°C to 15°C range, as shown in Figure 4D-31, indicating some influence from the chamber environmental controls on DUT temperature. A typical experimental arrangement is shown in **Figure 4D-79**, and a luminaire that failed during testing can be seen in the foreground surrounded by three other functional luminaires.

The electrical and photometric properties of the DUTs tested in this manner are given in Table 4D-12. After each 250-hour test interval, the luminaires were removed from the environmental chamber measured. Electrical property measurements included both device-level properties (e.g., power consumption, power factor, driver efficiency) and component level properties (e.g., capacitance, ESR, inductance, resistance, diode function). In addition, photometric flicker measurements were also taken later in the project when a handheld

flicker meter was purchased. These measurements provided some level of monitoring of device degradation before failure.

Figure 4D-79. Interior of Environmental Chamber Used to Simultaneously Expose both LEDs and Drivers in a Luminaire to AST Environments

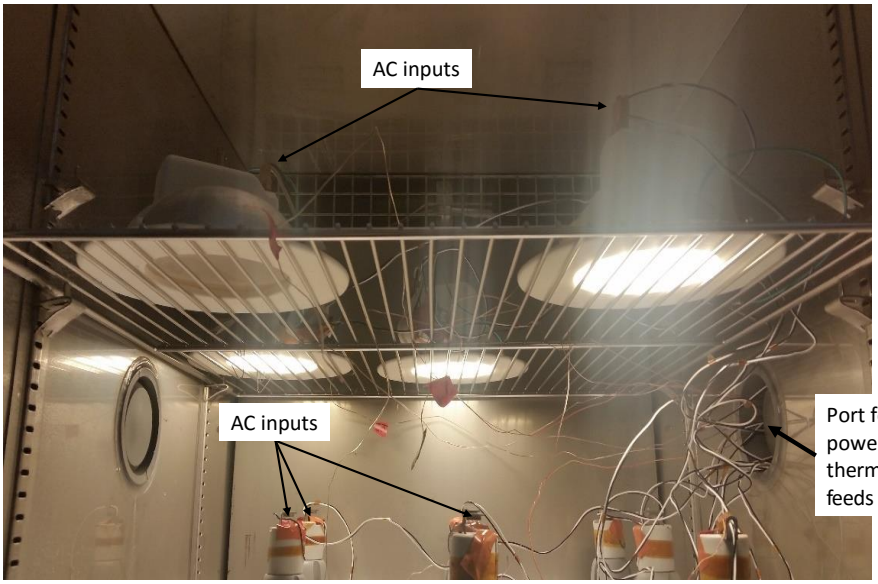

During the analysis of LED drivers, the criteria for failure were: (1) catastrophic failure with no light emission; (2) lumen maintenance failure with light emission less than 50% of the original value; or (3) excessive change in electrical properties, such as Power Factor. Lumen maintenance failures in excess of 50% were included in this list because such parametric failures often involve at least some component of driver degradation or failure. For example, this level of degradation could arise from reduced DC output voltages or the loss of DC voltage to some LEDs.

When luminaire failure occurred, the root cause was investigated using the procedure outlined in **Figure 4D-80**. The initial step in our failure analysis process was a basic check of electrical function including a measurement of power consumed, current, and power factor. The next step was a visual inspection of the luminaire to identify any parts that may have been damaged during the ALT. Examples of obvious damage that could be detected in this manner include electrolytic capacitors that were bulging or leaking, breeched film capacitors, discoloration of plastics or housing, and resistors that had obvious damage such as discoloration. At this point a deeper electrical analysis was performed, including a continuity check using a DMM that has the capability of checking diode performance. As part of this analysis, capacitance and equivalent series resistance of driver capacitors were

measured with a capacitance meter (Agilent U1733C) operating at 1 KHz. As a final step, the voltage across key components was measured using a DMM if the part is energized; however, care must be taken not to inadvertently short parts when performing a voltage check with the unit energized.

Figure 4D-80. Process Flow for Determining Failure Mechanisms of Luminaires Examined in this Study

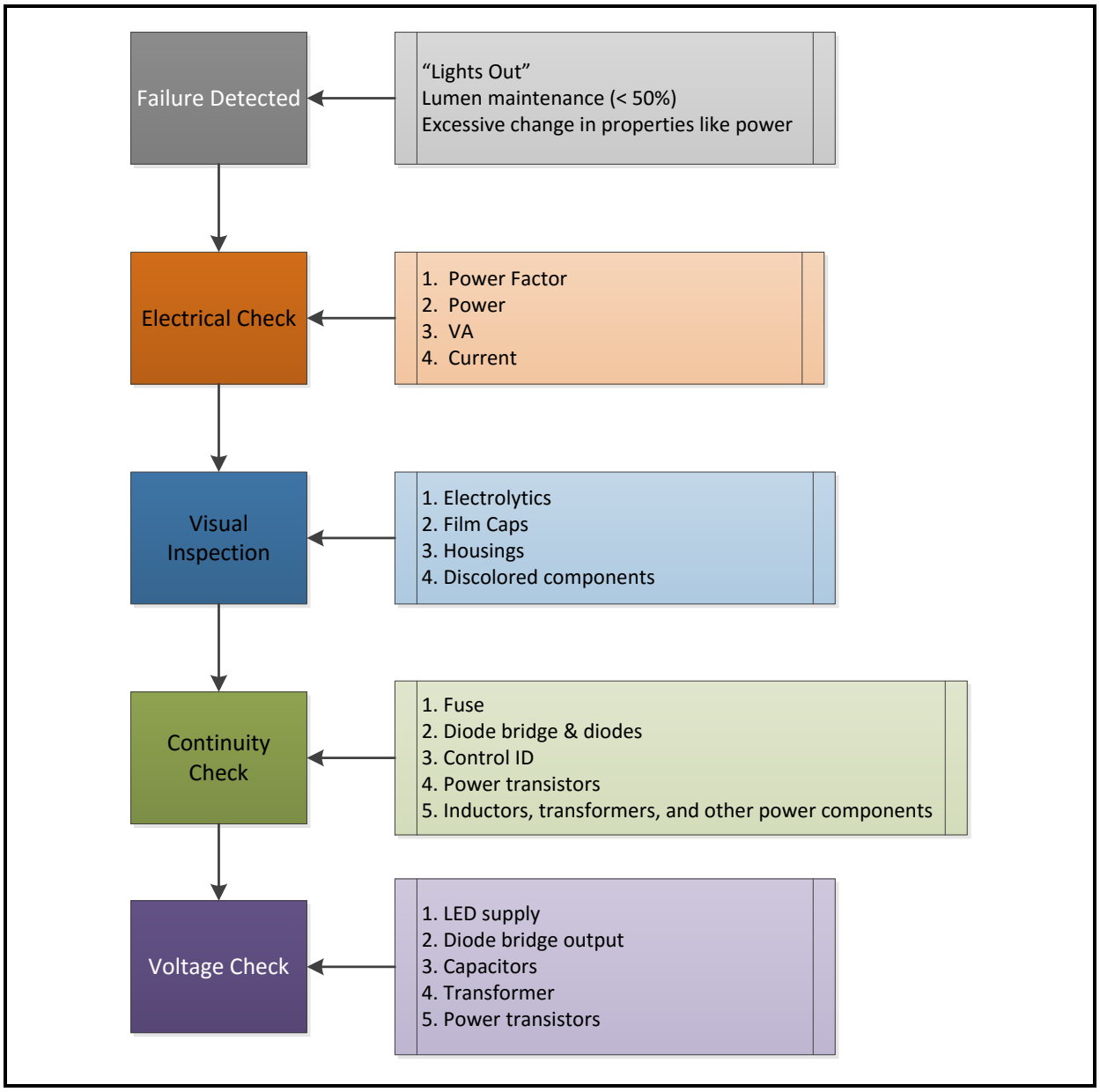

Separate populations of the luminaires examined in this study were tested in each of the WHTOL environments (i.e., 8585, 7575, and 6590). Utilizing the failure analysis protocol

given in Figure 4D-80, the failure sites of nearly all luminaire failures could be determined. In many cases, multiple components within the device failed during testing. One such common failure mode was an electrical short in the MOSFET which could result in large current surges that damage electrolytic capacitors, resistors, and fuses. A breakout of the common failure modes in 7575 is given in **Figure 4D-81**. In some luminaires, more than one component failed. In those instances, each failure was added to the tally, so some luminaires may have more than one part counted as a failure.

Figure 4D-81. Component Failure Distribution for 6" Downlights in 7575 Testing

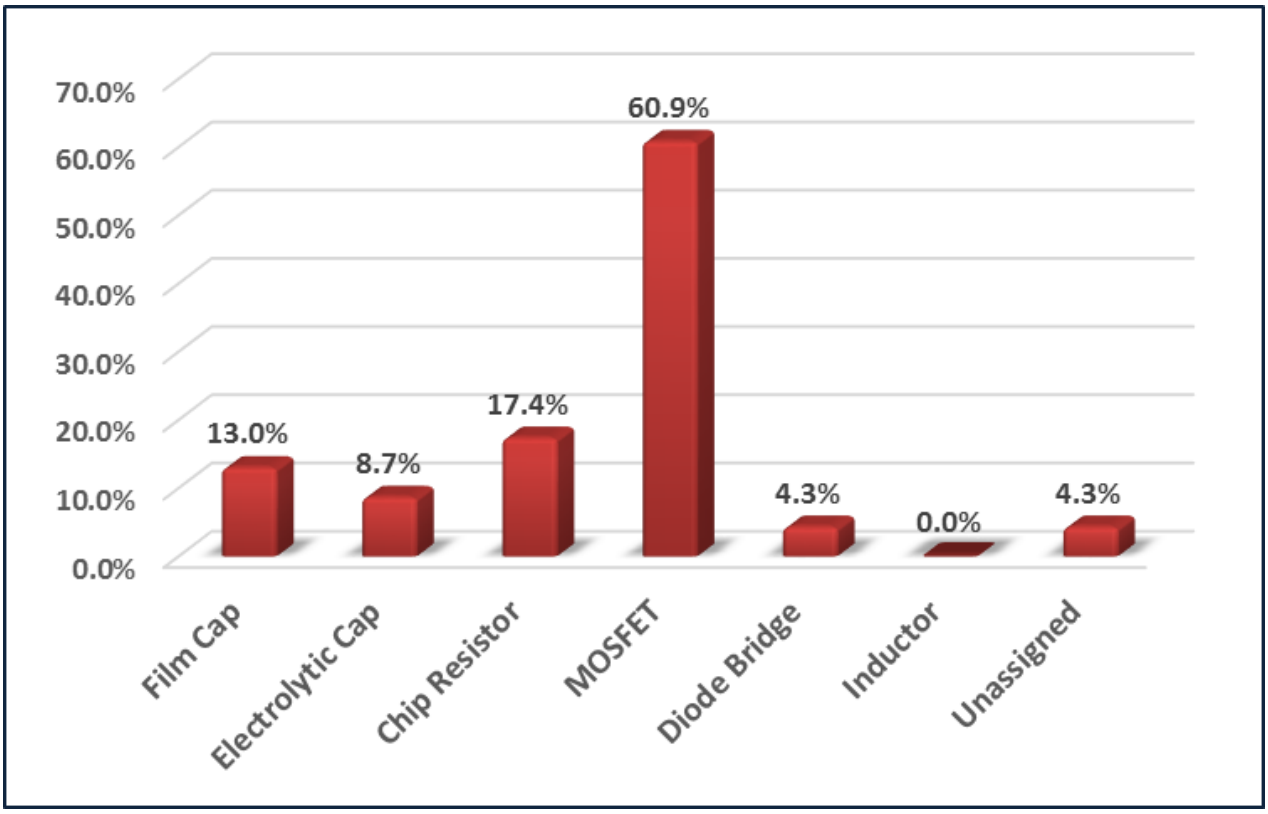

The test results from the WHTOL experiments can also be represented by the Weibull probability plot, shown in **Figure 4D-82** which was built assuming that both temperature and humidity has an impact on reliability. The data included in this plot encompasses all the 6” downlights that were tested in this study and provides an indication of the performance of similar products. This is essentially an industry-wide benchmark of reliability, and follows the same general approach that was used in the Hammer Test [37].

An alternative approach would be to consider the impact of temperature alone, and a temperature-only Weibull analysis is given in **Figure 4D-83**. At first, 8585 may be judged to be more accelerating that 7575, since the β value is higher in the temperature only

model. However, this analysis is skewed by a large number of early failures that occurred during the first 750 hours of testing. Consequently, there are significant deviations from the Weibull line for the last 30 percent of failures in 8585. In contrast, the 7575 data follows the temperature-only Weibull line for most of the range and. There are a minimal number of early failures during this test and DUT failures seem to be more randomly distributed about the Weibull line. Therefore, the 7575 line can be considered to be more representative of random failure that would occur in normal use. While the 7575 data may be a reasonable fit in a temperature only model, such an approach is insufficient to model the reliability of down lights in WHTOL testing since it ignores the impact of humidity. In addition, a temperature-only model cannot account for the higher failure rate of 6590 tests compare to 7575. Clearly, a temperature-only model is insufficient and other factors need to be considered. This work has already demonstrated that the impact of humidity on device aging can be higher than that of temperature alone and must be included in any model on product reliability [132, 133].

An analysis of the lifetime versus temperature and humidity stress levels reveals that both factors are important in describing lifetime and models that include both effects will be the most accurate [132; 133; 134]. The models shown in Figure 4D-82 were built taking both temperature and humidity into account and can be seen to provide a better fit to the data. The equation for lifetime based on a temperature-humidity model with an assumed Weibull lifetime distribution is:

$$\ln(L(T, RH)) = \ln(A) + \phi/T + b/RH \qquad (4D.1)$$

where

L = lifetime

T = temperature

RH = relative humidity

$\ln(A)$ = a constant

ϕ = a parameter related to temperature

B = a parameter related to humidity

An initial analysis of lifetime versus stress levels indicates that humidity has a larger impact on product lifetime than temperature so ignoring this effect in the lifetime model will ignore a major factor in product reliability.

Although many of the DUTs in the WHTOL tests closely followed the Weibull line for the test conditions, some of the early failures deviated from the Weibull lines for their respected test condition. This finding indicates that additional failure modes are occurring in these early

failures [36]. As an example, the failure rate for the first 5% of the samples in 75/75 was higher than that predicted by the Weibull line for this test condition. A higher failure rate is indicated by the higher local slope that would be present if a Weibull probability plot was constructed only for those points. Likewise, the first 25% of the failures in 85/85 occurred at a higher rate than accounted for in the Weibull model for these conditions. A similar number of premature failures were found for 6590. The causes of these premature failures are likely either manufacturing defects or poor products designs. This finding is consistent with our experimental observation that certain products had a greater tendency to fail premature than others during WHTOL testing.

Based upon the similarity of the slopes in the Weibull probability plot, similar failure mechanisms can be assumed to be operable under the different WHTOL conditions. This finding allows acceleration factors to be determined and for a projected use line to be constructed at any temperature and humidity. A projection for the case of 65°C and 45% RH is included in **Figure 4D-82** as a thick, dashed, green line. This condition was chosen for the baseline use state given the rise in DUT temperature found in the chamber measurements when no chamber controls are applied (see Figure 4D-30).

Figure 4D-82. Weibull Probability Plot Based on Temperature and Humidity Parameterization for 6" Downlights in WHTOL

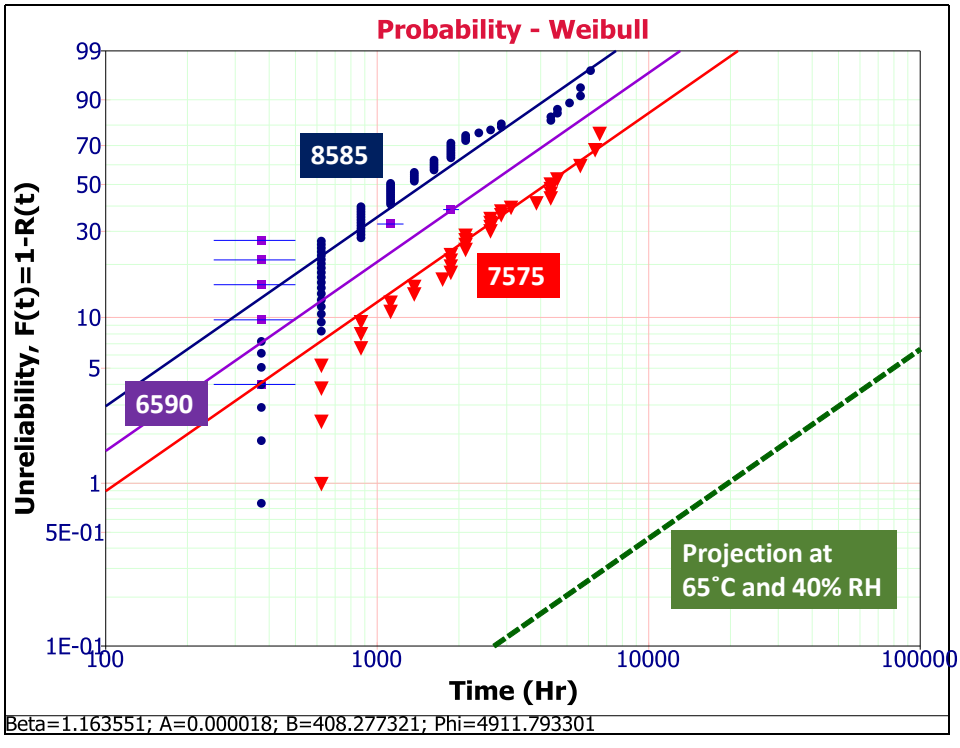

Figure 4D-83. Weibull Probability Plot for 6" Downlights Using Temperature as the only Parameter

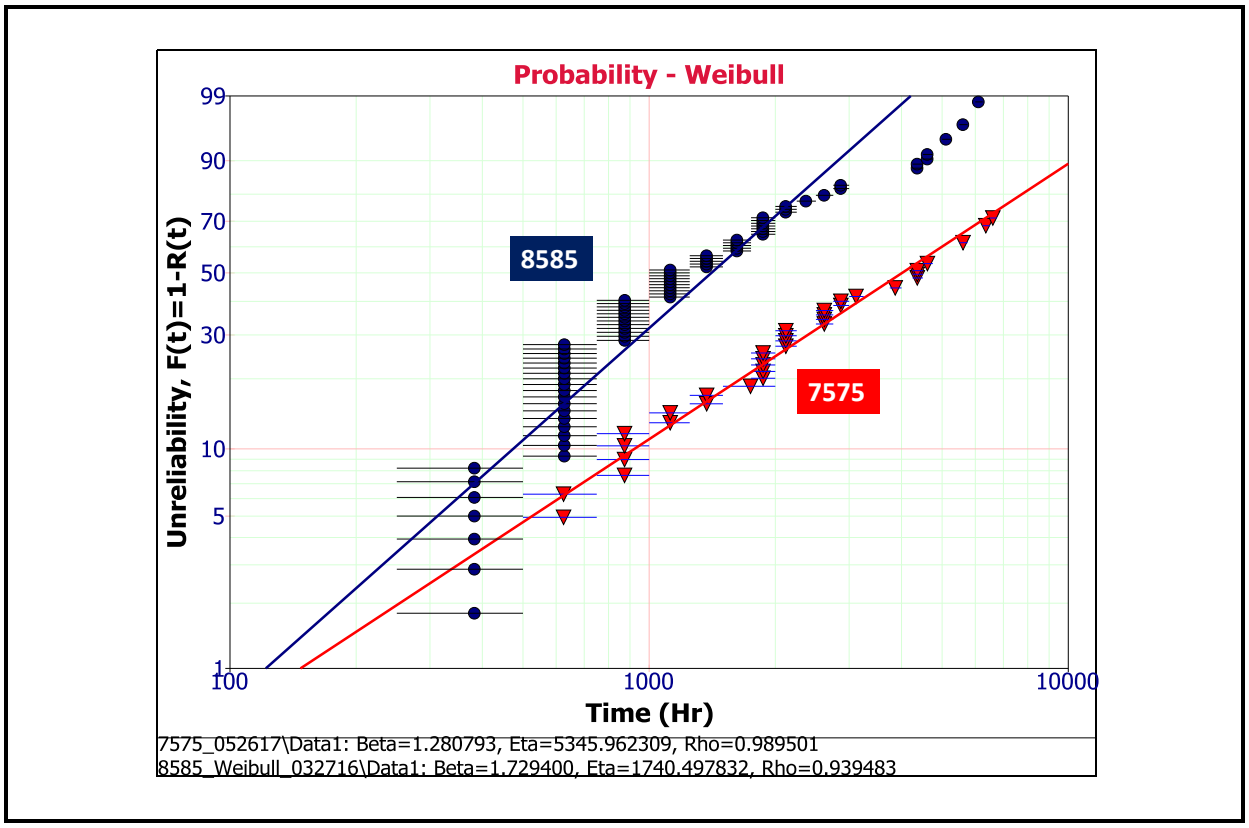

As part of this study, the power consumption of the DUTs was also measured at every 250 hours of exposure to the 7575 environment, and a graph of the average values for select products is given in **Figure 4D-84**. In all cases, the power consumption of the luminaire increased with the length of time in 7575; however, in examining the data, the observed behaviors seem to divide into two different groups. One group, consisting of the Lithonia Security Lamp, OptiLED Round150 WW, and OptiLED Round150 CW populations, displayed a rapid increase in power consumption followed by reaching an asymptotic value. A bounded exponential model of this behavior is shown in **Figure 4D-85** for the Lithonia Security Lamp, and an excellent, statistically significant fit was obtained with this type of model with R^2 = 0.764 and the Durbin-Watson statistic equally 2.503. It is worth noting that in some cases (e.g., OptiLED Round150 WW), DUTs nearing failure pulled down the overall population average, but the broader trend of bounded exponential behavior is still apparent. In contrast, the second group, consisting of the Cree CR6, Commercial Electric T65, LSG Glimpse Indirect, and Commercial Electrical FG-01942, exhibited a slow increase in power consumption over time. At least for the Cree CR6, the data indicates that there is also an upper limit to the extent of this power consumption increase. Consequently, we found that the power consumption of this group can be best modeled with a logistic function as also

shown in Figure 4D-85. This model was also found to be excellent fit to the data with a R^2 value of 0.959 and a Durbin-Watson statistic of 2.34.

The reason for these two different types of behavior is unknown. One conjecture that we are investigating is that devices that experience a rapid increase in power consumption, especially when first turned on, may be more susceptible to increases in impedance from resistors and connects. We are currently speculating that the longer-term nature of the power consumption increase in these products modeled with a generalized logistic function indicate that additional processes need to occur before these mechanism(s) responsible for the slow, bounded increase in power consumption become noticeable. It is possible that these processes involve slow-acting mechanisms such as contact corrosion or moisture diffusion into the body of a capacitor, inductor, or packaged IC [133].

Figure 4D-84. Average Power Consumption of Select Luminaires as a Function of Time in 7575

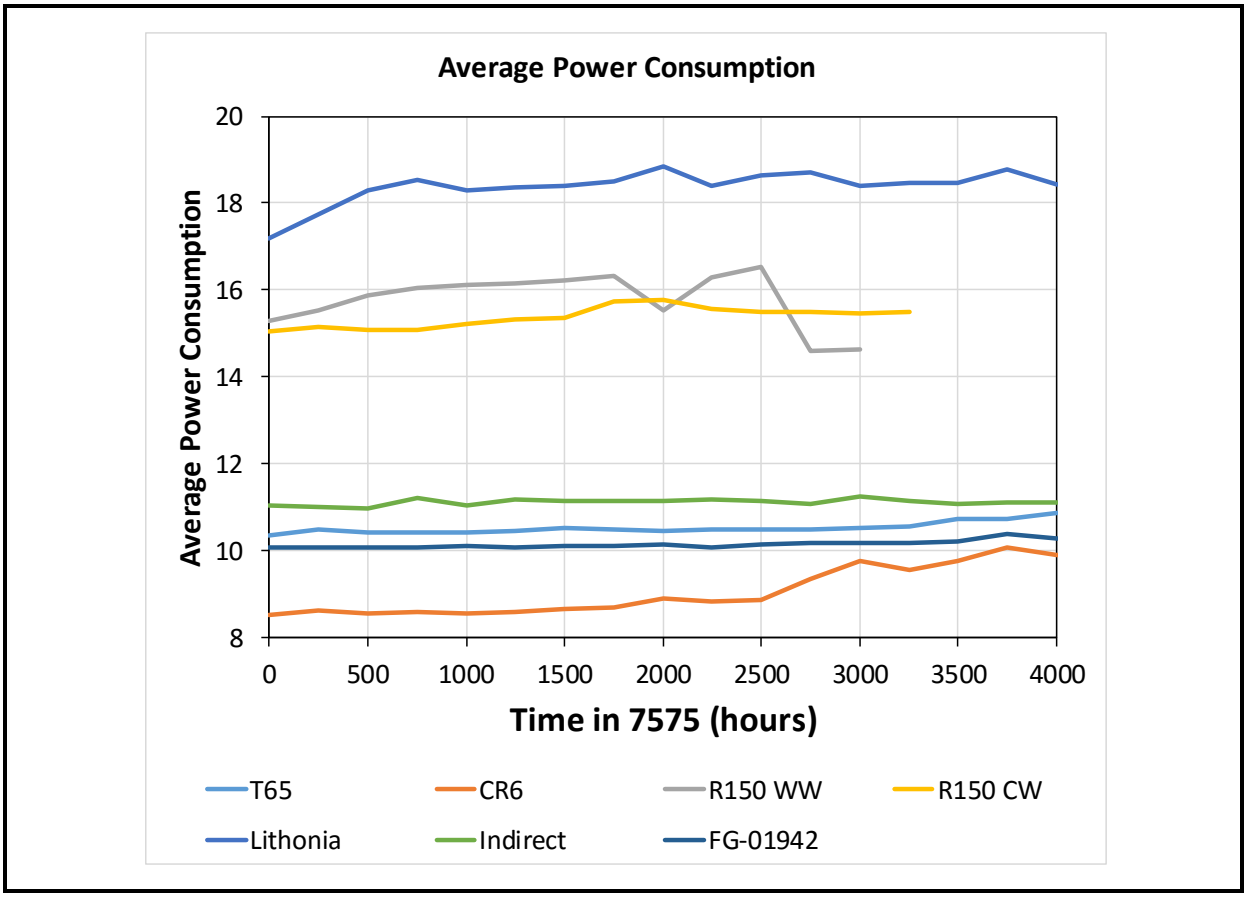

Figure 4D-85. Comparison of Data for Average Power Consumption and Appropriate Model for Two Luminaires Tested in this Study

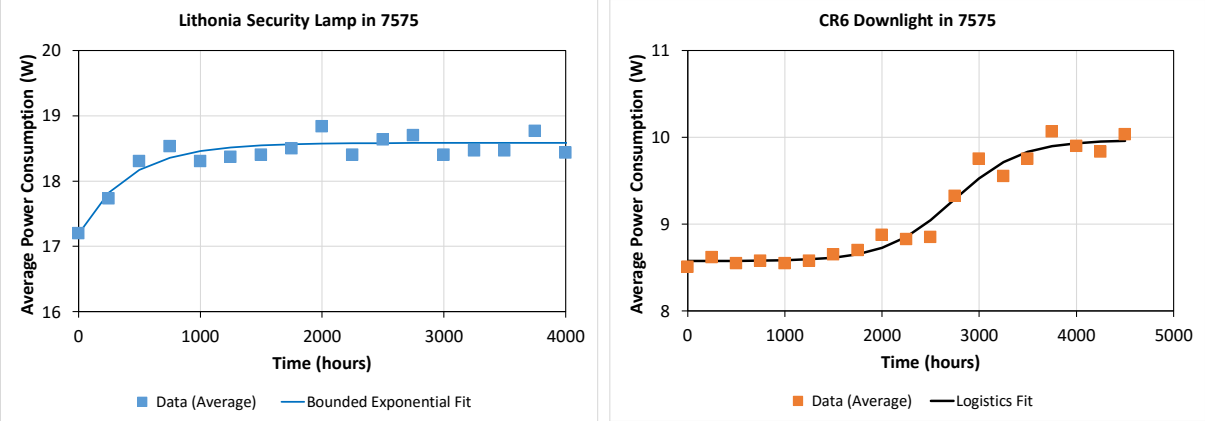

Note: For the bounded exponential model for the Lithonia Security Lamp, R^2 = 0.764 and the Durbin-Watson statistic is 2.503. For the logistic model for the CR6 downlight, R^2 = 0.959 and the Durbin-Watson statistic is 2.336.

A deeper investigation in the impact of WHTOL experience on the electrical performance of LED drivers was conducted. In performing this analysis, RTI contracted with Dr. Praneet Athalye of Buck-Boost, Ltd., a renowned developed of drivers for LED luminaires. Dr. Athalye used a Xitron 2802 two-channel power analyzer. The electrical analysis is shown in **Table 4D-16** and included measurement of the AC input power, DC output power, power factor, and THD. Photometric measurements were combined with the electrical measurements to determine the luminous efficacy (in lumens (lm) per watt).

Table 4D-16. Electrical Properties of LED Drivers and Controls after Operational Testing in 7575

Sample Description	WHTOL Test	Exposure Time (hours)	AC Input Power (W)	DC Output Power (W)	Power Loss (W)	Electrical Efficiency	Luminous Efficacy (lm/W)	Power Factor	THD
Lithonia Security Lamp	Unexposed	0	19.038	16.380	2.658	86.0%	76.4	0.81	65.6%
Lithonia Security Lamp	7575	6,000	20.437	17.000	3.437	83.2%	47.7	0.83	64.9%
Cree CR6	Unexposed	0	8.417	6.684	1.733	79.4%	71.3	0.85	57.0%
Cree CR6	7575	4,250	10.285	7.853	2.432	76.4%	51.9	0.87	55.3%
Cree CR6	7575	4,250	10.116	7.712	2.404	76.2%	51.1	0.89	47.9%
OptiLED Round150 (2700 K)	Unexposed	0	16.182	12.905	3.277	79.7%	41.2	0.99	10.3%

(continued)

Table 4D-16. Electrical Properties of LED Drivers and Controls after Operational Testing in 7575 (continued)

Sample Description	WHTOL Test	Exposure Time (hours)	AC Input Power (W)	DC Output Power (W)	Power Loss (W)	Electrical Efficiency	Luminous Efficacy (lm/W)	Power Factor	THD
OptiLED Round150 (2700 K)	7575	3,000	16.186	12.925	3.261	79.9%	29.2	1.00	9.9%
OptiLED Round150 (4000 K)	Unexposed	0	15.158	12.204	2.954	80.5%	51.4	0.99	10.4%
OptiLED Round150 (4000 K)	7575	3,250	16.064	12.270	3.795	76.4%	38.8	0.99	13.4%
Glimpse Indirect	Unexposed	0	11.039	9.479	1.559	85.87%	58.6	0.95	30.6%
Glimpse Indirect	7575	7,000	11.222	9.701	1.521	86.45%	45.8	0.95	31.3%
Glimpse Indirect	7575	7,000	11.602	10.026	1.577	86.41%	46.6	0.95	32.1%

This analysis confirmed that the total power consumption of the LED drivers increases with exposure to 7575. In addition, the DC output power of the drivers to the LEDs was also found to increase, but usually at a lower level than the AC power increase. As a result, the power losses in the driver also increased and electrical efficiency dropped by several percentage points in most cases. The electrical changes combined with the drop in luminous flux, which was measured separately with an integrating sphere, resulted in a sharp drop in luminous efficacy of the SSL devices after 7575 testing. Ironically, power factor remained largely unchanged as a result of 7575 exposure. This finding may be more of an indicator of the ability of the controller IC to maintain the power factor level than a indicator of the degradation of components in the power factor circuit. This topic will be discussed in more detail below with several case studies from RTI's test data.

Case Study Number 1—Lithonia Security Lamp

The Lithonia Security Lamp (Part Number OLAL-40K 120PE) is a general-purpose LED lamp sold through big box retailers. The unit is intended for outdoor use as a security lamp primarily in residential settings. The driver utilizes a flyback in the first stage and to provide electrical isolation of the AC mains from the DC output. To understand the changes in output current regulation induced by accelerated aging in WHTOL, the transistor switching waveforms of the MOSFET used in the Lithonia Security Lamp were recorded with an oscilloscope. The waveforms for an unexposed luminaire (i.e., control sample) and a second luminaire that had been exposed to 6,000 hours of 7575 are given in **Figure 4D-86**. When the gate of the MOSFET is switched to a higher voltage by the SMPS control IC, the drain

switches to a lower voltage and the source switches to a more positive one. In comparing the two waveforms, some oscillation of the source and drain voltages occur upon switching. These oscillations are common in flyback circuits and are quickly dampened. There is no oscillation on the gate signal since it originates from the controller IC. A comparison of the voltage oscillations (or ringing) demonstrates that they are similar in the unexposed and exposed DUTs.

Figure 4D-86. MOSFET Switching Waveform for Lithonia Security Lamp Samples Unexposed (left) and after 6,000 Hours of 7575 Exposure (right)

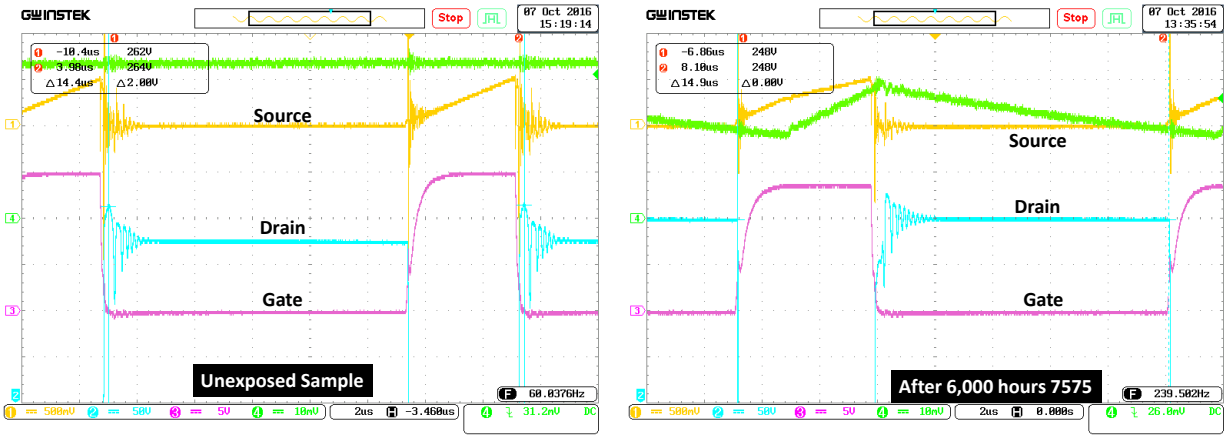

When the controller IC increases the gate voltage, this sets in action a series of voltage changes that switch the MOSFET into the on (i.e., conducting) state. When the gate voltage increases above the threshold voltage, the source voltage switches to a positive value and the drain switches to a lower voltage which enables current to flow through the component. As current flows through the source electrode, residual capacitance in the source structure is charged resulting in the slow, linear rise in source voltage shown in both DUTs. After one cycle, the controller IC switches the gate voltage off which also lowers the source voltage and raises the drain voltage above the source voltage effectively opening the switch. No current will flow in this state in a properly functioning MOSFET, although current will still flow in a failed MOSFET as shown in Figure 4D-64. In comparing the waveforms for the unexposed and exposed DUTs, the gate voltage is higher on the unexposed sample white the source voltage is roughly the same on the two. In addition, the time when the gate is switched to high voltage (i.e., the on state) is longer in the exposed sample than in the control. Both of these findings suggests that there is some degradation in the MOSFET and in the circuitry that feeds it. However, the luminaire continues to operate after 6,000 hours of 7575 exposure, albeit with lower efficiency and reduced luminous flux levels.

Case Study Number 2 – Cree CR6 Downlight

The Cree CR6 downlight (Part Number CR6 ECO-575L) is a general-purpose interior downlight sold through a big box retailer. The luminaire utilizes an integrated buck driver with a valley-fill circuit as part of the PFC network. Since this device was one of the most tested luminaires in this study, a detailed analysis was conducted on failure modes found in testing. A picture of the top of the driver is shown in **Figure 4D-87**. The MOSFET and other surface mount components are located on the bottom of the board. This circuit has some similarities with a reference design developed by National Semiconductor (subsequently acquired by Texas Instruments) and the circuit diagram of the reference design is given in **Figure 4D-88** [135, 136].

Figure 4D-87. Picture of the Top of the CR6 Driver PCB with Key Component Labeled

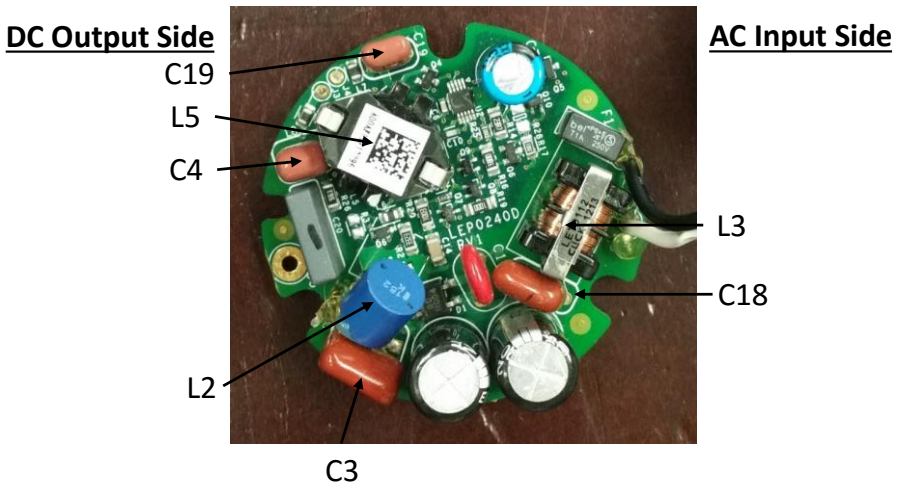

Figure 4D-88. Block Circuit Diagram of a Buck Driver Used in a 6" Downlight

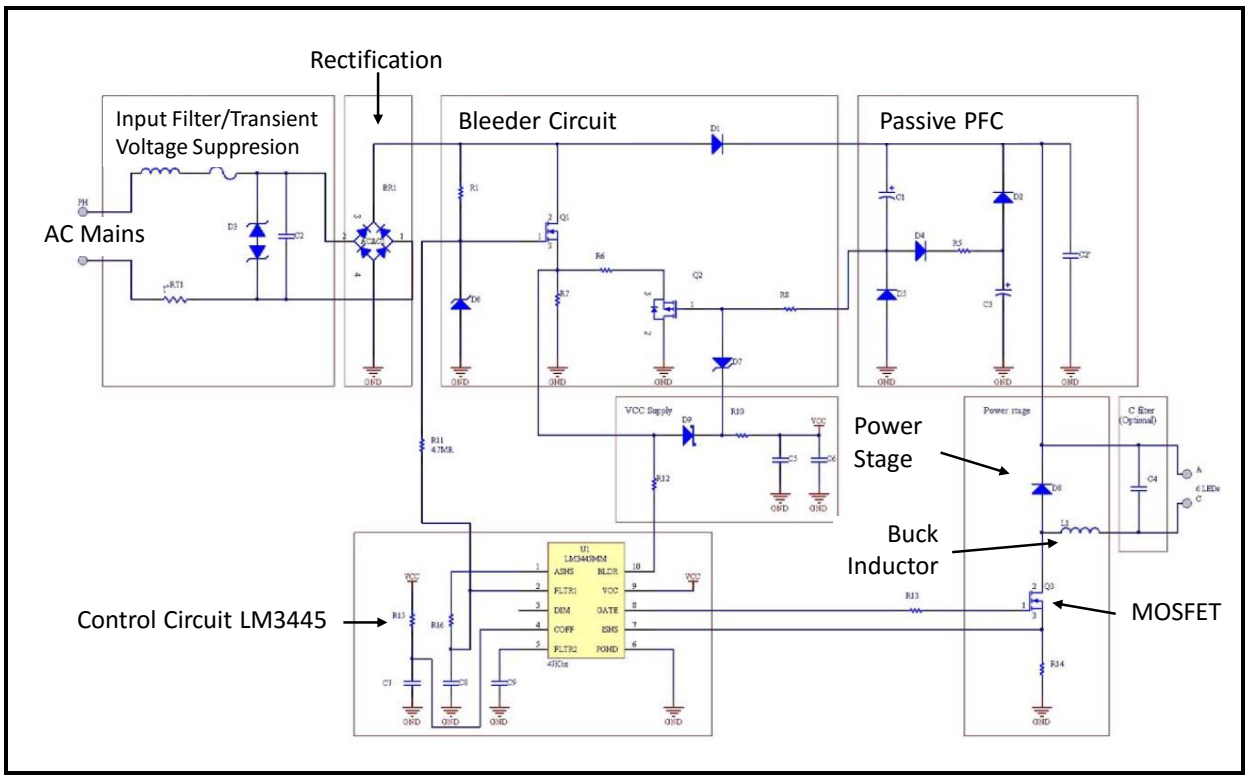

Note: Source [135, 136].

As part of the analysis of the degradation of the electrical circuit, the MOSFET switching waveforms were measured for an unexposed (i.e., control) luminaire and for a luminaire after 4,250 hours of 7575. The results for both are shown in **Figure 4D-89**. The unexposed sample exhibited a nearly ideal square wave switching waveform with sharp transitions during switching with practically no indications of overshot or ringing in the unexposed sample. As discussed above, capacitance on the source electrode produces a linear voltage increase when the MOSFET is switched on and current is flowing.

Figure 4D-89. MOSFET Switching Waveforms for CR6 Luminaires

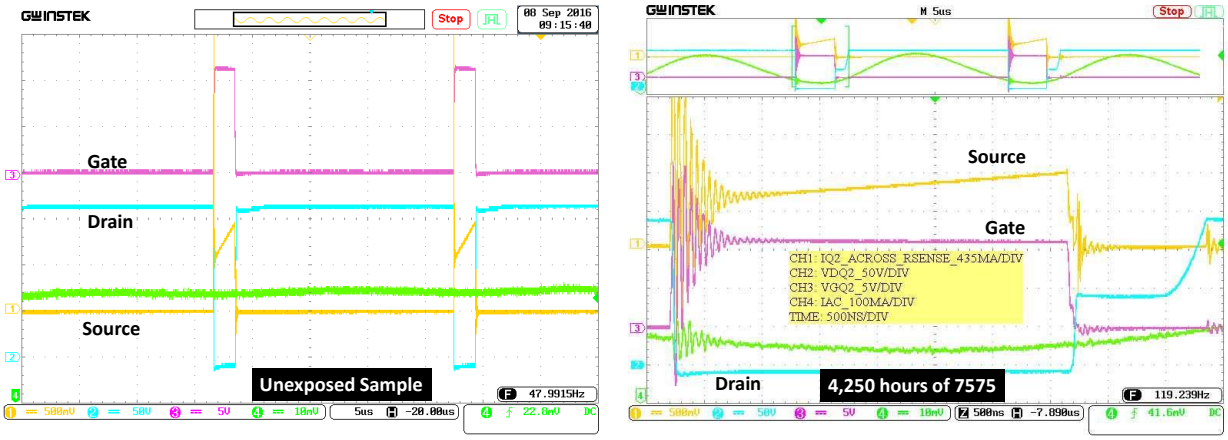

Note: An unexposed sample is shown on the left and a sample after 4,250 hours of 7575 is shown on the right.

In contrast, after 4,250 hours of exposure to the 7575 environment, significant degradation has occurred in the MOSFET and its feeder circuits. Instead of the source and gate switching waveforms being sharp, there is a significant amount of ringing in both when the device is turned on. The ringing produces large transient voltages that are up to twice that of the intended supply voltage. Similar voltage oscillations were also observed in samples exposed to just 2,000 hours of the milder 6590 environment, albeit at a much lower level, suggesting that this behavior is a failure mode that arises with aging. This effect may also be an explanation for the higher catastrophic failure rate found in 6590 compared to 7575. The presence of such voltage oscillations in the gate waveform is especially significant since the gate voltage is supplied by the controller IC. This ringing behavior suggest potential issues with the controller IC and the circuits (e.g., PFC) that are controlled by the main IC. When the device is turned off, the drain does not return directly to its off voltage, but instead has a short pause at a metastable voltage that is halfway between the two switching extremes. Both of these findings are suggestive of the loss of filtering in the supply circuits and degradation of the MOSFET. In addition, the large transients associated with the ringing will ultimately have an effect on the reliability of the MOSFET. Thus, although the device shown in Figure 4D-89 is still operational after 4,250 hours of AST, the degradation that has already occurred will ultimately produce device failure.

To find the root cause of this this ringing behavior and the associated transients, the capacitance and inductance of key components was measured for both an unexposed sample and two units that were exposed the 7575. The findings are presented in **Table 4D-17**. The capacitor and inductor on the AC input filter are barely affected by 7575 exposure and their values after 4,250 hours of testing are similar to those of the unexposed control. Likewise, the buck inductor (L5) on the output DC filter circuit seems to have change little after 4,250 hours of 7575. However, components of the PFC/EMI filtering

circuits have degraded significantly. Specifically, the capacitors that form the valley-fill circuit in the PFC stage seem to be affected this most. We believe that the reason that these capacitors are more susceptible to degradation is the across the line voltage drop produced by the rectifier circuit. Some of the capacitors (e.g., capacitor C3) experience the full voltage drop (~ 170 V peak voltage) while the voltage is divided for others. Consequently, the degradation of these components is thought to play a role in the transient oscillations found during MOSFET switching.

Table 4D-17. Comparison of the Properties of Key Components in the CR6 Luminaire

Component	Unexposed	DUT-140	DUT-143	Function
L3	18.52 mH	16.70 mH	20.05 mH	AC Input Filter
C18	67.19 nF	68.03 nF	68.74 nF	AC Input Filter
L2	1546.3 mH	1552.6 mH	12 mH	DC Side EMI/PFC
C3	456.7 nF	Replaced	147.33 nF	DC Side EMI/PFC
L5	983.5 mH	983.9 mH	975.8 mH	Buck Inductor
C4	790.4 nF	636.9 nF	Replaced	DC Output Filter
C19	457.0 nF	393.5 nF	111.35 nF	DC Output Filter

Note 1: The letters and numbers assigned to the key components refer to Figure 4D-87.

Note 2: Both DUT-140 and DUT-143 were subjected to 4,250 hours of 7575. Both devices were operational at the end of 7575 exposure and luminous flux of each was approximately 0.88.

Note 3: mH = millihenries and nF = nanoFarads

To understand the phenomena further, we investigated the capacitance and ESR and key capacitors during WHTOL testing. These measurements were taken with the capacitor still attached to the circuit and may be affected by readings from nearby components. In this test, capacitor C3 (see Figure 4D-87) consistently displayed a large increase in ESR and a corresponding large decrease in capacitance. Since this component sits across the output of the rectifier, it receives the full, unfiltered output of the rectifier stage. Although not apparent from the light output of this device, the degradation in this component and its impact on the other components in the PFC circuit eventually produce the transient ring waveforms shown in Figure 4D-89 that will stress the MOSFET and ultimately result in its failure. Consequently, the explanation for the delay in power supply increase found for this device (see Figure 4D-85) is the time necessary for component degradation to reach a sufficient level to have an impact and to begin propagating through the system.

Case Study Number 3—Commercial Electric T-65

The Commercial Electric T-65 is also a 6” downlight sold by a big box retailer and intended for residential applications. In contrast to the Cree CR6, this device contains a two-stage driver with the first stage being a flyback circuit to provide electrical isolation of the mains

voltage from the DC output. The second stage, which provides power to the LEDs, is a buck circuit. A picture of the top of the driver board is shown in **Figure 4D-90** with some key components and driver stages identified. The backside of the PCB contains various SMT components including the controller ID and the diode bridge.

Figure 4D-90. Top View of the Driver PCB for the Commercial Electric T-65 Downlight

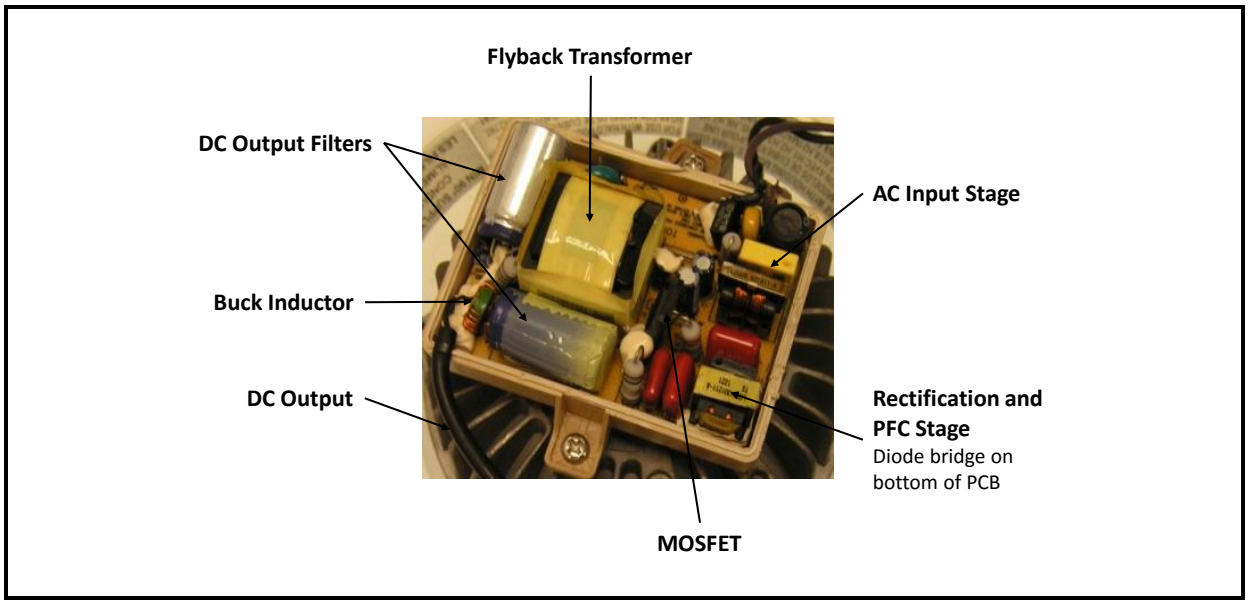

The switching waveforms of the device MOSFET were also studied and a comparison of the findings for an unexposed DUT and one following 4,000 hours of 7575 is shown in **Figure 4D-91**. Additional details on this testing can also be found in the literature [105].

Figure 4D-91. Comparison of the MOSFET Switching Waveforms for the Commercial Electric T-65 Downlight

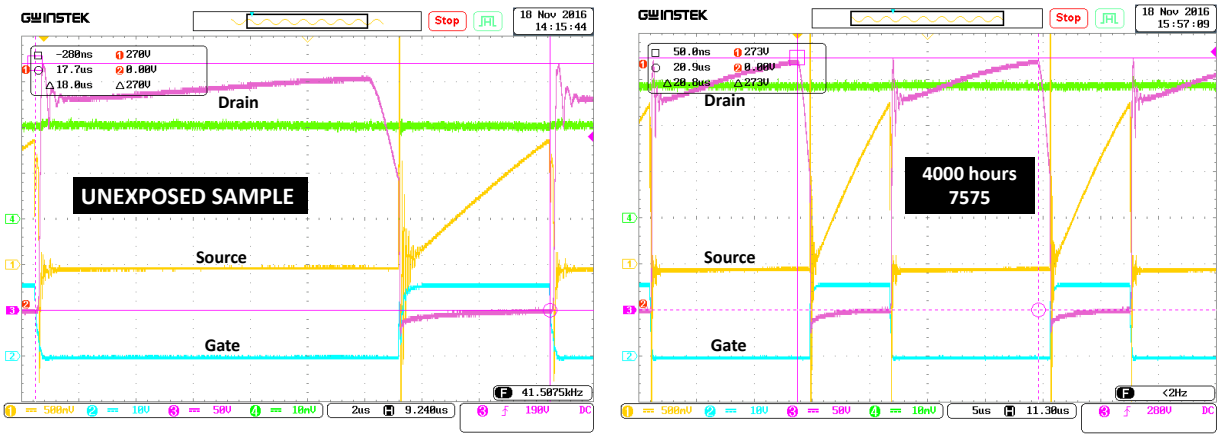

Note: The unexposed DUT is shown on the left and a different DUT subjected to 4,000 hours of 7575 is shown on the right.

A close comparison of these two waveforms identified the changes in device performance caused by degradation of the circuit and also identified another possible failure mechanism in SSL drivers. Since this is a flyback circuit, there is some residual ringing of the voltages that occurs upon switching as also shown in Figure 4D-86. However, this ringing appears to vary little between the unexposed and exposed DUTs and is quickly dampened which suggests proper circuit function. A close comparison of the gate waveform indicates that there is little if any change in the gate signal. In addition, there is no ringing in the gate signal since it originates from the controller IC. These findings provide an indication that the WHTOL environment has little impact on the controller IC in this design.

However, there were some differences in the switching waveforms of the source and drain between the unexposed and 7575-exposed DUTs. Specifically, the source waveform switched at a higher voltage after 7575 exposure resulting in faster charging of residual capacitance in the source structure. In addition, when the MOSFET is switched off and the drain is switched to a high voltage, a significant amount of parasitic capacitance at the drain electrode has been introduced into the circuit of the DUT exposed to 4,000 hours of 7575. This parasitic capacitance is evidenced by the slow, linear increase in the drain voltage after switching to the off state. Just before the MOSFET is switched back to the on state, the drain voltage can be seen to be higher than in the unexposed samples. Taken together, these changes in the source and drain waveforms indicate degradation in the MOSFET in the form of higher parasitic capacitances. Thus, although the device is still operating after 4,000 hours of testing, significant degradation in key components has already occurred and device failure is likely in the near future.

References

1. Illuminating Engineering Society. 2011. *TM-21-11: Projecting long term lumen maintenance of LED light sources*. New York, NY: Illuminating Engineering Society.

2. Illuminating Engineering Society. 2008. *IES LM-80-08, approved method: Measuring lumen maintenance of LED light sources*. New York, NY: Illuminating Engineering Society.

3. r-Project.org. *The R Project for statistical computing.* 2017. Available from http://www.r-project.org/.

4. Illuminating Engineering Society. 2015. *IES LM-80-15, approved method: Measuring luminous flux and color maintenance of LED packages, arrays, and modules*. New York, NY: Illuminating Engineering Society.

5. van Driel, W.D., M. Schuld, B. Jacobs, F. Commissaris, J. van der Eyden, and B. Hamon. 2015. Lumen maintenance predictions for LED packages using LM80 data. In *Proceedings of the 2015 16th International Conference of Thermal, Mechanical and Multiphysics Simulation and Experiments in Microelectronics and Microsystems (EuroSimE 2014)*.

6. van Driel, W.D., M. Schuld, B. Jacobs, F. Commissaris, J. van der Eayden, and B. Hamon. 2016. Lumen maintenance predictions for LED packages. *Microelectronics and Reliability* 63:39-44.

7. Yu, H.-F., and S.-T. Tseng. 1998. On-line procedure for terminating an accelerated degradation test. *Statistical Acta* 8 (1):207.

8. Bobashev, G., N. Baldasaro, K. Mills, and J.L. Davis. 2016. An efficiency decay model for lumen maintenance. *IEEE Transactions on Device and Materials Reliability* 16 (3):277-81. doi: 10.1109/TDMR.2016.2584926

9. Petrucci, R.H., W.S. Harwood, and F.G. Herring. 2002. *General Chemistry (8th ed.)*. Englewood Cliffs, NJ: Prentice-Hall.

10. Bokshtein, B.S., M.I. Mendelev, and D.J. Srolovitz, (Eds.). 2005. *Thermodynamics and kinetics in materials science: A short course*. Oxford, United Kingdom: Oxford University Press.

11. Crank, J. 1980. *The mathematics of diffusion*. Oxford, United Kingdom: Oxford University Press.

12. Greenwood, M. 1926. The natural duration of cancer. In *Reports of Public Health and Related Subjects, Vol. 33*. London: HMSO.

13. Tan, C.M., and P. Singh. 2014. Time evoluation degradation physics in high power white LEDs under high temperature-humidity conditions. *IEEE Transactions on Device and Materials Reliability* 14:742.

14. Zhang, J., and G.Q. Zhang. 2017. Advances in LED solder joint reliability testing and prediction. In *Solid-State Lighting Reliability: Components to Systems, Vol. 2*, edited by W. D. van Direl, X. J. Fan and G. Q. Zhang. New York, NY: Springer.

15. Meneghini, M., A. Tazzoli, G. Mure, G. Meneghesso, and E. Zanoni. 2010. A review on the physical mechanisms that limit the reliability of GaN-based LEDs. *IEEE Transactions on Electron Devices* 57:108-18.

16. Khalilullah, I., T. Reza, L. Chen, A.K.M. Moyanem, H. Mazumder, J. Fan, C. Qian, G. Zhang, and X. Fan. 2017, April 2-5. In situ characterization and moisture absorption and hygroscopic swelling of silicone-phosphor composite film and epoxy mold compound in LED packaging. In *Proceedings of the 18th International Conference on Thermal, Mechanical and Multi-Physics Simulation and Experiments in Microelectronics and Microsystems (EuroSimE 2017)*. Dresden, Germany.

17. Narendran, N., and Y. Gu. 2005, August 22. Life of LED-based white light sources. IEEE/OSA. *Journal of Display Technology* 1:167-71.

18. Koh, S., W. van Driel, and G.Q. Zhang. 2011, April. Degradation of epoxy lens materials in LED systems. In *Proceedings of the 12th International Conference of Thermal, Mechanical and Multi-Physics Simulation and Experiments in Microelectronics and Microsystems (EuroSimE April 18-10, 2011)*. Linz, Austria: IEEE Conference Publications, 1/5–5/5.

19. Lu, G., M.Y. Mehr, W. van Driel, X. Fan, J. Fan, K.M.B. Jansen, and G.Q. Zhang. 2015. Color shift investigations for LED secondary optical designs: Comparison between PBA-PC and PMMA. *Optical Materials* 45:37-41.

20. Davis, J.L., K.C. Mills, M. Lamvik, R. Yaga, S.D. Shepard, J. Bittle, N. Baldasaro, E. Solano, G. Bobashev, C. Johnson, and A.E. Evans. 2014, April 7-9. System reliability for LED-based products. In *Proceedings of the 2014 15th International Conference of Thermal, Mechanical and Multiphysics Simulation and Experiments in Microelectronics and Microsystems (EuroSimE 2014)*. Ghent, Belgium: IEEE Conference Publications, 1–7.

21. Lu, G., W.D. van Driel, X. Fan, M.Y. Mehr, J. Fan, K.M.B. Jansen, and G.Q. Zhang. 2015. Degradation of microcellular PET reflective materials used in LED-based products. *Optical Materials* 49:79-84.

22. Diepens, M., and P. Gijsman. 2007. Photodegradation of bisphenol A polycarbonate. *Polymer Degradation & Stability* 92:397-406.

23. Diepens, M., and P. Gijsman. 2008. Photo-oxidative degradation of bisphenol A polycarbonate and its possible initiation processes. *Polymer Degradation & Stability* 93:1383-8.

24. Mehr, M.Y., W.D. van Driel, H. Udono, and G.Q. Zhang. 2014. Surface aspects of discolouration in Bisphenol A Polycarbonate (BPA-PC) used as lens in LED-based products. *Optical Materials* 37:155-9.

25. Koh, S., H. Ye, M.Y. Mehr, J. Wei, W.D. van Driel , L.B. Zhao, and G.Q. Zhang. 2014. Investigation of color shift of LED-based lighting products. In *Proceedings of the 2014 15th International Conference of Thermal, Mechanical and Multi-Physics Simulation and Experiments in Microelectronics and Microsystems (EuroSimE April 7-9, 2014)*. Ghent, Belgium: IEEE Conference Publications, 1–5.

26. Davis, J.L., M. Lamvik, J. Bittle, S. Shepherd, R. Yaga, N. Baldasaro, E. Solano, and G. Bobashev. 2013. Insights into accelerated aging of SSL luminaires. In *Proceedings of SPIE 8835: LED-based Illumination Systems,* pp. 88350L-1–88350L-10. San Diego, CA.

27. Davis, J.L., J. Young, and M. Royer. 2016, February. *CALiPER Report 20.5: Chromaticity Shift Modes of LED PAR38 Lamps Operated in Steady-State Conditions* (prepared for the U.S. Department of Energy, Report Number PNNL-25201).

28. Tuttle, R. 2015, February 24. *LED System Lifetime and Reliability: LED Components*. Presented at the Strategies in Light conference, Las Vegas, NV.

29. Huang, J., D.S. Golubovic, S. Koh, D. Yang, X. Li, X. Fan, and G.Q. Zhang. 2015. Degradation mechanisms of mid-power white-light LEDs under high-temperature-humidity conditions. *IEEE Transactions on Device and Materials Reliability* 15 (2):220-8.

30. Yeh, C.-W., W.-T. Chen, R.-S. Liu, S.-F. Hu, H.-S. Sheu, J.-M. Chen, and H.T. Hintzen. 2012. Origin of thermal degradation of Sr(2-x)Si5N8:Eu(x) phosphors in air for light-emitting diodes. *Journal of the American Chemical Society* 134 (34):14108-17.

31. Lin, C.C., and R.-S. Liu. 2014. Thermal effects in (oxy)nitride phosphors. *Solid of Solid State Lighting* Vol. 1.

32. Wang, C.-Y. 2014. Thermal degradation of the green-emitting SrSi2O2N2:Eu2+ phosphor for solid state lighting. *Journal of Materials Chemistry. C, Materials for Optical and Electronic Devices* 2:2735-242.

33. Davis, J.L., K. Mills, M. Lamvik, C. Perkins, G. Bobashev, J. Young, R. Yaga, and C. Johnson. 2017. Understanding and controlling chromaticity shift in LED devices. In *Proceedings of the 18th International Conference on Thermal, Mechanical and Multi-Physics Simulation and Experiments in Microelectronics and Microsystems (EuroSimE 2017)*. Dresden, Germany.

34. EnergyStar. EnergyStar Program Requirements for Luminaires: Partner Requirements, version 2.0. EnergyStar 2015, May. Available from https://www.energystar.gov/sites/default/files/Luminaires%20V2%200%20Final_0.pdf.

35. Brentschneider, E. 2017. *Models for color point stability of LEDs: An introduction to differential chromaticity analysis*. Presented at the 2017 Strategies in Light conference, Santa Clara, CA.

36. Nelson, Wayne, B. 2004. A*ccelerated testing: statistical models, test plans, and data analysis*. Hoboken, NJ: John Wiley & Sons.

37. RTI International. *Hammer testing findings for solid-state lighting luminaires* (prepared for the U.S Department of Energy) 2013, December. Available from https://www1.eere.energy.gov/buildings/publications/pdfs/ssl/hammer-testing_Dec2013.pdf.

38. Koh, S., C. Yuan, B. Sun, B. Li, X. Fan, and G.Q. Zhang. 2013. *Product level accelerated lifetime test for indoor LED luminaires*. Presented at the 14th International Conference on Thermal, Mechanical and Multi-Physics Simulation and Experiments in Microelectronics and Microsystems (EuroSimE 2013), Wroclaw, Poland.

39. Tuttle, R., and M. McClear. 2014, February. Understanding the true cost of LED choices in SSL systems. *LEDs Magazine* (Issue 67):43.

40. Davis, J.L., A. Smith, T. Clark, K. Mills, and C. Perkins. 2017. *Lifetime predictions for dimmable two-channel tunable white LEDs*. 2017 16th Intersociety Conference on Thermal and Thermomechanical Phenomena in Electronic Systems, Orlando, FL.

41. EIA/JEDEC. 1997, April. *Standard test method A101-B: Steady state temperature humidity bias life test*.

42. Wu, B., X. Luo, Z. Zhao, and S. Liu. 2011. *Effect investigation of delamination on optical output of high power LEDs*. Presented at the International Conference on Electronic Packaging Technology and High Density Packaging (pp. 1072–1076).

43. Luo, X., B. Wu, and S. Liu. 2010. *Effects of moist environments on LED module reliability*. Presented at the 3rd Electronic System-Integration Technology Conference (ESTC). doi: 10.1109/ESTC.2010.5642942

44. Luo, X., B. Wu, and S. Liu. 2010. Effect of moist environments on LED module reliability. *IEEE Transactions on Device and Materials Reliability* 10 (2):182-6.

45. Tan, C.M., B.K. Chen, X. Li, and S.J. Chen. 2012. Rapid light output degradation of GaN-based packaged LED in the early stage of humidity test. *IEEE Transactions on Device and Materials Reliability* 12 (1):44-8.

46. Lall, P., H. Zhang, and J.L. Davis. 2016. *A comparison of temperature and humidity effects on phosphor converted LED packages and the prediction of remaining useful life with state estimator*. Presented at the Intersociety Conference on Thermal and Thermomechanical Phenomena in Electronic Systems (iTHERM2016).

47. Lall, P., H. Zhang, and J.L. Davis. 2015. *Failure mechanisms and color stability in light-emitting diodes during operation in high-temperature environments in presence of contaminations*. Presented at the 2015 Electronic Components and Technology Conference (pp. 1624–1632)

48. Tsai, C.-C., C.-H. Chung, J. Wang, W.-H. Cheng, M.-H. Chen, J.-S. Liou, . . . , and W.H. Cheng. 2010. *High thermal stability of high-power phosphor based white-light-emitting diodes employing Ce:YAG-doped glass*. Presented at the Electronic Components and Technology Conference (pp. 700–703).

49. Wang, J., C.-C. Tsai, W.-C. Cheng, M.-H. Chen, C.-H. Chung, and W.-H. Cheng. 2011. High thermal stability of phosphor-converted white light-emitting diodes employing Ce:YAG-doped glass. *IEEE Journal of Selected Topics in Quantum Electronics* 17 (3):741-6.

50. Tsai, C.-C., J.-S. Liou, W.-C. Cheng, C.-H. Chung, M.-H. Chen, J. Wang, and W.-H. Cheng. 2011. *High humidity resistance of high power white-light-emitting diode modules employing Ce:YAG doped glass*. Presented at the Electronic Components and Technology Conference (pp. 626–630).

51. Wang, J.-S., C.-C. Tsai, J.-S. Liou, W.-C. Cheng, S.-Y. Huang, G.-H. Chang, and W.-H. Cheng. 2012. Mean-time-to-failure evaluations of encapsulation materials for LED package in accelerated thermal tests. *Microelectronics Reliability* 52 (5):813-7.

52. Tuttle, R. 2017. *Design considerations with LED package primary optics.* Presented at the DOE SSL R&D Workshop, Long Beach, CA. Available from https://energy.gov/sites/prod/files/2017/02/f34/tuttle_optics_longbeach2017.pdf.

53. Sun, B., L. Zhao, T. Wei, X. Yi, Z. Liu, G. Wang, and J. Li. 2013. Shape designing for light extraction enhancement bulk-GaN light emitting diodes. *Journal of Applied Physics* 113:243104.

54. Lall, P., H. Zhang, and J.L. Davis. 2017. *Color shift analysis and modeling of high power warm white pcLED under high temperature and high humidity environment*. Presented at the Intersociety Conference on Thermal and Thermomechanical Phenomena in Electronic Systems (iTHERM2017), Orlando, FL.

55. Zhang, H. 2017. Failure modes analysis and life prediction modeling of phosphor converted white light emitting diode under harsh conditions (Unpublished doctoral dissertation), Auburn University, Auburn, AL.

56. Energy Star. 2014. Energy Star® TM-21 Calculator 2014 [cited Aug 28 2014]. Available from https://www.energystar.gov/products/spec/luminaires_specification_version_2_0_pd

57. Pacific Northwest National Laboratory. 2013, October. *CALiPER Report 20.1: Subjective Evaluation of Beam Quality, Shadow Quality, and Color Quality of LED PAR38 Lamps* (prepared for the U.S. Department of Energy).

58. Pacific Northwest National Laboratory. 2014, March. *CALiPER Report 20.2: Dimming, Flicker, and Power Quality Characteristics of LED PAR38 Lamps* (prepared for the U.S. Department of Energy, Report Number PNNL-SA-23263).

59. Pacific Northwest National Laboratory. 2014, December. *CALiPER Report 20.3: Robustness of LED PAR38 Lamps* (prepared for the U.S. Department of Energy, Report Number PNNL-SA-23971).

60. Pacific Northwest National Laboratory. 2014, December. *CALiPER Report 20.4: Lumen and Chromaticity Maintenance of LED PAR38 Lamps* (prepared for the U.S. Department of Energy, Report Number PNNL-SA-23988).

61. Pacific Northwest National Laboratory. 2014, February. *CALiPER Report 3: Retail Lamps Study 3* (prepared for the U.S. Department of Energy, Report Number PNNL-SA-23132).

62. Pacific Northwest National Laboratory. 2014, December. *CALiPER Report 3.1: Dimming, Flicker, and Power Quality Characteristics of LED A Lamps* (prepared for the U.S. Department of Energy, Report Number PNNL-SA-2394).

63. Pacific Northwest National Laboratory. 2014, December. *CALiPER Report 3.2: Lumen and Chromaticity Maintenance of LED A Lamps Operated in Steady-State Conditions* (prepared for the U.S. Department of Energy, Report Number PNNL-SA-23984).

64. Poplawski, M.E., M.R. Ledbetter, and M.A. Smith. *L-Prize® Stress Testing of the Philips 60W Replacement Lamp Entry* (prepared for the U.S. Department of Energy) 2012, April. Available from http://www.lightingprize.org/pdfs/lprize_60w-stress-testing.pdf.

65. Gordon, K.L., R.P. Hafen, J.E. Hathaway, and J.J. McCullought. 2016, September (updated). *L-Prize® Lumen Maintenance Testing of the Philips 60-watt Replacement Lamp L Prize Entry* (prepared for the U.S. Department of Energy).

66. Davis, J.L., K. Mills, R. Yaga, C. Johnson, M. Hansen, and M. Royer. 2017. Chromaticity maintenance in LED devices. In *Solid State Lighting Reliability: Components to Systems*, edited by W. D. van Driel, X. Fan and G. Q. Zhang. NY: Springer.

67. Hansen, M., and J.L. Davis. 2016. *Package impact on color shift in LEDs*. Presented at the 2016 Strategies in Light conference, Santa Clara, CA.

68. Next Generation Lighting Industry Alliance and LED Systems Reliability Consortium. 2017, April. *LED Luminaire Reliability: The Impact of Color Shift* (prepared for the U.S. Department of Energy).

69. Brodrick, J., ed. 2016, June. Solid-State Lighting R&D Plan (prepared for the U.S. Department of Energy SSL program, Document DOE/EE-1418).

70. Illuminating Engineering Society. 2014. *TM-28-14: Projecting Long-Term Luminous Flux Maintenance of LED Lamps and Luminaires*: Illuminating Engineering Society.

71. Smallwood, P. 2016. *Lighting, LEDs and Smart Lighting Market Overview*. Presented at the U.S. Department of Energy SSL Workshop, Raleigh, NC.

72. Miller, N.J., and M. Poplawski. 2014. *SSL flicker fundamentals and why we care.* Presented by the U.S. Department of Energy at 2014 Lightfair, Las Vegas, NV.

73. IEEE. 2015. *IEEE Standard 1789-2015: IEEE Recommended Practices for Modulating Current in High Brightness LEDs for Mitigating Health Risks to Viewers*. New York, NY: IEEE.

74. State of North Carolina. *Energy Efficient Lighting Guidance Document for New Construction and Retrofits: The State of North Carolina*. State Construction Office of the State of North Carolina. 2016, March. Available from https://ncdoa.s3.amazonaws.com/s3fs-public/documents/files/State-of-NC-SSL-Guidance-Document.pdf.

75. Hutcheson, R., R. Talley, and J.L. Davis. *LED Lighting Panel Discussion: Energy Efficient Lighting Guidance Document for New Construction and Retrofits.* Presented at the State Construction Conference (Webinar and Presentation) 2016. Available from https://ncdenr.s3.amazonaws.com/s3fs-public/Environmental%20Assistance%20and%20Customer%20Service/Utility%20Savings%20Initiative/SSL%20Webinar%20final_062216.pdf.

76. Talley, R. 2016. *Solid-state lighting: An owner's perspective*. Presented at the DOE SSL R&D Workshop, Raleigh, NC.

77. Nelson, W.B. 2004. *Applied Life Data Analysis*. Hoboken, NJ: John Wiley & Sons,.

78. Wang, J.-S., C.-C. Tsai, M.-H. Chen, Y.-C. Hsu, H.-L. Hu, C.-W. Lee, and W.H. Cheng. 2009. "Decay of lumen and chromaticity of high-power phosphor-converted white-light emitting diodes in thermal aging," in Light emitting diodes: Materials, devices, and applications for solid state lighting XIII. *Proceedings of the SPIE* 7231:723100-1.

79. She, H.J., and H. Feng. 2007. Accelerated life test for high-power white LED based on spectroradiometric measurement. Solid state lighting and solar energy technologies. *Proceedings of SPIE* Vol. 6841.

80. Ishizaki, S.H., H. Kimurz, and M. Suginoto. 2007. Lifetime estimation of high power white LEDs. *Journal of Light and Visual Environment* 31:11.

81. JEDEC Solid State Technology Association. JEDEC Standard: JESD22-A101C, Steady State Temperature Humidity Bias Life Test. JEDEC Solid State Technology Association, 2009. Available from www.jedec.org.

82. Mehr, M.Y., W.D. van Driel, K.M.B. Jensen, P. Deeben, M. Boutelje, and G.Q. Zhang. 2013. Photodegradation of bisphenol A polycarbonate under blue light radiation and its effect of optical properties. *Optical Materials* 35:504.

83. Neilson, J.B., and B.N. Crocker. 1993. UV aging of fluorescent reflectors. *Conference Record of the 1993 IEEE Industrial Applications Conference (IAS 1993)* 3:2348-50.

84. Christensen, P.A., A. Dilks, T.A. Egerton, and J. Temperley. 2000. Infrared spectroscopic evaluation of the photodegradation of paint: Part ii: The effect of UV intensity and wavelength on the degradation of acrylic films pigmented with titanium dioxide. *Journal of Material Science* 35:5353.

85. NGLIA and LSRC. *LED Luminaire Lifetime: Recommendations for Testing and Report, Third Edition* (prepared for the U.S. Department of Energy) 2014. Available from https://energy.gov/sites/prod/files/2015/01/f19/led_luminaire_lifetime_guide_sept2014.pdf.

86. NGLIA and LSRC. *LED Luminaire Reliability: Impact of Color Shift* (prepared for the U.S. Department of Energy) 2017. Available from https://energy.gov/sites/prod/files/2017/04/f34/lsrc_colorshift_apr2017.pdf.

87. JEDEC Solid State Technology Association. JEDEC Standard: JESD22-A104D, Temperature Cycling. JEDEC Solid State Technology Association, 2009. Available from www.jedec.org.

88. JEDEC Solid State Technology Association. JEDEC Standard: JESD22-A108C, Temperature, Bias, and Operating Life. JEDEC Solid State Technology Association, 2005. Available from www.jedec.org.

89. Narendran, N., Y.-W. Liu, X. Mou, D.R. Thotagamuwa, and O.V.M. Eschwarage. 2016. Project LED product life based on application. Fifteenth International Conference on Solid-State Lighting and LED-Based Illumination Systems. In *Proceedings of the SPIE*, edited by M. H. Kane, N. Dietz and I. T. Ferguson. San Diego, CA.

90. Ting, M., and E. Page. *Energy Star Lighting Webinar: CPUC LED Lab Test Study Update*. Presented at the September 2016 EnergyStar Webinar Series, 2016. Available from https://www.energystar.gov/sites/default/files/asset/document/Michael%20Ting%20CPUC%20LED%20Lab%20Test.pdf.

91. Lago, M.D., M. Meneghini, N. Trivellin, G. Mura, M. Vanzi, G. Meneghesso, and E. Zanoni. 2012. Phosphors for LED-based light sources: thermal properties and reliability issues. *Microelectronics Reliability* 52:2164.

92. Mehr, M.Y., W.D. van Driel, and G.Q. Zhang. 2014. Accelerated life time testing and optical degradation of remote phosphor plates. *Microelectronics Reliability* 54:1544.

93. Mehr, M.Y., W.D. van Driel, and G.Q. Zhang. 2014. *Reliability and accelerated test methods for plastic materials in LED-based products*. Presented at the Proceedings of the 2014 15th International Conference on Thermal, Mechanical, and Multi-physics Simulation and Experiments in Microelectronics and Microsystems (IEEE EuroSimE), Ghent, Belgium.

94. Davis, J.L., R. Yaga, M. Lamvik, K. Mills, and B. Fletcher. 2017. The influence of phosphor and binder chemistry on the aging characteristics of remote phosphor products. In *Solid State Lighting Reliability: Components to Systems, Vol. 2*, edited by W. D. van Driel, X. Fan and G. Q. Zhang. New York, NY: Springer.

95. Miller, N.J, Leon, F.A., Davis, J.L. September, 2016. *CALiPER Report 24: Photometric Testing, Laboratory Teardowns, and Accelerated Lifetime Testing of OLED Luminaires* (prepared for the U.S. Department of Energy)

96. Yang, S., A. Bryant, P. Mawby, D. Xiang, L. Ran, and P. Tavner. 2011. As industry-based survey of reliability in power electronic converters. *IEEE Transactions on Industrial Applications* 47:1441.

97. Next Generation Lighting Industry Alliance and LED Systems Reliability Consortium. 2014, September. *LED Luminaire Lifetime: Recommendations for Testing and Reporting* (prepared for the U.S. Department of Energy).

98. Winder, S. 2008. Power supplies for LED driving. Amsterdam, the Netherlands: Elsevier/Newnes.

99. On Semiconductor. 2008. *Transient Overvoltage Protection.* Publication Order Number TND335/D. Phoenix, AZ: On Semiconductor.

100. Phipps, K.O., and B.R. Connatser. 2005. Understanding MOVs for applying robust protection against surges. *Interference Technology EMC Directory and Design Guide* p. 116.

101. Keebler, P.F., K.O. Phipps, and D. Nastasi. Distinguishing between surge- and temporary overvoltage-related failures of metal oxide varistors in end-use equipment designs. *Interference Technology* 2006. Available from https://interferencetechnology.com/distinguishing-between-surge-and-temporary-overvoltage-related-failures-of-metal-oxide-varistors-in-end-use-equipment-designs/.

102. National Electrical Manufacturers Association. 2016. *NEMA 410-2015: Performance Testing for Lighting Controls and Switching Devices with Electronic Drivers and Discharge Ballast*. Washington, DC: NEMA.

103. Shepherd, S.D., K.C. Mills, R. Yaga, C. Johnson, and J.L. Davis. 2014. New understandings of failure modes in SSL luminaires. *Proceedings of the SPIE* 9190 (2014):919018.

104. Davis, J.L. *Accelerated life test results for SSL luminaire electronics.* Presented at the 2015 U.S. Department of Energy's Solid-State Lighting Research and Development Workshop, San Francisco, CA 2015. Available from http://www.energy.gov/sites/prod/files/2015/02/f19/davis-l_reliability_sanfrancisco2015.pdf.

105. Davis, J.L., C. Perkins, A. Smith, T. Clark, and K. Mills. 2017, April 2-5. *Leveraging accelerated testing to assess the reliability of two-stage and multi-channel drivers*. Presented at the 2017 18th International Conference on Thermal, Mechanical, and Multi-physics Simulation and Experiments in Microelectronics and Microsystems (EuroSimE), Dresden, Germany. doi: 10.1109/EuroSimE.2017.7926224

106. Valentine, N., D. Das, B. Sood, and M. Pecht. 2015, October 27–29. *Failure analysis of modern power semiconductor switching devices*. Presented at the IMAPS 48th International Symposium on Microelectronics, Orlando, FL. doi: http://dx.doi.org/10.4071/isom-2015-THA56

107. Li, X., J. Qin, and J.B. Bernstein. 2008. Compact modeling of MOSFET wearout mechanisms for circuit-reliability simulation. *IEEE Transactions on Device and Materials Reliability* 8 (1):98-121.

108. Lu, F., J. Shao, X. Liu, and X. Wang. 2012. *Validation test method of TDDB physics-of-failure model*. Presented at the 2012 Prognostics & System Health Management Conference (PHM-2012 Beijing), Beijing, pp. 1-4.

109. Zhou, Z., X. Liu, Q. Shi., Y. En, and X. Wang. 2013. *Failure rate calculation for NMOS devices under multiple failure mechanisms*. Presented at the 2013 IEEE Internaional Symposium on the Physical and Failure Analysis of Integrated Circuits (IPFA), pp. 362-365.

110. Celaya, J.R., A. Saxena, C.S. Kulkarni, S. Saha, and K. Goebel. 2012. *Prognostics approach for power MOSFET under thermal-stress aging*. Presented at the 2012 Proceedings of the Reliability and Maintainability Symposium (RAMS).

111. Saha, S., J.R. Celaya, V. Vashchenko, S. Mahiuddin, and K.F. Goebel. 2011. *Accelerated aging with electrical overstress and prognostics for power MOSFETs*. Presented at the 2011 IEEE EnergyTech conference.

112. Vaalasranta, I., J. Pippola, and L. Frisk. 2013. *Power MOSFET failure and degradation mechanisms in flyback topology under high temperature and humidity conditions.* Presented at the 2013 9th IEEE International Symposium on Diagnostics for Electric Machines, Power Electronics and Drives (SDEMPED), pp. 16–22. doi: 10.1109/DEMPED.2013.6645691

113. Lahyani, A., P. Venet, G. Grellet, and P.-J. Viverge. 1998. Failure prediction of electrolytic capacitors during operation of a switchmode power supply. *IEEE Transactions on Power Electronics* 13:1199.

114. Blais, P. *Ongoing LED R&D challenges: capacitors.* Presented at the U.S. Department of Energy's Solid-State Lighting Research and Development Workshop. San Francisco, CA 2015, February. Available from https://www.energy.gov/sites/prod/files/2015/02/f19/blais_led-challenges_2015.pdf.

115. Reliability Analysis Center. 1996. Reliable application of capacitors. Rome, NY: Reliability Analysis Center.

116. Kulkarni, C.S., J.R. Celaya, K. Goebel, and G. Biswas. 2012. *Physics based electrolytic capacitor degradation models for prognostic studies under thermal overstress*. Presented at the European Conference of the Prognostics and Health Management Society, p. 1.

117. Iman, A.M., D.M. Divan, R.G. Harley, and T.G. Habetler. 2007. Electrolytic capacitor failure mechanism due to inrush current. *Conference Record of the 2007 IEEE Industry Applications Conference, 42nd Annual Meeting of the Industry Applications Conference.,* pp. 730–736.

118. Lall, P., P. Sakalaukus, and J.L. Davis. 2015. Reliability and failure modes of solid-state lighting electrical drivers subjected to accelerated aging. *IEEE Access* 3:53.

119. Zhou, Y., X. Li, X. Ye, and G. Zhai. 2012. *A remaining useful life prediction method based on condition monitoring for LED driver*. Presented at the 2012 Prognostics & System Health Management Conference (PHM-2012 Beijing), MU3086. doi: 10.1109/PHM.2012.6228797

120. Wang, H., and F. Blaabjerf. 2013. *Reliability of capacitors for DC-link applications—An overview*. Presented at the 2013 IEEE Energy Conversion Conference and Exposition (ECCE), pp. 1866–1873.

121. Lin, F., X. Dai, Z. Yao, and J. Li. 2003. Research on electrode-end contact degradation of metallized polypropylene capacitors. *IEEE Transactions on Magnetics* 39 (1):353.

122. Brown, R.W. 2006. Linking corrosion and catastrophic failure in low-power metallized polypropylene capacitors. *IEEE Transactions on Device and Materials Reliability* 6 (2):326-33.

123. Sleegers, P.J.C., N.M. Moolenaar, M. Galetzka, A. Pruyn, B.E. Sarroukh, and B. van der Zande. 2013. Lighting affects students' concentration positively: Findings from three Dutch studies. *Lighting Research and Technology* 45:159-75.

124. Choi, K., and H.J. Suk. 2016. Dynamic lighting system for the learning environment: performance of elementary students. *Optics Express* 24 (10).

125. Poplawski, M., S. Brown, B. Hartman, C. Isaacson, and M. Phillips. 2015. *Workshop1: LED driver fundamentals for lamp and luminaire designers*. Presented at the Workshop at 2015 Strategies in Light, Las Vegas, NV.

126. IEEE Standard 1100-2005. 2005. IEEE recommended practice for powering and grounding electronic equipment.

127. Keebler, P.F. 2012. Ingredients for the success for LED lighting. Presented at the U.S. Department of Energy Solid-State Lighting Research and Development Workshop, Atlanta, Ga. January. http://apps1.eere.energy.gov/buildings/publications/pdfs/ssl/keebler_discussion_2012rdworkshop.pdf

128. Lall, P., M. Pecht, and E.B. Hakim. 1997. *Influence of Temperature on Microelectronics and System Reliability*. Boca Raton, FL: CRC Press.

129. Han, L., and N. Narendran. 2009. Developing an accelerated life test method for LED drivers. Ninth International Conference on Solid State Lighting. *Proceedings of the SPIE 7422:742209*.

130. Han, L., and Narendran, N. 2011. An accelerated test method for predicting the useful life of an LED driver. *IEEE Transactions on Power Electronics* 26(8):2249–2257.

131. Kulkarni C.S., J.R. Celaya, G. Biswa, and K. Goegel. 2012. *Accelerated aging experiments for capacitor health monitoring and prognostics*. 2012 IEEE AUTOTESTCON 356-361. doi: 10.1109/AUTEST.2012.6334580.

132. Sakalaukus, P.K. 2015. *Failure mode classification for life prediction modeling of solid-state lighting*. PhD Dissertation, Auburn University. https://etd.auburn.edu/handle/10415/4740.

133. Peck, D.S. 1986. *Comprehensive model for humidity testing correlation*. 24th Annual Reliability Physics Symposium. doi: 10.1109/IRPS.1986.362110.

134. Lall, P., Sakalaukus, P., and Davis, J.L. 2016. Improvements to the IES TM-28-14 lumen maintenance standard: A generalized acceleration factor approach for solid-state lighting. 2016 IEEE 66th Electronic Components and Technology Conference (ECTC). doi: 10.1109/ECTC.2016.273.

135. Kamal, N. 2009. *9W Retrofit Triac Dimming, Part Number LM3445MM*. National Semiconductor Application Note 2009-02-12. http://www.ti.com/lit/ug/snvu104/snvu104.pdf.

136. Texas Instruments. 2015. *120 V_{AC} valley fill buck triac dimmable LED driver*. Application Note published by Texas Instruments. http://www.ti.com/lit/ug/sluuba8/sluuba8.pdf

Appendix A:
Devices Under Test

Devices tested during this project included both LED and OLED devices and crossed many form factors, from bare LED to ceiling troffer, to luminaire drivers. Table A-1 lists the sample models, the type of device and what exposure methods were used during testing. In many cases, the same model of device was investigated with more than one AST exposure test during the project. However, each test sample only experienced one AST method in its test life.

Table A-1. Solid-state Lighting Leds, Lamps, and Luminaires Tested during this Investigation

Manufacturer	Model	Device Type	Test Performed
Osram	RT6	6" Downlight	Hammer, RTOL
Osram	RT6HO	6" Downlight	8585
Osram	RT6 (Gen2)	6" Downlight	8585, 7575
Osram	OT50W/PRG1400C/UNV/DIM/L (79631) DRVR +	Driver	7575
LSG	Glimpse	6" Downlight	Hammer, RTOL, 8585
LSG	Glimpse-Indirect	6" Downlight	8585, 7575
LSG	ECS DN6 W27 E26 120 BX	6" Downlight	7575
Cree	LR6	6" Downlight	Hammer, RTOL
Cree	CR6	6" Downlight	Hammer, RTOL, 8585, 7575, 6590
Cree	Essentia	6" Downlight	Hammer, 8585
Cree	T67	6" Downlight	8585, 7575
Cree	XP-E	HP-LED	8585, 7575
Cree	XP-G	HP-LED	8585, 7575
Cree	XT-E	HP-LED	8585, 7575, 6590
Cree	Original 60 W equivalent BA19-08027OMF-12DE26-1U_00	Lamp	8585, HTSL, WHTSL, RTOL
Finelite	77798 Dual LED	MP-LED Module	75 C Bake, 95 C Bake, 7575
Finelite	DMX Driver 4 Channel, 40 W Part#89661	Driver	7575
Finelite	2x2 Troffer	Luminaire	Flicker
Finelite	2x4 Troffer	Luminaire	LM-80
Finelite	Wallwash	Luminaire	Flicker

(continued)

Table A-1. Solid-state Lighting Leds, Lamps, and Luminaires Tested during this Investigation (continued)

Manufacturer	Model	Device Type	Test Performed
Philips Lightolier	Calculite 6” downlight	6" Downlight	Hammer, RTOL
Philips	Fortimo LED DLM 3000 30W/834	Light Engine	7575
Philips	Xitanium 39 W, 0.2 - 0.7A, 20-56 V 9137 012 13402	Driver	7575
Philips	Philips-40W Xitanium 0-10V	Driver	7575
Philips	L-Prize 60W equivalent	Lamp	8585, HTSL, WHTSL, RTOL
Philips	Gen 2 60W equivalent BC11A19/AMB/2700 DIM120V	Lamp	8585, HTSL, WHTSL, RTOL
Philips	Slimline - 60W equivalent	Lamp	8585, HTSL, WHTSL, RTOL
Lunera	2x2 Troffer	Luminaire	Hammer
Cordelia Lighting (Commercial Electric)	T65 6” Downlight	6" Downlight	8585, 7575, 6590
OptiLED	Round150	6" Downlight	8585, 7575, 6590
Lithonia	Security Lamp	Luminaire	8585, 7575
Everfine		Driver	7575
LG	DRVR-150W 54-C700 UNV 0-10 4CH LG	Driver	7575
EldoLED		Driver	7575

Appendix B:
Products—Experimental Methods

Table B-1. Accelerated Stress Test (AST) Methods Developed and/or Used during this Investigation

Test Name	Test Description
Hammer	https://www1.eere.energy.gov/buildings/publications/pdfs/ssl/hammer-testing_Dec2013.pdf.
HTSL	Dry, non-operational bake at 135°C
WHTOL	85°C/85% relative humidity (8585), 75°C/75% relative humidity (7575), 65°C/90% relative humidity (6590) with one-hour electric bias duty cycle
WHTSL	85°C/85% relative humidity (8585)
Bake	Dry bake at 45°C
RTOL	Real-time Operational Life - room temperature and ambient humidity

Several models developed during this investigation were based on AST data, particularly those for luminaire lenses and reflectors, which were used then incorporated in the DST.

The chemical kinetic models for chromaticity shift were also based on AST data from this investigation.

Models developed for LED types (HPLED, MPLED, COB) were developed from industry LM-80 data.

A simulated experiment was also performed by utilizing the ray-tracing program Photopia to create virtual luminaires and then degrading the materials in the luminaire and recalculating luminaire performance.

Appendix C:
Products—List of Papers and Presentations

Table C-1. Products—List of Papers and Presentations

Document Title	Authors	Publication	Year	Volume	Start Page	End Page	DOI
Prediction of lumen output and chromaticity shift in LEDs using Kalman Filter and Extended Kalman Filter based models	P. Lall; J. Wei; L. Davis	Prognostics and Health Management (PHM), 2013 IEEE Conference on	2013		1	14	*10.1109/ICPHM.2013.6621457*
L70 life prediction for solid state lighting using Kalman Filter and Extended Kalman Filter based models	P. Lall; J. Wei; L. Davis	2013 IEEE 63rd Electronic Components and Technology Conference	2013		1452	1465	10.1109/ECTC.2013.6575764
Prediction of L70 Life and Assessment of Color Shift for Solid-State Lighting Using Kalman Filter and Extended Kalman Filter-Based Models	P. Lall; J. Wei; L. Davis	Proceedings of the SPIE	2013	8835			10.1117/12.2027593
Insights into accelerated aging of SSL luminaires	L. Davis et al.	Proceedings of the SPIE	2013	8835			10.1117/12.2025295
Assessment of lumen degradation and remaining useful life of LEDs using particle filter	P. Lall; H. Zhang; L. Davis	AMSE 2013 International Technical Conference and Exhibition on Packaging and Integration of Electronic and Photonics Microsystems (IPACK2013)	2013				10.1115/IPACK2013-73305
Prognostics of damage accrual in SSL luminaires and drivers subjected to HTSL accelerated aging	P. Lall; P. Sakalaukus; L. Davis	AMSE 2013 International Technical Conference and Exhibition on Packaging and Integration of Electronic and Photonics Microsystems (IPACK2013)	2013				10.1115/IPACK2013-73250

(continued)

Table C-1. Products—List of Papers and Presentations (continued)

Document Title	Authors	Publication	Year	Volume	Start Page	End Page	DOI
Solid-state lighting life prediction using extended Kalman filter	P. Lall; J. Wei; L. Davis	AMSE 2013 International Technical Conference and Exhibition on Packaging and Integration of Electronic and Photonics Microsystems (IPACK2013)	2013	1	T05A016		10.1115/IPACK2013-73288
Hammer Testing Findings for Solid-State Lighting Luminaires	J.L. Davis; M. Lamvik; J. Bittle; S. Shepherd; R. Yaga	DOE SSL Website: http://apps1.eere.energy.gov/buildings/publications/pdfs/ssl/hammer-testing_Dec2013.pdf	2013				-
SSL and LED life prediction and assessment of CCT shift	P. Lall; P. Sakalaukus; J. Wei; L. Davis	Thermal and Thermomechanical Phenomena in Electronic Systems (ITherm), 2014 IEEE Intersociety Conference on	2014		1179	1185	10.1109/ITHERM.2014.6892413
Reliability of solid-state lighting electrical drivers subjected to WHTOL accelerated aging	P. Lall; P. Sakalaukus; L. Davis	Thermal and Thermomechanical Phenomena in Electronic Systems (ITherm), 2014 IEEE Intersociety Conference on	2014		1164	1170	10.1109/ITHERM.2014.6892411
Bayesian probabilistic model for life prediction and fault mode classification of solid-state luminaires	P. Lall; J. Wei; P. Sakalaukus	2014 IEEE Conference on Prognostics and Health Management (PHM)	2014				10.1109/ICPHM.2014.7036401
Prediction and classification of failure modes in solid-state luminaires using Bayesian Probabilistic Models	P. Lall; J. Wei; P. Sakalaukus	2014 IEEE Electronics Components and Technology Conference (ECTC)	2014				10.1109/ECTC.2014.6897585

(continued)

Table C-1. Products—List of Papers and Presentations (continued)

Document Title	Authors	Publication	Year	Volume	Start Page	End Page	DOI
New understandings of failure modes in SSL luminaires	S.D. Shepherd et al.	Proceedings of the SPIE	2014				10.1117/12.2062243
System reliability for LED-based products	J. Davis; K. Mills; M. Lamvik; R. Yaga; S. Shepherd; J. Bittle; N. Baldasaro; E. Solano; G. Bobashev; C. Johnson; A. Evans	2014 15th International Conference on Thermal, Mechanical, and Multi-Physics Simulation and Experiments in Microelectronics and Microsystems (EuroSimE)	2014				10.1109/EuroSimE.2014.6813879
Failure mechanisms and color stability in light-emitting diodes during operation in high-temperature environments in presence of contamination	P. Lall; H. Zhang; L. Davis	2015 IEEE 65th Electronic Components and Technology Conference (ECTC)	2015		1624	1632	10.1109/ECTC.2015.7159814
Reliability and Failure Modes of Solid-State Lighting Electrical Drivers Subjected to Accelerated Aging	P. Lall; P. Sakalaukus; L. Davis	IEEE Access	2015	3	531	542	10.1109/ACCESS.2015.2404812
Prognostics Health Management Model for LED Package Failure Under Contaminated Environments	P. Lall; H. Zhang; L. Davis	AMSE 2015 International Technical Conference and Exhibition on Packaging and Integration of Electronic and Photonics Microsystems (IPACK2015)	2015	2			10.1115/IPACK2015-48724
Discoloration and failure mechanism analysis of high power pc-LED under harsh environment in presence of contamination	P. Lall; H. Zhang; L. Davis	AMSE 2015 International Technical Conference and Exhibition on Packaging and Integration of Electronic and Photonics Microsystems (IPACK2015)	2015	2			

(continued)

Table C-1. Products—List of Papers and Presentations (continued)

Document Title	Authors	Publication	Year	Volume	Start Page	End Page	DOI
An investigation of catastrophic failure in solid-state lamps exposed to harsh environmental operational conditions	P. Lall; P. Sakalaukus; L. Davis	AMSE 2015 International Technical Conference and Exhibition on Packaging and Integration of Electronic and Photonics Microsystems (IPACK2015)	2015	2	T01A011		10.1115/IPACK2015-48257
Prognostication of LED remaining useful life and color stability in the presence of contamination	P. Lall; H. Zhang; L. Davis	2015 IEEE Conference on Prognostics and Health Management (PHM)	2015				10.1109/ICPHM.2015.7245065
Reliable LED Lighting Technologies: Key Factors and Procurement Guidance	J. L. Davis; A. Arquit-Niederberger	2015 IEEE Global Humanitarian Technology Conference (GHTC)	2015				10.1109/GHTC.2015.7343972
Improvements to the IES TM-28-14 Lumen Maintenance Standard: A Generalized Acceleration Factor Approach for Solid-State Lighting	P. Lall; P. Sakalaukus; L. Davis	2016 IEEE 66th Electronic Components and Technology Conference (ECTC)	2016		1342	1351	10.1109/ECTC.2016.273
A comparison of temperature and humidity effects on phosphor-converted LED packages and the prediction of remaining useful life with state estimation	P. Lall; H. Zhang; L. Davis	2016 15th IEEE Intersociety Conference on Thermal and Thermomechanical Phenomenon in Electronic Systems	2016		207	217	10.1109/ITHERM.2016.7517552
An efficiency decay model for lumen maintenance	G. Bobashev; N. Baldasaro; K. Mills; and J.L. Davis	IEEE Transactions on Device and Materials Reliability	2016	16	277		10.1109/TDMR.2016.2584926

(continued)

Table C-1. Products—List of Papers and Presentations (continued)

Document Title	Authors	Publication	Year	Volume	Start Page	End Page	DOI
CALiPER 20.5: Chromaticity Shift Modes of LED PAR38 Lamps Operated in Steady-State Conditions	J.L. Davis; J. Young; M. Royer	CALiPER Report 20.5: Chromaticity shift modes of LED PAR38 lamps operated in steady-state conditions. Report prepared for the U.S. Department of Energy	2016				http://energy.gov/sites/prod/files/2016/03/f30/caliper_20-5_par38.pdf
CALiPER 24: Photometric testing, laboratory teardowns, and accelerated lifetime testing of OLED luminaires	N. Miller; F. Leon; J. Lynn Davis	CALiPER Report 24: Photometric testing, laboratory tear downs, and accelerated life testing of OLED luminaires	2016				http://energy.gov/sites/prod/files/2016/10/f33/caliper-24_oled-luminaires.pdf
Assessing the reliability of electrical drivers used in LED-based lighting devices	J. L. Davis, K. Mills, R. Yaga, C. Johnson, M. Hansen, and M. Royer	Solid-State Lighting Reliability, 2nd Edition (Due out in June 2017)	2017				
Chromaticity maintenance in LED devices	J. L. Davis, K. Mills, R. Yaga, C. Johnson, J. Young	Solid-State Lighting Reliability, 2nd Edition (Due out in June 2017)	2017				
The influence of phosphor and binder chemistry on the aging characteristics of remote phosphor products	J. L. Davis, R. Yaga, K. Mills, M. Lamvik, and B. Flectcher	Solid-State Lighting Reliability, 2nd Edition (Due out in June 2017)	2017				
Modeling the impact of thermal effects on luminous flux maintenance for SSL luminaires	J.L. Davis, K. Mills, M. Lamvik, and C. Perkins	Proceedings of the 2017 IEEE iTHERM Conference (in development)	2017	TBD			

Appendix D:
Products—Networks and Collaborations Fostered

It is RTI's belief that the results of this project will be most useful to our client and the industry with a rich contribution from industry, itself. Through partnerships and expert input, RTI fostered industry buy-in to the concepts developed during this project.

Project Partners:

Organization Name: Auburn University
Location of Organization: Auburn, Alabama
Partner Contribution to the project

- Collaborative research with RTI on SSL luminaire reliability
- Facilities including test chambers and work on developing a Kalman filter for LM-80 data (to improve lifetime projections) and studies on the impact of accelerated life test of SSL driver components.
- Presentation of results at technical conferences.
- Financial support

Organization Name: Cree
Location of Organization: Sturtevant, Wisconsin and Research Triangle Park, North Carolina
Partner Contribution to the project

- Technical guidance on SSL lighting and failure modes
- Technical guidance on LED performance and reliability
- Participation on project Advisory Board

Organization Name: Agencies within the state government of North Carolina including the State Construction Office, Department of Environmental Quality, and Department of Public Instruction, Department of Public Safety, North Carolina State University, and University of North Carolina at Chapel Hill
Location of Organization: Raleigh, NC and Chapel Hill, NC
Partner Contribution to the project

- Information on the field performance of SSL installations
- Lessons learned from SSL installations compared to other lighting technologies
- Specifications for LED-based lighting systems in all environments
- Participation on project Advisory Board (N.C. State University)
- Financial support

Organization Name: SAS Institute
Location of Organization: Cary, North Carolina
Partner Contribution to the project

- In-kind contribution of software and training
- Financial support

Additional Project Collaborators:

- Pacific North National Laboratories
- LED System Reliability Consortium (LSRC)
- Ralph Tuttle of Cree
- Eric Haugaard of Cree
- Willem van Driel of Philips
- Xuejun Fan of Lamar University
- G.Q. Zhang, of Technical University of Delft
- Abhijit Dasgupta of the University of Maryland

Appendix E:
Products—Inventions/Patent Applications

No patents were filed nor any inventions disclosed during the POP of this project.